STRETCHED EXPONENTIAL DECLINE MODEL AS A PROBABILISTIC AND DETERMINISTIC TOOL FOR PRODUCTION FORECASTING AND RESERVE ESTIMATION IN OIL AND GAS SHALES

A Dissertation

by

BABAK AKBARNEJAD NESHELI

Submitted to the Office of Graduate Studies of
Texas A&M University
in partial fulfillment of the requirements for the degree of

DOCTOR OF PHILOSOPHY

May 2012

Major Subject: Petroleum Engineering

Stretched Exponential Decline Model As a Probabilistic and Deterministic Tool for Production Forecasting and Reserve Estimation in Oil and Gas Shales

Copyright 2012 Babak Akbarnejad Nesheli

STRETCHED EXPONENTIAL DECLINE MODEL AS A PROBABILISTIC AND DETERMINISTIC TOOL FOR PRODUCTION FORECASTING AND RESERVE ESTIMATION IN OIL AND GAS SHALES

A Dissertation

by

BABAK AKBARNEJAD NESHELI

Submitted to the Office of Graduate Studies of
Texas A&M University
in partial fulfillment of the requirements for the degree of

DOCTOR OF PHILOSOPHY

Approved by:

Chair of Committee,	Peter P. Valkó
Committee Members,	W. John Lee
	Christine Ehlig-Economides
	Frederick M. Chester
Head of Department,	A. Daniel Hill

May 2012

Major Subject: Petroleum Engineering

ABSTRACT

Stretched Exponential Decline Model As a Probabilistic and Deterministic Tool for Production Forecasting and Reserve Estimation in Oil and Gas Shales. (May 2012)

Babak Akbarnejad Nesheli, B.A., University of Tehran; M.S., Texas A&M University

Chair of Advisory Committee: Dr. Peter P. Valkó

Today everyone seems to agree that ultra-low permeability and shale reservoirs have become the potentials to transform North America's oil and gas industry to a new phase.

Unfortunately, transient flow is of long duration (perhaps life of the well) in ultra-low permeability reservoirs, and traditional decline curve analysis (DCA) models can lead to significantly over-optimistic production forecasts without additional safeguards.

Stretched Exponential decline model (SEDM) gives considerably more stabilized production forecast than traditional DCA models and in this work it is shown that it produces unchanging EUR forecasts after only two-three years of production data are available in selected reservoirs, notably the Barnett Shale.

For an individual well, the SEDM model parameters, can be determined by the method of least squares in various ways, but the inherent nonlinear character of the least squares problem cannot be bypassed. To assure a unique solution to the parameter estimation problem, this work suggests a physics-based regularization approach, based

on critical velocity concept. Applied to selected Barnett Shale gas wells, the suggested method leads to reliable and consistent EURs.

To further understand the interaction of the different fracture properties on reservoir response and production decline curve behavior, a series of Discrete Fracture Network (DFN) simulations were performed. Results show that at least a 3-layer model is required to reproduce the decline behavior as captured in the published SEDM parameters for Barnett Shale. Further, DFN modeling implies a large number of parameters like fracture density and fracture length are in such a way that their effect can be compensated by the other one. The results of DFN modeling of several Barnett Shale horizontal wells, with numerous fracture stages, showed a very good agreement with the estimated SEDM model for the same wells.

Estimation of P_{90} reserves that meet SEC criteria is required by law for all companies that raise capital in the United States. Estimation of P_{50} and P_{10} reserves that meet SPE/WPC/AAPG/SPEE Petroleum Resources Management System (PRMS) criteria is important for internal resource inventories for most companies. In this work a systematic methodology was developed to quantify the range of uncertainty in production forecast using SEDM. This methodology can be used as a probabilistic tool to quantify P_{90}, P_{50}, and P_{10} reserves and hence might provide one possible way to satisfy the various legal and technical-society-suggested criteria.

DEDICATION

To my dear family for their love, kindness, and encouragement.

ACKNOWLEDGEMENTS

I would like to thank and appreciate my teacher, adviser and committee chair Dr. Valkó for his guidance, support and encouragement. It is my great privilege that I had the opportunity to work with him. His knowledge and wisdom has provided me the strength to accomplish this work.

I would also like to thank my committee members, Dr. Lee, Dr. Ehlig-Economides, and Dr. Chester, for their guidance and support throughout the course of this research.

I also want to thank Chesapeake Corporation for providing me the data for this study.

Thanks also go to my friends and colleagues and the department faculty and staff for making my time at Texas A&M University a great experience.

Last but not least, I am thankful to my dear family for their encouragement and support throughout my study.

NOMENCLATURE

a	=Intercept constant defined by Eq. 7, Day $^{(m-1)}$
A	=Cross-section area of flow, ft^2
b	=Arps' decline exponent, dimensionless
D_∞	=Decline rate at infinite time in Ilk's PL model, 1/year
D_i	=Arps' decline constant, 1/Day
$EUR_{100\ MSCF/D}$	=Cumulative production forecast for q>100 Mscf/Day economic cutoff, Mscf
$EUR_{30\text{-}years}$	=Cumulative production for t=30 years, Mscf
$EUR_{t=\infty}$	=Contacted gas-in-place, Mscf
G_p	=Cumulative production, Mscf
m	=Slope defined by Eq. 7
M_a	=Air molecular weight=28.964 lbm mole
n	=Exponent parameter for SEPD model, dimensionless
p	=Pressure, psia
P_{10}	=The value smaller than 10% of the distribution
P_{50}	=The value smaller than 50% of the distribution
P_{90}	=The value smaller than 90% of the distribution
q	=Production, Mscf
q_0	=Production parameter common in Arps' model and in SEPD, Mscf/Days

q_1	=Production at Day 1, Mscf/Day
Q_c	=Critical gas flow rate, MMscf/D
q_D	=Production rate, Mscf/Day
R	=Universal gas constant=10.73147 psia-ft^3/°R-lbm mol
t	=Production time, Days
$T^{\circ R}$	=Temperature, °R
t(a,m)	=Time function based on Eq. 9
$t_{100\text{-Mscf/D}}$	=Time to reach the economic cutoff rate of q=100 Mscf/Days
	, Days
v_c	=Critical velocity, ft/sec
Z	=Gas compressibility factor
Γ	=Gamma function
γ_g	=Gas specific gravity
ρ_l	=Liquid density, lbm/ft^3
ρ_g	=Gas density, lbm/ft^3
σ	=Surface tension, dynes/cm
τ	=Characteristic time parameter for SEPD model, Days

TABLE OF CONTENTS

Page

LIST OF FIGURES

FIGURE Page

LIST OF TABLES

TABLE Page

1. INTRODUCTION: THE IMPORTANCE OF RESEARCH

Today everyone seems to agree that low-permeability and shale (both oil and gas) reservoirs have become the potentials to transform North America's oil and gas industry to a new phase. Now, the important question is how do we evaluate and interpret these potentials. The question of primary importance is: how much an individual well can produce during a certain time period of its life? The answer to this question is critical because it can change the economic cutoffs for exploration, drilling, and stimulation and ultimately a specific field's development strategy. Also it will determine how much reserve exists in a specific field.

Traditional production decline curve analysis (DCA), developed by Arps (1945), is a methodology based on actual production data of a specific well to forecast hydrocarbon production in the future. DCA uses empirical decline models such as exponential decline, harmonic decline, and hyperbolic decline. The hyperbolic decline is more general and the other two models can be considered as special cases of the hyperbolic decline model.

Over the decades traditional DCA has been accepted as a proven methodology–at least for conventional hydrocarbon wells. Direct application of the same methodology to unconventional oil and gas wells, however, has been found less reliable and even controversial.

Traditional DCA is often not reliable enough to accurately predict the estimated

---

This dissertation follows the style of *Journal of Petroleum Technology*.

ultimate recovery (EUR) for unconventional Oil and gas production forecasting.

This is because of complex, and maybe yet unknown, reservoir behavior and flow channel geometries in low-permeability and shale reservoirs. Traditional DCA was originally developed for production conditions that can be considered boundary-dominated in modern reservoir engineering terms. Boundary-dominated flow (BDF) occurs in medium-high permeability formations and usually the well reaches this regime in a short time. The behavior characteristics of the production history in tight-gas shale reservoirs can be and often are quite different. As a result, traditional DCA leads to unreasonable results. To improve traditional Arps hyperbolic decline model for production forecasting in ultra-low permeability reservoirs (including gas shales), the most common practice in the industry is: 1) to allow the decline exponent have a value of $b>1$ and 2) to incorporate a specified final (minimum) exponential decline rate in the model.

Robertson (1988) presented a production rate equation with a hyperbolic characteristics in the early life of the well but asymptotically exponential. Based on his ideas, now it is common to find a hyperbolic fit to the early production of a well, and adding to that an exponential "tail", chosen to represent later stages of the well life. But the question is how one obtains the asymptotic exponential decline rate from the production characteristics at early times. In practice, the cutoff becomes a 4^{th} parameter of the model. Most often this 4^{th} parameter comes from experience from the analogous wells or experience with a particular reservoir. While this might lead to reasonable

estimates, it represents a potential danger: the EUR will depend more on this 4th parameter than on the analyzed prediction on history.

Also Arps hyperbolic decline in production forecasting in unconventional reservoirs yields b-factor value of greater than one which is contradictory to the comment that b-factor should never be greater than one. Traditional Arps hyperbolic model was originally created for the BDF data, closed reservoir, and constant flowing bottomhole pressure conditions which results in $0<b<1$. However, in ultra-low permeability formations transient flow is dominant. This is why we get b-values greater than one in such reservoirs using traditional Arps decline. Fan et al. (2011) analyzed production data from 8700 horizontal wells in Barnett Shale and found that hyperbolic exponent b-factor ranges between 1.35 to 1.65 with an average of 1.5.

Unfortunately, transient flow is of long duration (perhaps life of the well) in these reservoirs, and Arps model can lead to significantly over-optimistic production forecasts (with $b>1$) without additional safeguards. Several empirical approaches have been developed to make these unconventional production forecasts more reliable. The most recent ones are by Ilk et al. (2008), the power law (PL) decline model, Mattar and Moghadam (2009), modified power law exponential decline model, Currie et al. (2009), continuous EOR, Valkó et al. (2009 and 2010), the Stretched Exponential Decline Model (SEDM) model, and Duong (2011), a rate-decline analysis method.

Ilk's PL model, like traditional DCA, uses flow rates and is purely empirical and can be used for both transient and BDF regimes. This model does not have the problem of over estimation of reserves associated with $b>1$ in traditional hyperbolic forecast.

However, it has 4 unknowns and this creates severe ill-conditioning when fitting this equation to field data. One drawback related to this many degrees of freedom is that those resulting EUR will depend on the "starting parameter estimates" of the non-linear minimization procedure.

Currie et al. (2010) presented "Continues EUR" methodology for reserve estimation in unconventional reservoirs. This methodology uses different rate-time relations to obtain the upper limit for EUR. For lower limit of EUR this methodology uses a straight line extrapolation technique and PL model which is influenced by transient flow period. The difference between the upper and lower limits of EUR estimation is supposed to decrease with time (with continues data acquisition). Their study on 38 field examples in tight and shale gas reservoirs shows that all wells are producing under transient condition and there is no sign of BDF. Also all hyperbolic matches resulted in b-parameter value greater than 1, showing that BDF condition was not reached in any of those examples.

Mattar and Moghadam (2009) pointed out some of these drawbacks of Ilk's PL model and emphasized the need to "tune" this model so it is compatible with mechanistic reservoir models. To do so, they compared the PL model with reservoir simulation models, and modified the PL model accordingly. One major difference between Ill's PL model and the Mattar and Moghadam model is that the transition from log-log straight line to constant D happens much longer in PL model which can be very long time in the well life. To do the modification they considered some constrains on the PL model to make it consistent with two common reservoir models: linear flow and

radial flow, each followed by BDF regime. This modified PL model consists of two sections: transient part and BDF part. For the transient part they got rid of the term D_∞ in Ilk's PL model and constrained n to 0 to -0.13. Using a radius of investigation equation they could obtain the start of BDF. We note that the PL model without the D_∞ is nothing else but the SEDM model.

The Stretched Exponential (SE) model, long used by applied physicists to model relaxation processes of various types, was introduced to the petroleum industry as an appropriate and reliable model for production rate decline in gas wells. SEDM gives considerably more stabilized production forecast than the Arps model (with or without minimum terminal decline), and it has been shown to produce unchanging EUR forecasts after only two-three years of production data are available in selected reservoirs, notably the Barnett Shale. Also, studies of synthetic and field data indicate that the model applies to both transient and stabilized flow data, with much of the model verification based on the Barnett Shale.

Perhaps one the most important characteristic of SE is that the relaxation of a system based on SE is equivalent to relaxation of a similar system containing many components that each decay independently under a specific relaxation rate. For petroleum engineering applications, Valko and Lee (2010) suggested that this characteristic of the SE model can be interpreted as the consequence of reservoir heterogeneity. Later, Kabir et al. (2011, SPE144311) has developed a semi-analytical approach, using the capacitance-resistance modeling (CRM) concept, to estimate production profile and EUR for unconventional reservoirs which incorporates this

concept of heterogeneity. In their formulation, a number of arbitrary reservoir segments were considered, each making variable contributions to production in a specific well. These contributions are analogues to the probability distribution of the decay rates considered in the glassy relaxation phenomenon by physicists, but in their model the exponential decay constants decrease with increasing the distance from the well within the stimulated reservoir volume (SRV). They applied their formulation on synthetic and field data and compared their results with the SEDM and found that CRM supports the solution obtained from SEDM. To investigate the capability of SEDM model in handling heterogeneity in unconventional reservoir a series of reservoir simulations have been performed using PETREL 2010 as the simulation tool. Then SEDM and hyperbolic model has been fit to the simulation result and the parameters for each model were estimated based on least-square fit. Hyperbolic parameter b for these simulation settings were estimated to be in the range of $1<b<2$ which is in agreement with the b range in the literature for tight reservoirs like shale gas. In all cases the *log (q) vs.* cumulative plot shows that SEDM model yielded a lower EUR compared to the hyperbolic model and shows how hyperbolic model can overestimate reserves and SEDM yields to a bounded and more conservative EUR.

One important aspect of Arps' original concept of DCA is associated with the "individual decline behavior" recognizable from one well's data. Indeed, most publications focus on analysis of individual production data and show such illustrations of concepts. Several investigations suggested, however, that the decline characteristics are valid for a group of wells. The big question however is, whether one well's

production data contains all the necessary information to extrapolate future behavior or some of the extrapolation should be "conditioned" on information gleaned from analysis of the field (group data). If field information is used, the question is in what form?

In the Barnett Shale the large number of wells –though most with short history of production – already allowed for some version of this conditioning process. In fields with lower number of wells and even shorter production history the method has to be worked out. Probably the answer will also depend on the quality and time span of the individual data series to be analyzed. Nevertheless, one should keep in mind that "unconventional" wells usually have more variable production history than conventional wells.

For an individual well the SEDM model parameters (n, τ, and q_0), can be determined by the method of least squares in various ways, but the inherent nonlinear character of the least squares problem cannot be bypassed. This non-uniqueness of SEDM 3-variable search method leads to different EUR estimations for each individual well. Noted by Seshadri and Mattar (2010), this is a drawback of the SEDM model. Two new strategies are introduced to take care of this parameter estimation non-uniqueness for 3-variable search method.

The first strategy, as an alternative for 3-variable (n, τ, and q_0) search, is to perform a 1-variable (just τ) search. The 1-variable search was done by setting q_0 equal to last cumulative production available divided by sum of all $\exp\left[-\left(\frac{t}{\tau}\right)^n\right]$ terms and setting n=0.247, based on the Valko and Lee (2010) for Barnett Shale, and searching for τ to obtain the best match on log of rate *vs.* cumulative production plot. Our study

shows that calculated EUR from both1 and 3-variable search methods are very close to each other.

As a second strategy (alternative) a 2-variable search based on Turner's critical velocity concept (1969) is introduced. The critical gas rate based on Turner's critical velocity can be used for conditioning the 3-variable search (n, τ, and q_0) in SEDM. In this parameter estimation strategy, for any specific well, it is assumed that inflection time in log(q) *vs.* rate plot is the time when the gas rate drops to the critical rate value. Therefore, in this new SEDM variable search only two parameters of n and τ are needed to be searched, and the third parameter (q_0) can be obtained using the critical gas rate. The advantage of this 2-variable search over the 3-variable search is that it does not have the problem of non-uniqueness and Excel's Solver always yields only one pair of n and τ (In contrast for the 3 or 4 parameter search).

To further investigate the SEDM parameter estimation and also reserve estimation in shale and other tight reservoirs, case studies on 25 horizontal shale gas wells in Newark East Field were performed. In these case studies SEDM parameters were estimated based on 3-parameter search and also 2-parameter search conditioned with Turner's critical gas rate. Then contacted gas in place and $EUR_{30\text{-years}}$ based on estimated parameters for each individual well and also based on published parameters for Barnett Shale were calculated for each individual well.

For comparison purposes, the same reserve parameters were determined for each individual well and based on Duong's methodology. This methodology is for wells producing from tight gas reservoirs in which fracture flow is dominant. Results of these

case studies show that $EUR_{30,\ SPE134231}$ and $EUR_{30,\ SPE137748}$, which are cumulative production after 30 years and were calculated using published parameters for Duong and SEDM methodology (Valko and Lee, 2010) for Barnett Shale, are consistent with the $EUR_{30\text{-}years}$ calculated from individual well SEDM parameter estimation.

These estimates ($EUR_{30,\ SPE134231}$ and $EUR_{30,\ SPE137748)}$ seem especially useful when the data set is short, or contain anomalies and hence do not allow for unique determination of all parameters for the SEDM and Duong models. Large discrepancy of the model estimates based on individual well decline parameters is a warning sign for uncertainty. Lee and Sidle (2010) provided an extensive critique of methods that are being used to forecast production estimate reserves in unconventional and poorly understood resource plays. They emphasized on importance of performing uncertainty analysis using statistical methods in such resources, as it can provide valuable insights on upper and lower limits of the reserves and makes it easier and more accurate to categorize those resources (proved, probable, and possible).

Can and Kabir (2011) presented a reserve-evaluation methodology which couples SEDM (as a DCA tool) with a probabilistic forecasting frame for wells with and without production history. They grouped production data based on the initial rates to obtain unified SEPD parameter sets (n, τ, and q_0) for similar wells in terms of productivity index. By grouping similar wells and then determining the distribution of the SEPD parameters they could come up with forecasting for individual wells. This way there will be less uncertainty involved compared to just one global parameter set for all wells. For new wells that have no history they used analogues wells to generate data for numerical

modeling. For existing wells, in case of irregularity in the production decline, they just used the dominant decline trend for curve-fitting, and then added the excluded production to the EUR as a constant. They used Valko and Lee (2010) methodology, which involves solving two non-linear equations, to obtain n and τ pairs. Then, after determining P10, P50 and P90 for each group they calculated high, medium, and low τ values by solving the two non-linear equations. For q_0, they assumed it is the maximum monthly rate for each well. Results of their study on 820 field data sets from three different shale types show that at least three-fourth of the wells' performance fall within the expected P10-P90 range.

Duong also performed statistical analysis in his methodology to obtain P10, P50, and P90 for reserve estimation purposes. Based on his study on various gas plays, he showed that there is a correlation between ***a*** and ***m*** parameters and it can be used to construct q/q_1 *vs.* time (days) type-curves.

The dual porosity (DP) concept, first introduced by Warren and Root (1963), adds a second interacting continuum which reflects storage and permeability characteristics of fractured reservoirs. However, because DP approaches simplify connectivity and imply scale-dependent heterogeneity, they cannot effectively address the connectivity between natural fractures and induced hydraulic fractures and their interaction (Fig. 1). The discrete fracture network (DFN) approach is geologically more realistic than DP model. Moreover, DFN models have many advantages over conventional dual porosity (DP) approaches, especially in heterogeneous reservoirs where the dominant flow mechanism is through the network of fractures rather than the

reservoir matrix. The DFN approach is based on the stochastic modeling concept and therefore every realization of the discrete fracture network will produce different results. As such, the DFN-type modeling is not a direct competitor to DP reservoir models. Rather it provides an additional insight into the potential variability of production histories.

The flow behavior in shale gas reservoirs, especially Barnett shell, was investigated using a Discrete Fracture Network (DFN) simulator (FracGen and NFflow). The interaction of the different stochastic properties of the fracture network on reservoir response was studied.

In particular, we aimed to connect the fracture network characteristics to SEDM parameters. For this purpose, FRACGEN/NFFLOW (2010) has been used. FRACGEN/NFFLOW is a fractured reservoir modeling software package that originally has been developed by the National Energy Technology Laboratory (NETL) Geological and Environmental Sciences on-site research group.

In our study, published parameters for SEDM from Valko and Lee (2010) have been used to first investigate the compatibility of the SEDM behavior in Barnett Shale gas wells with DFN concept. These SEDM parameters are $n=0.247$, $\tau=24$ days, and an average initial rate of $q_0=1667$ MSCF/D based on average Barnett Shale gas wells rate. These parameters yield to an inflection time of 2188 days.

In addition to single layer reservoir, to further understand the effect of reservoir heterogeneity on the SEDM behavior and inflection time location, multiple layer reservoirs have been investigated. For this purpose a different combination of 2-Layer

and 3-Layer reservoir with different reservoir and fracture properties have been simulated to get the best fit for our SEDM model based on published parameters for SEDM.

With single-layer and then a 2-layer model it was not possible to match the exact inflection time of the SEDM based on published SEDM parameters. Therefore a 3-layer reservoir model was considered, to investigate the effect of the number of reservoir layers (or different created fractured zones) on the SEDM behavior and inflection time. Results from 3-layer case shows that at least 3-layer model (or 3 different zones of fracture network) is required to have the same inflection time and decline behavior as captured by the published SEDM parameters for Barnett. Some of the observations from DFN simulations for multiple-layered reservoir are:

- Some parameters like Fracture density and fracture length are interchangeable from the point of view of decline behavoirs.
- Keeping all parameters fixed and just comparing 10 realizations explains the great variability of reserves that main production comes from network of natural and enhanced fractures.
- In the 3-layer model fracture aperture has the dominant effect on early time concavity of the overall decline curve.
- Porosity of the adjacent layers (L1 and L3) has the dominant effect on late time decline shape.

Since compatibility of published SEDM parameters with DFN modeling was confirmed, the applicability of DFN modeling for individual well histories was examined on several

Barnett Shale horizontal wells with numerous fracture stages, and then the results were compared with the estimated SEDM model for the same wells.

The main objectives of this research are

- Comparison of the performance of the new empirical methods in reserve estimation and production forecasting for unconventional shale oil and gas wells using:
    - SEDM
    - Duong's method
- Further development of the SEDM methodology to low and ultra-low permeability reservoirs, with especial emphasis on incorporating information obtained via simultaneous analysis of a large group of wells.
- Investigating the applicability of SEDM in handling the heterogeneity in shale gas and oil reservoirs.
- Investigating the compatibility of SEDM with DFN concept and applicability of DFN model for horizontal wells in Barnett Shale.
- Developing systematic methods to quantify proved (1P), probable (2P), and possible (3P) reserves based on forecasts using the SEDM model.

2. STRETCHED-EXPONENTIAL DECLINE MODEL (SEDM)

2.1. Stretched Exponential (SE) Function

The concept of applying stretched-exponential model in decline curve analysis was introduced by Valko (2009) as a performance prediction tool with an innate physical basis. This model is based on Johnston's (2006) investigation on SE decay properties and their physical meaning which was first described by Kohlrausch (1847). Stretched exponential decay behavior has been observed for decaying processes of many physical quantities in nature, and also in economy, in different systems and research areas (Laherrere and Sornette, 2008).

For any relaxing quantity like q, stretched exponential decaying function can describe the time, t, dependence of q according to Equation 2.1 (Valko, 2009).

$$q = q_0 \, exp\left[-\left(\frac{t}{\tau}\right)^n\right], \quad (2.1)$$

where q_o=q(t=0), τ is a characteristic relaxation rate, and the stretching exponent, n, is in the range 0<n<1. Figure 2.1 shows log-linear and linear-log plots of the normalized stretched exponential function, q/q_0, versus normalized time, t/τ. Figure 2.1 shows that all of the plots corresponding to different n values cross at a time $t=\tau$ at which the normalized stretched exponential function has the value of e^{-1} for all n values. Also stretched exponential function with n=1 corresponds to the pure exponential decay and in Figure 2.1 (a) it plots as a straight line. For small times and for $t/\tau \ll 1$ a Taylor series expansion of Eq. 2.1 yields to:

$$\frac{n}{n_0}(t \to 0) \approx 1 - \left(\frac{t}{\tau}\right)^n, \quad \text{.....(2.2)}$$

Eq. 2.2 clarifies that stretched exponential function for 0<n<1 is singular with an infinitely negative slope at t=0.

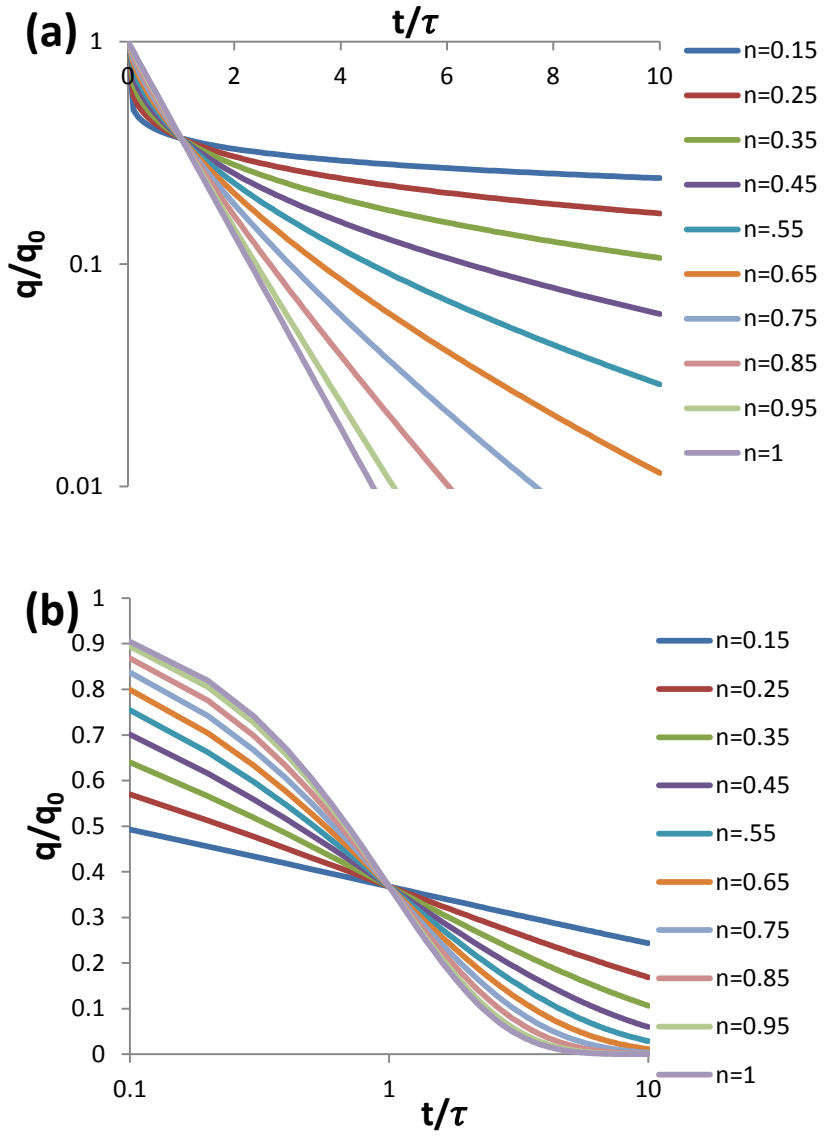

Figure 2.1—Log-linear (a) and linear-log (b) plots of the normalized stretched exponential function in Equation 2.1 *vs.* normalized time.

An important interpretation of stretched exponential relaxation concept is the global relaxation of a system containing many independently relaxing species, each of which decays exponentially in time with a specific fixed relaxation rate of τ' in the form of $e^{-(\frac{t}{\tau'})}$. Using this interpretation stretched exponential function can be explained as a sum of pure exponential decays, with a specific probability distribution P of τ' values for a given value of n. For such systems the Eq. 2.1 can be written as:

$$e^{-(\frac{t}{\tau})^n} = \int_0^\infty P(s,n)\exp\left[-\left(\frac{s}{\tau}\right)t\right]ds, \quad \text{.....(2.3)}$$

Where s=$\frac{\tau}{\tau'}$.

Because $P(s,n)$ is a probability density function it is clear that $\int_0^\infty P(s,n)\,ds = 1$. From Eq. 2.3 the SE decay function can be understood as a Laplace transform of a probability distribution function, with non-negative values. In other words for any values of n, this probability distribution function is the inverse Laplace transform of the stretched exponential and can be written as (Johnston, 2006):

$$P(s,n) = \frac{1}{\pi}\sum_{k=1}^{\infty}\frac{(-1)^{k+1}\Gamma(kn+1)}{k!s^{kn+1}}\mathrm{Sin}(k\pi n), \quad \text{.....(2.4)}$$

where Γ is the gamma function. Using Mathematica 8.0 probability density, P(s,n), was obtained for several rational values of n and the results are plotted in Figure 2.2.

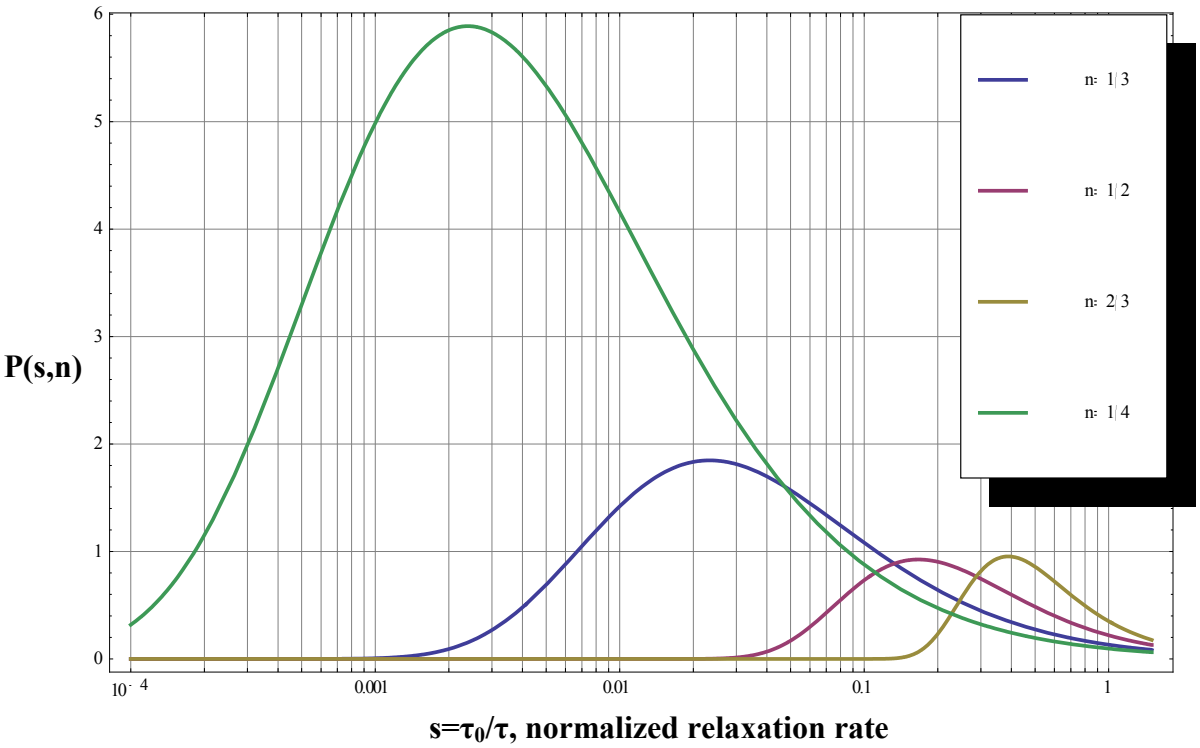

Figure 2.2—Plots of the probability density, P(s,n), for the relaxation rate in *Eq. 2.1* versus normalized relaxation rate s for several rational values of n.

2.2. Stretched Exponential Characteristics

2.2.1. SE As a Sum of Independent Exponentials

As it was mentioned previously, stretched exponential concept comes up from the global decay of a system containing independent exponentially decaying components. In this section this concept will be further investigated for three different n values of 0.25, 0.33, and 0.5. Figure 2.3 shows 21 different τ values and their corresponding probabilities that have been calculated from Eq. 2.4.

s	τ	P(s,0.25)
0.0001	7760	0.465675
0.0002	4363.769	1.275136
0.0003	2453.927	2.61361
0.0006	1379.945	4.214101
0.0010	776	5.569262
0.0018	436.3769	6.241462
0.0032	245.3927	6.100815
0.0056	137.9945	5.323625
0.0100	77.6	4.227687
0.0178	43.63769	3.10446
0.0316	24.53927	2.135864
0.0562	13.79945	1.391854
0.1000	7.76	0.866879
0.1778	4.363769	0.519883
0.3162	2.453927	0.302076
0.5623	1.379945	0.170928
1.0000	0.776	0.094589
1.7783	0.436377	0.051373
3.1623	0.245393	0.027464
5.6234	0.137994	0.014488
10.0000	0.0776	0.007557

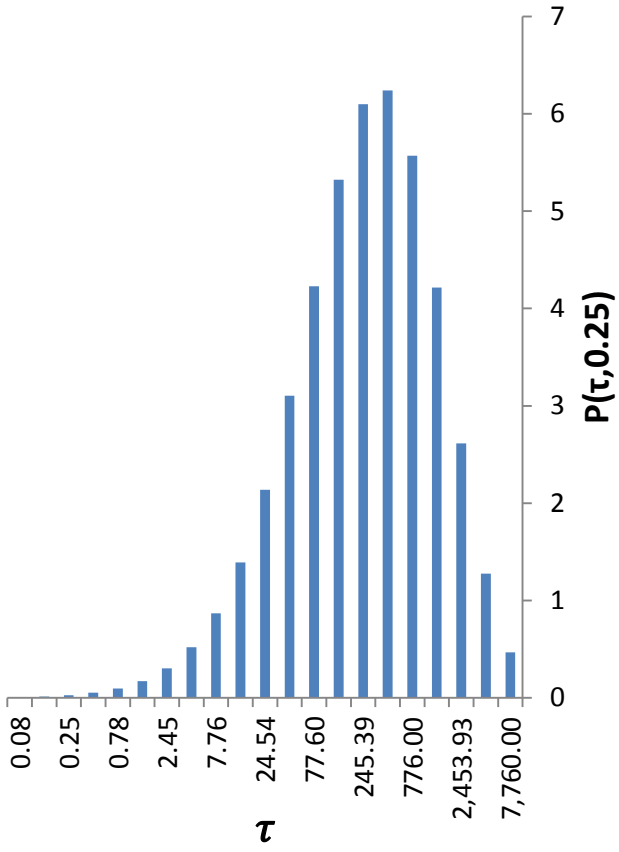

Figure 2.3—Probability distribution function for n=0.25 and different τ values.

Using these characteristic time constants and their corresponding probabilities the SE decay for n=0.25 and τ=0.776, which are the corresponding SE pair for Barnett Shale reservoirs, can be written as a sum of independently decaying exponential components. Figure 2.4 shows how only 19 independent exponentials with different relaxation constants have been used to explain a SE function for the case of n=0.25 and τ=0.776.

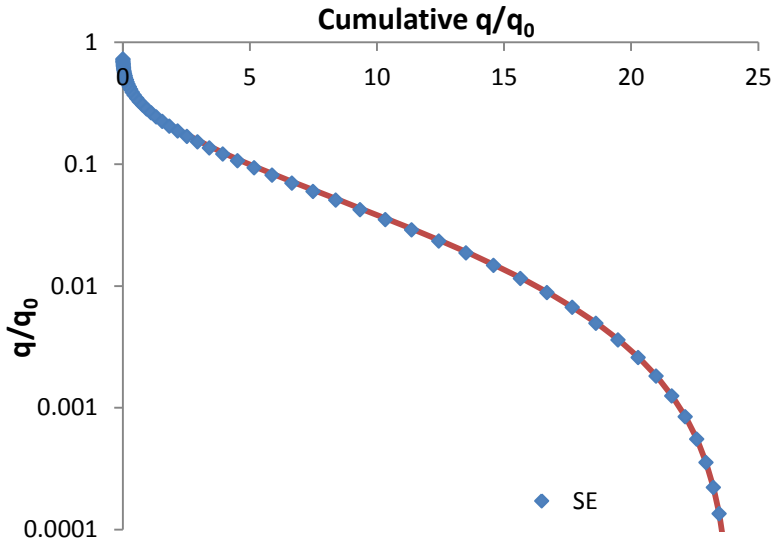

Figure 2.4—SE function as a sum of 19 independent exponentials for n=0.25 and τ=0.776 months.

For n=0.33 and n=0.5 and results are shown in Figure 2.5 and Figure 2.6.

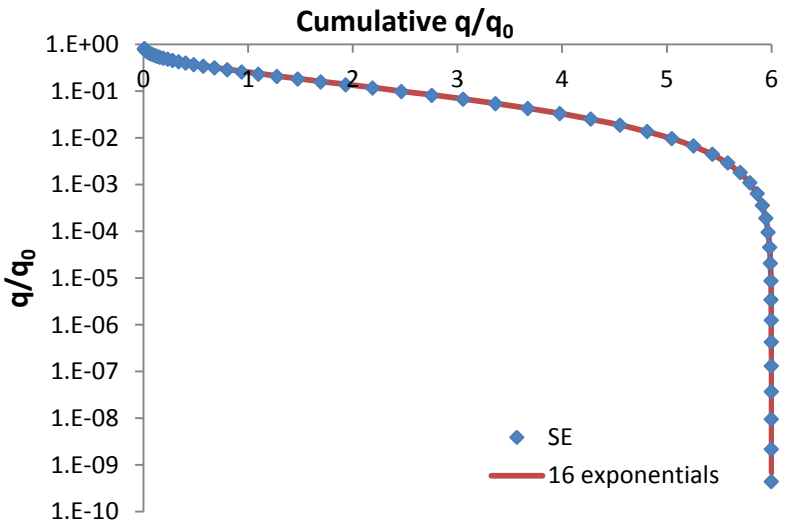

Figure 2.5—SE function as a sum of 16 independent exponentials for n=0.33 and τ=0.776 months.

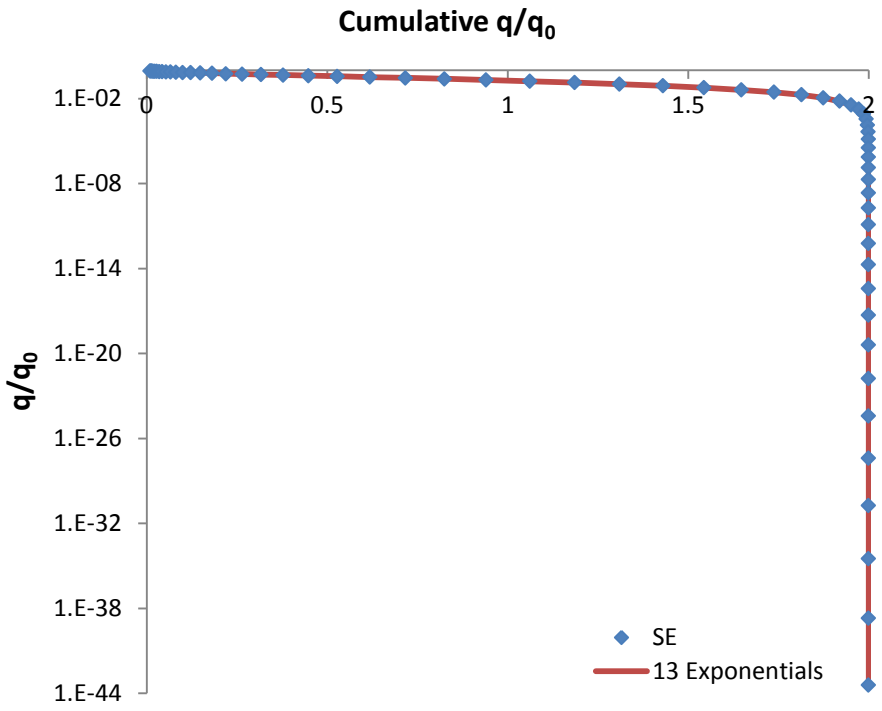

Figure 2.6—SE function as a sum of 13 independent exponentials for n=0.5 and τ=0.776 months.

2.2.2. "Inflection Point"

For Arp's hyperbolic model the decline is always concave with $0 < b < 1$ on the *log (q) vs.* cumulative plot and gives finite area under the curve. However, for harmonic and super-harmonic declines where b=1 and $b > 1$ (as for tight gas reservoirs) the decline is always convex. This decline model (convex) physically cannot be sustained forever and there will be infinite area under q(t) curve (Figure 2.7 and Figure 2.8). This is why in classical decline analysis harmonic decline was considered the extreme. Also this difference between concave and convex behavior for b<1 and b>1 is only detectable on *log (q) vs.* cumulative plot and it does not show up on other common plots in DCA like q *vs.* t or G_p *vs.* t.

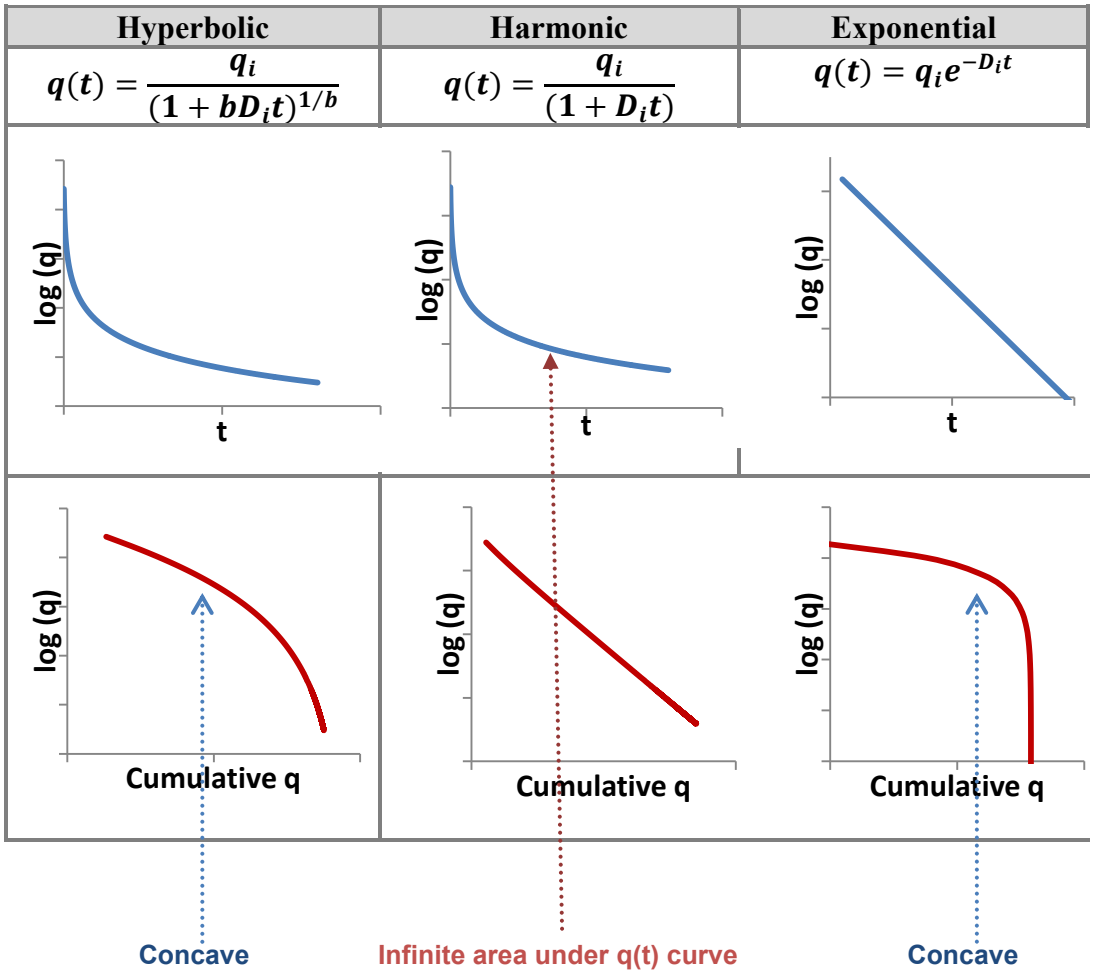

Figure 2.7—Classical Arp's models

One of the big advantages of SEDM is that it puts together the concave and convex portions. In the SEDM "Inflection Point" is where convex turns into concave in *log (q) vs.* cumulative plot and it has the maximum slope. The SE model always has an inflection point and as it is illustrated in Figure 2.8.

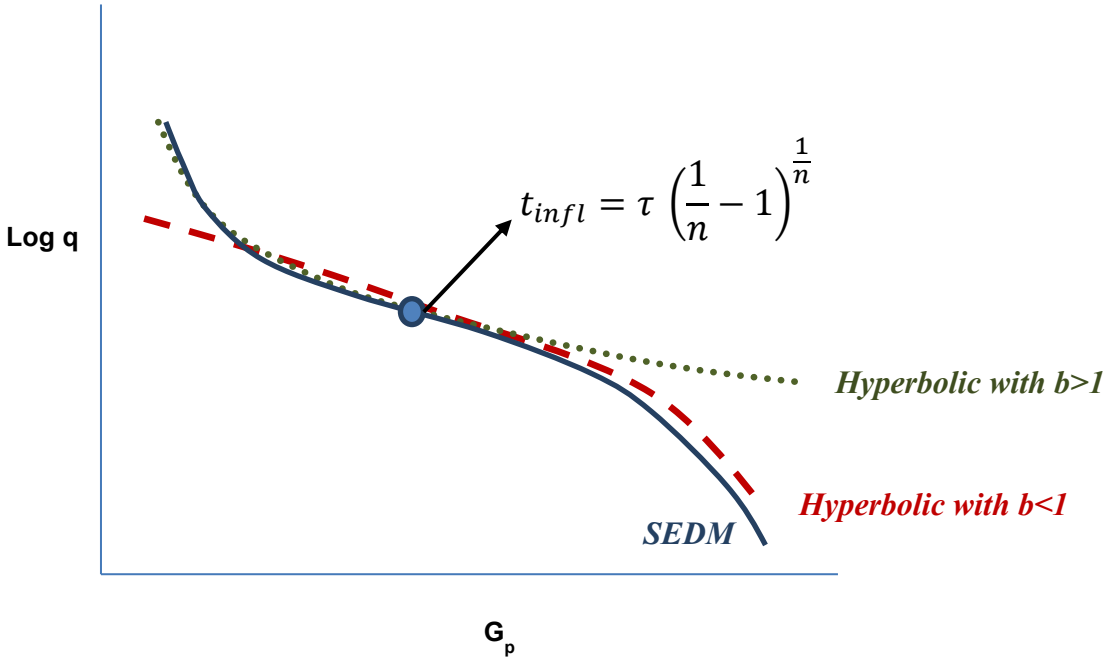

Figure 2.8—Inflection point in SEDM

The concave portion is necessary for finite contacted gas in place but the convex part is often dominant within the first several years of these shale data series.

To obtain the inflection time first we calculate the slope of the plot in Figure 2.8:

$$\text{Slope} = \frac{d\log[q]}{d\,Gp} = \frac{d\log[q(t)]/dt}{q(t)}, \quad \text{.....(2.5)}$$

Putting q from **Eq. 2.1** to **Eq. 2.5** we get:

$$\text{Slope} = -\frac{e^{\left(\frac{t}{\tau}\right)^n} n\left(\frac{t}{\tau}\right)^n}{q_0 t}, \quad \text{.....(2.6)}$$

Now, if we take the derivative of the slope with respect to time we have:

$$\frac{d(\text{Slope})}{\text{dt}} = \frac{e^{\left(\frac{t}{\tau}\right)^n} n\left(\frac{t}{\tau}\right)^n}{q_0 t^2} - \frac{e^{\left(\frac{t}{\tau}\right)^n} n^2\left(\frac{t}{\tau}\right)^{-1+n}}{q_0 t\tau} - \frac{e^{\left(\frac{t}{\tau}\right)^n} n^2\left(\frac{t}{\tau}\right)^{-1+2n}}{q_0 t\tau}, \quad \text{.....(2.7)}$$

By setting **Eq. 2.7** to zero and solve it for t we obtain t_{infl}, which is the inflection time where convex character changes to concave in SEDM model:

$$t_{infl} = \tau\left(\frac{1}{n} - 1\right)^{\frac{1}{n}}, \quad \text{.....(2.8)}$$

Using **Eq. 2.8** two limits for t_{infl} can be obtained. As n approaches 1(exponential decline), the inflection point approaches to zero. The other end is when n approaches to zero and in this case inflection point moves toward infinity.

2.2.3. Finite Value of EUR

Integrating Eq.2.1 the cumulative production is obtained as:

$$G_p = q_0 \frac{\tau}{n}\left\{\Gamma\left[\frac{1}{n}\right] - \Gamma\left[\frac{1}{n}, \left(\frac{t}{\tau}\right)^n\right]\right\}, \quad \text{.....(2.9)}$$

$\Gamma(a,x)$ is the incomplete gamma function, which needs two variables (Abramowitz and Stegun, 1972). For positive n, τ and q_0, SEDM gives a finite (bounded) value of the EUR, with no need of any cutoffs in time or in rate. In contrast, the Arps family of curves leads to an unbounded and non-physical estimation of EUR for $b \geq 1$. Ilk at al. (2008) added an additional parameter to the model (called infinite time decline, D_{inf}). Seshadri and Mattar (2010) later found that Ilk's 4-parameter model leads to difficulties due to ill-conditioning in the parameter estimation process (non-uniqueness).

2.2.4. SE Model in Handling the Reservoir Heterogeneity

Perhaps one the most important characteristic of SE is that the relaxation of a system based on SE is equivalent to relaxation of a similar system containing many components that each decay independently under a specific relaxation rate. For petroleum engineering applications, Valko and Lee (2010) suggested that this characteristic of the SE model can be interpreted as the consequence of reservoir heterogeneity in reservoir performance and production forecast applications. Later, Kabir et al. (2011, SPE144311) has developed a semi-analytical approach, using the capacitance-resistance modeling (CRM) concept, to estimate production profile and EUR for unconventional reservoirs which incorporates this concept of heterogeneity. In their formulation, a number of arbitrary reservoir Segments were considered, each making variable contributions to production in a specific well. These contributions are analogues to the probability distribution of the decay rates investigated by Johnston for many exponential decays and decrease with increasing the distance from each segment to the stimulated reservoir volume (SRV). They applied their formulation on the synthetic and field data and compared their results with the SEDM and found that CRM supports the solution obtained from SEDM.

In this section to investigate the capability of SEDM model in handling heterogeneity in unconventional reservoir a series of reservoir simulations have been performed using PETREL 2010 as the simulation tool.

2.2.4.1. Case-1

In this simple simulation case the aim was to investigate the applicability of SEDM model with the production from a horizontal well in a low permeability matrix and through a set of induced hydraulic fractures. A 2000ft lateral in a 2000 by 1000 ft. flow region has been considered. It was assumed that the matrix permeability was 0.001 md *vs.* Hydraulic fracture permeability of 10,000 md. Figure 2.9 illustrates the gridding and structure of the wellbore and hydraulic fractures for this simulation case.

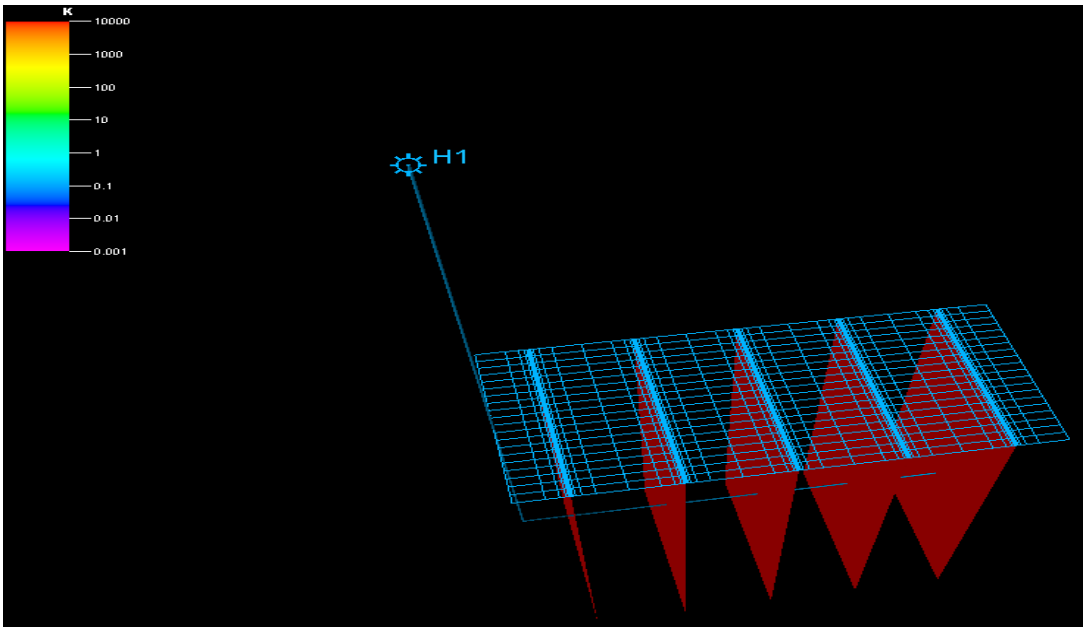

Figure 2.9—Grid and skeleton including the 2000 ft. lateral (H1) and a set of 5 hydraulic fractures for case-1 simulation.

Dry gas was produced from this reservoir and Figure 2.10 shows the pressure change in the reservoir after 40 years of production.

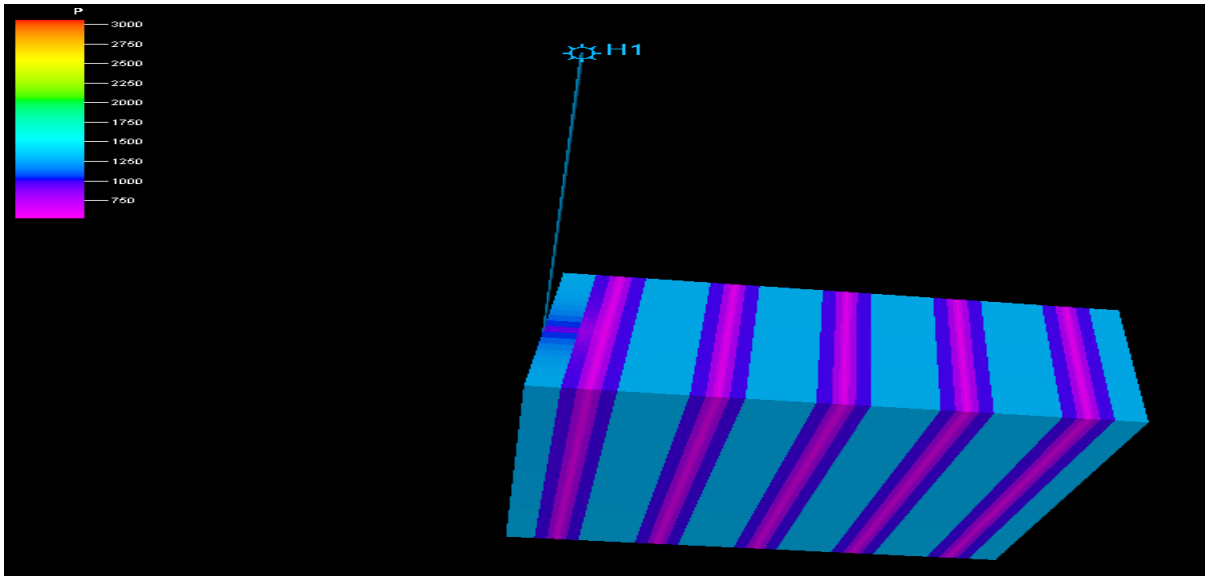

Figure 2.10—Pressure plot for case-1 after 40 years of production and with 5 HF.

Using the production results from this simulation a log(q) *vs.* cumulative rate plot was constructed for this case (Figure 2.11). Using Excel-SOLVER a stretched exponential fit was found for this plot and the three SE parameters are shown on the Figure 2.11.

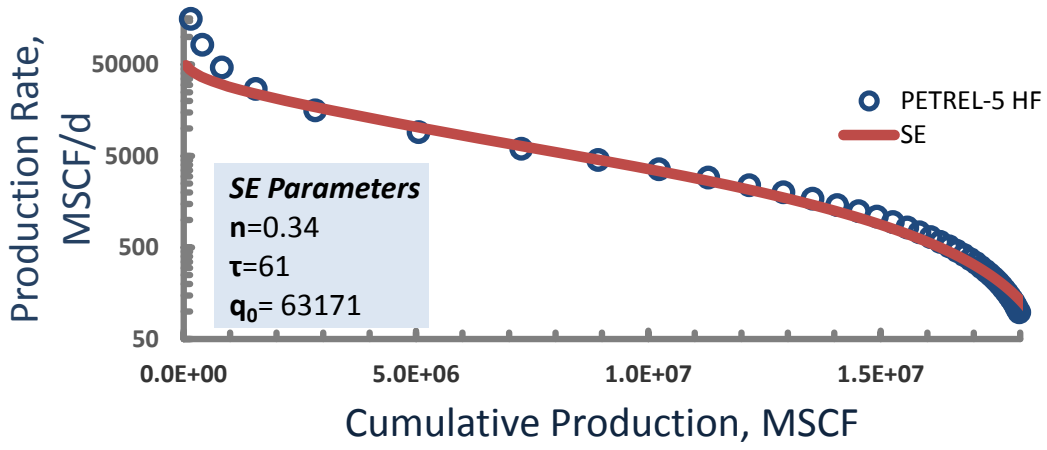

Figure 2.11—*log (q) vs.* cumulative for Case-1 and the estimated SEDM parameters with 5 HF.

For the same setting and without any hydraulic fracture and for 40 years of production the simulation resulted in estimated SEDM parameters as shown in Figure 2.12.

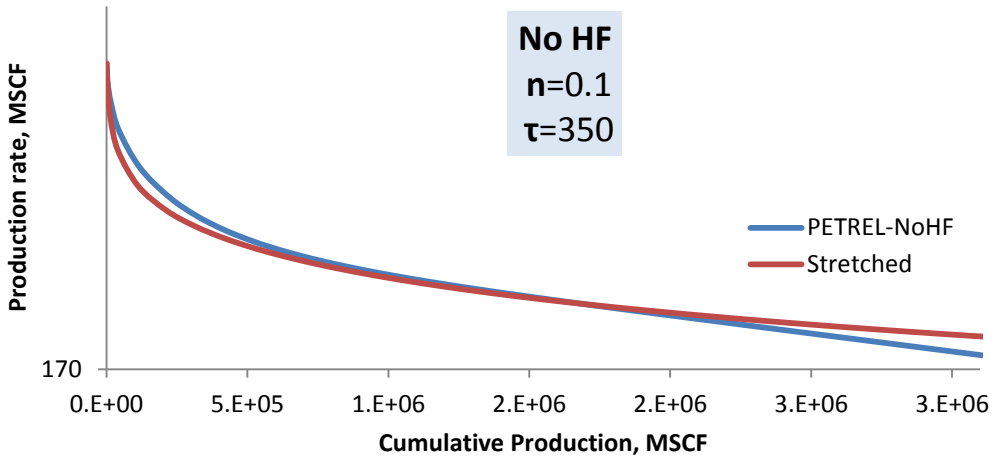

Figure 2.12—*log (q) vs.* cumulative for Case-1 and the estimated SEDM parameters with no HF.

Figure 2.13 shows how pressure changed in the reservoir after 40 years of production if there was no stimulation in the low permeability matrix.

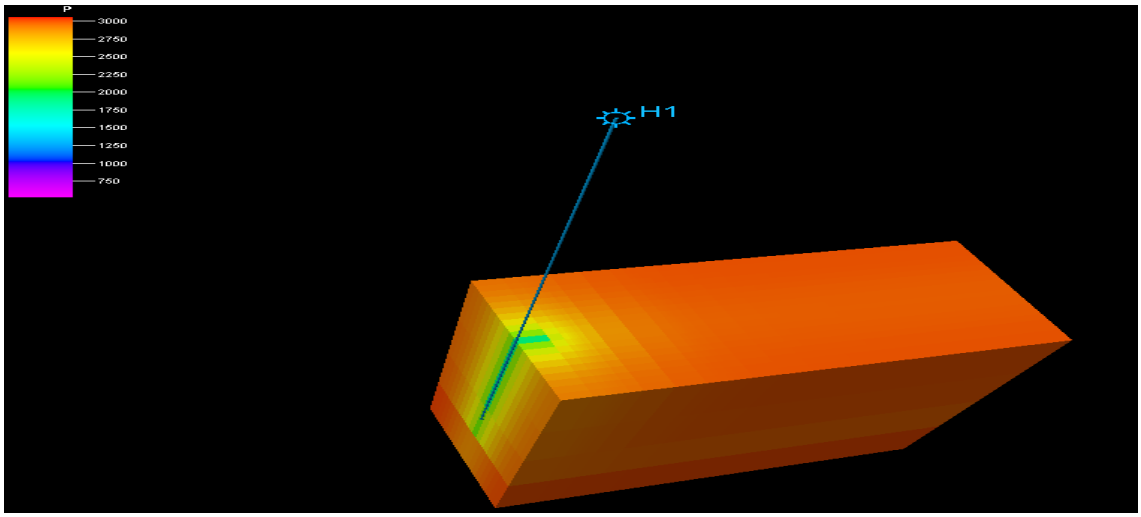

Figure 2.13—Pressure plot for case-1 after 40 years of production and with no HF.

Comparing Figure 2.11 and 2.12 it is clear that in a low permeability reservoir when production is only through the permeability of the matrix and there is no stimulation and consequently no network of fracture the production will be so low that even after 40 years of production it has not reached the inflection point.

2.2.4.2. Case-2

All parameters for this case are similar to Case-1 except the matrix permeability of 1 nd (0.000001 md) has been considered. Also two sets of natural fractures (5 of each) perpendicular to the hydraulic fractures with permeability of 0.1 and 0.01 md are assumed to be part of the fracture network in this reservoir. Figure 2.14 shows the network of fracture that was used for this simulation case.

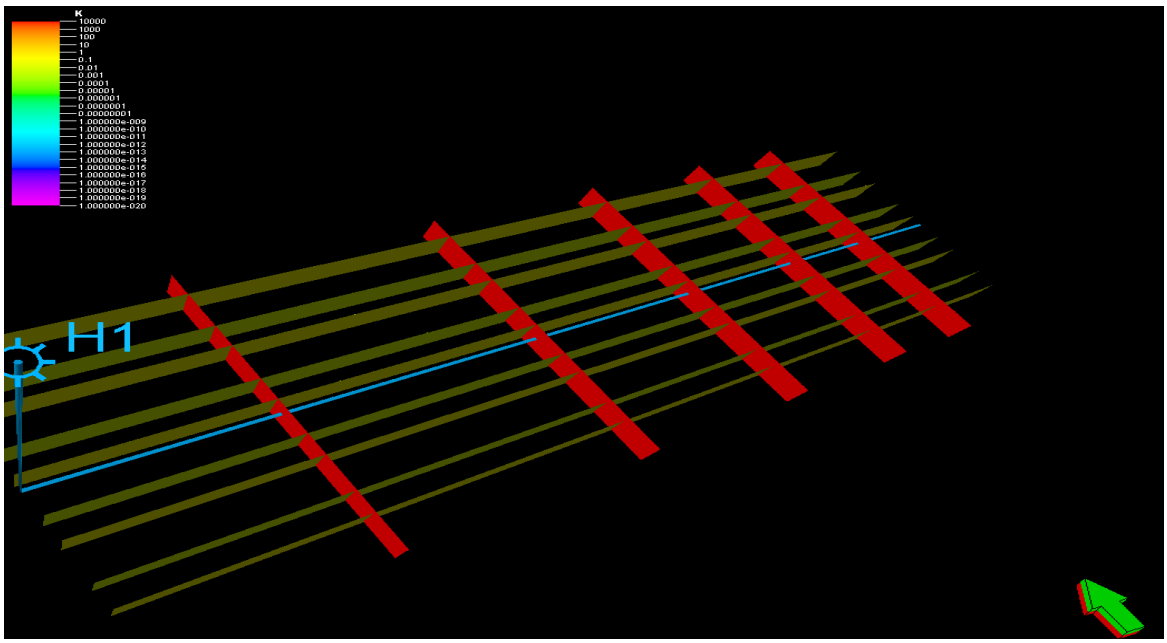

Figure 2.14—Network of fractures including the 2000 ft. lateral (H1) for case-2 simulation.

Figure 2.15 shows how pressure changed in the reservoir after 40 years of production. As it is clear from the pressure plot, because of the permeability contrast between the nano-darcy matrix and high permeability fracture network, most of the pressure drop is in the HF and natural fractures.

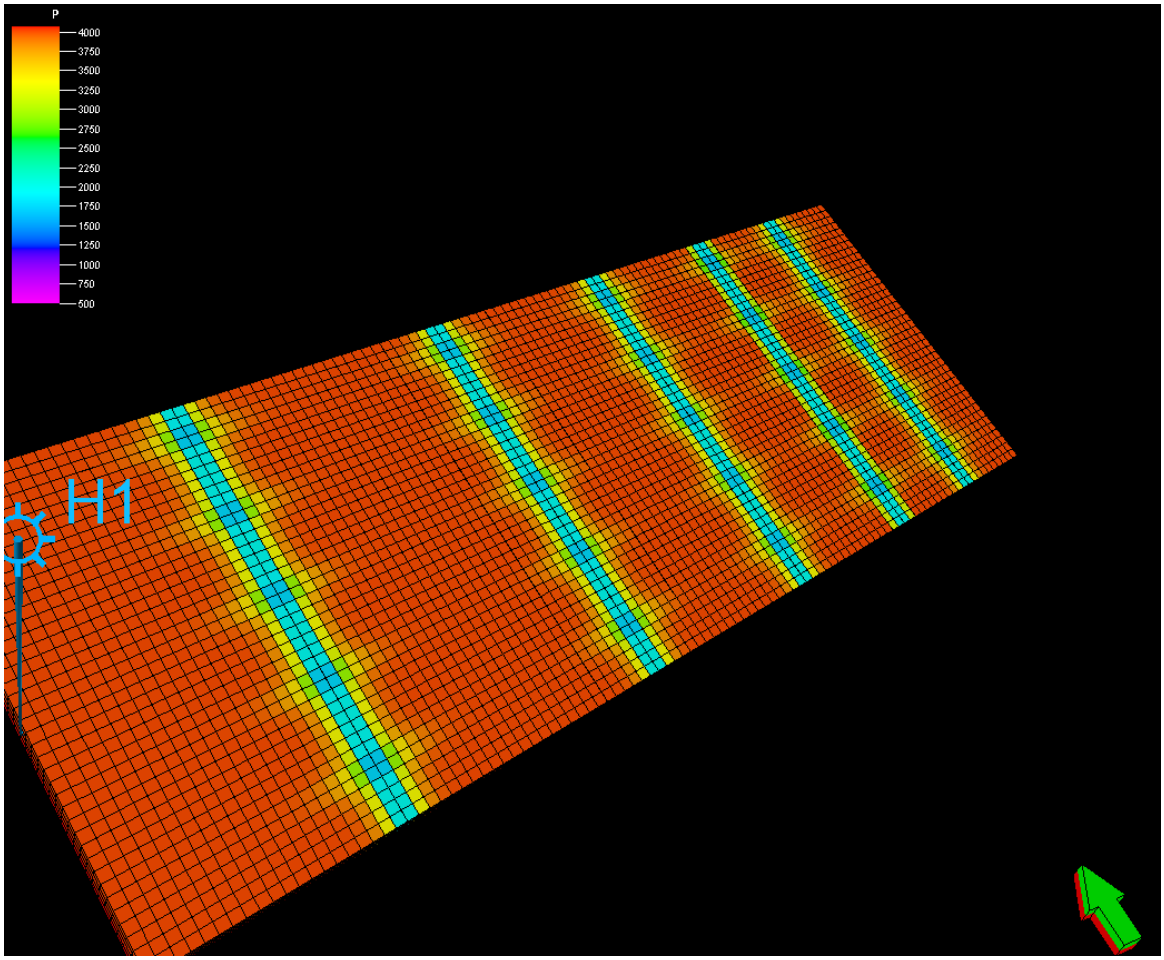

Figure 2.15—Pressure plot for case-2 after 40 years of production.

Figure 2.16 plots the *log (q) vs.* cumulative production after 40 years of production for case-2 simulation. SEDM and hyperbolic model has been fit to the curve.

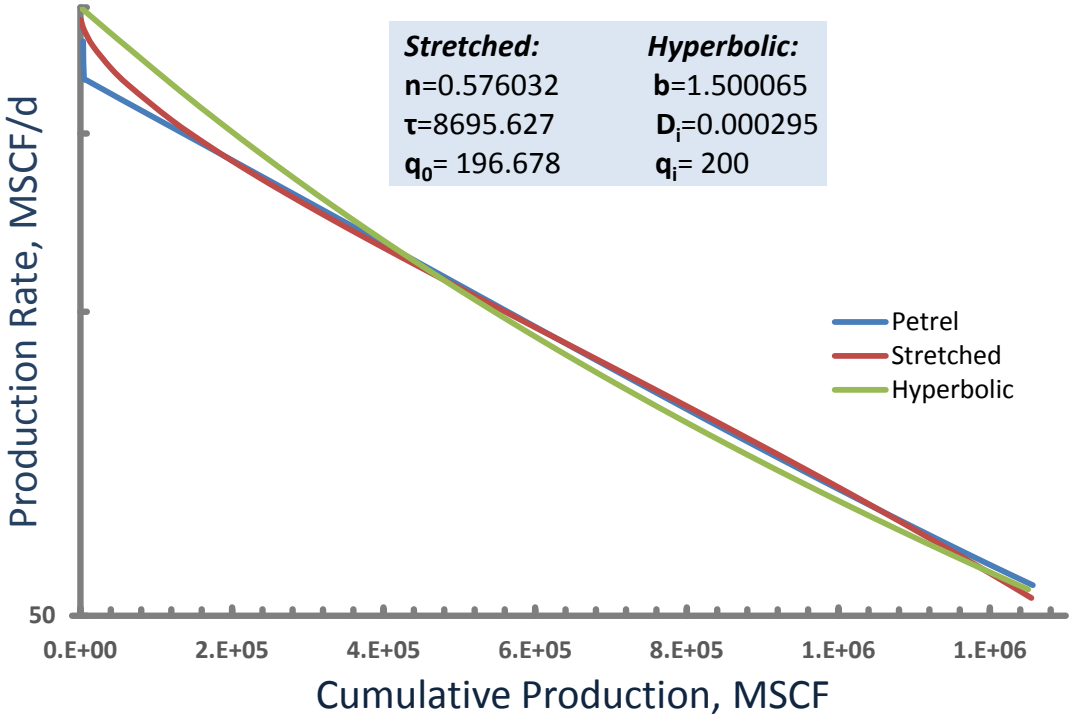

Figure 2.16—*log (q) vs.* cumulative for Case-2 and the estimated SEDM and Hyperbolic parameters.

To add more heterogeneity to the simulation case two separate cases with similar geometry and different permeability setting has been considered. The reservoir consisted of 5 segments with different sizes and there are no-flow boundaries (pink dashed lines in Figure 2.18 and 2.21) between them. Also in both cases a matrix porosity of 4% for all Segments has been assumed.

The fracture network for both cases consists of 5 hydraulic fractures with permeability of 10,000 md (red dashed lines in Figure 2.18 and 2.21) and also two sets of natural fractures (yellow and orange lines in figure 2.18 and 2.21) with permeability of 10 md and 0.1 md which are parallel to each other and perpendicular to the hydraulic fractures (figure 2.17).

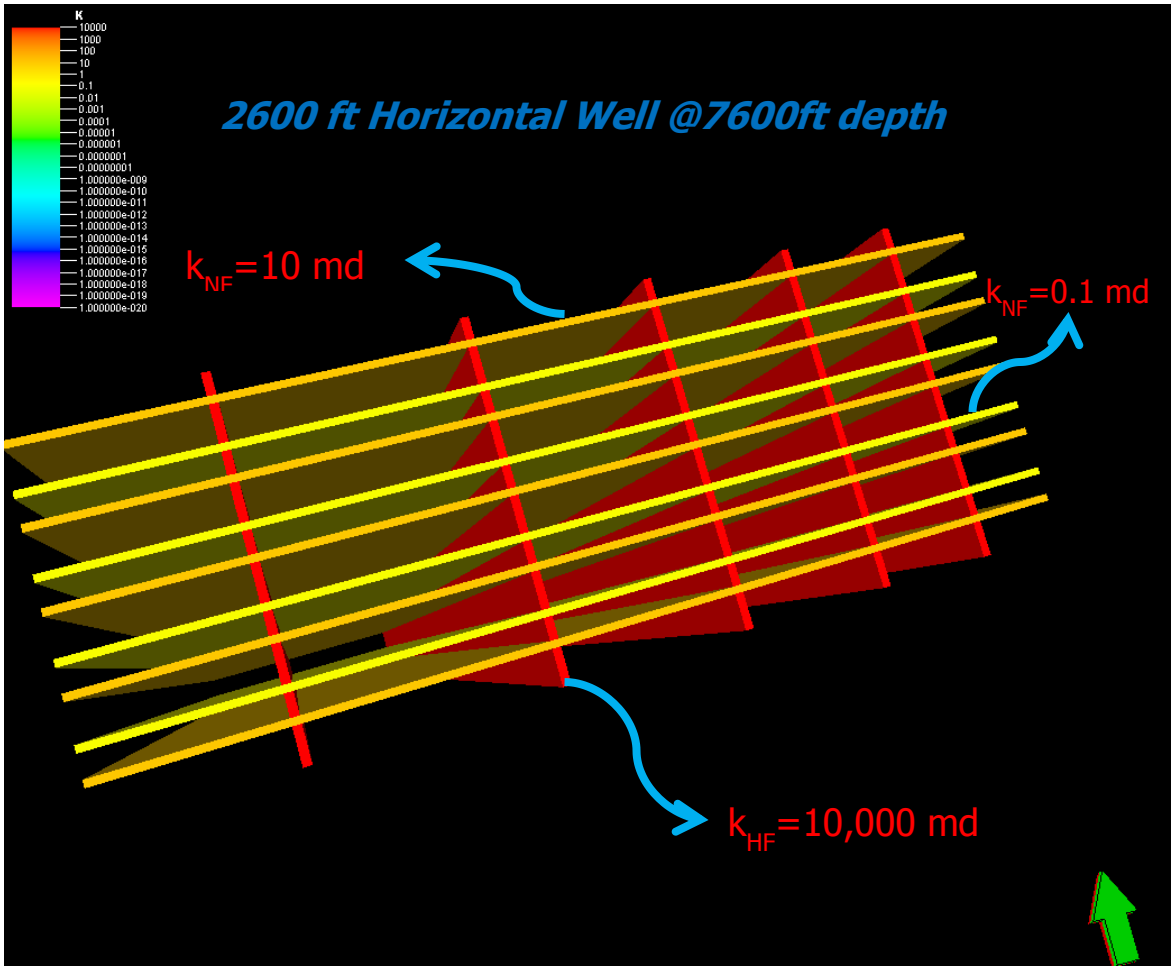

Figure 2.17—Network of fractures for case-3 and case-4 simulations.

2.2.4.3. Case-3

In this case, permeability of matrix decreases from the largest to the smallest segment as shown in Figure 2.18. The reservoir was 7600 ft. deep and dry gas was produced with a 2600 ft. long horizontal wellbore.

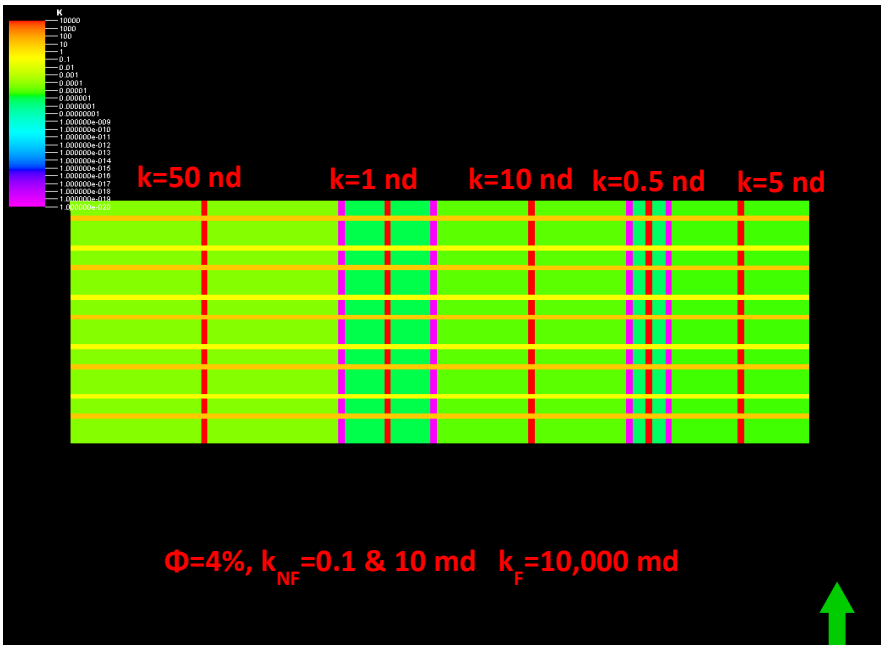

Figure 2.18—5 reservoir segments and their permeability for case-3 simulation.

After 40 years of production and under constant bottomhole pressure of 500psi the pressure in the reservoir changed as Figure 2.19.

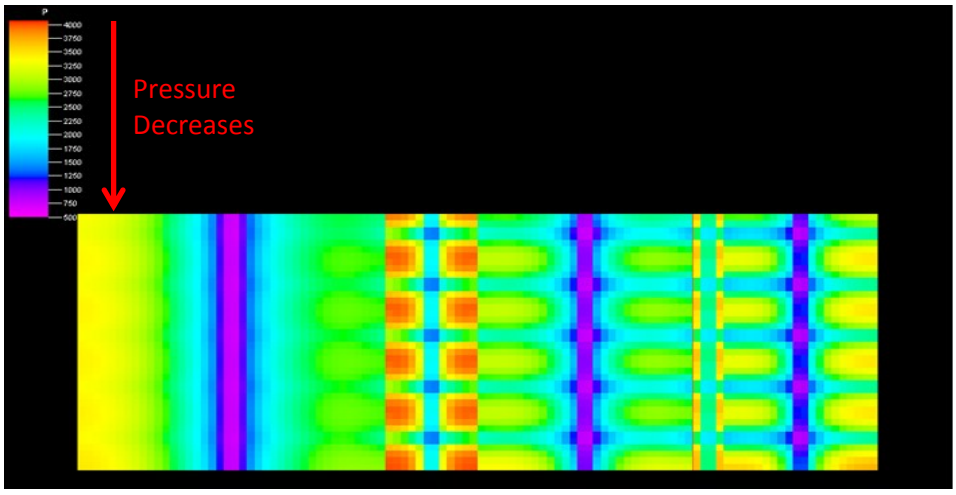

Figure 2.19—Pressure plot for case-3 after 40 years of production.

Figure 2.20 plots the *log (q) vs.* cumulative production after 40 years of production for case-3 simulation. SEDM and hyperbolic model has been fit to the curve and the estimated parameters for each model are shown in the plot. Hyperbolic parameter b for this simulation setting was estimated to be 1.9 which is in agreement with the b range in the literature for tight reservoirs like shale gas.

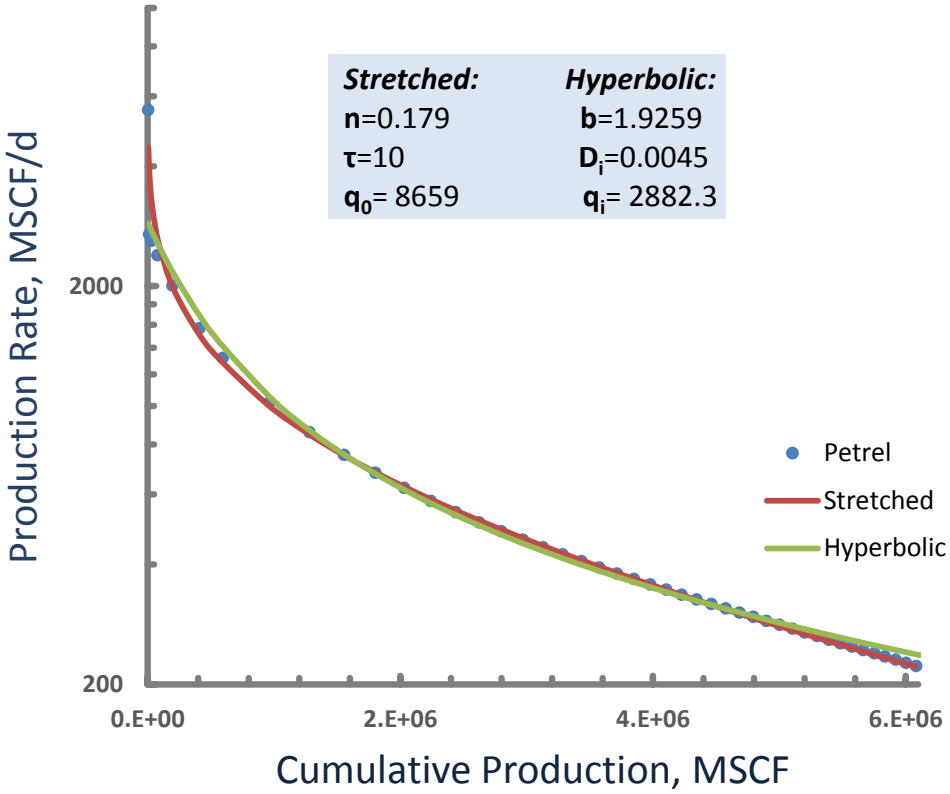

Figure 2.20—*log (q) vs.* cumulative for Case-3 and the estimated SEDM and Hyperbolic parameters.

2.2.4.4. Case-4

In this case, permeability of matrix increased from the largest to the smallest segment as shown in Figure 2.21. The reservoir was 7600 ft. deep and dry gas was produced with a 2600 ft. long horizontal wellbore.

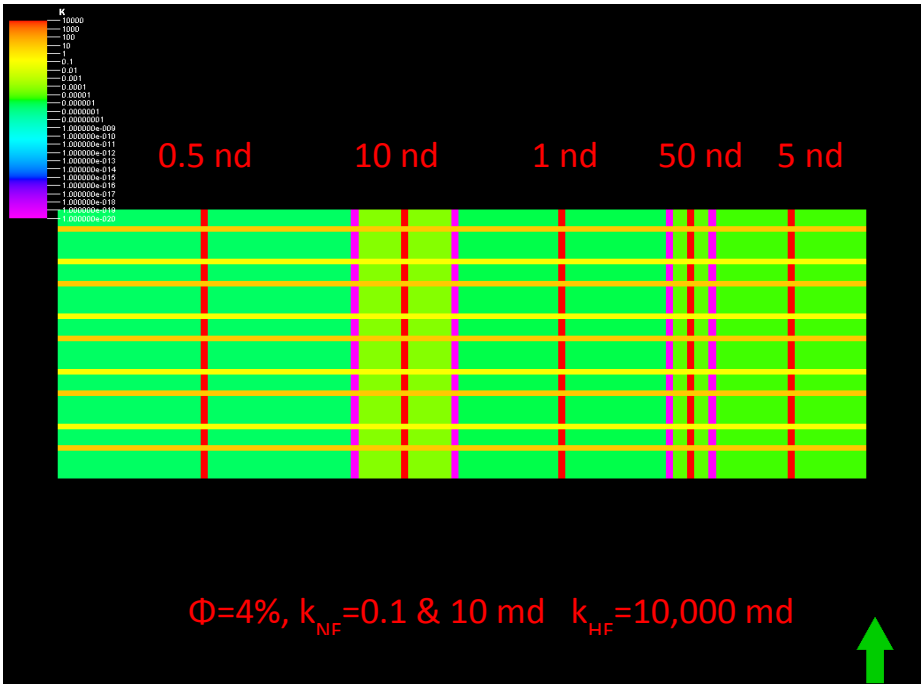

Figure 2.21—5 reservoir segments and their permeability for case-4 simulation.

After 40 years of production and under constant bottomhole pressure of 500psi the pressure in the reservoir changed as Figure 2.22.

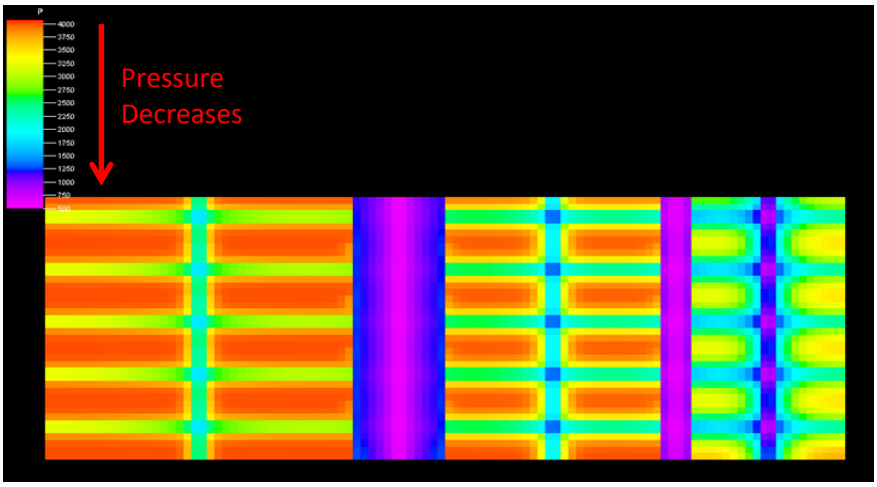

Figure 2.22—Pressure plot for case-4 after 40 years of production.

Figure 2.23 plots the *log (q) vs.* cumulative production after 40 years of production for case-4 simulation. SEDM and hyperbolic model has been fit to the curve and the estimated parameters for each model are shown in the plot. Hyperbolic parameter b for this simulation setting was estimated to be 1.4 which is in agreement with the b range in the literature for tight reservoirs like shale gas.

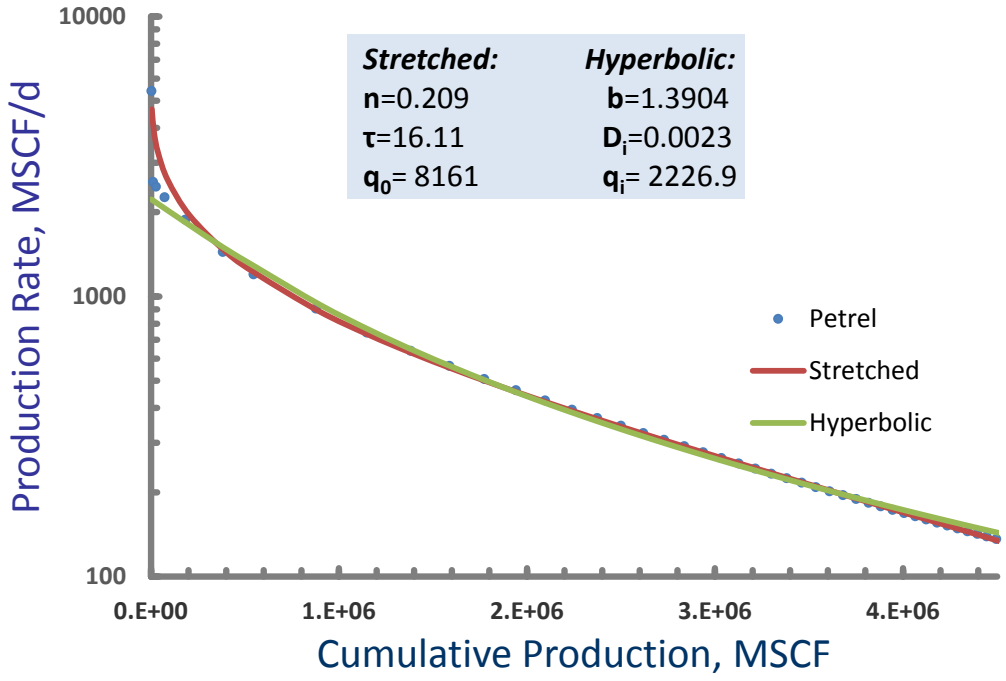

Figure 2.23—*log (q) vs.* cumulative for Case-4 and the estimated SEDM and Hyperbolic parameters.

In both cases the *log (q) vs.* cumulative plot shows that SEDM model yields a lower EUR compared to the hyperbolic model. For case-3 the SEDM and hyperbolic has been projected in Figure 2.24 to show how hyperbolic model can overestimate reserves and SEDM yields to a bounded and more conservative EUR.

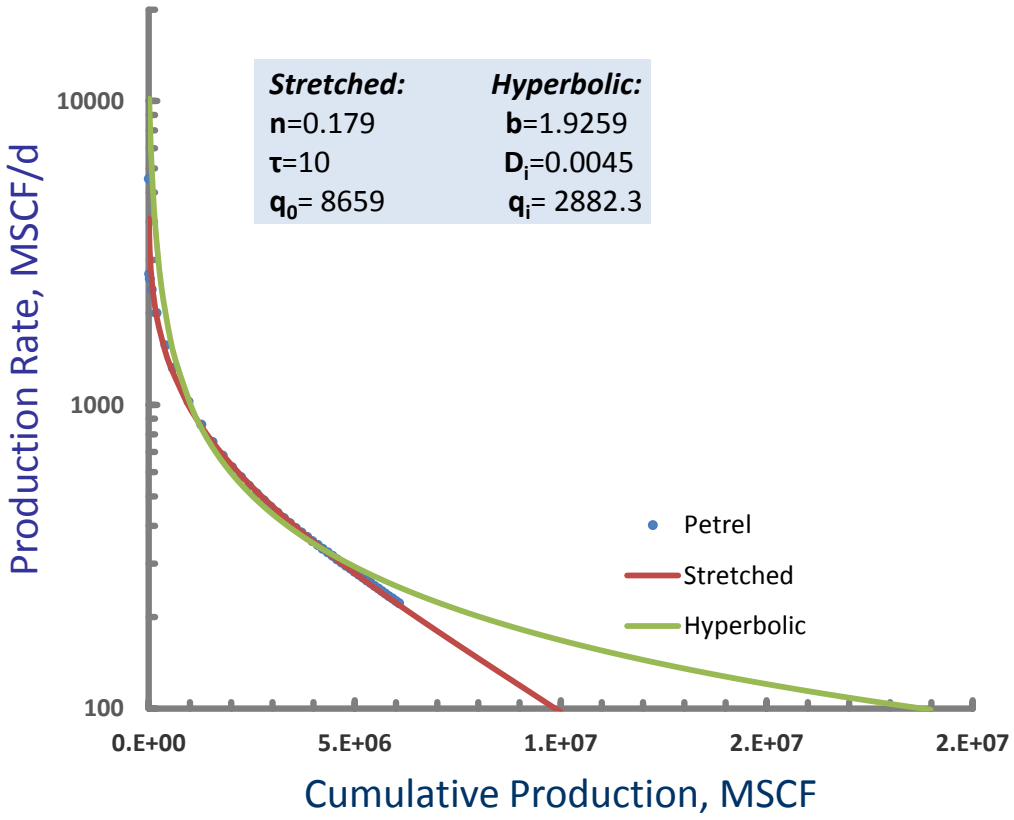

Figure 2.24—*log (q) vs.* cumulative for Case-3 and the projected SEDM and Hyperbolic.

Also Case-3 and Case-4 are better reservoir representative for the SEDM behavior compared to Case-2 and the reason could be more heterogeneity in the reservoir model. Indeed, including the reservoir segments in Case-3 and Case-4 is very similar to the concept of explaining the SE decay as a sum of independent exponentials where each reservoir segment can be similar to one of the independent exponentials. Inflection time of 9,400 days for Case-3 and 50,000 days for Case-4 have been estimated based on SEDM (Figure 2.25).

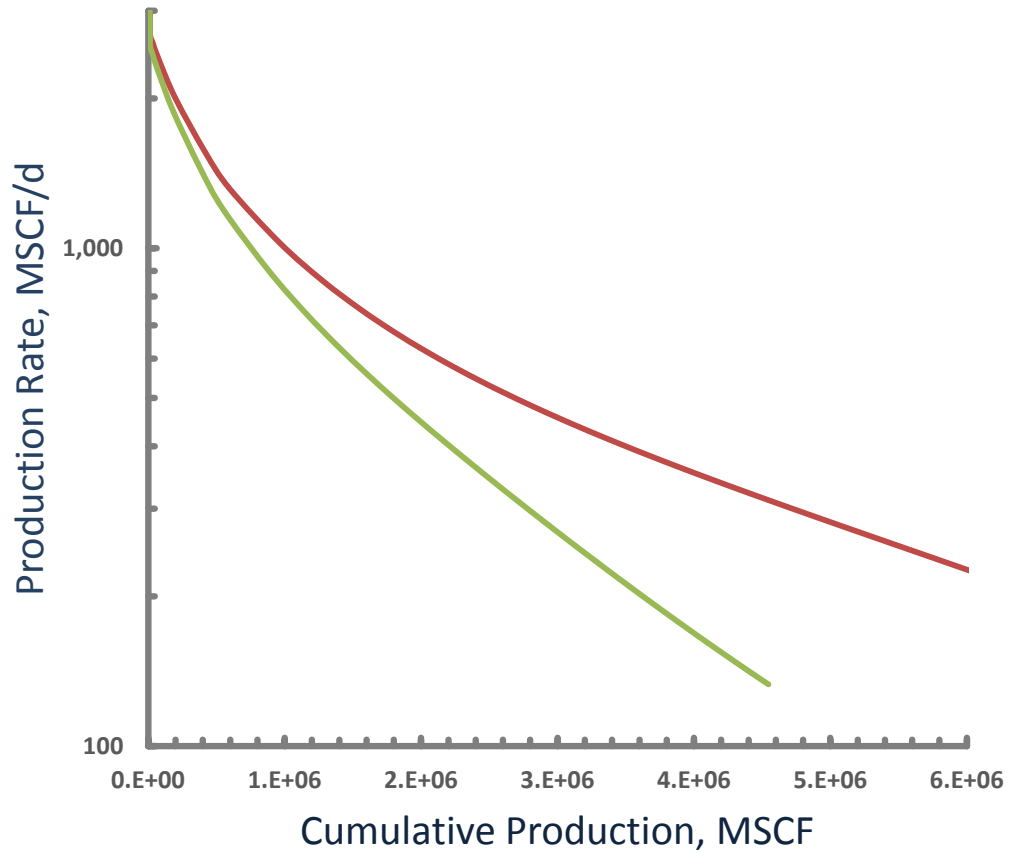

Figure 2.25—*log (q) vs.* cumulative for Case-3 (red) and case-4 (green) from simulation results.

2.2.4.5. Case-5

The only difference between this case and Case-4 is that the 5 reservoir sections are hydraulically communication with each other and there is no no-flow boundary. In this case, permeability of matrix increased from the largest to the smallest segment as shown in Figure 2.21. The reservoir was 7600 ft. deep and dry gas was produced with a 2600 ft. long horizontal wellbore. Figure 2.26 shows the pressure change in these 5 sections after 40 years of production and under constant bottomhole pressure of 500 psi.

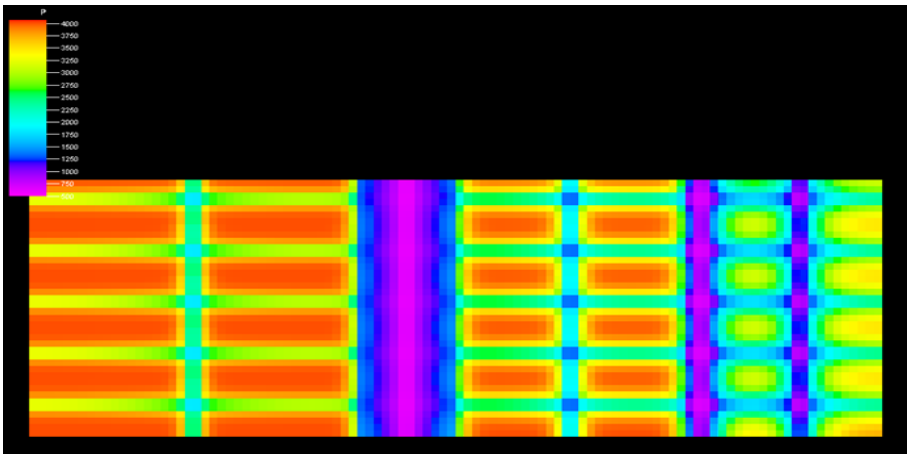

Figure 2.26—Pressure plot for case-5 after 40 years of production.

Figure 2.27 plots the *log (q) vs.* cumulative production after 40 years of production for case-5 simulation. Hyperbolic parameter b for this simulation setting was estimated to be 1.5 which is in agreement with the b range in the literature for tight reservoirs.

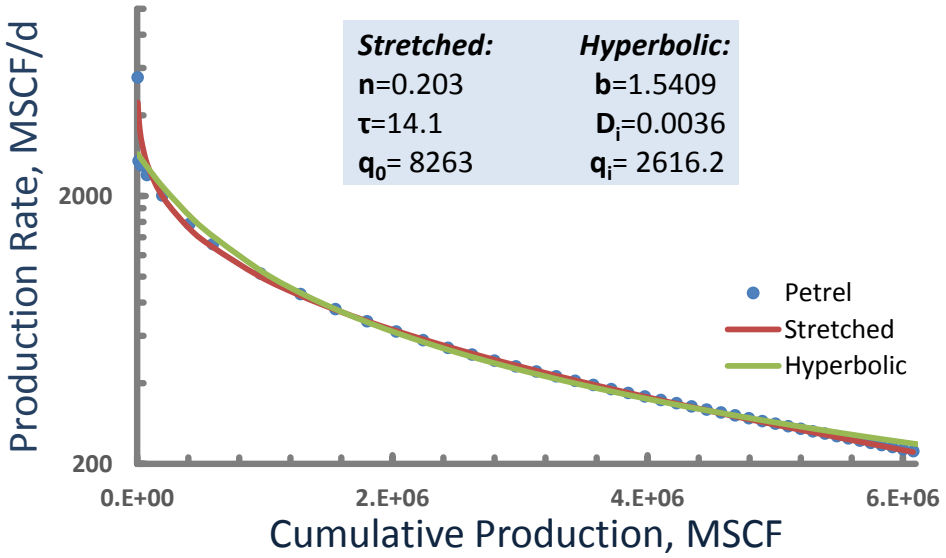

Figure 2.27—*log (q) vs.* cumulative for Case-5 and the estimated SEDM and Hyperbolic parameters.

In summary, SEDM is capable to describe the overall effect of various kinds of reservoir heterogeneity.

2.2.5. Monotonicity of SEDM

SEDM is completely monotonic for $0<n<1$. A monotonic function is the one whose successive values are increasing, decreasing or constant. It means that the order of function values maintain as independent variable changes. From the point of view of monotonic behavior, SEDM can be classified as "strictly decreasing" and in case of eq. 2.1 it means for a specific n and τ pair if $t_1<t_2$ then $q_1>q_2$.

A non-negative function f(t) , $t > 0$, is said to be completely monotonic if its derivatives satisfies $(-1)^n f^{(n)}(t)\geq 0$ for all t and n = 1,2, etc. (Miller and Samko, 2001). It also means that f is continuous on $[0, \infty)$ and infinitely differentiable on $(0, \infty)$. Also, Bernstein's Theorem (Alzer and Berg, 2006) states that f is completely monotonic if and only if $f(x) = \int_0^\infty e^{-xt}\, d\mu(t)$, where μ is a nonnegative measure on $[0,\infty)$ such that the integral converges for all $x > 0$.This is the necessary and also sufficient condition for the representation of the completely monotonic function (such as $\exp\left[-\left(\frac{t}{\tau}\right)^n\right]$ in eq. 2.1) as an infinite sum of exponentials with non-negative weights. While not particularly emphasized in the DCA literature, complete monotonicity should be a reasonable mathematical requirement for any specific empirical model of production decline.

For the Arps family the decline model is only completely monotonic for $b\geq 0$ and like SEDM it can be represented as a sum of non-negative exponentials (Brenstein theory). For $b>1$ however, the distribution of weights (in contrast to SEDM) goes to

infinity at zero time constant, indicating that the b>1 case is not possible to interpret as a result of individual exponential declines with physically meaningful exponents and weights.

3. COMPARISON OF TWO NOVEL DCA MODELS

The Stretched Exponential (SE) model, long used by applied physicists to model relaxation processes of various types, was introduced to the petroleum industry as an appropriate and reliable model for production rate decline in gas wells. SEDM gives considerably more stabilized production forecast than the Arps model (with or without minimum terminal decline), and it has been shown to produce unchanging EUR forecasts after only two-three years of production data are available in selected reservoirs, notably the Barnett Shale. Also, studies of synthetic and field data indicate that the model applies to both transient and stabilized flow data, with much of the model verification based on the Barnett Shale.

One important aspect of Arps' original concept of DCA is associated with the "individual decline behavior" recognizable from one well's data. Indeed, most publications focus on analysis of individual production data and show such illustrations of concepts. The big question however is, whether one well's production data contains all the necessary information to extrapolate future behavior or some of the extrapolation should be "conditioned" on information gleaned from analysis of the field (group data). If field information is used, the question is in what form?

In the Barnett Shale the large number of wells –though with short history of production – already allowed for some version of this conditioning process. In fields with lower number of wells the method has to be worked out. Probably the answer will also depend on the quality and time span of the individual data series to be analyzed.

It is now timely and appropriate to determine applicability of the model to a wider variety of shale and other tight reservoirs, including those that produce wet gas or that produce liquid hydrocarbons. Although there is no reason in principle that the model should not be appropriate, testing with actual field data will be required to determine the validity of the model in broader applications.

In this section, two empirical methods of SEDM and Duong's method have been applied to estimate reserves on 25 horizontal Barnett Shale gas wells (Figure 3.1). SEDM concepts and characteristics were discussed in previous section and Duong's method is explained in the next section.

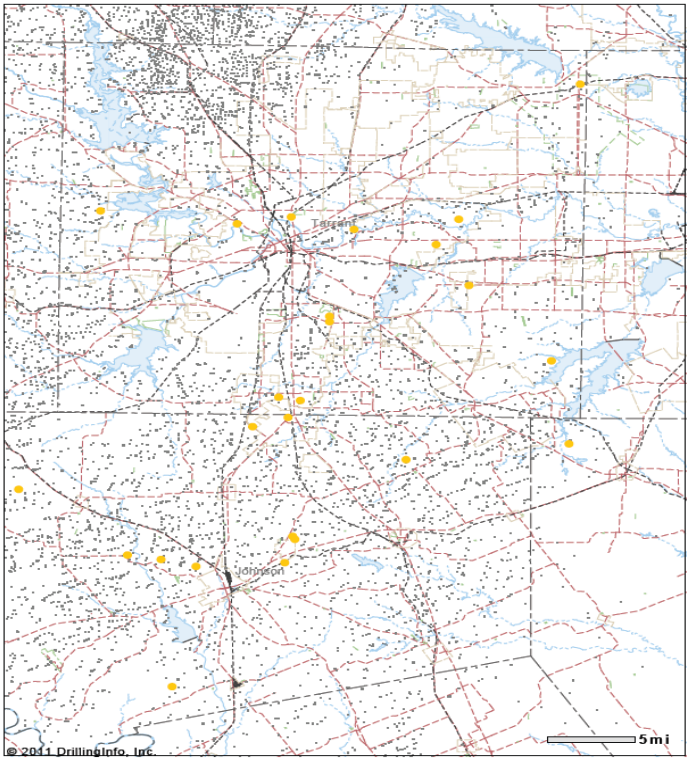

Figure 3.1—25 horizontal Barnett Shale gas wells located in Tarrant and Johnson Counties.

3.1. Duong's Model

Duong (2011) proposed an alternative approach for traditional decline methods such as Arp's rate/time relations for wells producing from tight gas reservoirs in which fracture flow is dominant. In his method for fracture flows at a constant bottomhole pressure, a log-log plot of rate over cumulative production *vs.* time will yield a straight line with a unit slope regardless of whether the flow is bilinear or linear type. In practice however, a slope of greater than one is normally observed because of "non-idealities", field operations and flow regime changes.

Duong's basic equations for q_D and G_p are:

$$\frac{q_D}{q_1} = t^{-m} e^{\frac{a}{1-m}(t^{1-m}-1)}, \quad (3.1)$$

$$G_p = \frac{q_1}{a} e^{\frac{a}{1-m}(t^{1-m}-1)}, \quad (3.2)$$

To better clarify the Duong's procedure for reserve estimations, one of the 25 wells in Barnett Shale will be discussed as an example. Figure 3.2 shows gas production for this horizontal well.

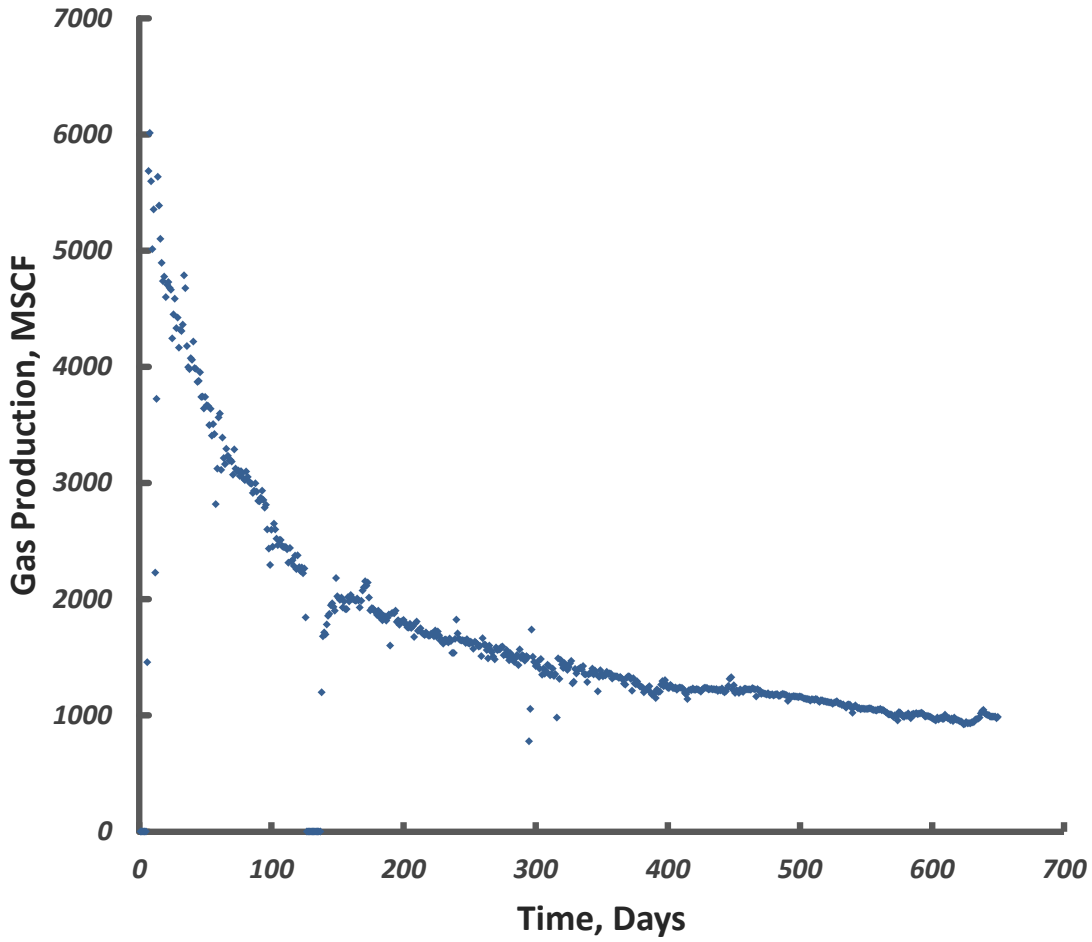

Figure 3.2—Gas production for a horizontal gas well in Barnett Shale

The very first step is to check the data and do any correction required. It can include deleting all zero rates and also all outlier points that exist in the production history.

Next a log-log plot of q_D/G_p *vs.* time in days (Figure 3.3) will be constructed to determine ***a*** and ***m*** values which are slope and intercept defined by Eq. 3.1. The R^2 value can be used to determine the best fit of the data. An R^2 value of more than 0.95 is recommended by Duong.

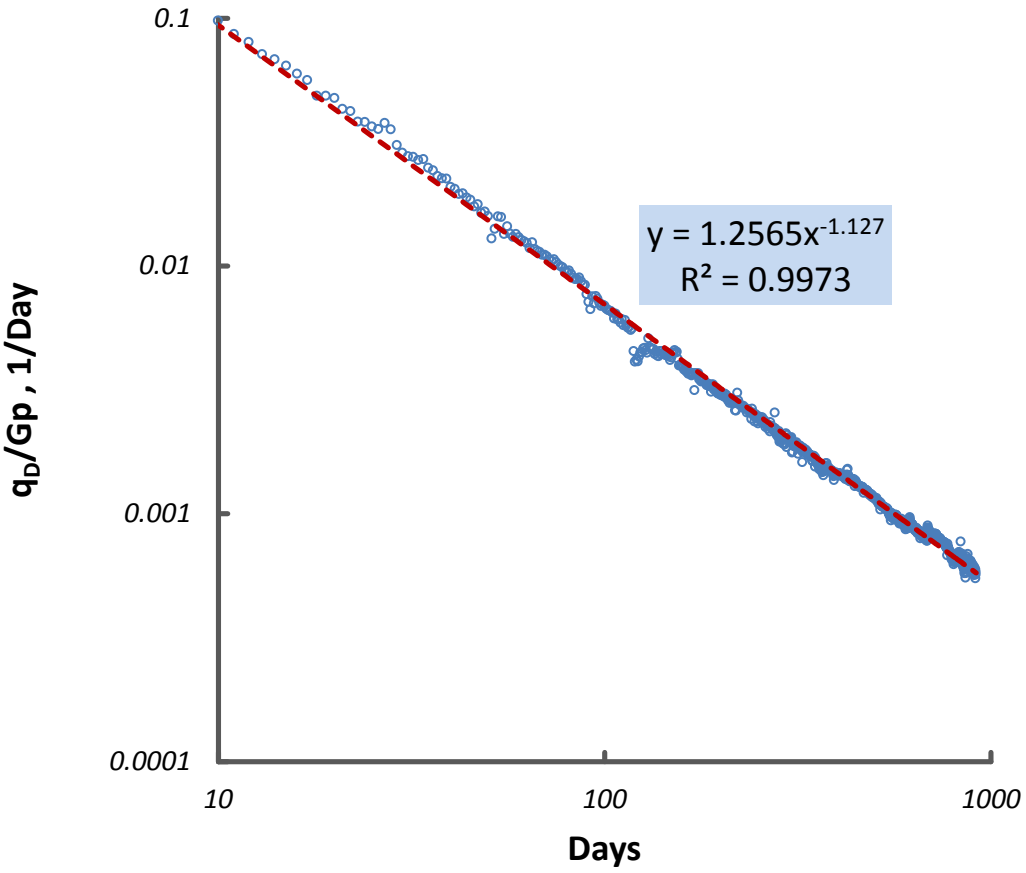

Figure 3.3—*a* and *m* determination for the same well

To determine rate at day 1, q_1, in Eq. 3.1, first we need to determine ***t(a,m)***, which is a time function based on Eq. 3.3:

$$q_D = q_1 t(a,m), \quad \text{.....} (3.3)$$

where t(a,m)= $t^{-m} e^{\frac{a}{1-m}(t^{1-m}-1)}$.

Now a q_D *vs.* t(a,m) plot will give a straight line with slope of q1. (Figure 3.4).

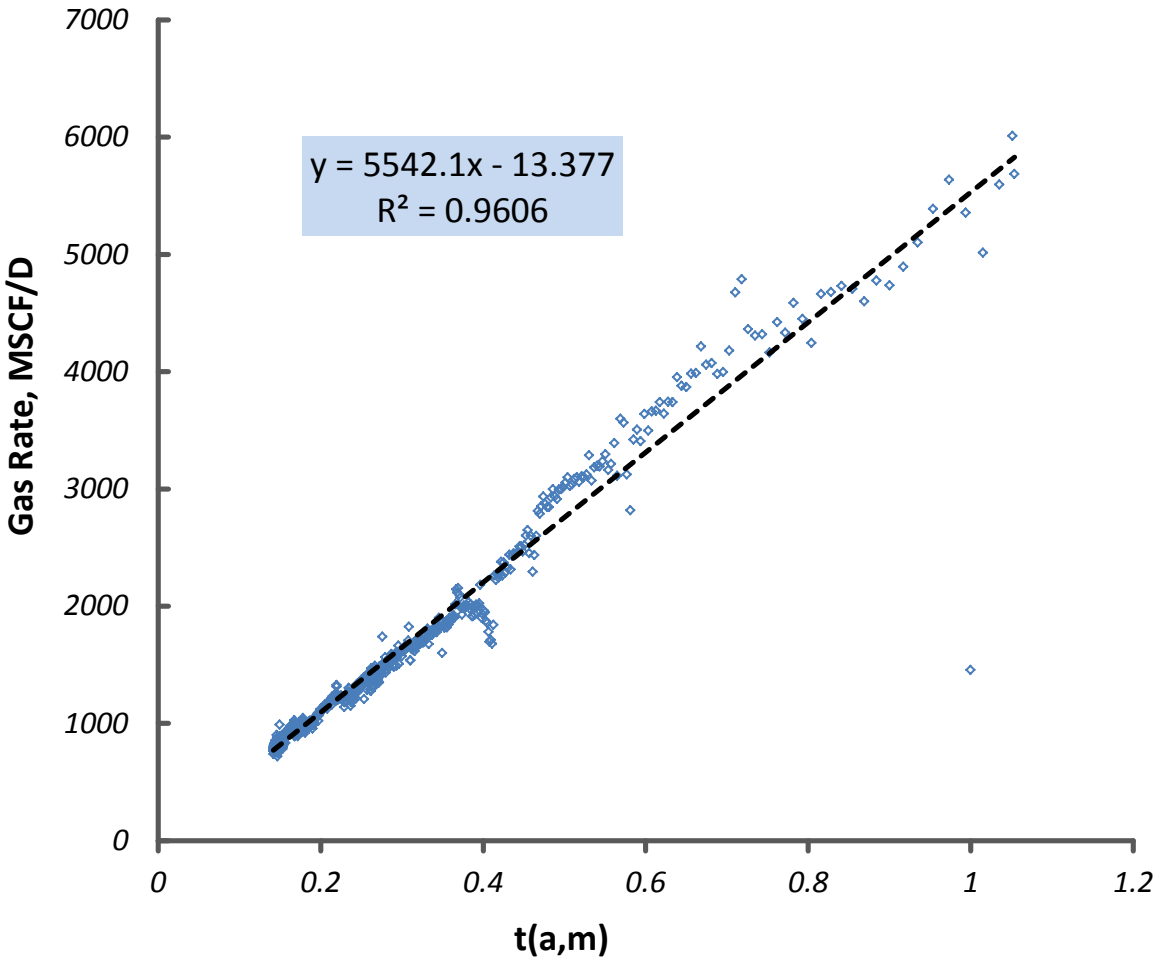

Figure 3.4—q_1 determination for the same well

Since only linear regression is used and no differentiation of the data is required once the data preparation is done, the method is straightforward and reproducible. The same procedure has been done for all 25 wells and the results can be find in APPENDIX A. *Table 3.1* summarizes all Duong's parameters calculated for 25 gas wells in Barnett Shale.

Table 3.1—Duong's parameters for all 25 wells in Barnett Shale

Well Name	m	a	t_{Max}	q_{Max}	q_1	Deleted Reserve, Bscf
WELL#1	1.14	1.418596	4.797428	2971.207	3950.644	0.041575
WELL#2	1.08	1.068207	0.897385	6833.719	4292.015	0.063722
WELL#3	1.186725	1.884511	11.90244	11836.39	4146.96	0.082907
WELL#4	1.120848	1.184537	1.579835	1728.116	2261.551	0.006475
WELL#5	1.200112	1.822821	8.074238	2564.646	2128.442	0.027683
WELL#6	1.13918	1.534403	8.49861	7315.48	2984.713	0.035304
WELL#7	1.14567	1.596515	9.756993	1884.346	2570.157	0.016948
WELL#8	1.130269	1.422716	5.849933	16.43483	3577.883	0.056412
WELL#9	1.15	1.4666	4.749312	2491.558	6904.28	0.017696
WELL#10	1.13	1.256548	2.353062	1538.074	5542.104	0.025269
WELL#11	1.158678	1.474422	4.566352	3255.868	4668.916	0.019813
WELL#12	1.108866	1.323993	5.097415	1531.5	2730.969	0.47338
WELL#13	1.196345	1.735773	6.656218	53.89156	2950.038	0.034492
WELL#14	1.127483	1.322317	3.491549	2364.361	2131.243	0.044207
WELL#15	1.098045	1.094296	0.965723	3071.111	3774.934	0.01624
WELL#16	1.130058	1.497097	8.693415	4181.396	6910.401	0.049701
WELL#17	1.151009	1.515604	8.693415	4181.396	6910.401	0.01917
WELL#18	1.09	1.187028	2.417051	3960.897	5742.725	0.04109
WELL#19	1.163222	1.541426	5.611066	2227.906	1306.817	0.060538
WELL#20	1.073186	1.044004	0.686123	3498.002	3376.927	0.071922
WELL#21	1.275688	2.556315	12.44421	10372.23	1437.956	0.029589
WELL#22	1.172493	1.809259	12.36417	1715.908	2179.324	0.01189
WELL#23	1.20773	1.833671	7.464713	4175.804	2345.537	0.010758
WELL#24	1.147492	1.561528	8.075517	1045.384	828.1863	0.004003
WELL#25	1.08862	1.202983	3.087064	1932.21	2834.233	0.038079

3.1.1. Some Characteristics of Duong's Model

Following the same procedure in previous section for SEDM and using Eq. 3.1, we can investigate the inflection point for Duong's method as below:

$$Slope = \frac{e^{-\frac{2(-1+t^{1-m})}{1-m}} t^{2m}\left(-e^{\frac{-1+t^{1-m}}{1-m}} m q_1 t^{-1-m} + e^{\frac{-1+t^{1-m}}{1-m}} q_1 t^{-2m}\right)}{{q_1}^2}, \quad \text{.....(3.4)}$$

Inflection point on log (q_D) *vs.* rate is where the slope is maximum. To find this maximum slope, the derivative of slope respect to time was calculated as:

$$\frac{d(Slope)}{dt} = \frac{e^{-\frac{2(-1+t^{1-m})}{1-m}} t^{2m}\left(-3e^{\frac{-1+t^{1-m}}{1-m}} m q_1 t^{-1-2m} - e^{\frac{-1+t^{1-m}}{1-m}}(-1-m) m q_1 t^{-2-m} + e^{\frac{-1+t^{1-m}}{1-m}} q_1 t^{-3m}\right)}{{q_1}^2} -$$

$$\frac{2e^{-\frac{2(-1+t^{1-m})}{1-m}} t^{m}\left(-e^{\frac{-1+t^{1-m}}{1-m}} m q_1 t^{-1-m} + e^{\frac{-1+t^{1-m}}{1-m}} q_1 t^{-2m}\right)}{{q_1}^2} +$$

$$\frac{2e^{-\frac{2(-1+t^{1-m})}{1-m}} m t^{-1+2m}\left(-e^{\frac{-1+t^{1-m}}{1-m}} m q_1 t^{-1-m} + e^{\frac{-1+t^{1-m}}{1-m}} q_1 t^{-2m}\right)}{{q_1}^2}, \quad \text{.....(3.5)}$$

By setting Eq. 3.5 to zero and solve it for t we obtain two t_{infl} for Duong's method:

$$t_{infl} = \{2^{-\frac{1}{1-m}}\left(m - \sqrt{4m-3m^2}\right)^{\frac{1}{1-m}},\ 2^{-\frac{1}{1-m}}(m + \sqrt{4m-3m^2})^{\frac{1}{1-m}}\}, \quad \text{.....(3.6)}$$

It is interesting to note that the Duong model on a log (q_D) *vs.* cumulative curve provides either no inflection point at all (if m > 4/3) or two inflection points (m < 4/3). If there is no inflection point, the curve has only a concave portion as Arp's hyperbolic model with 0 < b < 1.

Also, unlike SEDM, Duong's model is not completely monotonic (not monotonic at all).The starting rate at time zero is always zero and then it goes to a maximum. Strictly

speaking it is not a decline model, but it describes a behavior that is often seen in actual data series. Duong emphasizes, that when his model is fitted to actual data, the maximum will occur in the first 1-3 months of the production.

3.2. Parameter Estimation

Parameter estimation for the Arps model has been discussed extensively in the literature. Nonlinear least squares search for 3 parameters, nonlinear search combined with 2 parameter linear regression (Towler and Bansal), and numerical differentiation first and then linear regression (to obtain b) are the most common methods. All three approaches have serious drawbacks. In the case of unconventional gas especially application of the numerical differentiation of the rate data introduces a great deal of sensitivity to the algorithmic parameters.

Similarly, For an individual well the SEDM model parameters can be determined by the method of least squares in various ways, but the inherent nonlinear character of the least squares problem cannot be bypassed. The subsequent results were obtained by using the Solver of Excel fitting the cumulative production (APPENDIX A). The Solver needs a careful strategy to switch between search methods and additional constraints on the parameters. Noted by Seshadri and Mattar (2010), this is a drawback of the SEDM model. Table 3.2 summarizes all SEDM parameters calculated for 25 gas wells in Barnett Shale using 3-variable search method.

Table 3.2—SEDM parameters for all 25 wells in Barnett Shale						
Well Name	**n**	**τ Days**	**q_0 MSCF**	**t_{infl} Days**	**$t_{100mscfd}$ Days**	Days Produced
WELL#1	0.29	63.86	8424	1362	10661	135
WELL#2	0.24	38.04	6750	4785	15501	1347
WELL#3	0.27	41.92	20841	1785	21764	455
WELL#4	0.31	44.46	3287	540	2398	525
WELL#5	0.33	51.18	7021	474	4332	1359
WELL#6	0.24	41.25	10063	4469	22375	522
WELL#7	0.26	44.47	9112	2332	14049	381
WELL#8	0.26	43.81	9084	2178	13348	564
WELL#9	0.32	49.46	14829	495	7275	302
WELL#10	0.30	41.38	9089	695	6258	926
WELL#11	0.31	48.75	9919	607	6421	148
WELL#12	0.24	39.61	6914	4424	15420	184
WELL#13	0.33	42.26	8635	361	3915	1041
WELL#14	0.27	33.35	4586	1476	5097	2159
WELL#15	0.26	23.44	6102	1166	5031	619
WELL#16	0.24	65.52	18641	7978	64449	126
WELL#17	0.26	31.83	9133	1717	10255	824
WELL#18	0.24	33.52	11592	4465	23460	641
WELL#19	0.28	31.29	3732	935	3136	1198
WELL#20	0.26	41.69	5274	2475	8636	544
WELL#21	0.36	50.88	11164	265.68	3931.68	1839
WELL#22	0.28	42.53	10486	1407	11203	1081
WELL#23	0.30	40.31	7311	666	5113	1320
WELL#24	0.26	37.54	2778	2059	3777	1593
WELL#25	0.22	24.03	7136	7698	17757	965

To take care of this issue, as an alternative, 1-variable (just τ) search instead of 3-variable (n, τ, and q_0) search has been done. The 1-variable search was done by setting q_0 equal to last cumulative production available divided by sum of all $\exp\left[-\left(\frac{t}{\tau}\right)^n\right]$ terms and setting n=0.247, based on the Valko and Lee (2010) for Barnett Shale, and searching for τ to get the best match on log of rate *vs.* cumulative production plot. Our study shows that calculated EUR from both1 and 3-variable search methods are very close to each other. Table 3.3 shows some of the findings from 1-variable search method.

Table 3.3—Parameter Estimations for gas wells in Barnett Shale (1-variable search).

Well Name	n	τ Days	q_0 MSCF	t_{infl} Days	Contacted G_p BSCF	Days Produced
WELL#2	0.247	50.03	6240.24	4562.17	8.06	1347
WELL#5	0.247	9.1	12240.68	829.79	2.88	1359
WELL#8	0.247	46.04	8623.92	4198.13	10.26	564
WELL#9	0.247	17.02	19610.29	1551.78	8.62	302
WELL#14	0.247	25.53	4717.87	2328.32	3.11	2160
WELL#15	0.247	17.29	6569.10	1576.74	2.93	619
WELL#17	0.247	20.93	10378.41	1908.33	5.61	824
WELL#18	0.247	43.33	10826.30	3950.96	12.12	641
WELL#22	0.247	26.44	11771.51	2410.65	8.04	1080
WELL#23	0.247	7.49	13535.43	682.85	2.62	1320
WELL#24	0.247	26.74	3063.53	2438.2	2.12	1593
WELL#25	0.247	67.32	5370.57	6138.43	9.34	1593

3.3. Reserves Estimations

For comparison purposes different reserves estimation procedures have been performed for both SEDM and Duong's models.

3.3.1. EUR $_{30\text{-years}}$

This is the cumulative production after t=30 years. Using Eq. 2.9 and Eq. 3.2 and having SE and Duong's parameters it can be calculated for each individual well. The individual well data are used to obtain the three parameters for each well.

3.3.2. EUR $_{30,\ SPE134231}$ and EUR $_{30,\ SPE137748}$

These two estimates of $EUR_{30\text{-years}}$ are based solely on the time-cumulative production pair and published parameters (n and τ for SEDM and a and m for Duong, therefore they might be useful for wells that have limited production data and/or the data are heavily influenced by operational issues.

For instance in case of one of the 25 horizontal gas wells in Barnett Shale, such estimates based on published data will be about 10 Bscf instead of 17 Bscf, and are more conservative than estimates based on individual well data. Indeed, for this specific well the 150 days available for analysis and seemingly the data are not enough to determine "individual decline characteristics".

$EUR_{30,\ SPE134231}$ is based on Valko and Lee (2010) findings for Barnett Shale. Using their constants of n= 0.247 and τ=23.6 days along with Eq. 2.9 for last t and last G_p available in the data set for each individual well q_0 can be determined. Then using

$EUR_{30,SE} = q_0 \frac{\tau}{n} \left(\Gamma[\frac{1}{n}] - \Gamma[\frac{1}{n}, \left(\frac{t}{\tau}\right)^n] \right)$ with t =*30×365* days $EUR_{30,\ SPE134231}$ can be determined.

$EUR_{30\text{-}years,\ 30,\ SPE137748}$ is based on Duong's findings (2011). Using his constants of a = 1.41 and m = 1.14 for Barnett wells along with Eq. 3.2 for last for last t and last G_p available in the data set for each individual well q_1 can be determined. Then using $EUR_{30,Duong} = \frac{q_1}{a} e^{\left(\frac{a}{1-m}\right)(t^{1-m}-1)}$ with $t = 30 \times 365$ days $EUR_{30\text{-}years,\ 30,\ SPE137748}$ can be determined. These estimates show remarkable consistency.

3.3.3. EUR $_{100\ MSCF/D}$

This is the cumulative production forecast for q>100 Mscf/Day. To calculate the reserve on the basis of this economical cutoff rate, first we derive the time that this cut off being reached. In Eq. 2.1 if we set q=100 Mscf/D and then solve it for t we will have:

$$t_{100Mscf/D} = \tau \left(Log \frac{q_0}{100} \right)^{\frac{1}{n}}, \quad \text{.....(3.7)}$$

Now using ***Eq. 2.9*** and ***Eq. 3.7***, $EUR_{100\ MSCF/D}$ can be determined for SEDM.

In case of Duong's model, Solver has been used to find the cutoff time, t_{eco}, which gives the rate of 100 Mscf/Day having constants of a and m and q_1 for each individual well. Then having t_{eco} and using Eq. 3.2 one can determine $EUR_{100\ MSCF/D}$ for Duong's model.

The $EUR_{100\ MSCF/D}$ values were obtained using the individual well data and hence with the same parameters as the $EUR_{30\text{-}years}$ estimates.

3.3.4. Contacted Gp

For SEDM Contacted G_p or EUR at t=∞ can be determined if we calculate the limit of G_p in Eq. 2.9 when t→∞, and therefore:

$$EUR_{SE,\infty} = q_0 \frac{\tau}{n} \Gamma\left[\frac{1}{n}\right], \quad \text{.....(3.8)}$$

The limit of G_p in Eq. 3.2 when t→∞ gives Contacted G_p for Duong's model as:

$$EUR_{Duong,\infty} = \left(\frac{q_1}{a}\right) e^{\left(\frac{a}{m-1}\right)}, \quad \text{.....(3.9)}$$

Just by looking at *Eq. 3.9*, one can realize that Duong's method always yields finite contacted gas in place. If m approaches 1, contacted gas tends to infinity and for m<1 contacted gas in place has no meaning.

Table 3.4 gives all reserves estimations for both SEDM and Duong's model for 25 wells in Barnett Shale. For each model the lowest value between EUR $_{30\text{-years}}$ and EUR $_{100\ MSCF/D}$ is distinguished with red font color.

	Table 3.4—Reserves Estimations for 25 wells in Barnett Shale (3-variable search).							
	SE	SE	Duong	Duong	SE	Duong	SE	Duong
Well Name	EUR 30-years	EUR 100 MSCF/D	EUR 30-years	EUR 100 MSCF/D	EUR 30, SPE134231	EUR 30, SPE137748	Contacted G_p	Contacted G_p
WELL#1	4.32	4.29	4.57	5.7	4.35	4.53	5.73	67.02
WELL#2	4.09	4.63	4.82	9.72	3.48	3.77	8.1	4127.18
WELL#3	9.85	11.54	8.99	12.6	9.74	10.34	14.13	53.16
WELL#4	1.01	0.71	1.43	0.96	1.46	1.56	1.12	34.49
WELL#5	2.16	1.84	2.56	2.24	2.96	3.2	2.35	10.55
WELL#6	6.18	7.81	5.82	8.85	4.95	5.27	11.94	119.36
WELL#7	4.8	5.15	5.48	7.9	4.46	4.72	7.44	92.59
WELL#8	4.66	4.93	5.39	8.02	4.42	4.71	7.07	139.18
WELL#9	4.58	4.32	6.64	8.95	6.97	7.33	5.01	64.74
WELL#10	3.01	2.7	4.26	5.27	3.91	4.21	3.48	101.52
WELL#11	3.33	3.03	4.05	4.37	4.73	4.93	3.75	30.37
WELL#12	4.17	4.7	4.76	7.91	3.24	3.38	8.03	394.61
WELL#13	2.15	1.86	2.83	2.55	3.35	3.62	2.27	11.74
WELL#14	1.85	1.48	2.17	1.9	1.97	2.13	2.53	51.52
WELL#15	1.97	1.6	2.74	2.92	2.31	2.47	2.54	242.67
WELL#16	15.52	27.94	14.87	37.49	9.69	10.09	37.77	460.7
WELL#17	3.82	3.75	4.15	4.85	3.94	4.24	5.43	48.76
WELL#18	6.59	8.42	7.78	19.17	5.46	5.85	12.71	1633.06
WELL#19	1.24	0.88	1.35	0.9	1.46	1.58	1.52	10.71
WELL#20	2.76	2.55	3.7	6.26	2.58	2.75	4.36	5070.23
WELL#21	2.60	2.34	2.93	2.58	3.96	4.29	2.68	5.99
WELL#22	4.6	4.63	5.25	6.62	4.96	5.36	6.19	43.26
WELL#23	2.35	2.02	2.43	2.07	2.92	3.17	2.7	8.72
WELL#24	1.32	0.9	1.43	0.98	1.3	1.41	1.97	21.02
WELL#25	4.13	4.97	4.81	9.71	3.27	3.52	9.76	1851.73

3.4. Observations Based on the 25-Well Barnett Sample

1) Finite contacted gas in place ($EUR_{t=\infty}$):
    a. Arp's hyperbolic model with b >= 1 does not have finite value, but with a cut-off to switch to exponential decline it does have.
    b. Duong's model seems to yield m > 1 in all cases and that implies finite value, (though it may still be very large.)
    c. SEDM always yields 0 < n < 1 and that implies finite value, most often a moderate value, already having some physical meaning by itself.
2) Ease of use:
    a. Arps is heavily dependent on cutoff to exponential decline and on the way how the b exponent is determined (for instance numerical differentiation with smoothing.)
    b. Duong's model is very easy to use and leaves little doubt about non-uniqueness. This is due to two facts: one is that it does not need numerical determination of derivatives and it can be cast as sequence of two consecutive linear regression procedures.
    c. SEDM needs non-linear fitting (solver or similar) and constraints on the parameters. It is the most difficult model to work with and the results depend on the actions taken during the fitting procedure.
3) Inflection point:
    a. Arp's with b > 0 has a break point where the cutoff is reached (no inflection point, an artificial switch from convex to concave character.)

b. Duong's model usually puts the inflection point at very far; practically it always uses the convex part for the 30-yr prediction in the examples we considered. Therefore, it usually implies a very large contacted gas in place ($EUR_{t=\infty}$) having little or no physical meaning. In this respect, the finiteness of contacted gas in place does always exist. However, when the m parameter is near to 1, the contacted gas in place is very large and there might be a very large difference between EURs corresponding to the 30–yr and economic rate conditions.

c. SEDM usually puts the inflection point on the order of 1 – 8 years. This implies a limited value of contacted gas in place ($EUR_{t=\infty}$), that is already on the order of the $EUR_{t=30\text{-yr}}$ value and leads to possible physical interpretation.

The question is how these multi-stage fractured horizontal wells will behave after the first couple of years. Will there be a manifest inflection point on the log(q) *vs.* cumulative curve or it remains convex for many years? At this point we do not know the answer in general, though we have already some experience from the longer data sets.

4) Prediction with published parameters:

a. For Arps, There are no reliable suggestions for the Barnett Shale, and the decline cutoff is questionable.

b. Duong: SPE 137748 provides a reasonable way to estimate $EUR_{t=\ 30\text{-yr}}$ from only one time-cumulative pair.

c. SEDM: SPE 134231 provides a reasonable way to estimate $EUR_{t= 30\text{-yr}}$ from only one time-cumulative pair.

It is interesting that $\boldsymbol{EUR}_{30,\ SPE134231}$ and $\boldsymbol{EUR}_{30,\ SPE137748}$ are consistent, with the SEDM being always about 5 – 10 % less. The average parameter values for Barnett in these two papers were published approximately at the same time and independently.

These estimates seem especially useful when the individual well's data set is short, or contain anomalies and hence do not allow for unique determination of all three parameters.

4. LIQUID-LOADING IN GAS WELLS

Beside reservoir depletion, other factors also affect the decline of gas production rate. Accumulation of some liquids like water in the bottom of the wellbore can further reduce the production of gas by creating an increase hydrostatic pressure against the formation pressure. Liquid-loading is the term used to describe inability of a gas well to remove the liquid from the wellbore. There could be three sources of liquids in the gas: 1) free water entries directly from the reservoir, 2) water condensed from vapor in the upper portion of the tubing, or 3) hydrocarbon condensates in the wellbore.

Figure 4.1 shows different flow regimes for a gas well that also produces liquid. For mist and annular flow regimes the gas phase is the dominant continuous phase in the well. Liquid is present within the gas as a mist. In annular flow, the inside of the tubular is covered with a thin layer of liquid travelling up the pipe. In slug flow, the gas is found in large bubbles, separating slugs of fluid. In the bubble flow regime the liquid is the continuous phase along the tubular. This flow regime starts when the tubular in the well is almost filled with liquid and gas is present as small bubbles in the liquid.

The above two-phase terms are defined for steady-state flow and hence should be used with some cautions in the dynamically changing conditions of a producing well.

To ensure that liquids will be unloaded from the wellbore the gas phase should stay as continues phase. The liquid-loading problem is inherently associated with low gas velocities. If during the production of a gas well the gas production rate drops, the

energy of the gas phase will not be enough to lift the liquid and therefore the liquid starts to accumulate in the wellbore.

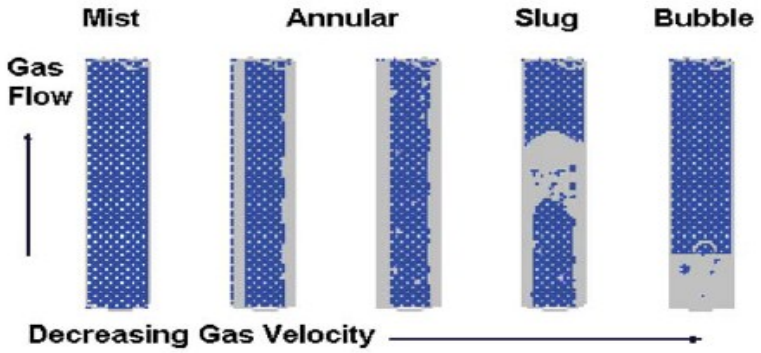

Figure 4.1—Flow regimes in gas wells producing liquids (Lea et al., 2008).

4.1. Liquid-loading Indicators

If a well has liquid-loading problem it may still produce for a long time. That's why it is not always easy to recognize it. Some indicators for liquid-loading in a gas well are (Lea and Nickens, 2004):

- Sharp drops in a decline curve.
- Liquid slugs observation at the surface of well.
- Increasing the differential pressure between the tubing and casing with time.
- Sharp changes in gradient of a flowing pressure survey.

Generally speaking, as the reservoir depletes over time, the production decline curve should be smooth. Any sharp drop in the general trend of the decline curve (as seen in Figure 4.2) or any oscillations unexplained otherwise can be an indication of liquid-loading problem.

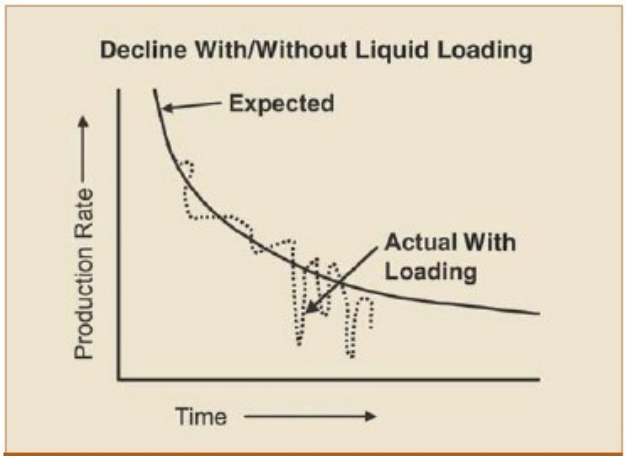

Figure 4.2—Liquid-loading indication from decline curve analysis (Lea et al., 2008).

Figure 4.3 shows an expected decline curve (SE) and also real production data with possible fluctuations due to liquid-loading in a log(q) *vs.* cumulative rate plot for a horizontal gas well in Barnett Shale.

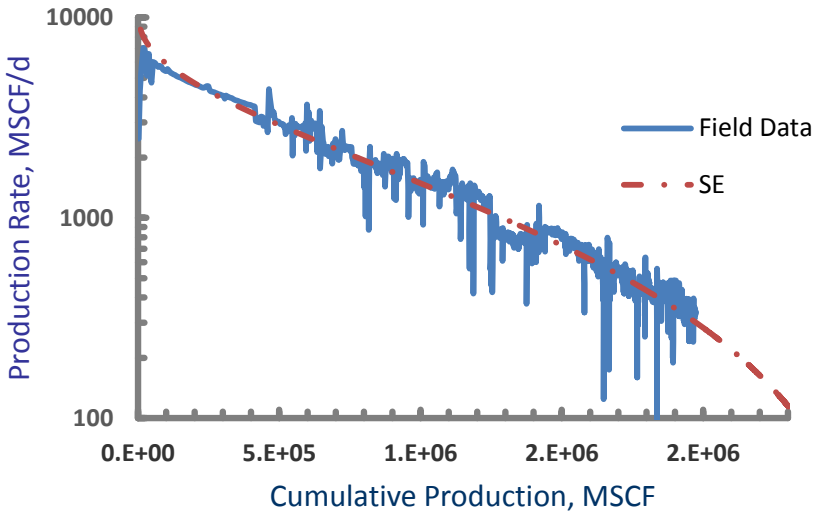

Figure 4.3—Log(q) *vs.* cumulative plot showing possible "liquid-loading" in a Barnett Shale horizontal gas well with 5 fracture stages of 228398, 296259, 457091, 515647, and 422733 lbs of Ottawa sand.

4.2. Critical Rate Theory

Critical velocity is the minimum gas rate that can lift the droplets of liquid upward and prevent liquid-loading in the wellbore. Two physical models were proposed by Turner et. al (1969) to model the presence of liquid phase in the wellbore with gas phase; (1) liquid forming a continuous film inside the wall of the production string moved upward by interfacial stress and (2) liquid droplets existing in the string of flowing gas. His study showed that droplet model was a better fit to the well data.

The concept of Turner's model is the determination of the minimum gas velocity needed to prevent the liquid droplets to fall down. In other words, for liquid droplets, this minimum gas rate is needed to overcome the terminal fall velocity, which is the maximum velocity it can attain against gravity. Turner's proposed the following equation for critical velocity:

$$v_c = 1.5934\left(\frac{\sigma(\rho_l-\rho_g)}{{\rho_g}^2}\right)^{0.25}, \quad (4.1)$$

where v_c is the critical velocity in ft/sec. σ is the surface tension in dynes/cm, ρ_l is liquid density in lbm/ft^3, and ρ_g is gas density in lbm/ft^3.

If water is the liquid phase, surface tension of 60 dynes/cm and density of 67 lbm/ft^3 can be assumed.

The gas density can be determined using the real gas equation of:

$$\rho_g = \frac{p\,\gamma_g M_a}{ZRT_{^\circ R}}, \quad (4.2)$$

where, p is the pressure in psia, γ_g is the gas specific gravity, M_a is air molecular weight=28.964 lbm mole, Z is gas compressibility factor, R is universal gas

constant=10.73147 psia-ft^3/°R-lbm mol, and $T_{\circ R}$ is temperature in°R. Having the critical velocity for a gas in specific production string geometry the corresponding critical gas rate can be obtained using Eq. 4.3 (Lea and Nickens, 2004):

$$Q_c = \frac{3.06pAv_c}{T_{\circ R}Z}, \quad (4.3)$$

where, Q_c is critical gas flow rate in MMscf/D and A is the cross-section area of flow in ft^2.

Critical velocity and gas rate have been calculated for 25 gas wells in Barnett Shale (Table 4.1). In the following section we use this interpolation for conditioning the SEDM model.

4.3. SEDM Variable Search Conditioned with Turner's Critical Gas Rate

The critical gas rate based on Turner's critical velocity can be used for conditioning the 3-variable search (n,τ, and q_0) in SEDM. From section 2, Eq. 2.1 and Eq. 2.8 give the SEDM rate and inflection time as following:

$$q = q_0 \, exp\left[-\left(\frac{t}{\tau}\right)^n\right], \quad (2.1)$$

$$t_{infl} = \tau\left(\frac{1}{n} - 1\right)^{\frac{1}{n}}, \quad (2.8)$$

If for any specific well, it is assumed that inflection time in log(q) *vs.* rate plot is the time when the gas rate drops to the critical rate value, then:

$$\begin{cases} t=t_{infl} \\ q=Q_c \end{cases}, \quad (4.4)$$

Table 4.1—Critical velocity and critical rate for 25 Barnett Shale gas wells.

Well	TVD, ft.	Tbg. Depth, MD	Tbg. ID, in.	P_{ri}, psia	T_r,F	γ_g	Avg. Tbg. Pressure	Z	ρ_g lbm/ft^3	v_c ft./sec	Q_c MMscf/D
WELL#1	6990	7630	1.995	3088	173	0.577	257	0.955	0.663	15.547	0.439
WELL#2	7177	7285.3	1.995	3163	175	0.577	210	0.957	0.538	17.262	0.396
WELL#3	7319	7905.3	2.441	3546	188	0.577	269	0.970	0.667	15.499	0.659
WELL#4	7625	7948.7	1.995	3335	181	0.577	222	0.963	0.560	16.912	0.404
WELL#5	7040	7378	1.995	3115	174	0.577	127	0.956	0.327	22.169	0.309
WELL#6	7541	7955.5	1.995	3286	180	0.577	331	0.961	0.839	13.806	0.494
WELL#7	8629	8898.5	1.995	3826	198	0.577	220	0.981	0.531	17.369	0.393
WELL#8	8376	8575.4	1.995	3754	195	0.577	329	0.978	0.800	14.144	0.482
WELL#9	7519	7841.1	2.441	3335	181	0.577	169	0.963	0.427	19.393	0.528
WELL#10	8321	8543	1.995	3578	189	0.577	147	0.971	0.363	21.022	0.326
WELL#11	8404	8694.9	1.995	3693	193	0.577	306	0.976	0.748	14.626	0.466
WELL#12	8093	8097.9	1.995	3309	180	0.577	356	0.962	0.901	13.323	0.512
WELL#13	7225	7710.6	1.995	3159	175	0.577	235	0.957	0.602	16.311	0.419
WELL#14	7037	7464.3	1.995	3059	172	0.577	120	0.954	0.310	22.754	0.301
WELL#15	7559	7974.7	1.995	3335	181	0.577	231	0.963	0.583	16.577	0.412
WELL#16	7297	7705.3	2.441	3094	173	0.577	376	0.955	0.969	12.841	0.794
WELL#17	7318	7670.8	1.995	3226	178	0.577	182	0.959	0.464	18.597	0.368
WELL#18	7310	7951.1	1.995	3226	178	0.577	195	0.959	0.497	17.964	0.381
WELL#19	6572	6781.8	1.995	2822	164	0.577	165	0.949	0.434	19.221	0.356
WELL#20	7080	7573	1.995	3100	173	0.577	252	0.955	0.649	15.709	0.435
WELL#21	7227	7192.9	1.995	3200	177	0.577	277	0.958	0.707	15.045	0.454
WELL#22	7389	7558.5	1.995	3200	177	0.577	271	0.958	0.692	15.211	0.449
WELL#23	7959	8040.1	1.995	3488	186	0.577	207	0.968	0.516	17.631	0.388
WELL#24	6478	7349.9	1.995	2872	166	0.577	106	0.950	0.278	24.039	0.285
WELL#25	6581	6761.4	1.995	2901	167	0.577	168	0.950	0.440	19.105	0.358

Using Eq. 2.1 and 2.8 along with critical rate from Eq. 4.3 in Eq. 4.4 condition gives the initial rate (q_0) as:

$$q_0 = Q_c exp\left[\frac{1}{n} - 1\right], \quad \text{.....(4.5)}$$

Substituting q_0 from Eq. 4.5 for initial rate in Eq. 2.1 yields to:

$$q = Q_c\ exp\ \left[\left(\frac{1}{n} - 1\right) - \left(\frac{t}{\tau}\right)^n\right], \quad \text{.....(4.6)}$$

Eq. 4.6 along with Eq. 4.5 can be used for a conditioned SEDM parameter estimation procedure. In this new approach only two parameters (n and τ) are needed to be searched, and the third parameter (q_0) can be obtained using the critical gas rate and Eq. 4.5. The advantage of this 2-variable search over the 3-variable search described in Section 3 is that it leads to a unique set of parameters (i.e. avoids the non-uniqueness) while it still provides enough flexibility to fit the actual data. To further investigate the validity of this new 2-variable SEDM parameter search conditioned with Turner's critical gas velocity, all of the previously investigated 25 wells in Barnett Shale will be studied. Then contacted gas in place and $EUR_{30\text{-years}}$ will be calculated for each individual well for comparison purposes.

Figure 4.4 compares the SEDM based on the best 3-variable search and new conditioned 2-variable search based on Turner's critical gas rate for ***WELL#5***.

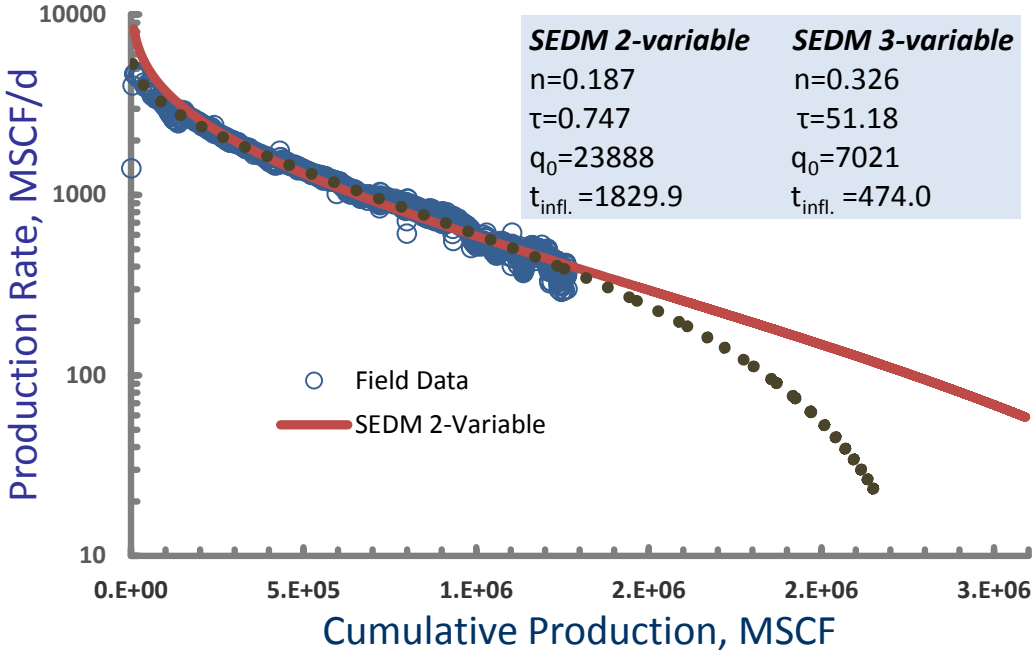

Figure 4.4—Log (q) *vs.* cumulative plot for two SEDM and field data for WELL#5.

Critical gas rates for the 25 Barnett Shale gas wells from Table 2.1 along with Eq. 4.5 and 4.6 were used to estimate SEDM parameters and reserves based on Turner's critical velocity conditioning and the results can be found in APPENDIX B. Table 4.2 shows how the new 2-variable search for SEDM conditioned with Turner's critical gas rate yielded a much closer $EUR_{30\text{-years}}$ compared to the $EUR_{30\text{-SPE134231}}$ based on the published data for the studied 25 Barnett Shale gas wells.

Table 4.2—Reserves Estimations for 25 gas wells in Barnett Shale (2-variable search).

Well	n	τ	q_0	$t_{infl.}$	$EUR_{30\text{-}years}$	$EUR_{30,SPE134231}$	Contacted Gp
WELL#1	0.253	57.58	8356.4	4091.1	5.69	4.35	10.65
WELL#2	0.279	95.44	5237.3	2856.0	3.95	3.48	6.52
WELL#3	0.211	11.44	27700.2	5905.4	11.52	9.74	24.46
WELL#4	0.332	55.69	3024.0	458.3	0.95	1.46	1.03
WELL#5	0.187	0.747	23888	1829.9	2.60	2.96	3.92
WELL#6	0.253	51.00	9433.2	3656.5	5.95	4.95	10.71
WELL#7	0.251	69.64	7832.8	5520.3	6.15	4.46	12.92
WELL#8	0.271	84.29	7108.5	3252.3	5.28	4.42	9.12
WELL#9	0.208	6.45	24013.4	4092.6	7.32	6.97	13.65
WELL#10	0.201	3.31	17273.7	3140.5	3.81	3.91	6.53
WELL#11	0.234	18.84	12357.5	3016.2	5.07	4.73	8.55
WELL#12	0.312	185.14	4646.4	2341.5	4.36	3.24	6.73
WELL#13	0.216	3.81	15787.8	1490.4	2.78	3.35	3.89
WELL#14	0.288	65.36	3569.3	1518.7	1.92	1.97	2.62
WELL#15	0.279	34.24	5435.2	1017.3	1.94	2.31	2.42
WELL#16	0.268	661.9	12142.5	27850.5	26.84	9.69	129.00
WELL#17	0.226	13.12	11282.2	3036.4	4.05	3.94	6.85
WELL#18	0.223	24.75	12327.3	6570.7	6.93	5.46	15.41
WELL#19	0.319	60.11	3016.8	651.6	1.14	1.46	1.30
WELL#20	0.312	113.45	3929.7	1419.8	2.60	2.58	3.47
WELL#21	0.148	0.01	141916.2	1432.5	3.22	3.96	4.65
WELL#22	0.232	19.37	12380.3	3432.9	5.33	4.96	9.39
WELL#23	0.208	2.37	17354	1443	2.53	2.92	3.53
WELL#24	0.356	168.93	1744.9	899.8	1.18	1.3	1.40
WELL#25	0.283	128.46	4527.9	3462.8	4.03	3.27	7.13

5. IMPLICATIONS OF NATURAL FRACTURE NETWORK

5.1. Background

The dual porosity (DP) model, first introduced by Warren and Root (1963), conventionally has been used for certain formations, because it adds a second interacting continuum which reflects storage and conductivity characteristics of "fractured reservoirs" including many shale reservoirs. However, because DP approaches simplify connectivity and scale-dependent heterogeneity, they cannot effectively address the connectivity between natural fractures and induced hydraulic fractures and their interaction (Figure 5.1). The discrete fracture network (DFN) approach is geologically more realistic than DP model. Moreover, DFN models have many advantages over conventional dual porosity (DP) approaches, especially in heterogeneous reservoirs where the dominant flow mechanism is through the network of fractures rather than the reservoir matrix. The advantages come with some disadvantages, as well. The DFN approach is based on the stochastic modeling concept and therefore every realization of the discrete fracture network will produce different results. Dershowitz et al. (1998) developed techniques to integrate DFN and DP approaches. They introduced fracture system porosity and permeability for every portion of the fractured reservoir based on the number of fractures per unit volume, the fracture size distribution and fracture aperture distribution.

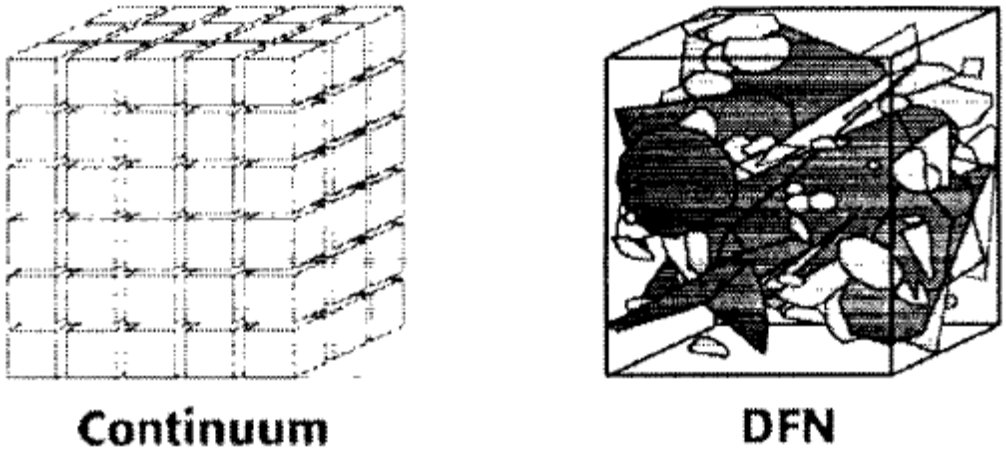

Figure 5.1- Dual Porosity and Discrete Fracture network concepts (Dershowitz et al., 1998)

In the following we use DFN model to interpret the SEDM results obtained previously. Our study proposes that the exponent parameter for SEDM, n, can be conditioned based on the scale independent characteristics of the created fracture network that in turn can be considered non-varying in a given field (or larger group of wells in the same geological settings.) Our hypothesis is supported by dry gas flow simulation involving stochastic generation of the discrete fracture network with various characteristics. The effect of variations in natural fracture lengths, apertures, density, and connectivity are considered along with induced hydraulic fracture dimensions. In view of our findings we present another conditioning approach to DCA of selected Barnett Shale wells.

In this section the flow behavior in shale gas reservoirs, especially Barnett Shale, will be investigated by using a Discrete Fracture Network (DFN) simulator (FracGen and NFflow) for fracture modeling of a shale gas reservoir. We study the interaction of

the different fracture properties on reservoir response. Finally we propose a conditioning procedure of SEDM fitting, based on our findings.

5.2. DFN Simulation

The Discrete fracture networks (DFN) concept involves *"analysis and modeling which explicitly incorporates the geometry and properties of discrete features as a central component controlling flow and transport."* (Dershowitz et al., 2004). DFN are stochastic models of fracture architecture that incorporate statistical scaling rules derived from analysis of fracture length, height, spacing, orientation, and aperture (Guohai, 2008).

To better understand the flow behavior in shale gas reservoirs based on Discrete Fracture Network (DFN) concept and relating the fracture network characteristics to SEDM parameters, FRACGEN/NFFLOW (2010) has been used. FRACGEN/NFFLOW is a fractured reservoir modeling software package that originally has been developed by the National Energy Technology Laboratory (NETL) Geological and Environmental Sciences on-site research group.

Some assumptions that need to be taken in consideration when using this simulation package are:

- The reservoir produces relatively dry gas, with little interference from water or oil.
- The reservoir rock (matrix) has less than 1 millidarcy (md) permeability.

- Variations in fracture apertures, density and connectivity are the dominate causes of heterogeneity in gas flow.
- Flow conductors are oriented nearly vertical and are strata-bound (extend from bottom to top of beds that can be modeled individually).
- Faults do not divide the reservoir into tightly sealed compartments or produce significant offsets in the productive strata.

5.3. FRACGEN Simulator

FracGen generates a stochastic network of lines that represent some of the patterns of fractures commonly found within thin strata-bound petroleum reservoirs and aquifers. All fractures are intrinsically two-dimensional, strata-bound and vertical. It also assumes that bed thickness is constant. Because FracGen works based on stochastic modeling each realizations of fracture system will be different from another one with the same input file.

Fracture lengths may be generated based on uniform, exponential, or lognormal. In our study, uniform distribution for fracture length has been assumed which generates fracture between a minimum and a maximum lengths and the distribution is rectangular in shape (i.e. no peak).

It has been avoided to generate fractures with lognormal distribution of length because it can generate very long fractures that expand the generation region and, as a result, significantly increase the number of fractures that must be analyzed.

The three different methods in FRACGEN that can be used for termination/intersection frequency control for fractures are: fracture endpoint shifting, T-termination frequency control, and fracture intersection-frequency control. In this study all fractures have been generated with T-termination frequency control which involves fracture end-point shifting coupled with synthetic annealing to achieve specified T-termination frequencies. In this method, a fracture is either reoriented or relocated from one location to another. If the two and one T-terminations fracture frequencies improve as a result of the effort, then the program begins to generate the next fracture; otherwise, the annealing process continues up to a specified limit on the number of swaps. This process works well for modeling early-formed fractures or master fractures.

5.3.1. FRACGEN Multilayer Input, General Description

For multi-layer the concept of "strata-bound" fracture networks was followed. Each layer is a "strata-bound" fracture network layer, even if 100% of the fractures extend into adjacent layers. For multi-layer modeling, layers were defined as rock units that have a different matrix permeability or porosity but the same sets of fracture as layers above or below. However some charactristics like fracture aperture or fracture density may change from one layer to another one.

Fractures were considered to propagate out of a layer by extending into and through the overlying layer. Fractures propagate upward, not downward. In reality, longer fractures have a greater tendency to extend into adjacent layers, so a correlation

coefficient between fracture length and the occurrence of cross-layer propagation into the overlying layer has been considered for natural fracture settings.

5.4. NFflow Natural Gas Flow Modeling

NFflow simulates the flow of dry gas through tight (<1 md matrix permeability) fractured reservoirs and it can be used under either rate-controlled mode or pressure-controlled mode. In our study gas flow through the fracture network, will be simulated with NFflow using pressure-controlled mode. In this model, gas flows out of the reservoir primarily through the fracture network, and gas from the rock matrix recharges its adjacent fracture segment at a rate determined, in part, by the gas pressure history at the fracture segment midpoint. Flow through the rock is modeled with Darcy's Law. Also it is assumed that flow along fractures changes as a linear (cubic law) function of the pressure difference between the recharge points and the fracture intersections. This linear function incorporates the real gas pseudo-potential which allows viscosity and the Z-factor to vary with pressure. Flow through the fracture network requires mass balance at all fracture intersections, which couples the individual recharge models together.

5.5. Geology and Natural Fracture Specifications in Barnett Shale Reservoirs

One of the most controversial topics in low permeability shale gas plays is how induced hydraulic fractures will interact with natural fractures and whether they can improve the production or they are detrimental to the reservoir performance. Montgomery et al. (2005) performed an overall evaluation of the Barnett Shale play and identified several features that make it exceptional compared with other shale gas plays. Some of these

features are great depth and high pressure of the reservoir and the complex thermal history, which has influenced the geochemistry of hydrocarbon generation and storage. They also stated that natural fractures are not essential for production and they could reduce well performance in some circumstances.

On the other hand, microseismic monitoring study by Fisher et al. (2004) and Warpinski et al. (2005) has shown that the hydraulic fractures stimulate the natural fractures to open. This reopening of natural fractures produces a complex network that enhances reservoir performance (Figure 5.2). In many reservoirs natural fractures act as a barrier for hydraulic fractures propagation (Warpinski and Teufel, 1987), but in case of the Barnett Shale natural fractures are not a barrier because the tensile strength of the contact between the calcite fracture fill and the shale wall rock is low (Gale et al. 2007). This low strength is because calcite in the fracture is not growing in crystallographic continuity with grains in the wall rock and no crystal bond exists between the wall rock and the calcite cement. Therefore, it is now commonly accepted, that the re-opened natural fracture network provides the pathway from the matrix pores to the propped hydraulic fracture and –ultimately- to the wellbore.

Two distinct sets of natural fractures can be distinguished in the Fort Worth Basin, an older north-south–trending set and a main, younger, west-northwest–east-southeast–trending set. Because of the type of cementation in the fractures, fractures act as planes of weakness that can reactivate. The direction of the maximum horizontal stress (S_{Hmax}) in the Fort Worth Basin is northeast-southwest (Figure 5.2).

5.6. Assumptions for All Simulation Cases

Based on the literatures two sets of natural fractures have been considered for DFN simulation purpose in Barnett Shale play. A primary set of natural fracture with azimuth of 115 degrees and tolerance of 2.5 degrees which we call it SET-1 and a secondary set of natural fracture in N-S direction (azimuth of zero degrees) and we call this SET-2.

The directions of the two sets of natural fractures are fixed for all simulation cases in this study. Some fracture specifications that may change case by case are:

- Natural fracture length
- Natural fracture aperture
- Density of natural fracture center points
- Number of hydraulic fracture stages
- Spacing of the hydraulic fractures

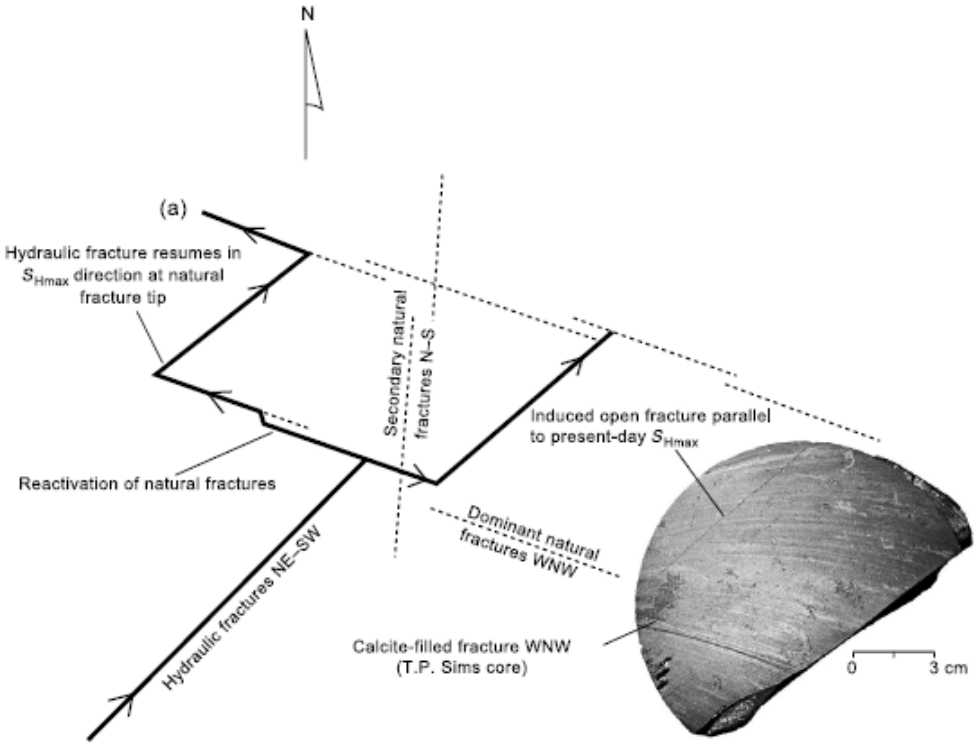

Figure 5.2—Hydraulic fracture growth proceeds northeast-southwest and reactivates natural fractures (dashed lines) trending west-northwest– east-southeast and north-south. Arrows indicate the propagation direction of hydraulic fractures (Gale et al., 2007).

All natural fractures were stochastically generated by choosing Model 1 in FRACGEN. It generates randomly located fractures and because of the stochastic nature of the fracture generation, each realization of the FRACGEN for the same data set will be different. All simulations are assumed to be under 500 psi constant bottomhole pressure.

5.7. General Trend Based on Published Parameters for Barnett Shale

Published parameters from Valko and Lee (2010) have been used to first investigate the compatibility of the SEDM behavior in Barnett Shale gas wells with DFN concept. These SEDM parameters are n=0.247, τ=24 days, and an average initial rate of q_0=1667

MSCF/D based on average Barnett Shale gas wells rate. This parameters yield to an inflection time of 2188 days.

5.7.1. Case 1: Single Layer Reservoir Simulation

As a first step, we attempted to reproduce the behavior computed by the SEDM model with a single layer model. Table 5.1 shows reservoir properties that have been used for this simulation.

Table 5.1—Reservoir parameters for simulating published SEDM parameters in Barnett Shale for case-1.

Parameter	Value
Wellbore Radius (ft)	0.3
Wellbore Lateral Length (ft)	2900
Depth (ft)	7500
Pay Zones Thickness (ft)	250
Reservoir Pressure (psi)	2040
Gas Specific Gravity	0.6
Temperature (F)	285
BHFP (psi)	500
Reservoir Size (ft)	3000×800
Reservoir Permeability (nd)	50
Reservoir Porosity (%)	3

Table 5.2 summarizes the expected fracture parameters for Barnett Shale that have been used to generate the fracture network consisting SET-1 and SET-2 natural fracture sets and also 8 hydraulic fractures for Case-1.

Table 5.2—Fractures parameters for simulating published SEDM parameters in Barnett Shale for case-1.	
Parameter	**Value**
Number of Hydraulic Fractures	8
Hydraulic Fractures Spacing (ft)	400
Hydraulic Fractures Length (ft)	600
Hydraulic Fractures Aperture (ft)	0.0800E-03
SET-1 Length (ft)	200
SET-2 Length (ft)	200
SET-1 Aperture (ft)	0.100E-05
SET-2 Aperture (ft)	0.800E-05
SET-1 Density (ft/ft^2)	0.00002
SET-2 Density (ft/ft^2)	0.00002

Figure 5.3 depicts the stochastically generated natural fractures in FRACGEN and also induced hydraulic fractures based on the fracture data in Table 2.

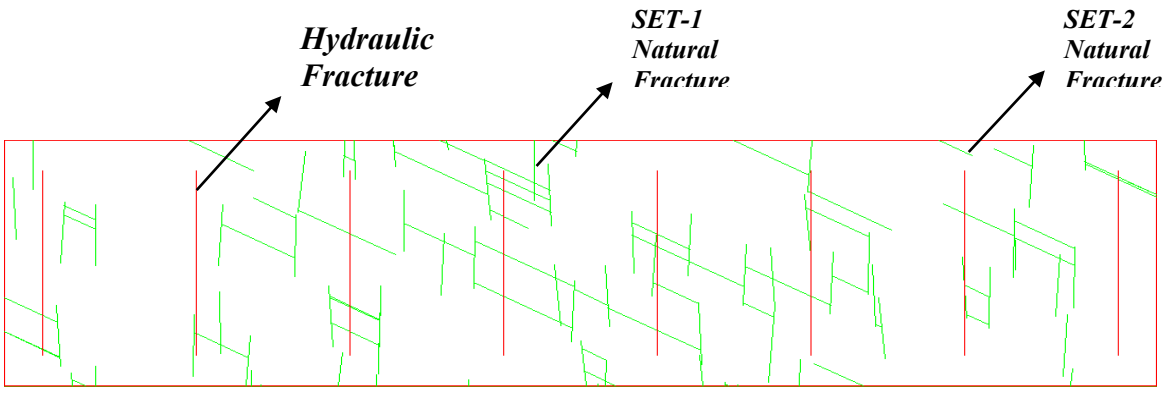

Figure 5.3—Stochastically generated natural fractures SET-1 & SET-2 and induced hydraulic fractures.

After feeding the result of the FRACGEN as an input file to the NFflow, this decline behavior of the single layer reservoir was simulated for 4020 days (almost 11 years) and under 500psi constant bottomhole pressure. Figure 5.4 compares the results from the simulation and the SEDM. As it can be seen in the plot simulation results overestimates the initial gas rate. Simulation yields first month rate of 862 MCF/D *vs.* SEDM first month rate of 579 MCF/D.

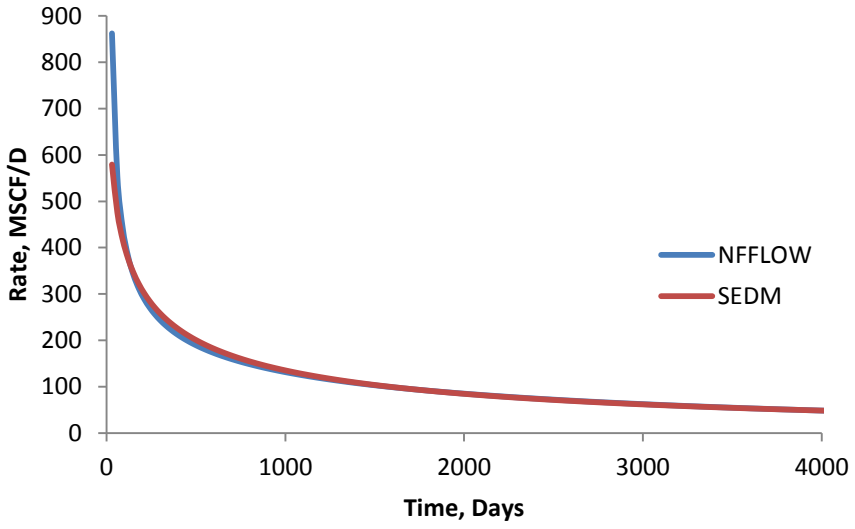

Figure 5.4—Case-1: Rate *vs.* time for NFflow simulation and SEDM.

The difference between early time decline behaviors of the two models is more apparent in the *log (q) vs.* cumulative plot (Figure 5.5). Different fracture parameters and also reservoir parameters have been tried to get a better match, but Figure 5.5 is the best match could be obtained based on single layer reservoir model. For the first 9 months

there is an over prediction of the simulation results for produced gas. Also the simulation resulted in an inflection time of 1650 days *vs.* 2188 for the SEDM.

Some of the observations from these simulations are:

1) The lower matrix permeability is the higher decline in rate will occur at the beginning period of the production.
2) Early Production and initial rate depend on the number of natural of fractures intersect wellbore, their permeability, and lengths.

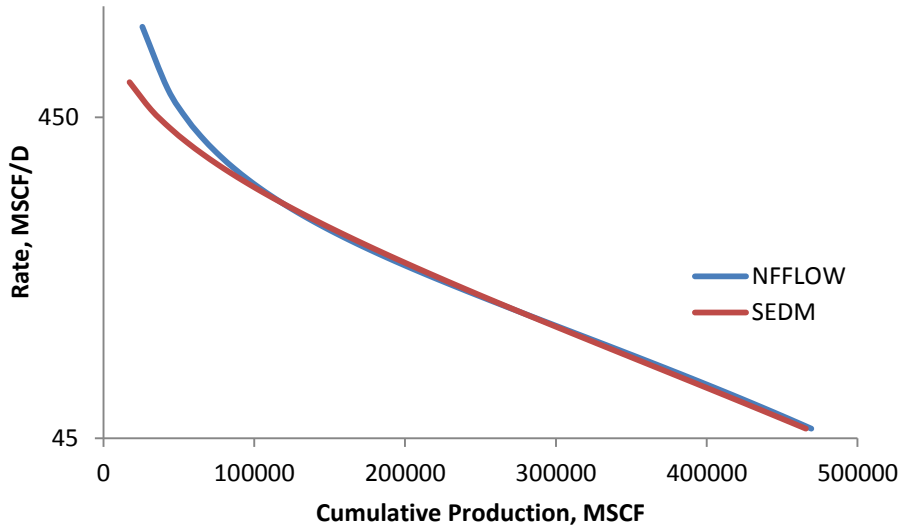

Figure 5.5—Case-2.1: *log (q) vs.* cumulative for NFflow simulation and SEDM.

For mid-period to late-production:

- The number of natural fractures intersecting by Wellbore has less effect on the production decline.
- Created network of fracture and how induced hydraulic fractures connected natural fractures to the wellbore will have a major impact on the decline.
- Reservoir press does not change inflection time
- Increasing Porosity increases inflection time

Next, to further understand the effect of reservoir heterogeneity on the SEDM behavior and inflection time location multiple layer reservoirs have been investigated. For this purpose a different combination of 2-Layer and 3-Layer reservoir (Figure 5.6) with different reservoir and fracture properties have been simulated to get the best fit for our SEDM model based on published parameters for SEDM.

Figure 5.6—Schematic of 2-Layer (left) and 3-Layer (right) reservoir setting used for simulation.

5.7.2. Case 2.1: 2-Layer Reservoir Simulation

Table 5.3 shows reservoir properties that have been used for this simulation.

Table 5.3—Reservoir parameters for simulating published SEDM parameters in Barnett Shale for case-2.1.

Parameter	Value
Wellbore Radius (ft)	0.3
Wellbore Lateral Length (ft)	1400
Depth of L1 (ft)	7500
L1 Thickness (ft)	30
L2 Thickness (ft)	200
Reservoir Pressure (psi)	2100
Gas Specific Gravity	0.6
Temperature (F)	285
BHFP (psi)	500
Reservoir Size (ft)	1500×800
L1 Permeability (nd)	270
L2 Permeability (nd)	25
L1 Porosity (%)	7.7
L2 Porosity (%)	3.5

Table 5.4 summarizes the expected fracture parameters for Barnett Shale that have been used to generate the fracture network consisting SET-1 and SET-2 natural fracture sets for both layers and also 8 hydraulic fractures for Case-2.1. For this simulation case the same fracture properties have been considered for both L1 and L2 layers.

Table 5.4—Fractures parameters for simulating published SEDM parameters in Barnett Shale for case-2.1	
Parameter	**Value**
Number of Hydraulic Fractures	4
Hydraulic Fractures Spacing (ft)	400
Hydraulic Fractures Length (ft)	600
Hydraulic Fractures Aperture (ft)	0.1E-03
SET-1 Length (ft)	200
SET-2 Length (ft)	200
SET-1 Aperture (ft)	0.265E-04
SET-2 Aperture (ft)	0.515E-04
SET-1 Density (ft/ft^2)	0.00004
SET-2 Density (ft/ft^2)	0.00004

Figure 5.7 depicts the stochastically generated natural fractures in FRACGEN and also induced hydraulic fractures based on the fracture data in Table 5.4 for L1 and L2 layers for case-2.1.

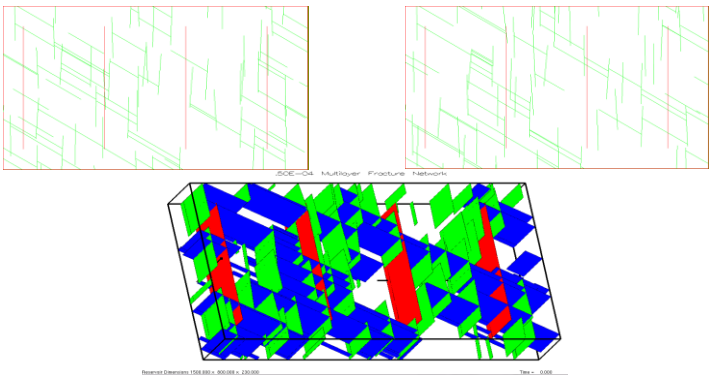

Figure 5.7—Stochastically generated natural fractures SET-1 & SET-2 and induced hydraulic fractures for L1 (left), L2 (right), and fracture network (bottom) for Case-2.1.

Figure 5.8 shows decline behavior of the 2-Layer reservoir that was simulated for 4020 days (almost 11 years) and under 500psi constant bottomhole pressure based on L1 and L2 generated with FRACGEN. This 2-Layer simulation gives a much closer initial rate compared to single-layer reservoir and yields a first month rate of 639 MCF/D *vs.* SEDM first month rate of 579 MCF/D.

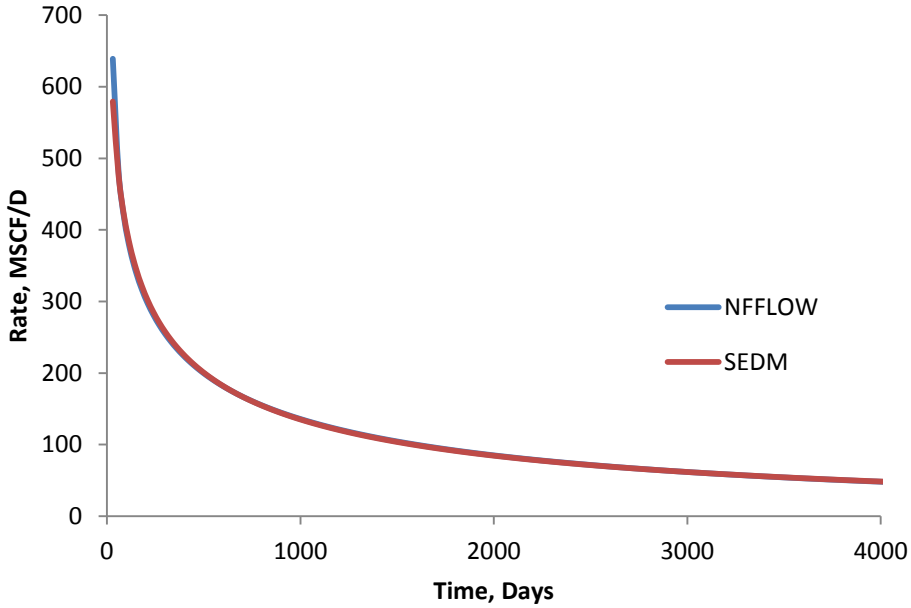

Figure 5.8—Case-2.1: Rate *vs.* time for NFflow simulation and SEDM.

Also, the discrepancy in early time decline behaviors of the two models is much less in the *log (q) vs.* cumulative plot (Figure 5.9) and it is only the first 2 months compared to 9 months for the single-layer case. This results in a closer inflection time to the SEDM for 2-Layer model which is 1860 days.

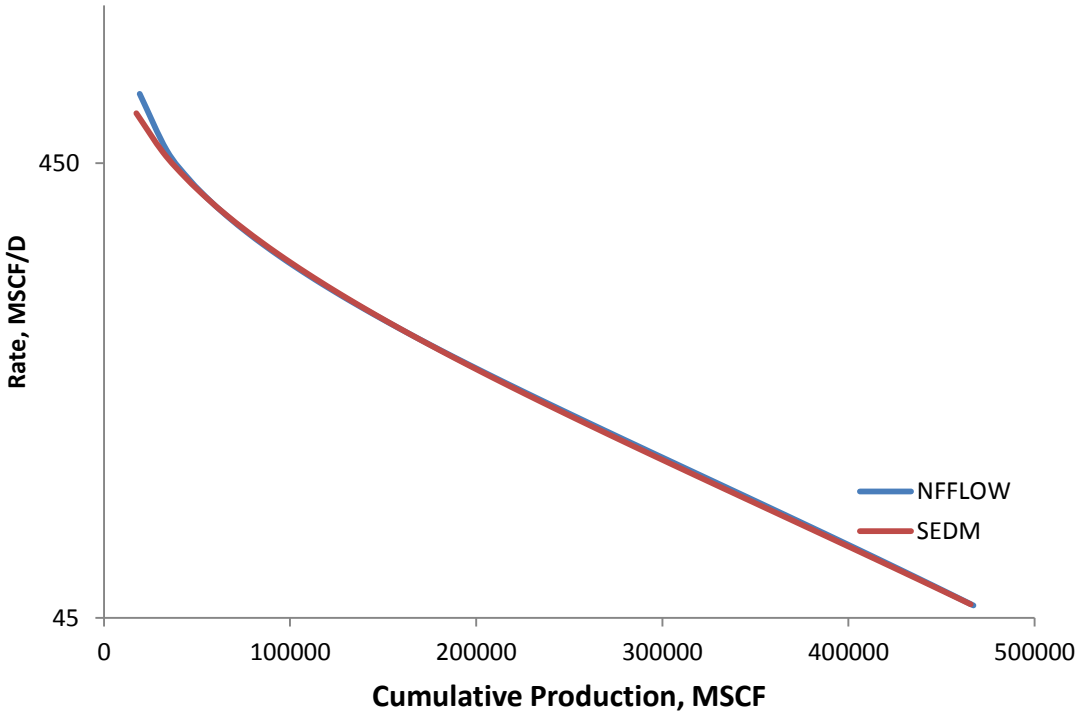

Figure 5.9—Case-2.1: *log (q) vs.* cumulative for NFflow simulation and SEDM.

To better understand how different realizations of created fracture network from FRACGEN with the same input data can affect the decline behavior of the simulated reservoir in Case-2.1, 10 different realizations of L1 and L2 have been simulated with NFflow. Figure 5.10 compares the *log (q) vs.* cumulative for these 10 realizations. These results show that even if all fracture and reservoir parameters are fixed the decline behavior can considerably change for different stochastic realization of the fracture network. This provides a physically sound explanation to the variability of individual well responds, even if geological settings and completion details are very similar.

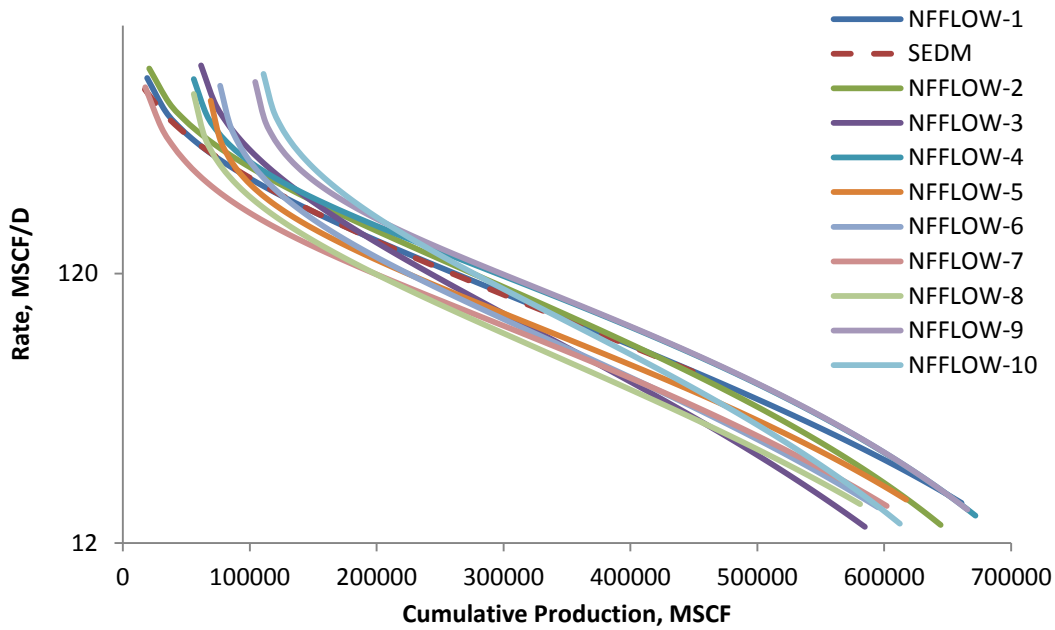

Figure 5.10—Case-2.1: *log (q) vs.* cumulative for NFflow simulation and SEDM for 10 different realization of L1 and L2 from FRACGEN.

Figure 5.11 shows EUR $_{30\text{-years}}$ for these 10 different realizations changes between 0.58 and 0.67 BSCF compared to the EUR $_{SEDM,\ 30\text{-years}}$ of 0.66 BSCF.

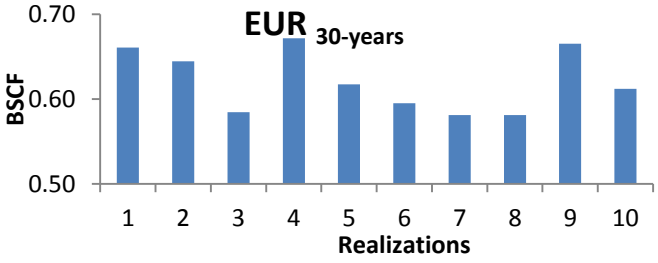

Figure 5.11—Case-2.1: EUR $_{30\text{-years}}$ for 10 different realizations of L1 and L2.

Inflection time for all of the realizations is between 1170 to 2430 days (Figure 5.12).

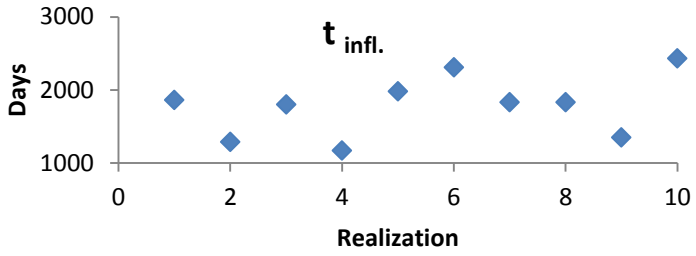

Figure 5.12—Case-2.1: Inflection Time for 10 Different Realizations of L1 and L2.

5.7.3. Case 2.2: 2-Layer Reservoir Simulation with Different Fracture Network Settings

For this simulation case all reservoir parameters are the same as Casse-2.1. However natural fracture density has been doubled and natural fracture length has been halved to investigate the effect of different fracture network specification on the rate decline behavior. Table 5.5 summarizes the fracture parameters used in this simulation case.

Table 5.5—Fractures parameters for simulating published SEDM parameters in Barnett Shale for case-2.2.

Parameter	Value
Number of Hydraulic Fractures	4
Hydraulic Fractures Spacing (ft)	400
Hydraulic Fractures Length (ft)	600
Hydraulic Fractures Aperture (ft)	0.1E-03
SET-1 Length (ft)	100
SET-2 Length (ft)	100
SET-1 Aperture (ft)	0.3500E-04
SET-2 Aperture (ft)	0.5700E-04
SET-1 Density (ft/ft^2)	0.00008
SET-2 Density (ft/ft^2)	0.00008

Figure 5.13 depicts the stochastically generated natural fractures in FRACGEN and also induced hydraulic fractures based on the fracture data in Table 5.5 for L1 and L2 layers for case-2.2.

Using L1 and L2 from case2.2, decline behavior of the 2-Layer reservoir model was simulated for 4020 days (almost 11 years) and under 500 psi constant bottomhole pressures.

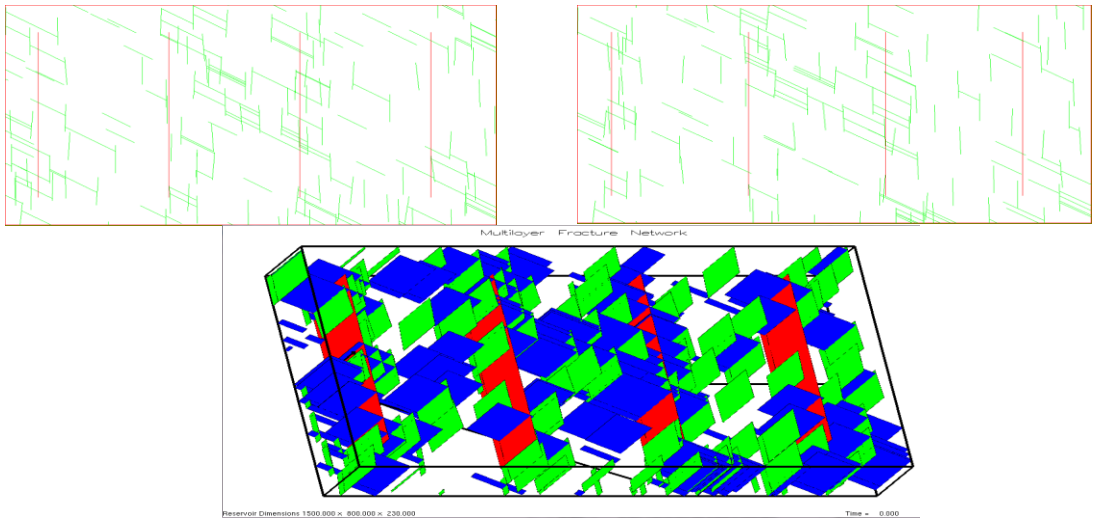

Figure 5.13—Stochastically generated natural fractures SET-1 & SET-2 and induced hydraulic fractures for L1 (left), L2 (right), and fracture network (bottom) for Case-2.2.

This 2-Layer setting which has half-length and twice density compared to case 2.1 yields almost the same first month rate of 634 MCF/D compared to rate of 639 MCF/D for case 2.1 (Figure 5.14).

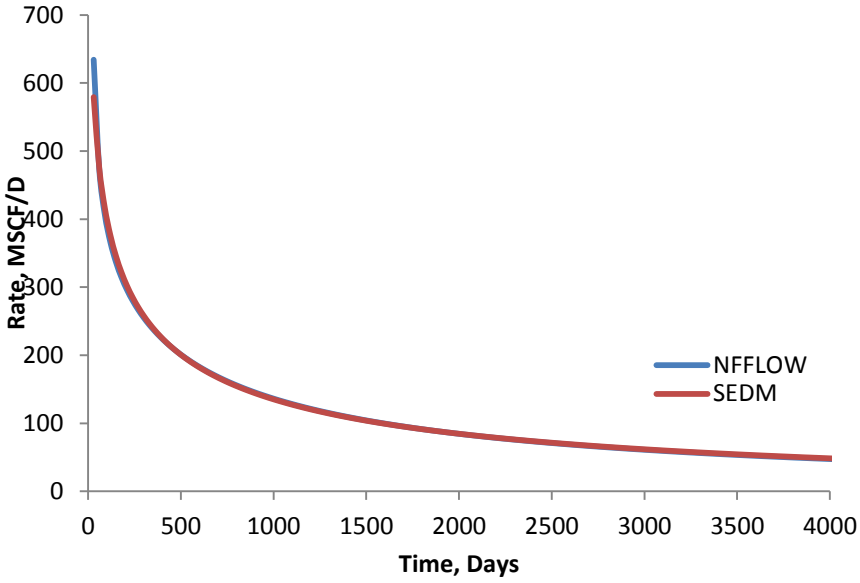

Figure 5.14—Case-2.2: Rate *vs.* time for NFflow simulation and SEDM.

Also inflection time of 1740 days for case-2.2 has been observed in *log (q) vs.* cumulative plot (Figure 5.15) and it is slightly earlier than case2.1 with inflection time of 1860 days. EUR $_{4020\ days}$ of 0.465 BCF for case-2.2 *vs.* EUR $_{4020\ days}$ of 0.467 BCF for cae-2.1 shows that both reservoir settings have the same EUR for 11 years and fracture parameters like density and length are interchangeable, meaning that if we double one and halve the other one the production decline behavior and EUR won't change much and almost stay the same.

With 2-layer model it was not possible to get the exact inflection time as SEDM inflection time based on published SEDM parameters. Therefore a 3-layer reservoir model was considered to investigate the effect of the number of reservoir layers (or different created fractured zones) on the SEDM behavior and inflection time location.

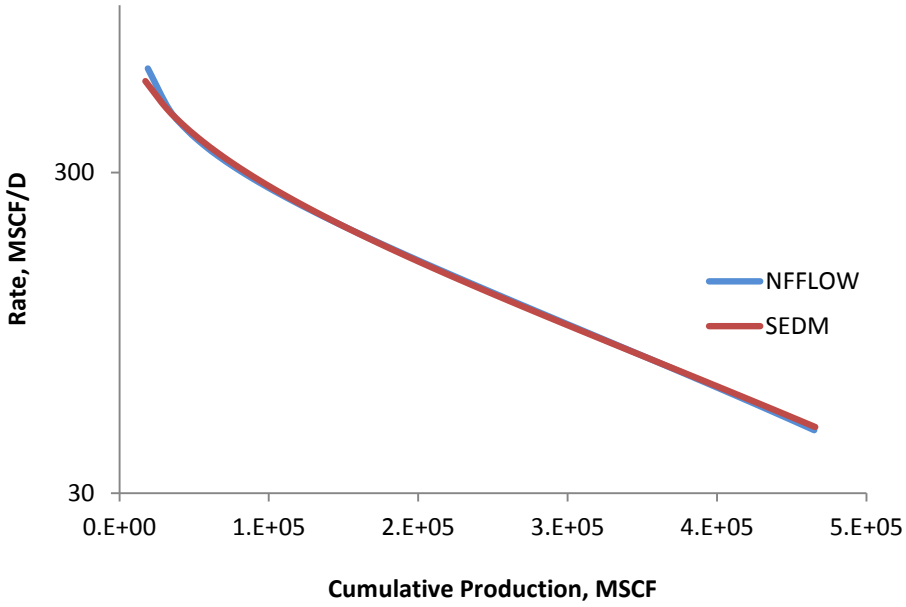

Figure 5.15—Case-2.2: *log (q) vs.* cumulative for NFflow simulation and SEDM.

To do this two different 3-Layer reservoir settings (Figure 5.6) were simulated to get the best fit for our SEDM model based on published SEDM parameters, which will be discussed in case3.1 and 3.2.

5.7.4. Case 3: 3-Layer Reservoir Simulation

Table 5.6 summarizes the expected fracture and reservoir parameters for Barnett Shale that have been used to generate the fracture network consisting SET-1 and SET-2 natural fracture sets for the three layers and also 8 hydraulic fractures for Case-3. All fracture parameters stayed the same except the natural fracture apertures for SET-1 and SET-2. Again, the same fracture properties have been considered for all L1 and L2, and L3 layers in this simulation case also.

Table 5.6—Input parameters and assumptions for simulating published SEDM parameters in Barnett Shale for case-3.	
WELLBORE DATA	
Tubing ID, inches	4.5
Pipe Roughness Factor	0.0008691
Wellhead Temperature, ℉	45.0
Bottomhole Flowing Pressure, psi	500.0
Wellbore Radius, ft.	0.3
Wellbore Lateral length, ft.	2900.0
FRACTURE NETWORK SPECIFICATIONS	
Total Number of Fractures	386
SECONDARY NATURAL FRACTURE (SET-1)	
Mean and SDEV of Fracture Orientation, Degrees	120.0, 0.0
Fracture Length Distribution	Uniform
Fracture Length	200.0
Fracture Aperture, ft.	0.273E-04
Density of Fracture Center Points	0.00004
Relative Frequencies of T-Terminations (T2,T1)	70, 0
PRIMARY NATURAL FRACTURE (SET-2)	
Mean and SDEV of Fracture Orientation, Degrees	0.0, 2.5
Fracture Length Distribution	Uniform
Fracture Length	200.0
Fracture Aperture, ft.	0.470E-04
Density of Fracture Center Points	0.00004
Relative Frequencies of T-Terminations (T2,T1)	50, 0
INDUCED HYDRAULIC FRACTURE	
Number of Hydraulic Fractures	4
Hydraulic Fractures Spacing, ft.	400
Hydraulic Fractures Length, ft.	600
Hydraulic Fractures Aperture, ft.	0.1E-03
RESERVOIR DESCRIPTION	
Reservoir Length, ft.	1500.0
Reservoir Width, ft.	800.0
Simulated Productive Volume, ft^3	0.126109E+08
Effective Depth of mid-Layer (L2), ft.	74350.0
Effective thickness of mid-Layer (L2), ft.	30.0
Permeability of mid- Layer (L2), nano-darcy	300
Porosity of mid- Layer (L2), %	6.7
Effective thickness of Bounding Layers (L1&L3), ft.	100.0
Permeability of Bounding Layers (L1&L3), nano-darcy	10
Porosity of Bounding Layers (L1&L3), %	4.25
Initial Pressure, psi	2250.0
Reservoir Temperature, ℉	320.0
Gas Specific Gravity (air = 1.0)	0.6
Pseudo-critical Temperature (Rankine)	351.0
Pseudo-critical Pressure (psia)	673.0
Pore Volume, MMCF	12.6109
Initial Volume Factor, $MSCF/ft.^3$	0.11256
Initial Gas in Place, BSCF	1.41946

Figure 5.16 shows stochastically generated natural fractures in FRACGEN and also induced hydraulic fractures based on the fracture characterization in Table 5.6 for L1, L2, and L3 layers for case-3. Also it has been assumed that 50% of the SET-1 and SET-2

fractures are allowed to penetrate from L1 to L2 and from L2 to L3. A correlation between penetrating fractures and length of fractures has been considered, meaning that the loner the fracture is the more chance it has to penetrate to the overlying layer.

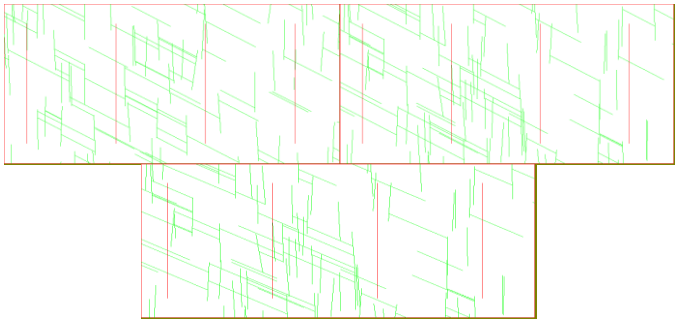

Figure 5.16—Stochastically generated natural fractures SET-1 & SET-2 and induced hydraulic fractures for L1 (left), L2 (right), and L3 (bottom) for Case-3.

Figure 5.17 shows the fracture network consisting of L1, L2, and L3 and also 4 induced hydraulic fractures.

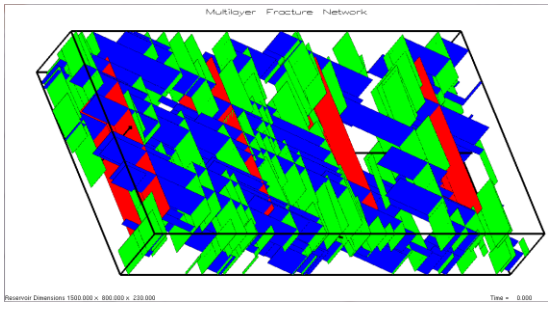

Figure 5.17—Stochastically generated fracture network for Case-3.

Using L1, L2, and L3 from case3, decline behavior of the 3-Layer reservoir model was simulated for 4020 days (Figure 5.18) and under 500 psi constant bottomhole pressures. This 3-Layer setting, yields a first month rate of 658 MCF/D compared to the rate of 579 MCF/D for SEDM. Also inflection time of 2160 days for case-3 has been observed in *log (q) vs.* cumulative plot (Figure 5.19) and it is very close to the SEDM inflection time of 2188 days.

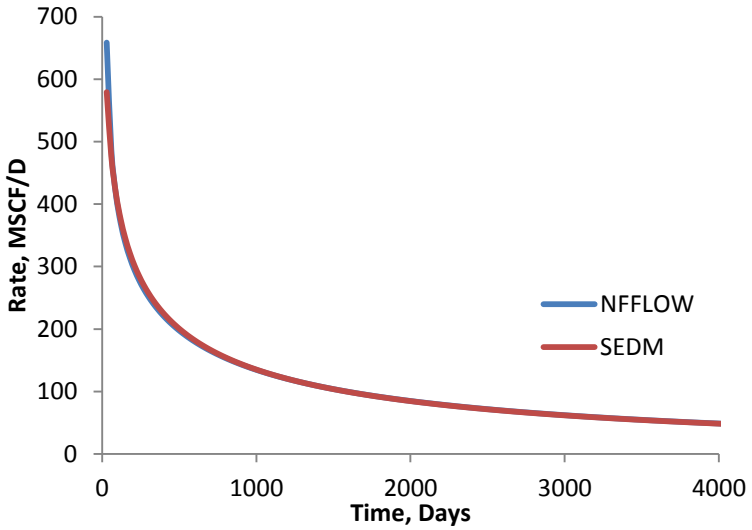

Figure 5.18—Case-3: Rate *vs.* time for NFflow simulation and SEDM.

EUR $_{4020\ days}$ of 0.465 BCF for case-2.2 *vs.* EUR $_{4020\ days}$ is the exactly the same for both SEDM and case-3 simulation with the value of 0.466 BCF. Results from this case shows that at least 3-layer model (or 3 different zones of fracture network) is required to have the same inflection time location and decline behavior for published SEDM parameters.

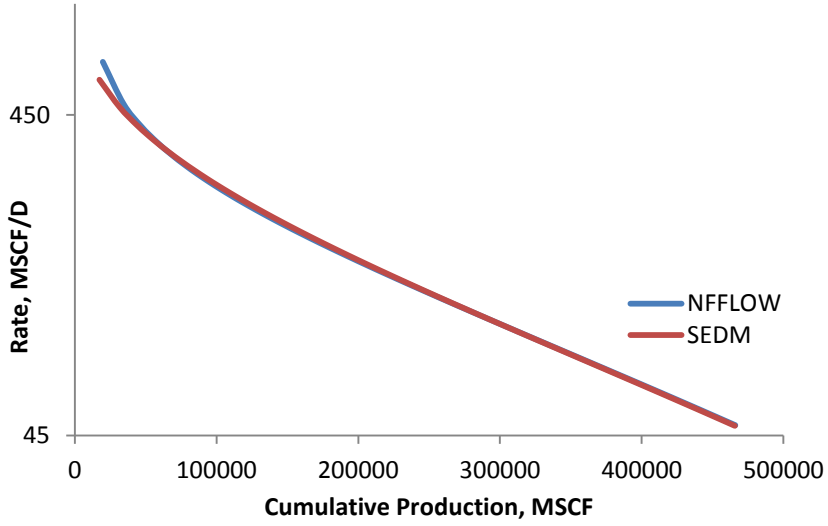

Figure 5.19—Case-3: *log (q) vs.* cumulative for NFflow simulation and SEDM.

Some of the observations from DFN simulations for multiple-layered reservoir are:

- Some parameters like Fracture density and fracture length are interchangeable.
- Keeping all parameters fixed and just comparing 10 realizations shows how reserve estimation can be tricky in reservoirs which main production comes from network of natural and enhanced fractures.
- In 3-layer model fracture aperture has the dominant effect on early time concavity.
- Porosity of the top and bottom layers (L1 and L3) has the dominant effect on late time decline shape.

Since compatibility of published SEDM parameters with DFN modeling has been confirmed in previous cases, the applicability of DFN modeling in real field cases can be

examined. In the next sections this approach will be applied to several Barnett Shale gas horizontal wells and then the results will be compared with the estimated SEDM parameters for the same wells.

5.8. Case Studies

5.8.1. Case-4: WELL#5

This is a horizontal well located in Johnson County. Table 5.7 summarizes the reservoir parameters and fracture specifications that were used to simulate the decline behavior of WELL#5 with NFflow. A daily production rate data for 1359 days was available for this well that was used in the simulation. The fracture network consists of SET-1 and SET-2 natural fracture sets for the three layers and also 21 hydraulic fractures for WELL#5.

Table 5.7—Input parameters and assumptions used to simulate decline behavior of WELL#5 for case-4.	
WELLBORE DATA	
Tubing ID, inches	4.5
Pipe Roughness Factor	0.0008691
Wellhead Temperature, F	45.0
Bottomhole Flowing Pressure, psi	500.0
Wellbore Radius, ft.	0.3
Wellbore Lateral length, ft.	3420.0
FRACTURE NETWORK SPECIFICATIONS	
Total Number of Fractures	386
SECONDARY NATURAL FRACTURE (SET-1)	
Mean and SDEV of Fracture Orientation, Degrees	120.0, 0.0
Fracture Length Distribution	Uniform
Fracture Length	200.0
Fracture Aperture, ft.	0.35E-04
Density of Fracture Center Points	0.00004
Relative Frequencies of T-Terminations (T2,T1)	70, 0
PRIMARY NATURAL FRACTURE (SET-2)	
Mean and SDEV of Fracture Orientation, Degrees	0.0, 2.5
Fracture Length Distribution	Uniform
Fracture Length	200.0
Fracture Aperture, ft.	0.50E-04
Density of Fracture Center Points	0.00004
Relative Frequencies of T-Terminations (T2,T1)	50, 0
INDUCED HYDRAULIC FRACTURE	
Number of Hydraulic Fractures	21
Hydraulic Fractures Spacing, ft.	151
Hydraulic Fractures Length, ft.	600
Hydraulic Fractures Aperture, ft.	0.1E-03
RESERVOIR DESCRIPTION	
Reservoir Length, ft.	3420.0
Reservoir Width, ft.	800.0
Simulated Productive Volume, ft^3	0.317360E+08
Effective Depth of mid-Layer (L2), ft.	7040.0
Effective thickness of mid-Layer (L2), ft.	120.0
Permeability of mid- Layer (L2), nano-darcy	90
Porosity of mid- Layer (L2), %	3.0
Effective thickness of Bounding Layers (L1&L3), ft.	200.0
Permeability of Bounding Layers (L1&L3), nano-darcy	20
Porosity of Bounding Layers (L1&L3), %	2.0
Initial Pressure, psi	3115.0
Reservoir Temperature, F	285.0
Gas Specific Gravity (air = 1.0)	0.6
Pseudo-critical Temperature (Rankine)	351.0
Pseudo-critical Pressure (psia)	673.0
Pore Volume, MMCF	31.7360
Initial Volume Factor, $MSCF/ft.^3$	0.10264
Initial Gas in Place, BSCF	3.25746

The completion for this well consisted of 3 stages slickwater fracturing that all completed before the first day of production. The horizontal section of the wellbore is 3420 ft. Each stimulation job covered 905 ft. of the horizontal section and accounts for 7

hydraulic fractures with spacing of 151 ft. The spacing between these three stimulation intervals is 299 ft (Figure 5.20).

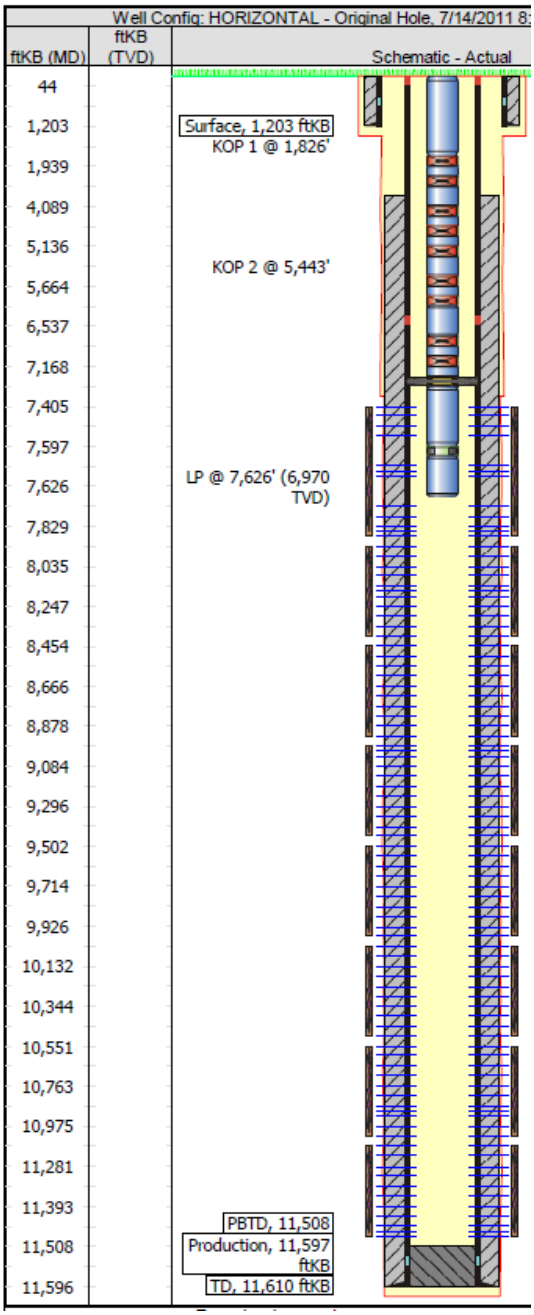

Figure 5.20—Wellbore diagram for WELL#5 horizontal gas well in Barnett Shale.

Again, it has been assumed that 50% of the SET-1 and SET-2 fractures are allowed to penetrate from L1 to L2 and from L2 to L3 with a correlation between penetrating fractures and length of fractures.

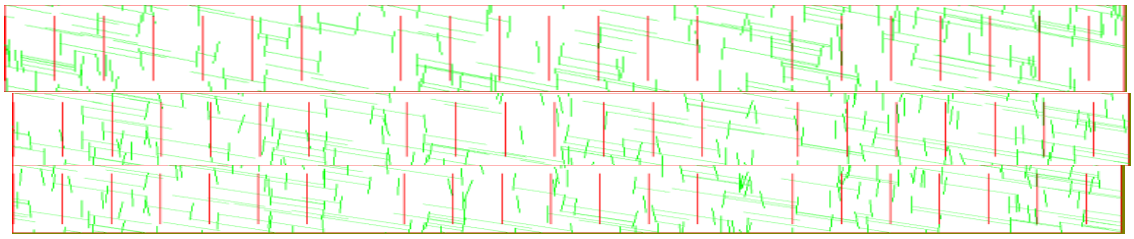

Figure 5.21—Stochastically generated natural fractures SET-1 & SET-2 and induced hydraulic fractures for L1 (top), L2 (midle), and L3 (bottom) for WELL#5.

Figure 5.22 compares the results of DFN simulation based on the expected fracture characteristics of Barnett Shale and also known reservoir parameters for WELL#5 horizontal well and for 30 years of production. The simulation resulted in a 15th day production rate of 4788 MCF/D versus 4035 MCF/D for the actual production for WELL#5.

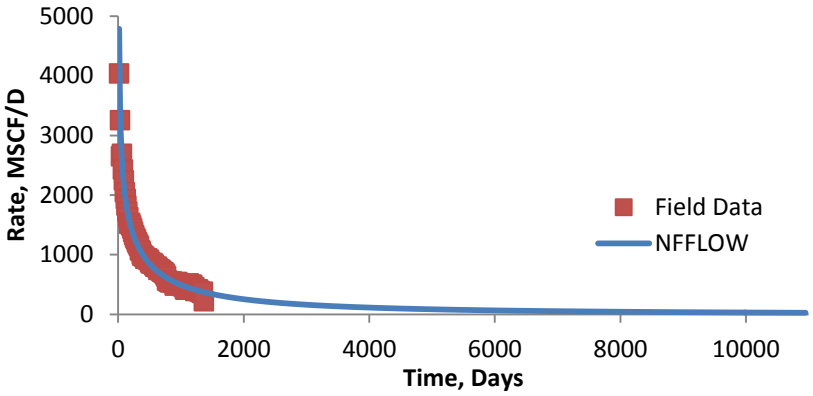

Figure 5.22—Rate *vs.* time based on NFflow simulation for WELL#5 and field data.

Table 5.8 compares some of the simulation results from 30 years of production for WELL#5 from NFflow and also SEDM parameter estimation that previously has been done for the same well.

Table 5.8—Estimated parameters and simulation results for WELL#5.

Parameter	SEDM	NFflow
$t_{infl.}$ (days)	474	510
$EUR_{30\text{-years}}$ (BCF)	2.16	2.17
$EUR_{100\text{-MCF}}$ (BCF)	1.84	1.84

An inflection time of 510 days for WELL#5 has been observed in *log (q) vs.* cumulative plot (Figure 5.23) based on NFflow simulation results and it is very close to the SEDM inflection time of 474 days for the same well.

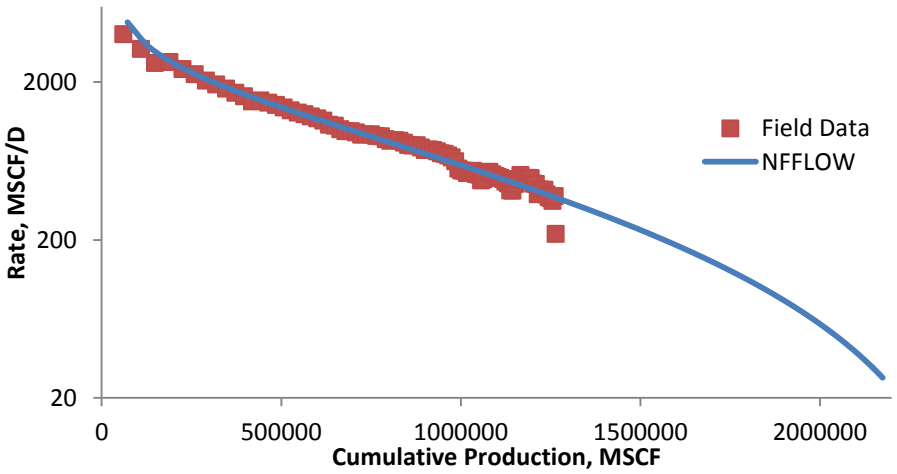

Figure 5.23—*log (q) vs.* cumulative based on NFflow simulation for WELL#5 and field data.

To better understand how different realizations of created fracture network from FRACGEN with the same input data can affect the decline behavior of the simulated reservoir for this well, 10 different realizations of L1, L2, and L3 have been simulated with NFflow. Figure 5.24 compares the *log (q) vs.* cumulative for these 10 realizations. These results indicate why it is needed that some kind of probabilistic reserve estimation should be done for this type of reservoirs to give a range for EUR.

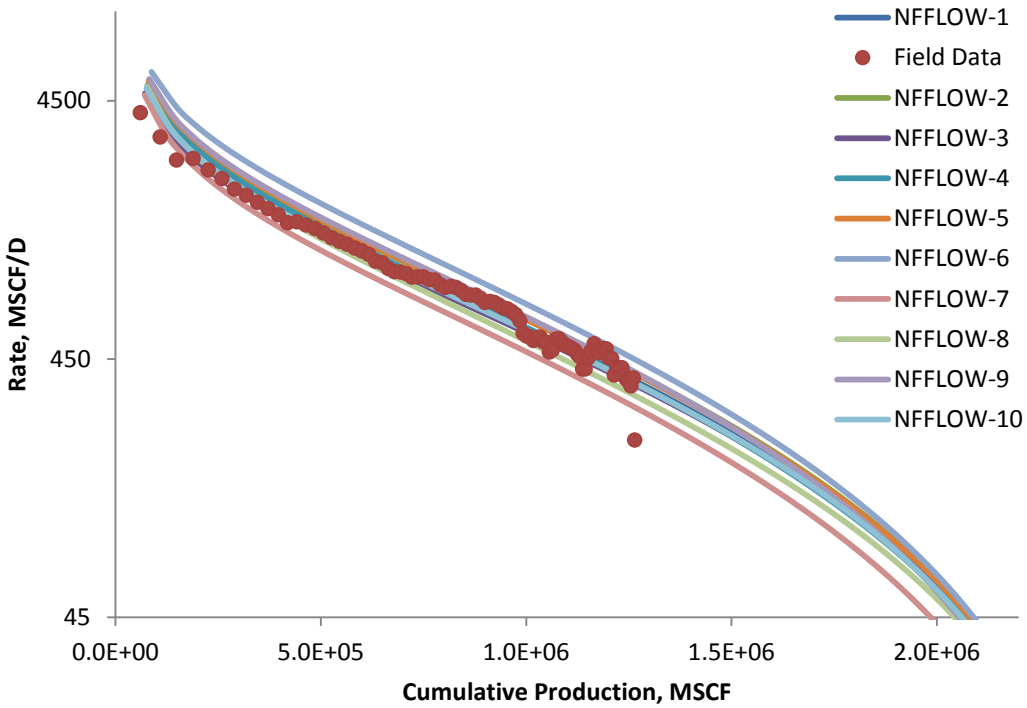

Figure 5.24—*log (q) vs.* cumulative for 10 different realizations of L1, L2, and L3.

Simulation for theses realizations resulted in EUR $_{30\text{-years}}$ of 2.07 to 2.19 BCF (Figure 5.25) compared to the EUR $_{SEDM,30\text{-years}}$ of 2.16 BCF and EUR $_{30,\ SPE134231}$ of 2.96 based on published SEDM parameters for this well.

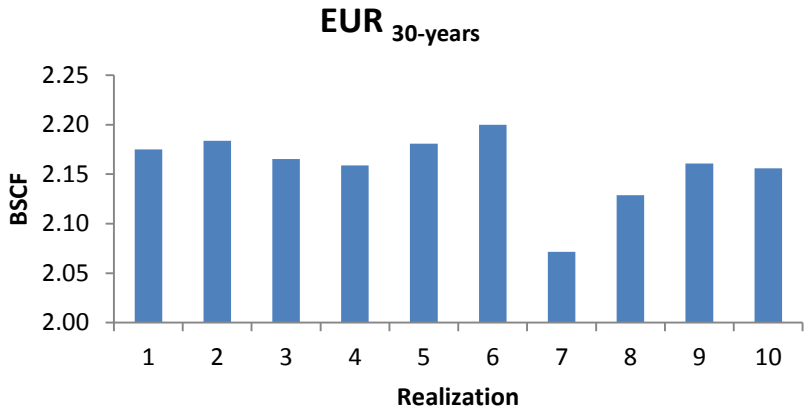

Figure 5.25—EUR $_{30\text{-years}}$ for 10 different realizations of L1, L2, and L3.

Inflection time for these realizations is between 435 and 675 (Figure 5.26).

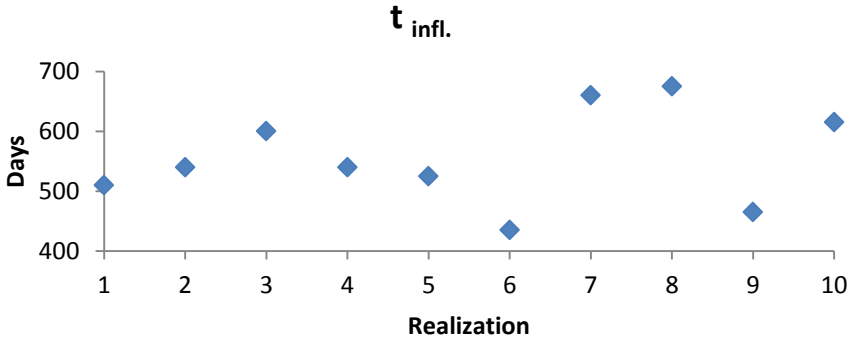

Figure 5.26—Inflection time for 10 different realizations of L1, L2, and L3.

To understand the effect of reservoir depletion degree on simulated decline curve behavior, fracture pressure plots for two extreme cases of NFFLOW-6 (the highest curve

in Figure 5.24) and NFFLOW-7 (the lowest curve in Figure 5.24) have been compared in Figure 5.27.

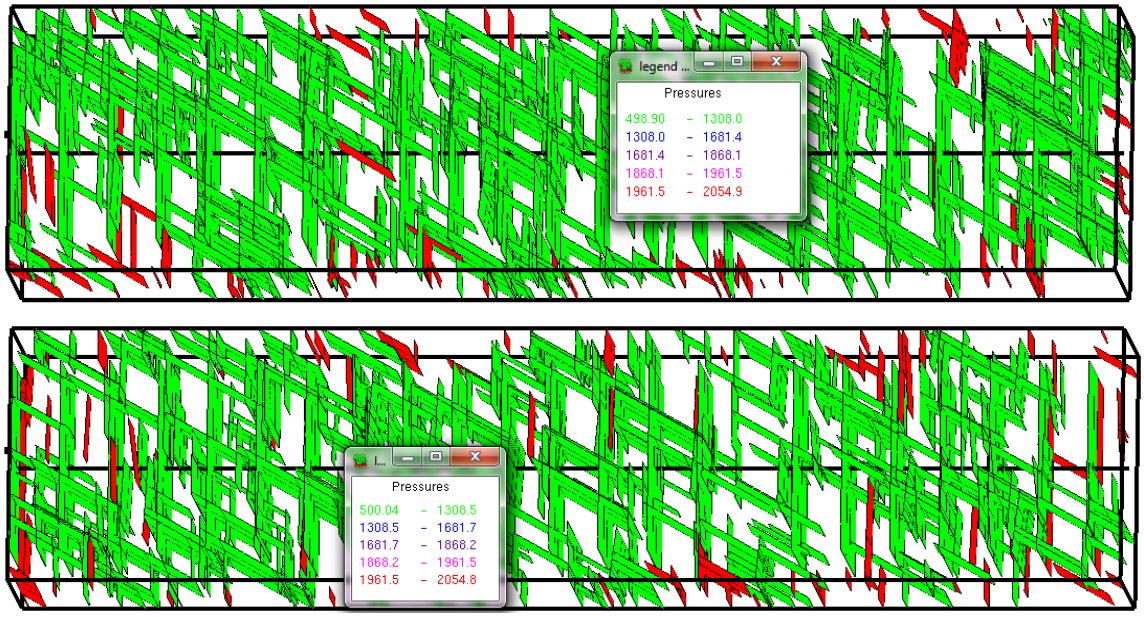

Figure 5.27—Pressure change in the fracture network after 30 years for NFFLOW-6 (top) and NFFLOW-7 (bottom).

After 30 years of production NFFLOW-7 had slightly more untouched pockets (fractures) of gas that were not connected to the main fracture network which yielded a lower $EUR_{30\text{-year}}$ of 2.07 BSCF *vs.* 2.2BSCF for NFFLOW-6. The initial Gas in Place (GIP) for all realizations was 3.25746 BSCF.

A similar simulation for WELL#5 was done with the same reservoir properties except there is no heterogeneity in matrix permeability for three different layers and they all have matrix permeability of 90 nd and fracture parameters were changed as shown in

Table 5.9. The natural fracture lengths have been halved and natural fracture density was doubled. Fracture apertures have changed as below.

Table 5.9—Different fracture parameters used to simulate decline behavior of WELL#5.	
Parameter	**Value**
Number of Hydraulic Fractures	21
Hydraulic Fractures Spacing (ft)	151
Hydraulic Fractures Length (ft)	600
Hydraulic Fractures Aperture (ft)	0.1E-03
SET-1 Length (ft)	100
SET-2 Length (ft)	100
SET-1 Aperture (ft)	0.270E-04
SET-2 Aperture (ft)	0.325E-04
SET-1 Density (ft/ft^2)	0.00008
SET-2 Density (ft/ft^2)	0.00008

As Figure 5.28 shows, the decline behavior did not change too much, except it gave an inflection time of 495 days which is closer to the SEDM inflection time, compared to previous simulation case. $EUR_{30\text{-years}}$ and $EUR_{100\text{-MCF}}$ of 2.13 and 1.81 BCF were obtained which are almost the same as previous simulation case and also SEDM estimation.

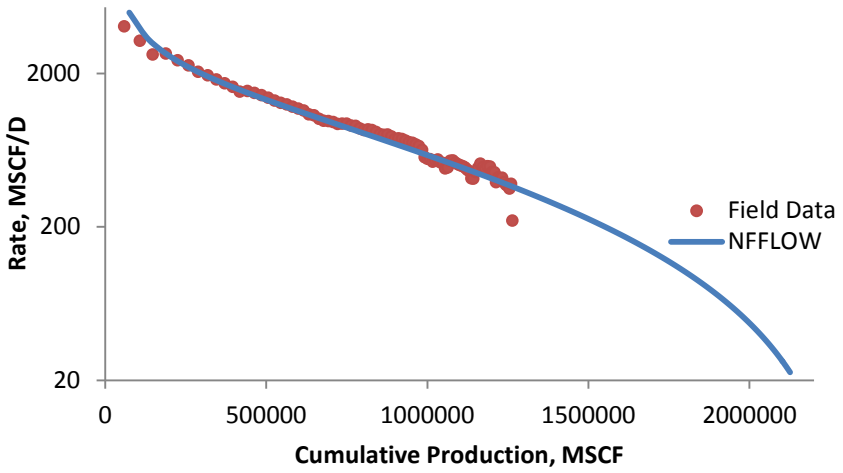

Figure 5.28—*log (q) vs.* cumulative based on second simulation data set for WELL#5.

For this case also 10 different realizations of L1, L2, and L3 have been simulated with NFflow. Figure 5.29 compares the *log (q) vs.* cumulative for these 10 realizations. These results indicate why it is needed that some kind of probabilistic reserve estimation should be done for this type of reservoirs to give a range for EUR.

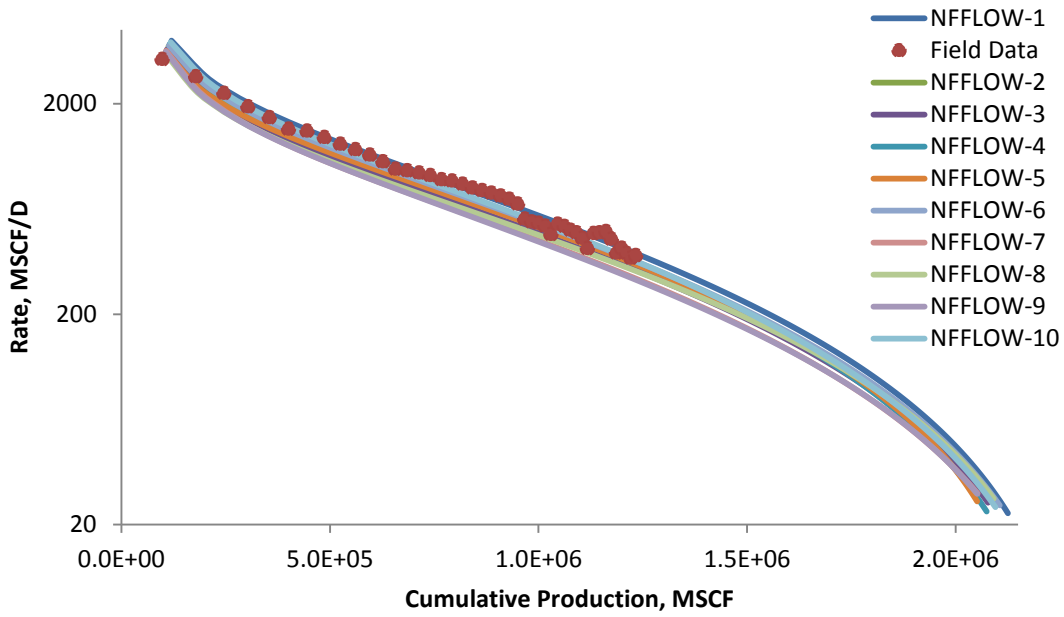

Figure 5.29—*log (q) vs.* cumulative for 10 different realizations of L1, L2, and L3.

Simulation for theses realizations resulted in EUR $_{30\text{-years}}$ of 2.05 to 2.13 BCF (Figure 5.30) compared to the EUR $_{SEDM,30\text{-years}}$ of 2.16 BCF and EUR $_{30,\ SPE134231}$ of 2.96 based on published SEDM parameters for this well.

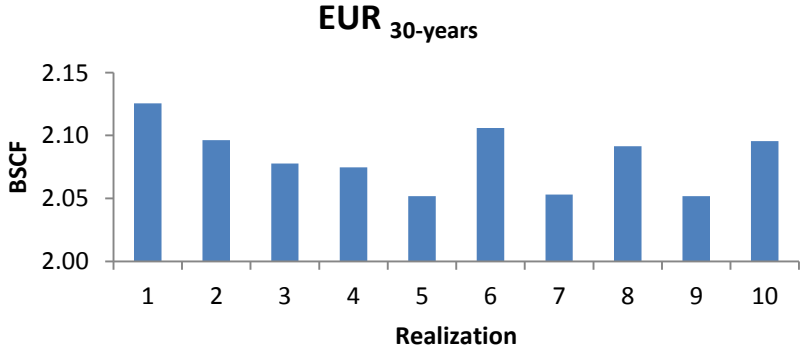

Figure 5.30—EUR $_{30\text{-years}}$ for 10 different realizations of L1, L2, and L3.

Inflection time for these realizations is between 540 and 720 (Figure 5.31).

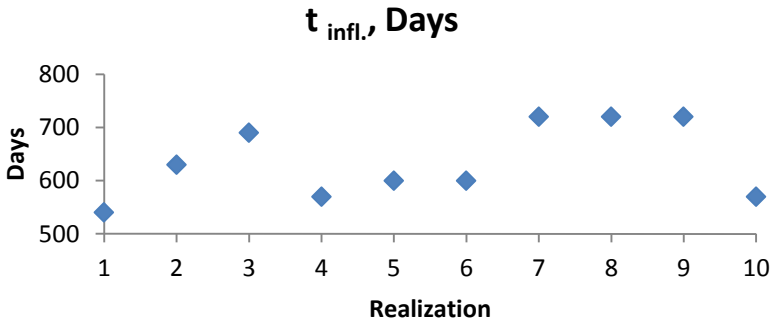

Figure 5.31—Inflection time for 10 different realizations of L1, L2, and L3.

Fracture pressure plots for two extreme cases of NFFLOW-1 (the highest curve in Figure 5.29) and NFFLOW-9 (the lowest curve in Figure 5.29) have been compared in Figure 5.32.

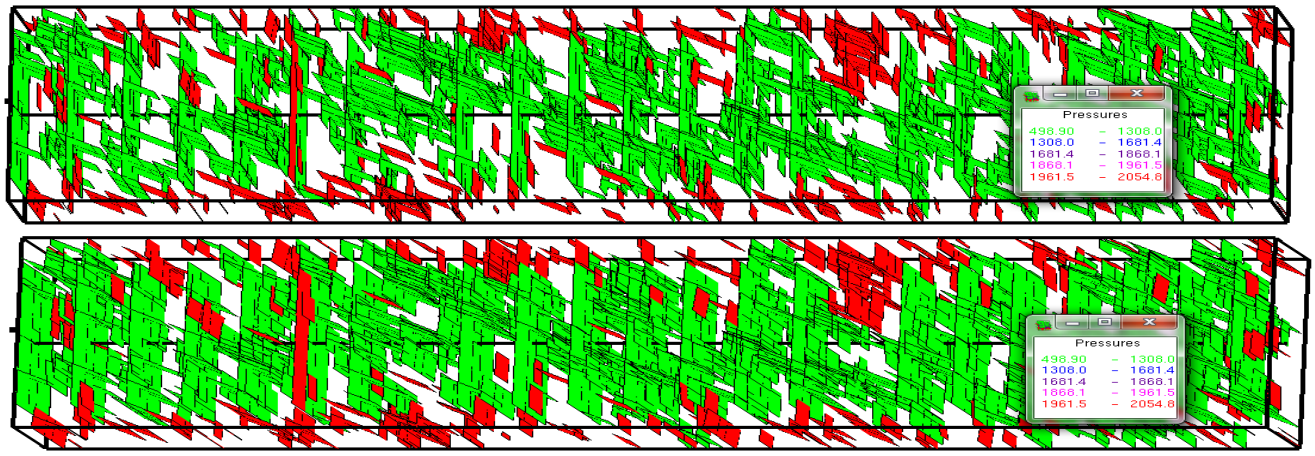

Figure 5.32—Pressure change in the fracture network after 30 years for NFFLOW-1 (top) and NFFLOW-9 (bottom).

After 30 years of production NFFLOW-9 had slightly more untouched pockets (fractures) of gas that were not connected to the main fracture network which yielded a lower $EUR_{30\text{-year}}$ of 2.05 BSCF *vs.* 2.13BSCF for NFFLOW-1. The initial Gas in Place (GIP) for all realizations was 3.20134 BSCF. This setting had slightly less connectivity in the fracture network compared to the previous case.

5.8.2. Case-5: WELL#10

This is a horizontal well located in Tarrant County. Table 5.10 summarizes the reservoir parameters that were used to simulate the decline behavior of WELL#10 with NFflow. The completion for this well consisted of 4 stages slickwater fracturing that all completed before the first day of production. The horizontal section of the wellbore is 4850 ft. Each stimulation job covered 967 ft. of the horizontal section and accounts for 7 hydraulic fractures with spacing of 161 ft. The spacing between these four stimulation intervals is 299 ft (Figure 5.33).

Table 5.10—Reservoir parameters used to simulate decline behavior of WELL#10.	
Parameter	**Value**
Wellbore Radius (ft)	0.3
Wellbore Lateral Length (ft)	4850
Depth of L2 (ft)	8321
L1 Thickness (ft)	230
L2 Thickness (ft)	40
L3 Thickness (ft)	230
L′1 Thickness (ft)	***240***
L′2 Thickness (ft)	***20***
L′3 Thickness (ft)	***240***
Reservoir Pressure (psi)	3578
BHFP (psi)	500
Reservoir Size (ft)	4850×800
L1& L3 Permeability (nd)	1.5
L′1& L′3 Permeability (nd)	***3***
L2 Permeability (nd)	10
L′2 Permeability (nd)	***35***
L1& L3 Porosity (%)	4.0
L′1& L′3 Porosity (%)	***3.0***
L2 Porosity (%)	3.7
L′2 Porosity (%)	***4.7***

A daily production rate data for 926 days was available for this well that was used in the simulation. Two different cases have been considered for DFN simulation of this well. The thicker mid-layer setting was called (L1, L2, and L3) and the thinner mid-layer setting was called (***L'1, L'2, and L'3***).

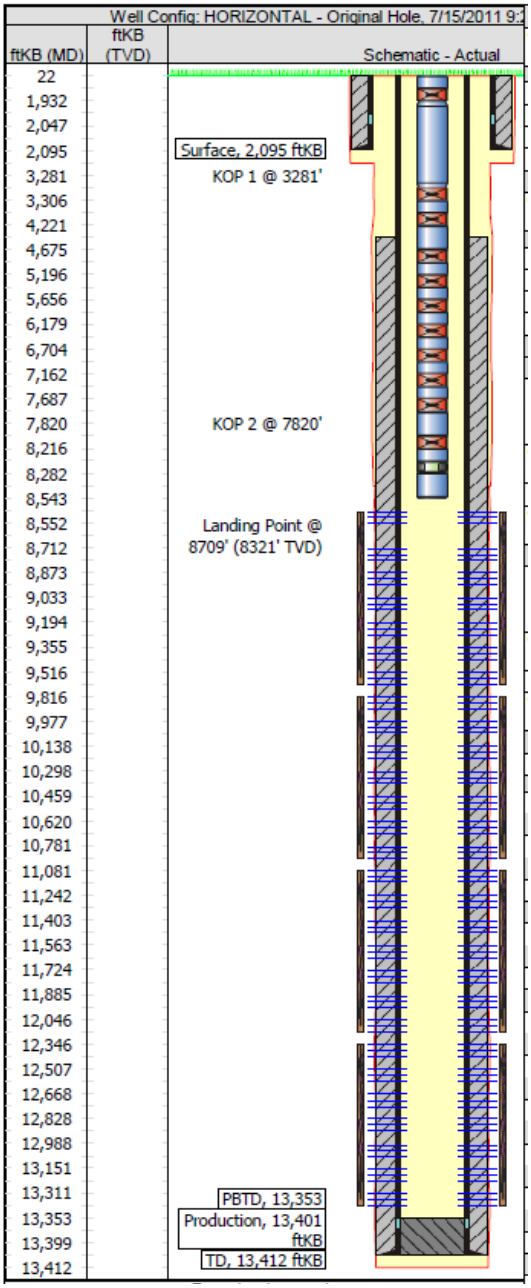

Figure 5.33—Wellbore diagram for WELL#10 horizontal gas well in Barnett Shale.

Table 5.11 summarizes two sets of fracture parameters that have been used to generate the fracture network consisting SET-1 and SET-2 natural fracture sets for the three

layers and also 28 hydraulic fractures for WELL#10. For the thin-mid layer fracture setting the only fracture parameter were changed are natural fracture apertures and they are called ***SET-1'*** and ***SET-2'*** in table 5.11.

Table 5.11—Two sets of fractures used to simulate decline behavior of WELL#10.

Parameter	Value
Number of Hydraulic Fractures	28
Hydraulic Fractures Spacing (ft)	161
Hydraulic Fractures Length (ft)	600
Hydraulic Fractures Aperture (ft)	0.1E-03
SET-1 Length (ft)	100
SET-2 Length (ft)	100
SET-1 Aperture (ft)	0.40E-04
SET-1' Aperture (ft)	***0.60E-04***
SET-2 Aperture (ft)	0.60E-04
SET-2' Aperture (ft)	***0.70E-04***
SET-1 Density (ft/ft^2)	0.00008
SET-2 Density (ft/ft^2)	0.00008

Figure 5.34 compares the results of two different DFN simulations based on the expected fracture characteristics of Barnett Shale and also known reservoir parameters for WELL#10 horizontal well and for 30 years of production. From this plot there is not much difference between the two different simulation cases.

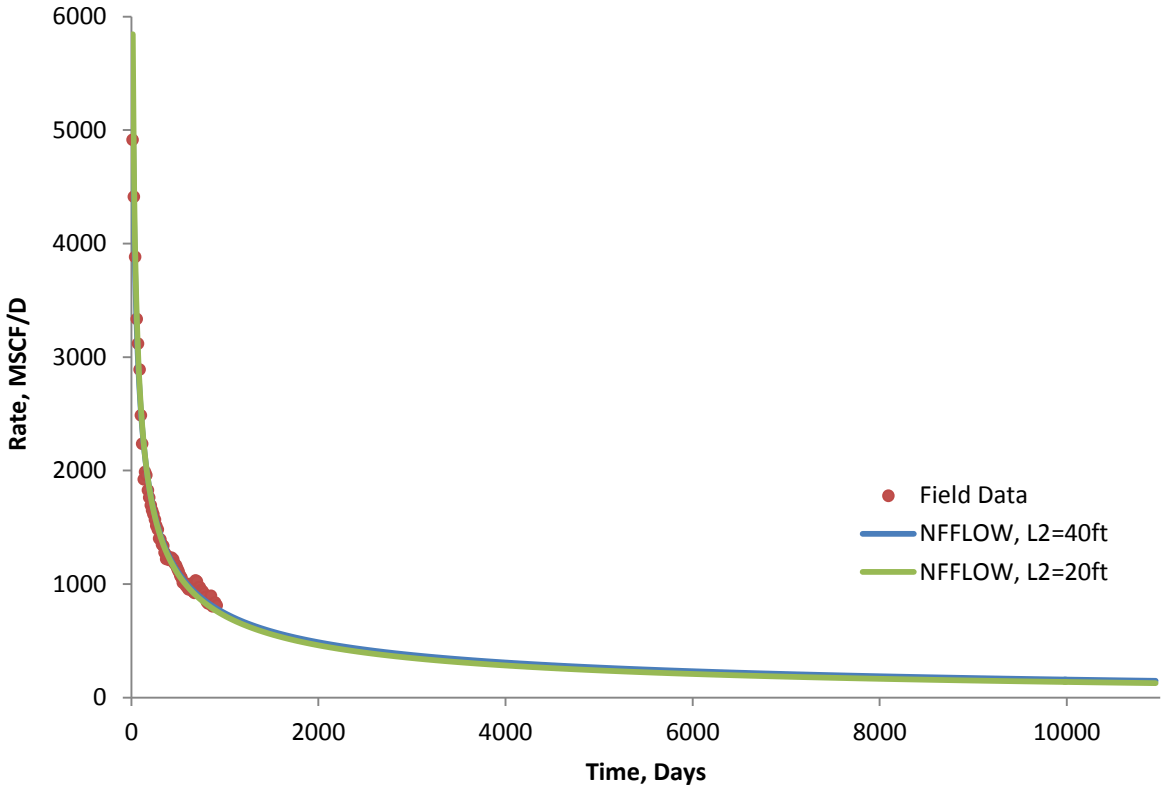

Figure 5.34—Rate *vs.* time based on two different NFflow simulations for WELL#10.

However, Figure 5.35 clearly shows that the fracture setting with ticker mid-layer yields to a slightly higher $EUR_{30\text{-years}}$. Table 5.12 compares the results of these two simulation cases with SEDM parameter estimation for the same well. Second simulation case (thinner mid-layer) yields closer $EUR_{30\text{-years}}$ to the $EUR_{30,\ SPE134231}$ of 3.91 BCF.

Table 5.12—Estimated parameters and simulation results for *WELL#10*.

Parameter	SEDM	NFflow, L2=40 ft.	NFflow, L2=20 ft.
$t_{infl.}$ (days)	695	-	9975
$EUR_{30\text{-years}}$ (BCF)	3.01	4.20	3.96
$EUR_{100\text{-MCF}}$ (BCF)	2.70	-	4.34

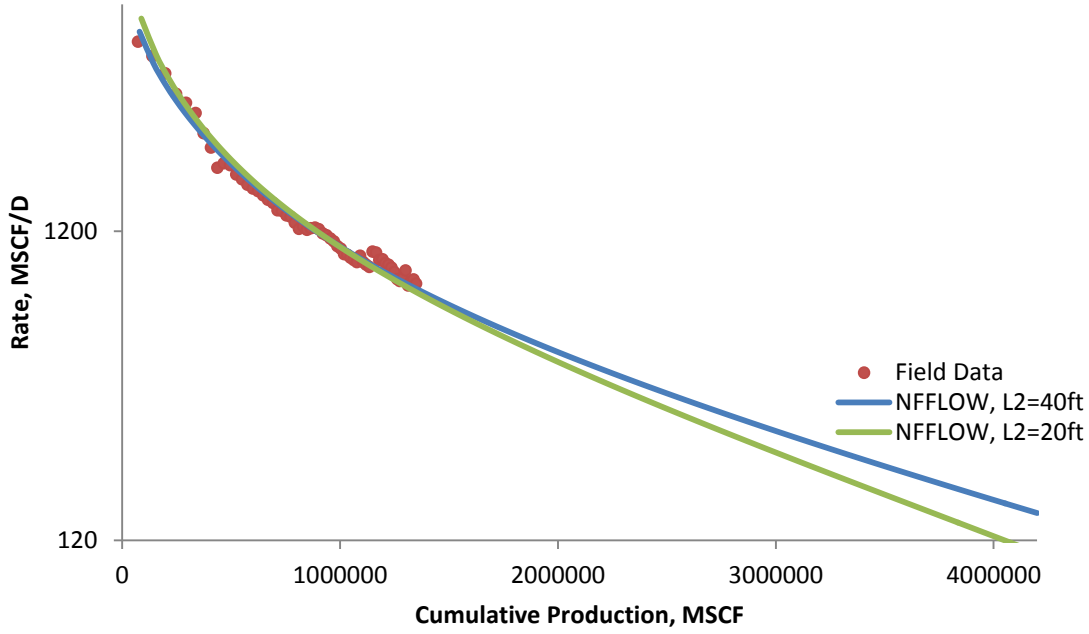

Figure 5.35—*log (q) vs.* cumulative based on two different NFflow simulations for WELL#10.

5.8.3. Case-6: WELL#16

This is a horizontal well located in Johnson County. Table 5.13 summarizes the reservoir parameters that were used to simulate the decline behavior of WELL#16 with NFflow. The completion for this well consisted of 12 stages slickwater fracturing that all completed before the first day of production. The horizontal section of the wellbore is

6020 ft. Each stimulation job covered 418 ft. of the horizontal section and accounts for 5 hydraulic fractures with spacing of 84 ft. The spacing between these 12 stimulation intervals is 98 ft (Figure 5.36). A daily production rate data for 126 days was available for this well that was used in the simulation. Two different cases have been considered for DFN simulation of this well. The setting with lower permeability for three layers was called (L1, L2, and L3) and the higher permeability setting was called (***L'1, L'2, and L'3***).

Table 5.13—Reservoir parameters used to simulate decline behavior of WELL#16.

Parameter	Value
Wellbore Lateral Length (ft)	6020
Depth of L2 (ft)	7297
L1 Thickness (ft)	150
L2 Thickness (ft)	55
L3 Thickness (ft)	150
L′1 Thickness (ft)	***150***
L′2 Thickness (ft)	***55***
L′3 Thickness (ft)	***150***
Reservoir Pressure (psi)	3094
BHFP (psi)	500
Reservoir Size (ft)	6020×800
L1& L3 Permeability (nd)	30
L′1& L′3 Permeability (nd)	***65***
L2 Permeability (nd)	1
L′2 Permeability (nd)	***4***
L1& L3 Porosity (%)	7.2
L′1& L′3 Porosity (%)	***5.2***
L2 Porosity (%)	5.2
L′2 Porosity (%)	***4.2***

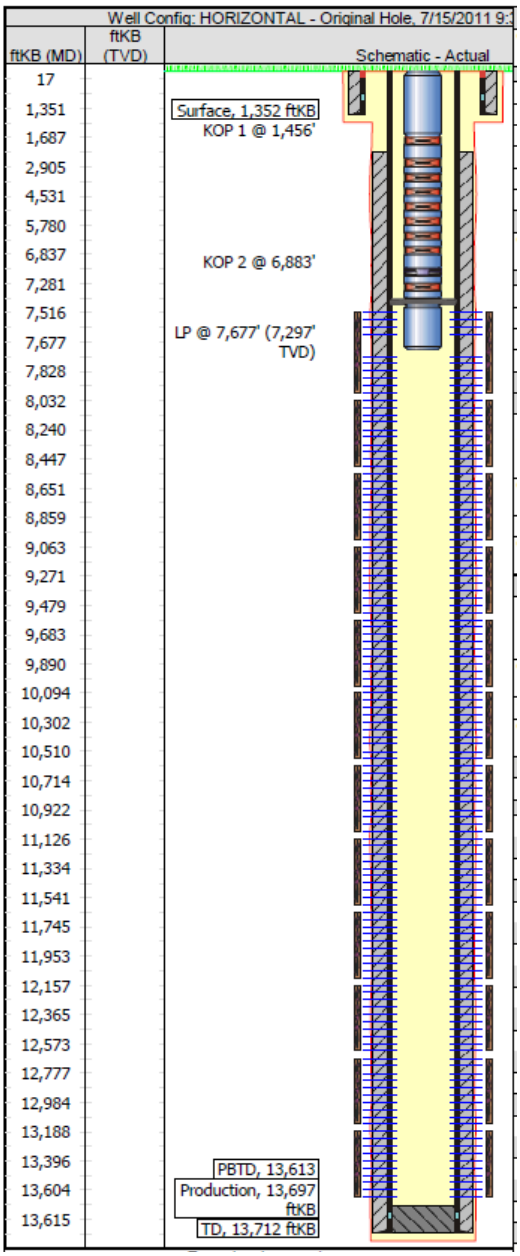

Figure 5.36—Wellbore diagram for WELL#16 horizontal gas well in Barnett Shale.

Table 5.14 summarizes two sets of fracture parameters that have been used to generate the fracture network consisting SET-1 and SET-2 natural fracture sets for the three layers and also 61hydraulic fractures for WELL#16. For the thin-mid layer fracture

setting the only fracture parameter was changed is SET-2 natural fracture aperture and it is called ***SET-2'*** in table 5.14.

Table 5.14—Two sets of fractures used to simulate decline behavior of WELL#16.	
Parameter	**Value**
Number of Hydraulic Fractures	28
Hydraulic Fractures Spacing (ft)	84
Hydraulic Fractures Length (ft)	600
Hydraulic Fractures Aperture (ft)	0.1E-03
SET-1 Length (ft)	100
SET-2 Length (ft)	100
SET-1 Aperture (ft)	0.50E-04
SET-2 Aperture (ft)	0.40E-04
SET-2' Aperture (ft)	***0.365E-04***
SET-1 Density (ft/ft^2)	0.00008
SET-2 Density (ft/ft^2)	0.00008

Table 5.15 compares the results of these two simulation cases with SEDM parameter estimation for the same well. First simulation case (lower permeability setting) yields a higher $EUR_{30\text{-years}}$ estimation and second simulation case (higher permeability setting) yields a lower $EUR_{30\text{-years}}$ estimation compared to the $EUR_{30,\ SPE134231}$ of 9.69 BCF.

Table 5.15—Estimated parameters and simulation results of WELL#16.			
Parameter	**SEDM**	**NFflow, High Perm.**	**NFflow, low Perm.**
$t_{infl.}$ (days)	7978	845	1445
$EUR_{30\text{-years}}$ (BCF)	15.52	8.84	10.20
$EUR_{100\text{-MCF}}$ (BCF)	27.94	-	-

Again rate *vs.* time plot for WELL#16 does not show significant difference between two different simulation cases (Figure 5.37).

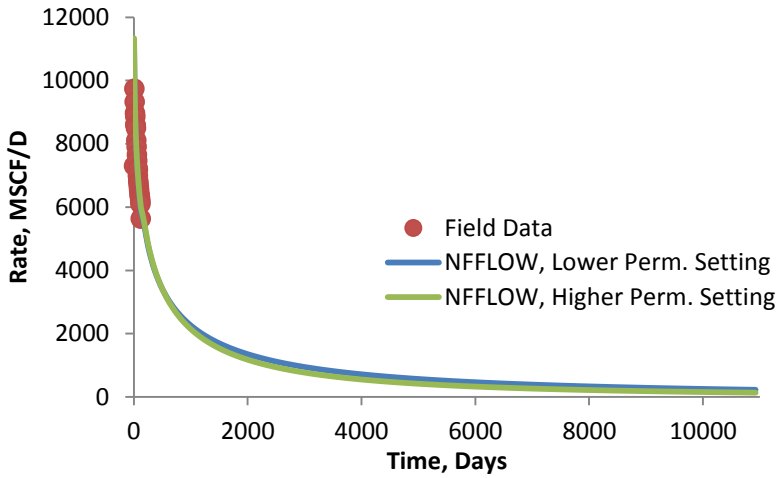

Figure 5.37—Rate *vs.* time based on two different NFflow simulations for of WELL#16.

Figure 5.38 compares the results of two different DFN simulations based on the expected fracture characteristics of Barnett Shale and also known reservoir parameters for WELL#16 horizontal well and for 30 years of production.

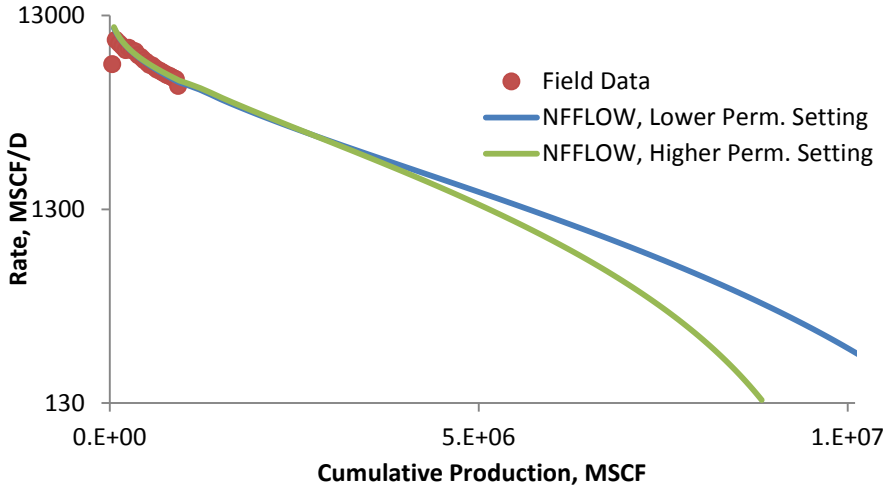

Figure 5.38—*log (q) vs.* cumulative based on two different NFflow simulations for WELL#16.

For higher permeability setting case 10 different realizations of L1, L2, and L3 have been simulated with NFflow. Figure 5.39 compares the *log (q) vs.* cumulative for these 10 realizations.

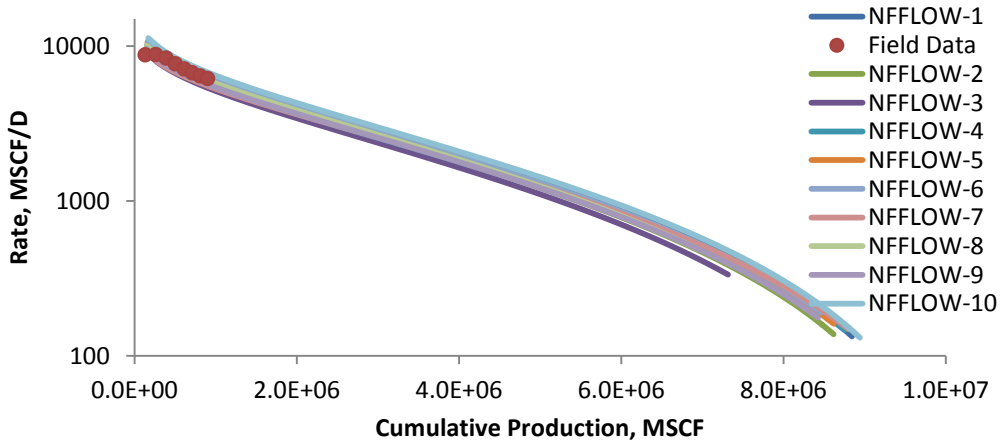

Figure 5.39—*log (q) vs.* cumulative for 10 different realizations of L1, L2, and L3.

Simulation for theses realizations resulted in EUR $_{30\text{-years}}$ of 6.94 to 8.88 BCF (Figure 5.40) compared to the EUR $_{SEDM,30\text{-years}}$ of 15.52 BCF and EUR $_{30,\ SPE134231}$ of 9.69 based on published SEDM parameters for this well.

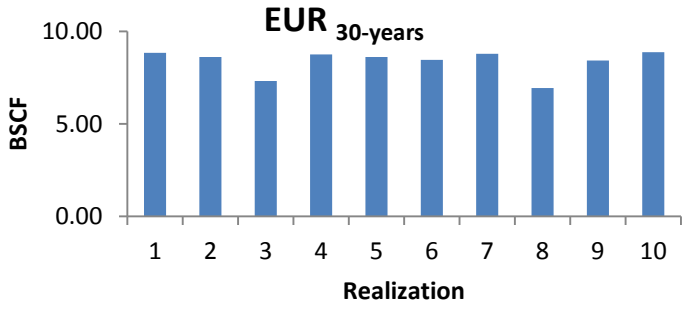

Figure 5.40—EUR $_{30\text{-years}}$ for 10 different realizations of L1, L2, and L3.

Inflection time for these realizations is between 540 and 720 (Figure 5.41).

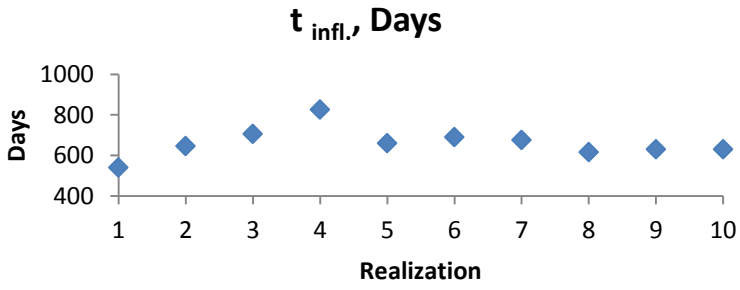

Figure 5.41—Inflection time for 10 different realizations of L1, L2, and L3.

Fracture pressure plots for two extreme cases of NFFLOW-1 (the highest curve in Figure 5.39) and NFFLOW-3 (the lowest curve in Figure 5.39) have been compared in Figure 5.42.

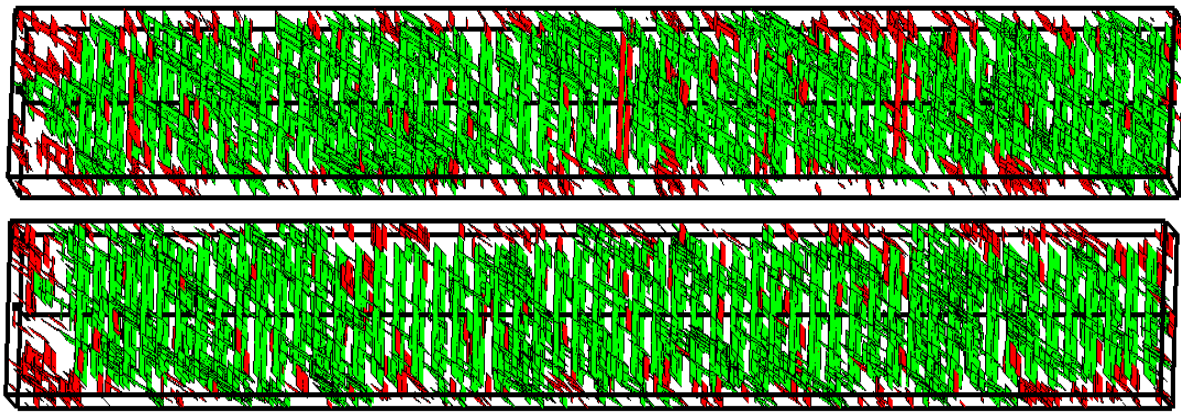

Figure 5.42—Pressure change in the fracture network after 30 years for NFFLOW-1 (top) and NFFLOW-3 (bottom).

NFFLOW-3 setting had untouched pockets (fractures) of gas that were not connected to the main fracture network and although there was more gas to be produced but because of these abandonment of such pockets (fractures) reservoir stopped production after 16 years with a EUR of 7.32. NFFLOW-1 case yielded a $EUR_{30\text{-}year}$ of 8.85 BSCF. The initial Gas in Place (GIP) for all realizations was 13.14144 BSCF.

In summary, we conclude that the basic decline characterizations of the individual wells can be described using the DFN approaches. The model provides a physical insight into the factors affecting the overall production decline and its variability. It is however not a

practical tool for routine forecast and EUR determination, because of the inherent ambiguity of the many parameters necessary to specify.

6. PROBABILISTIC STUDY IN SEDM

6.1. Background

Large discrepancy of the model estimates based on individual well decline parameters is a warning sign for uncertainty. Lee and Sidle (2010) provided an extensive critique of methods that are being used to forecast production estimate reserves in unconventional and poorly understood resource plays. They emphasized on importance of performing uncertainty analysis using statistical methods in such resources, as it can provide valuable insights on upper and lower limits of the reserves and make it easier and more accurate to categorize those resources (proved, probable, and possible).

Can and Kabir (2011) presented a reserve-evaluation methodology which couples SEPD (as a DCA tool) with a probabilistic forecasting frame for wells with and without production history. They grouped production data based on the initial rates to obtain unified SEPD parameter sets (n, τ, and q_0) for similar wells in terms of productivity index. By grouping similar wells and then determining the distribution of the SEPD parameters they could come up with forecasting for individual wells. This way there will be less uncertainty involved compared to just one global parameter set for all wells. For new wells that have no history they used analogues wells to generate data for numerical modeling. For existing wells, in case of irregularity in the production decline, they just used the dominant decline trend for curve-fitting, and then added the excluded production to the EUR as a constant. They used Valko and Lee (2010) methodology, which involves solving two non-linear equations, to obtain n and τ pairs. Then, after

determining P_{10}, P_{50} and P_{90} for each group they calculated high, medium, and low τ values by solving the two non-linear equations. For q_0, they assumed it is the maximum monthly rate for each well. Results of their study on 820 field data sets from three different shale types show that at least three-fourth of the wells' performance fall within the expected P_{10}-P_{90} range.

Duong also performed statistical analysis in his methodology to obtain P10, P50, and P90 for reserve estimation purposes. Based on his study on various gas plays, he showed that there is a correlation between a and m parameters and it can be used to construct q/q_1 *vs.* time (days) type-curves.

6.2. Need for Uncertainty Analysis in Reserve Estimation

In previous chapters it was shown that SEDM is considerably more accurate than the Arps model (with or without minimum terminal decline) for forecasting production and it is perhaps one of the best candidates for DCA in low to ultra-low permeability reservoirs. Also based on the deterministic reserve estimation of 25 horizontal shale gas wells using SEDM it has been shown that SEDM produces stabilized (unchanging) EUR forecasts after only two-three years of production data are available in selected reservoirs, notably the Barnett Shale.

However, only preliminary work has been reported on quantification of the uncertainty of SEDM production forecasts, which will be needed to establish acceptable estimates of proved reserves (1P or P_{90} i.e. having a 90% certainty of being produced), proved plus probable reserves (2P or P_{50} i.e. having a 50% certainty of being produced), and proved plus probable plus possible reserves (3P or P_{10} i.e. having a 10% certainty of

being produced). Estimation of 1P reserves that meet SEC criteria is required by law for all companies that raise capital in the United States. Estimation of 2P and 3P reserves that meet SPE/WPC/AAPG/SPEE Petroleum Resources Management System (PRMS) criteria is important for internal resources inventories for most companies. Rigorous quantification is needed for all the types of reservoirs in which SEDM proves to be applicable, including tight gas and various shale reservoirs producing oil and gas.

The objectives of this section is to (1) develop a systematic method to quantify the range of uncertainty in production forecasts using SEDM and; (2) develop systematic method to provide P_{90}, P_{50}, and P_{10} reserves; and (3) apply this reserve estimation method to low and ultra-low permeability reservoirs.

6.3. Range of Uncertainty for SEDM Parameters in Barnett Shale Gas Reservoirs

As first step in the probabilistic reserve estimation using SEDM, P_{10}, P_{50}, and P_{90} values for SEDM parameter will be determined. Stretched exponent value (n) has been estimated for each individual 25 horizontal Barnett Shale gas wells in section-3 (Table 3.2). Using these values a probability plot of parameter “n” was constructed (Figure 6.1).

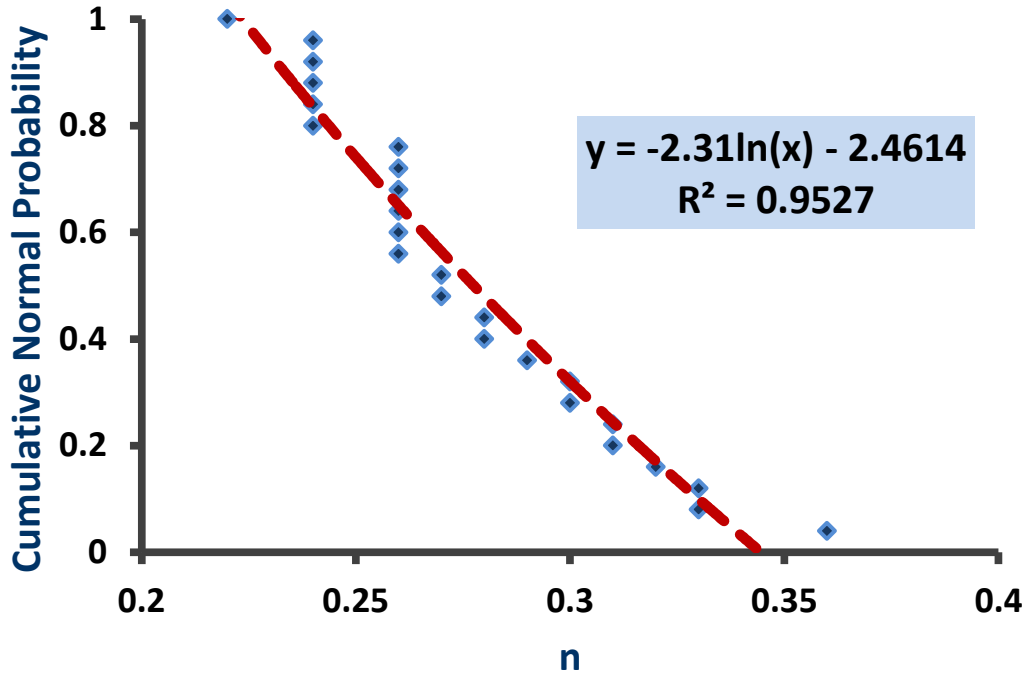

Figure 6.1—Probability plot of parameter "n" in SEDM based on 25 horizontal shale gas wells in Barnett.

Also, inflection time ($t_{infl.}$) has been estimated for each individual 25 horizontal Barnett Shale gas wells in section-3 (Table 3.2). Using these values a probability plot of parameter "$t_{infl.}$" was constructed (Figure 6.2).

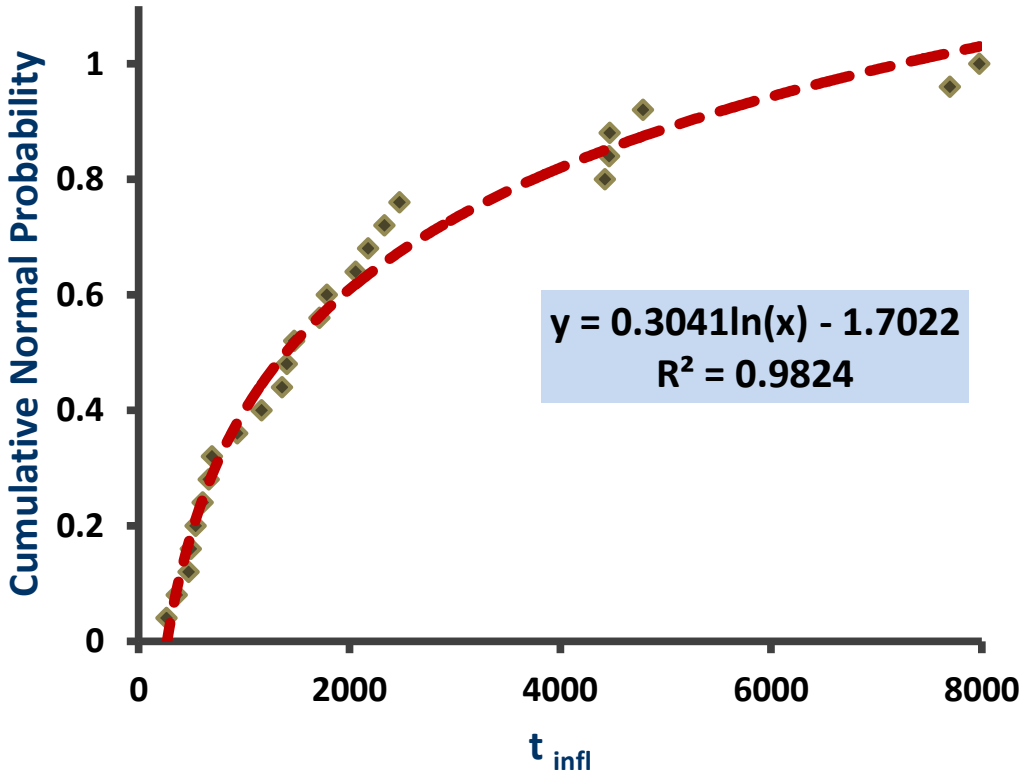

Figure 6.2—Probability plot of parameter "$t_{infl.}$" in SEDM based on 25 horizontal shale gas wells in Barnett.

From Eq. 2.1 ($q = q_0\, exp\left[-\left(\frac{t}{\tau}\right)^n\right]$) it is clear that higher EUR values are associated with lower values of "n" parameters.

In the following, we will not repeat a similar approach for the τ parameter because the two estimated parameters are highly correlated. Instead here we suggest incorporating our findings regarding the inflection point location. This approach can be rationalized by the fact that the inflection point is physically related to the liquid-loading phenomena.

Also, Eq. 2.1 and Eq. 2.8 ($t_{infl} = \tau\left(\frac{1}{n} - 1\right)^{\frac{1}{n}}$) can be used to rewrite SEDM as:

$$q = q_0 \exp[-(\frac{t}{t_{\text{infl.}}})^n(\frac{1}{n} - 1)], \quad (6.1)$$

From Eq. 6.1 it can be understood that higher EUR values are associated with higher values of "$t_{infl.}$" parameters. Therefore, EUR_{P90} will be associated with n_{P10}, and $t_{infl.,P90}$ and EUR_{P10} will be associated with n_{P90}, and $t_{infl.,P10}$.

For example in Figure 6.1, n_{P10} is the value of "n" where the cumulative normal probability is equal to 0.1 and n_{P90} is the value of "n" where the cumulative normal probability is equal to 0.9. Table 6.1 shows "n" and "$t_{infl.}$" values for P_{10}, P_{50}, and P_{90} based on 25 horizontal shale gas wells in Barnett.

Table 6.1—Range of uncertainty for SEDM parameters in Barnett Shale gas.

	n	**$t_{infl.}$ (Days)**
P_{10}	0.23	5203
P_{50}	0.28	1396
P_{90}	0.33	375

6.4. Type Curves of SEDM for Barnett Shale Gas Reservoirs

Using Eq. 6.1 and SEDM parameter values from Table 6.1 P_{10}, P_{50}, and P_{90} type curves for Barnett Shale gas have been generated based on a sample of 25 horizontal wells.

Figure 6.3 shows the plot of normalized rate *vs.* time of these P_{10}, P_{50}, and P_{90} type curves and all 25 horizontal wells in Barnett Shale gas reservoir.

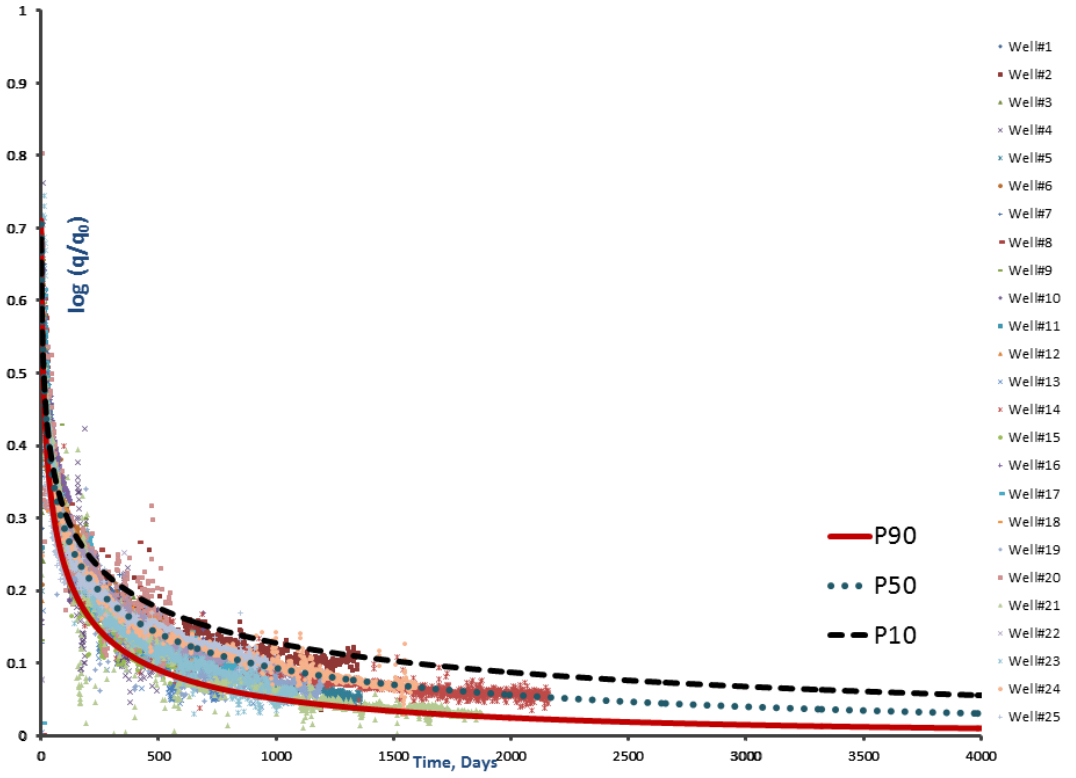

Figure 6.3—Normalized rate *vs.* time type curves for Barnett Shale gas based on a 25 wells sample.

Similarly Eq. 6.1 and SEDM parameter values from Table 6.1 were used to generate P_{10}, P_{50}, and P_{90} type curves for Barnett Shale gas. Figure 6.4 depicts the plot of normalized rate *vs.* normalized cumulative rate of these P_{10}, P_{50}, and P_{90} type curves and all 25 horizontal wells in Barnett Shale gas reservoir.

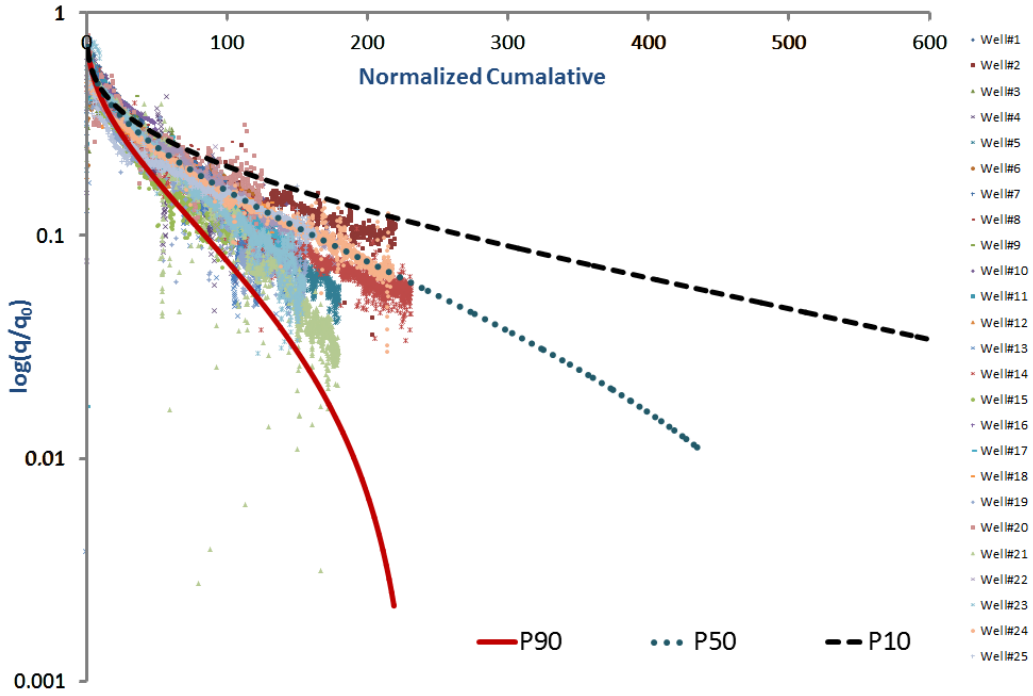

Figure 6.4—Log of normalized rate *vs.* normalized cumulative type curves for Barnett Shale gas based on a 25 wells sample.

6.5. Range of Uncertainty in SEDM for Individual Wells

From Table 6.1, P_{10}, P_{50}, and P_{90} for SEDM parameters "n" and "$t_{infl.}$" were used to determine the decline behavior of each individual shale gas well. Using Eq. 6.1 for all production history available for any specific well q_0 could be written in the form of:

$$q_0 = \frac{\sum_{i=1}^{n} q_i}{\sum_{i=1}^{n} [-(\frac{t}{t_{\text{infl.}}})^n (\frac{1}{n} - 1)]} \quad \text{.....(6.2)}$$

$\sum_{i=1}^{n} q_i$ for any specific well is the same as the last cumulative rate for that well. Then using "n" and "$t_{infl.}$" values from Table 6.1, q_0 values related to P_{10}, P_{50}, and P_{90} could be calculated for each well. For example these values for one of the 25 wells called WELL#19 with 1198 days of production data were calculated as 3798, 3093, and 3000 MSCF/D (Figure 6.5). Having initial rate (q_0) related to P_{10}, P_{50}, and P_{90} for each well along with "n" and "$t_{infl.}$" from Table 6.1 and using Eq. 6.1 SEDM can be evaluated for each individual well.

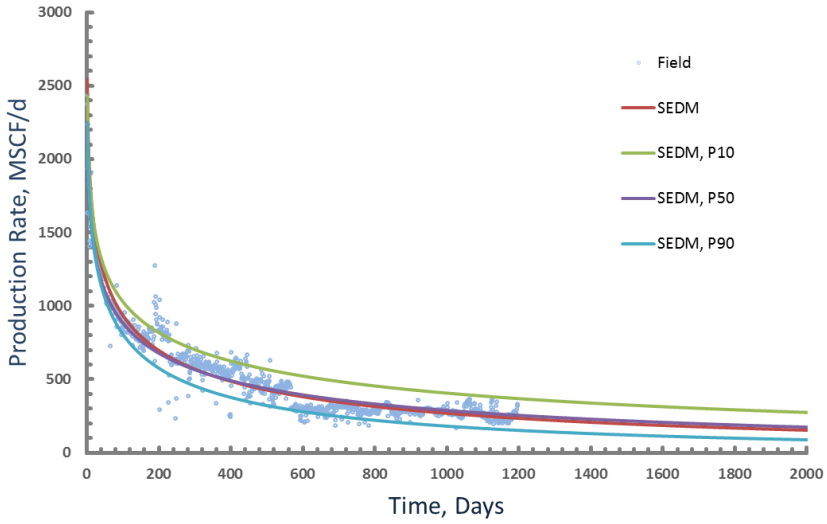

Figure 6.5—Range of uncertainty in rate *vs.* time for WELL#19.

Similarly Eq. 6.1 and SEDM parameter values from Table 6.1 along with calculated q_0 values were used to generate P_{10}, P_{50}, and P_{90} of log (rate) *vs.* cumulative rate for WELL#19 (Figure 6.6).

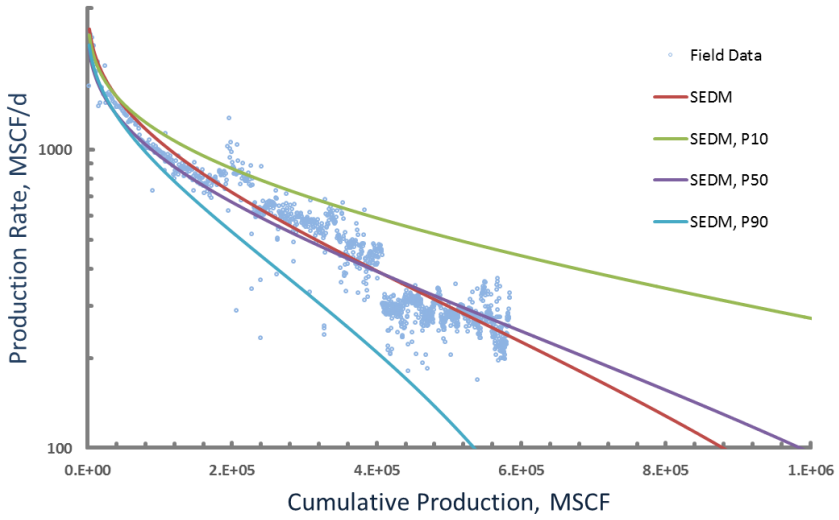

Figure 6.6—Range of uncertainty in log(rate) *vs.* cumulative for WELL#19.

These procedures have been done for each individual well from the sample of 25 horizontal wells from Barnett Shale gas reservoir and plots of rate *vs.* time and *log (q) vs.* cumulative of each well can be found in Appendix C. Similar to the procedure that was done in section 3.3 can be applied here to obtain the range of the uncertainty in $\mathbf{EUR}_{\mathbf{30\text{-}years}}$ (P_{10}, P_{50}, and P_{90}) for each individual well. The most expected SEDM parameter "n" and "$t_{infl.}$" for Barnett Shale gas (Table 6.1) along with q_0 values calculated for each individual well were used to obtain the uncertainty ranges for

$\mathbf{EUR}_{\mathbf{30\text{-}years}}$ .Table 6.2 compares these obtained range of uncertainties for each well with $EUR_{30\text{-}years}$ that were calculated previously based on least square SEDM parameter search method in Table 3.4. These results show that for almost all wells (>90%) $\mathbf{EUR}_{\mathbf{30\text{-}years}}$ based on least square SEDM parameter search falls within the range of P_{10} and P_{90}.

Table 6.2—Range of uncertainty in reserves estimations of 25 wells in Barnett Shale using SEDM.							
Well	EUR $_{30\text{-years}}$	EUR $_{100}$ MSCF/D	P_{90}	P_{50}	P_{10}	EUR 30, SPE134231	Contacted G_p
WELL#1	4.32	4.29	2.57	4.12	5.44	4.35	5.73
WELL#2	4.09	4.63	1.82	3.28	5.33	3.48	8.1
WELL#3	9.85	11.54	5.45	9.14	13.17	9.74	14.13
WELL#4	1.01	0.71	0.81	1.37	2.01	1.46	1.12
WELL#5	2.16	1.84	1.55	2.79	4.54	2.96	2.35
WELL#6	6.18	7.81	2.75	4.65	6.78	4.95	11.94
WELL#7	4.8	5.15	2.52	4.19	5.94	4.46	7.44
WELL#8	4.66	4.93	2.44	4.15	6.09	4.42	7.07
WELL#9	4.58	4.32	3.98	6.55	9.11	6.97	5.01
WELL#10	3.01	2.7	2.10	3.68	5.70	3.91	3.48
WELL#11	3.33	3.03	2.79	4.48	5.95	4.73	3.75
WELL#12	4.17	4.7	1.89	3.06	4.12	3.24	8.03
WELL#13	2.15	1.86	1.79	3.16	4.97	3.35	2.27
WELL#14	1.85	1.48	1.30	2.34	3.81	1.97	2.53
WELL#15	1.97	1.6	1.27	2.17	3.21	2.31	2.54
WELL#16	15.52	27.94	5.74	9.19	12.10	9.69	37.77
WELL#17	3.82	3.75	2.14	3.71	5.67	3.94	5.43
WELL#18	6.59	8.42	3.00	5.13	7.64	5.46	12.71
WELL#19	1.24	0.88	0.77	1.38	2.21	1.46	1.52
WELL#20	2.76	2.55	1.43	2.42	3.55	2.58	4.36
WELL#21	2.60	2.34	2.46	4.43	7.20	3.96	2.68
WELL#22	4.6	4.63	2.64	4.67	7.39	4.96	6.19
WELL#23	2.35	2.02	1.54	2.76	4.47	2.92	2.7
WELL#24	1.32	0.9	0.74	1.34	2.17	1.3	1.97
WELL#25	4.13	4.97	1.75	3.08	4.79	3.27	9.76

In previous Sections we demonstrated the application of the SEDM to production-forecast and EUR determination.

However, for quantifying uncertainty, the actual parameterization (q_0, τ, n) might not be the best choice, mostly because n and τ are highly interdependent in the investigated cases.

While the n parameter reflects some basic characteristics of the hydraulic fracture-natural fracture network-matrix system, it is not quite obvious that the τ parameter bears equal amount of significant information. In this Section we opted for inflection time that was previously related to the physics of the wellbore flow, rather than to the reservoir characteristics. Considering the inflection time as a second "parameter" more consistent stochastic description could be obtained. In other words, an alternate parameterization of the same model might be advantageous, if it is stronger related to the physical processes behind the model.

We conclude that the inflection behavior of the model is a key aspect of SEDM worth further exploiting.

7. OBSERVATIONS AND CONCLUSIONS

- SE functions can be written as a sum of independently decaying exponential components. 19 independent exponentials with different relaxation constants have been used to explain a SE function for the case of n=0.25 and τ=0.776, which are the published parameters for Barnett Shale reservoir.
- A series of reservoir simulations have been performed to investigate the capability of SEDM model in handling heterogeneity in unconventional reservoirs.
- Two empirical methods of SEDM and Duong's method have been applied to estimate reserves on 25 horizontal Barnett Shale gas wells.
- For comparison purposes different reserves estimation procedures have been performed for both SEDM and Duong's models. Some observations based on the 25-well Barnett sample are:

    1) Finite contacted gas in place ($EUR_{t=\infty}$):

        d. Arp's hyperbolic model with b >= 1 does not have finite value, but with a cut-off to switch to exponential decline it does have.
        e. Duong's model seems to yield m > 1 in all cases and that implies finite value, (though it may still be very large.)
        f. SEDM always yields 0 < n < 1 and that implies finite value, most often a moderate value, already having some physical meaning by itself.

2) Ease of use:

    a. Arps is heavily dependent on cutoff to exponential decline and on the way how the b exponent is determined (for instance numerical differentiation with smoothing.)

    b. Duong's model is very easy to use and leaves little doubt about non-uniqueness. This is due to two facts: one is that it does not need numerical determination of derivatives and it can be cast as sequence of two consecutive linear regression procedures.

    c. SEDM needs non-linear fitting (solver or similar) and constraints on the parameters. It is the most difficult model to work with and the results depend on the actions taken during the fitting procedure.

3) Inflection point:

    a. Arp's model with $b > 0$ has a break point where the cutoff is reached (no inflection point, an artificial switch from convex to concave character.)

    b. Duong's model usually puts the inflection point at very far; practically it always uses the convex part for the 30-yr prediction in the examples we considered. Therefore, it usually implies a very large contacted gas in place ($EUR_{t=\infty}$) having little or no physical meaning. In this respect, the finiteness of contacted gas in place does always exist. However, when the m parameter is near to 1, the contacted gas

in place is very large and there might be a very large difference between EURs corresponding to the 30–yr and economic rate conditions.

c. SEDM usually puts the inflection point on the order of 1 – 8 years. This implies a limited value of contacted gas in place ($EUR_{t=\infty}$), that is already on the order of the $EUR_{t=30\text{-yr}}$ value and leads to possible physical interpretation.

4) Prediction with published parameters:

a. For Arps, there are no reliable values for the Barnett Shale, and the decline rate cutoff is questionable.

b. Duong: SPE 137748 provides a reasonable way to estimate $EUR_{t=30\text{-yr}}$ from only the time-cumulative pair.

c. SEDM: SPE 134231 provides a reasonable way to estimate $EUR_{t=30\text{-yr}}$ from only the time-cumulative pair. It is interesting that $\boldsymbol{EUR}_{30,\,SPE134231}$ and $\boldsymbol{EUR}_{30,\,SPE137748}$ are consistent with the SEDM being always about 5 – 10 % less. The average parameter values for Barnett in these two papers were published approximately at the same time and independently. These estimates seem especially useful when the data set is short, or contain anomalies and hence do not allow for unique determination of all three parameters for the SEDM and Duong models.

5) Large discrepancy of the model estimates based on individual well decline parameters is a warning sign for uncertainty.

- The critical gas rate based on Turner's critical velocity can be used for conditioning the 3-variable search (n,τ, and q_0) in SEDM into a 2-variable search. The advantage of this conditioning is that it does not have the problem of non-uniqueness and Solver (based on least square criteria) always yields only one pair of n and τ.
- Flow behavior in shale gas reservoirs, especially Barnett shell, was investigated by using a Discrete Fracture Network (DFN) simulator (FracGen and NFflow) for fracture modeling of a shale gas reservoir. Also the interaction of the different fracture properties on reservoir response was studied.
- Published parameters from Valko and Lee (2010) have been used to first investigate the compatibility of the SEDM behavior in Barnett Shale gas wells with DFN concept. Some of the observations from the single-layer simulations are:

  1) The lower matrix permeability is the higher decline in rate will occur at the beginning period of the production.
  2) Early Production and initial rate depend on the number of natural of fractures intersect wellbore, their permeability, and lengths.

And for mid-period to late-production:

3) The number of natural fractures intersecting by Wellbore has less effect on the production decline.

4) Created network of fracture and how induced hydraulic fractures connected natural fractures to the wellbore will have a major impact on the decline.
5) Reservoir press does not change inflection time
6) Increasing Porosity increases inflection time

Some of the observations from DFN simulations for multiple-layered reservoir are:

1) Some parameters like Fracture density and fracture length are interchangeable.
2) Keeping all parameters fixed and just comparing 10 realizations shows how reserve estimation can be tricky in reservoirs which main production comes from network of natural and enhanced fractures.
3) In 3-layer model fracture aperture has the dominant effect on early time concavity.
4) Porosity of the top and bottom layers (L1 and L3) has the dominant effect on late time decline shape.
5) The best fit is from 3-layer reservoir model and at least 3-layer model (or 3 different zones of fracture network) is required to have the same inflection time location and decline behavior for published SEDM parameters.

- Inflection time and reserve parameters were estimated using DFN simulation for three Barnett Shale gas horizontal wells using the most recent production and completion data, well geometry, and reservoir parameters available and the results were compared with the estimated SEDM parameters for the same wells.

- A systematic methodology was developed to quantify the range of uncertainty in production forecasts using SEDM. This methodology could be used as a probabilistic tool to quantify P_{90}, P_{50}, and P_{10} reserves based on forecasts using SEDM.
- The most expected SEDM parameter "n" and "$t_{infl.}$" for Barnett Shale gas (Table 6.1) along with q_0 values calculated for each individual well were used to obtain the uncertainty ranges for **EUR $_{30\text{-years}}$**. These results show that for almost all 25 wells (>90%) **EUR $_{30\text{-years}}$** based on least square SEDM parameter search falls within the range of P_{10} and P_{90}.

REFERENCES

Abramowitz, M. and Stegun, I.A. eds. 1972. Handbook of Mathematical Functions With Formulas, Graphs, and Mathematical Tables, New York: Dover Publications.

Alzer, H. and Berg, C., "*Some classes of completely monotonic functions.II*", Ramanujan J. 11 (2006), no. 2, 225-248.

Arps, J.J. 1945. Analysis of Decline Curves. Trans. AIME 160: 228-247.

Can, B. and Kabir, C.S., 2011, Probabilistic Performance Forecasting for Unconventional. Reservoirs with Stretched-Exponential Model. SPE 143666.

Currie, S. M., Ilk, D., and Blasingame, T. A. 2010. Continues Estimation of Ultimate Recovery. Paper SPE 132352 presented at the SPE Unconventional Gas Conference, Pittsburgh, Pennsylvania, 23-25 February.

Dershowitz, W., LaPointe, P., Eiben, T. & Wei, L. 1998. Integration of discrete feature network methods with conventional simulator approaches. SPE, 49069.

Dershowitz, W.S., La Pointe, P.R. and Doe, T.W. 2004. Advances in Discrete Fracture Network Modeling. *Proc.*, US EPA/NGWA Fractured Rock Conference, Portland, Maine.

Duong, A.N. 2011. Rate-Decline Analysis for Fracture-Dominated Shale Reservoirs. SPE Res Eval & Eng 14 (3): 377-387. SPE-137748-PA. doi: 10.2118/137748-PA.

Fan, L., et al, 2011. "The Bottom Line of Horizontal Well Production Decline in the Barnett Formation. " Paper SPE 141263 presented at the SPE Production and Operations Symposium in Oklahoma City, OK 27-29 March, 2011.

Fisher, M. K., J. R. Heinze, C. D. Harris, B. M. Davidson, C. A. Wright, and K. P. Dunn, 2004, “Optimizing horizontal completion techniques in the Barnett Shale using microseismic fracture mapping”, Proceedings of the Society of Petroleum Engineers Annual Technical Conference, Houston, Texas, SPE Paper 90051, 11 p.

“FracGen & NFflow Naturally-Fractured Natural Gas Reservoir Simulator Users Gale, J.F.W., Reed, R.M., Holder, J., 2007, “National Fractures in the Barnett Shale and their importance for hydraulic fracture treatments”, AAPG Bulletin, 91, p. 603-622.

Guohai, J. Pashin, J.C. 2008. Discrete Fracture Network Models of the Secarb Carbon Sequestration Test Site, Deerlick Creek Field, Black Warrior Basin, Alabama. *Proc.*, International Coalbed & Shale Gas Symposium, Tuscaloosa, Alabama.

Ilk, D, Rushing, J.A., Petrego, A.D. and Blasingame, T.A.: Exponential *vs.* Hyperbolic decline in tight gas sands – Understanding the origin and implications for reserve estimates using Arps' Decline curves, SPE 116731, 2008.

Johnston, D.C. 2006. Stretched Exponential Relaxation Arising From a Continuous Sum of Exponential Decays. Phys. Rev. B 74: 184430.

Kohlrausch R. 1847. Ann. Phys., Lpz. 12 393.

Laherrere J. and Sornette D.: "Stretched exponential distributions in Nature and Economy: Fat tails with characteristic scales". *European Physical Journal* **B 2**, 2008.

Lea, J.F., Nickens, H.V.: Solving Gas-Well Liquid-Loading Problems, SPE 72092, *Journal of Petroleum Technology*, April 2004, pp. 30-31, 69-74.

Lea, James F., Nickens, Henry V. and Wells, Mike R., "Gas Well Deliquification," Second Edition, Elsevier Press, Cambridge, 2008.

Lee, J. and Sidle, R. 2010. Gas-Reserves Estimation in Resource Plays. SPE Econ & Mgmt 2 (2): 86-91. SPE-130102-PA. doi: 10.2118/130102-PA.

Mattar, L., and Moghadam, S. 2009. Modified Power Law Exponential Decline for Tight Gas. Paper 2009-198 presented at the 2009 Canadian International Petroleum Conference, Calgary, Alberta, 16-18 June.

Miller, K. S. and Samko, S. G., "Completely monotonic functions" , Integral Transform. Spec. Funct. 12 (2001), 389–402.

Montgomery, S. L., D.M. Jarvie, K. A. Bowker, and R. M. Pollastro, 2005, Mississippian Barnett Shale, Fort Worth Basin, north central Texas: Gas-shale play with multi–trillion cubic foot potential: AAPG Bulletin, v. 89, p. 155–175.

Robertson, S. "Generalized Hyperbolic Equation." Unsolicited SPE Paper 18731. (1988).

Seshadri, J. and Mattar, L. Comparison of Power Law and Modified Hyperbolic decline methods, SPE 137320, 2010.

Sutton, Robert P., Cox, Stuart A., Lea, James F. and Rowlan O. Lynn, "Guidelines for the Proper Application of Critical Velocity Calculations," paper SPE 120625, presented at the 2009 SPE Productions & Operations Symposium, USA, April 4-8.

Towler, B., and Bansal, S.: "Hyperbolic decline-curve analysis using linear regression," *Journal of Petroleum Science and Engineering* **8**, 1993, pp.257-68.

Turner, R.G., Hubbard, M.G. and Dukler, A.E., "Analysis and Prediction of Minimum Flow Rate for Continuous Removal of Liquids from Gas Wells," paper SPE 2198, *JPT* (November 1969).

Valkó, P.P. 2009. Assigning Value to Stimulation in the Barnett Shale: a Simultaneous Analysis of 7000 Plus Production Histories and well Completion Records. Paper SPE 119369 presented at the SPE Hydraulic Fracturing Technology Conference, The Woodlands, Texas, 19–21 January.

Valkó, P.P. and Lee, J. W. 2010. A Better Way to Forecast Production From Unconventional Gas Wells. Paper SPE 134231 Presented at the SPE Annual Technical Conference and Exhibition, Florence, Italy, 19-22 September.

Warpinski, N. R., and L. W. Teufel, 1987, Influence of geologic discontinuities on hydraulic fracture propagation: *Journal of Petroleum Technology* **39**, p. 209–220.

Warpinski, N. R., R. C. Kramm, J. R. Heinze, and C. K. Waltman, 2005, Comparison of single- and dual array microseismic mapping techniques in the Barnett Shale: Proceedings of Society of Petroleum Engineers Annual Technical Conference, Dallas, Texas, SPE Paper 95568, 10 p.

Warren, J.E. and Root, P.J. 1963. The Behavior of Naturally Fractured Reservoirs. *SPE Journal* **3** (3): 245 – 255. SPE-426-PA. doi: 10.2118/426-PA.

APPENDIX A

This section contains the results of parameter estimation for Duong's methodology and also SEDM for a series of 25 horizontal shale gas wells in Newark East Field. For each individual well the SEDM model parameters (q_0, τ, n) and Duong's model parameters (q_1, a, m) were determined. For SEDM parameter estimation was performed by using the Solver of Excel and fitting the cumulative production based on the method of least squares. In this section for SEDM a 3-parameter search has been performed for each individual well.

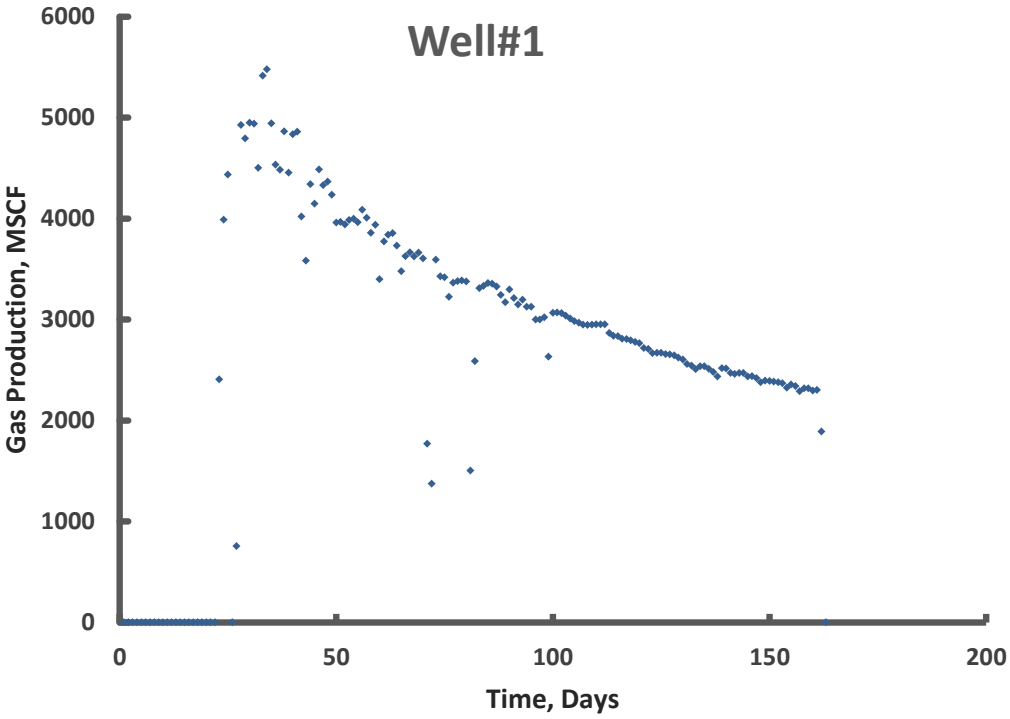
Well#1
Gas Production, MSCF
6000
5000
4000
3000
2000
1000
0
0
50
100
150
200
Time, Days

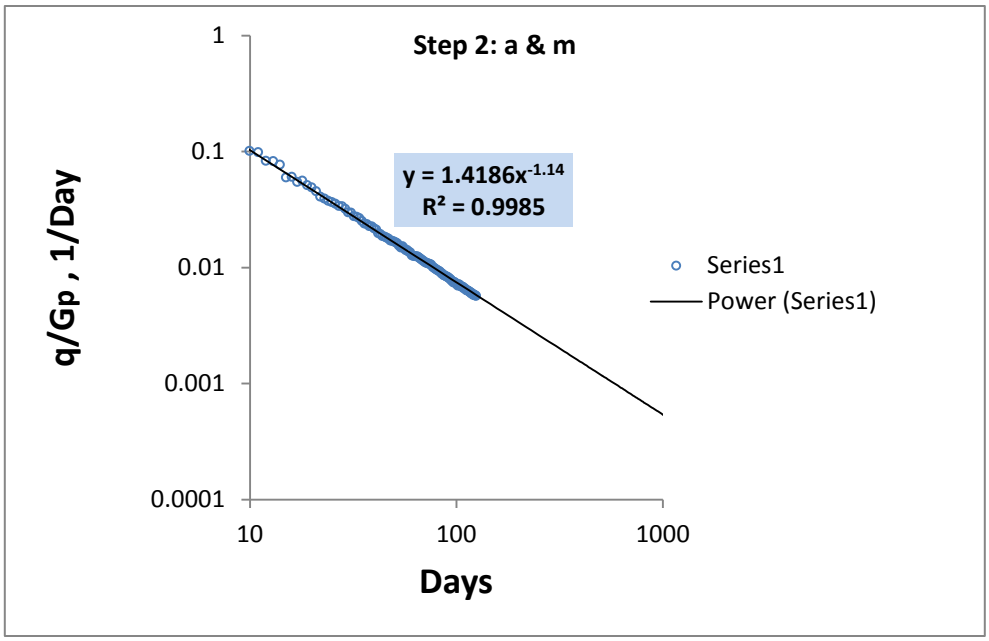
Step 2: a & m
q/Gp , 1/Day
1
0.1
0.01
0.001
0.0001
y = 1.4186x-1.14
R² = 0.9985
Series1
Power (Series1)
10
100
1000
Days

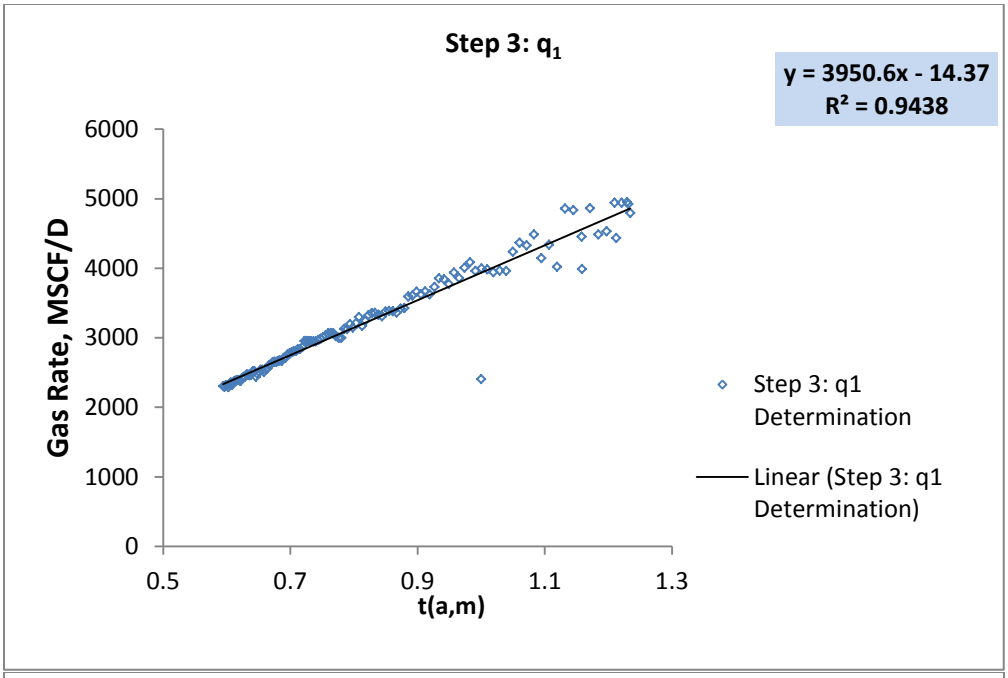
Step 3: q1
y = 3950.6x - 14.37
R² = 0.9438
Gas Rate, MSCF/D
6000
5000
4000
3000
2000
1000
0
0.5
0.7
0.9
1.1
1.3
t(a,m)
Step 3: q1 Determination
Linear (Step 3: q1 Determination)

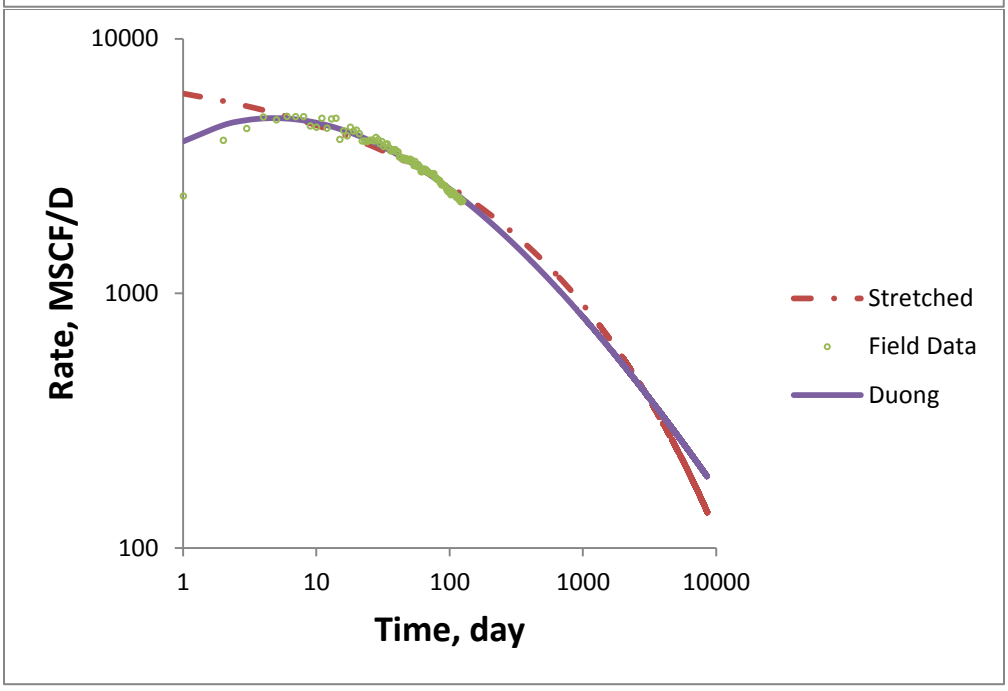
Rate, MSCF/D
10000
1000
100
1
10
100
1000
10000
Time, day
Stretched
Field Data
Duong

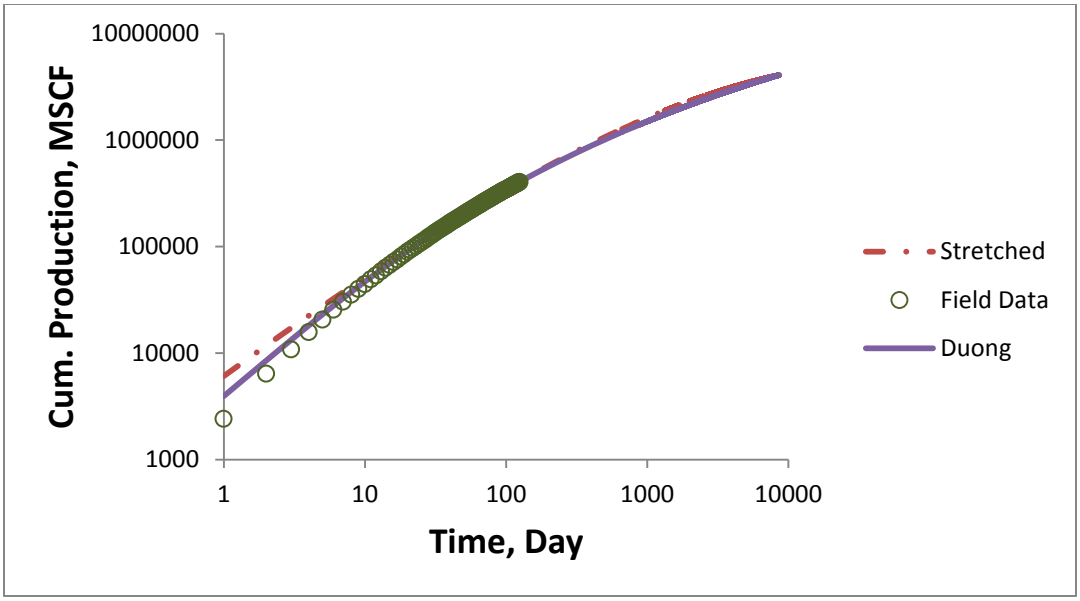
10000000
1000000
100000
10000
1000
Cum. Production, MSCF
1
10
100
1000
10000
Time, Day
Stretched
Field Data
Duong

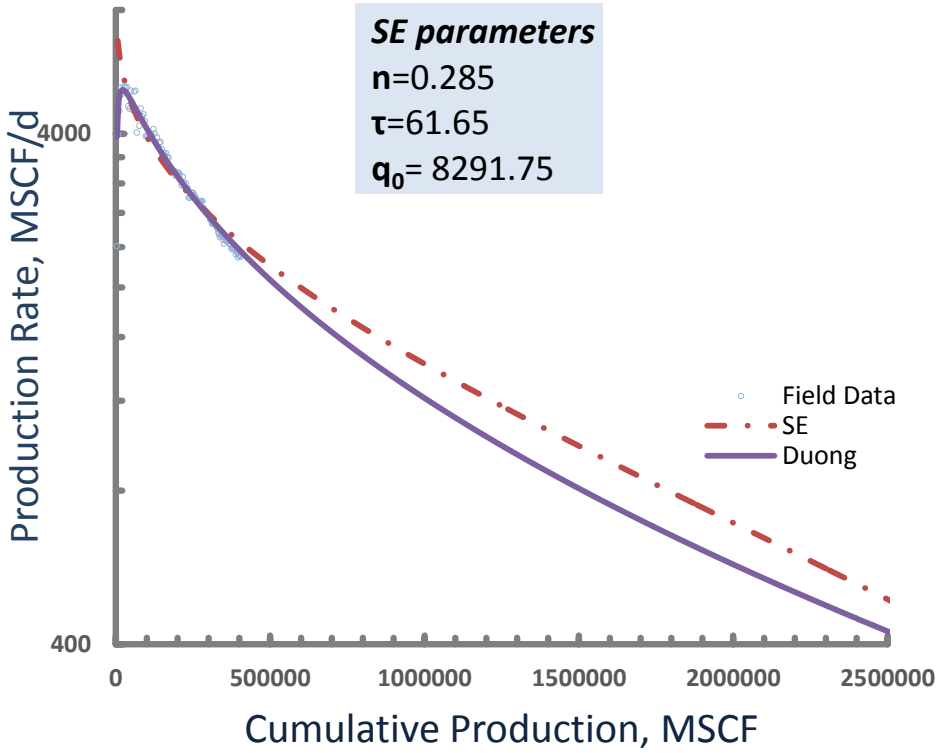
SE parameters
n=0.285
τ=61.65
q0= 8291.75
4000
400
Production Rate, MSCF/d
0
500000
1000000
1500000
2000000
2500000
Cumulative Production, MSCF
Field Data
SE
Duong

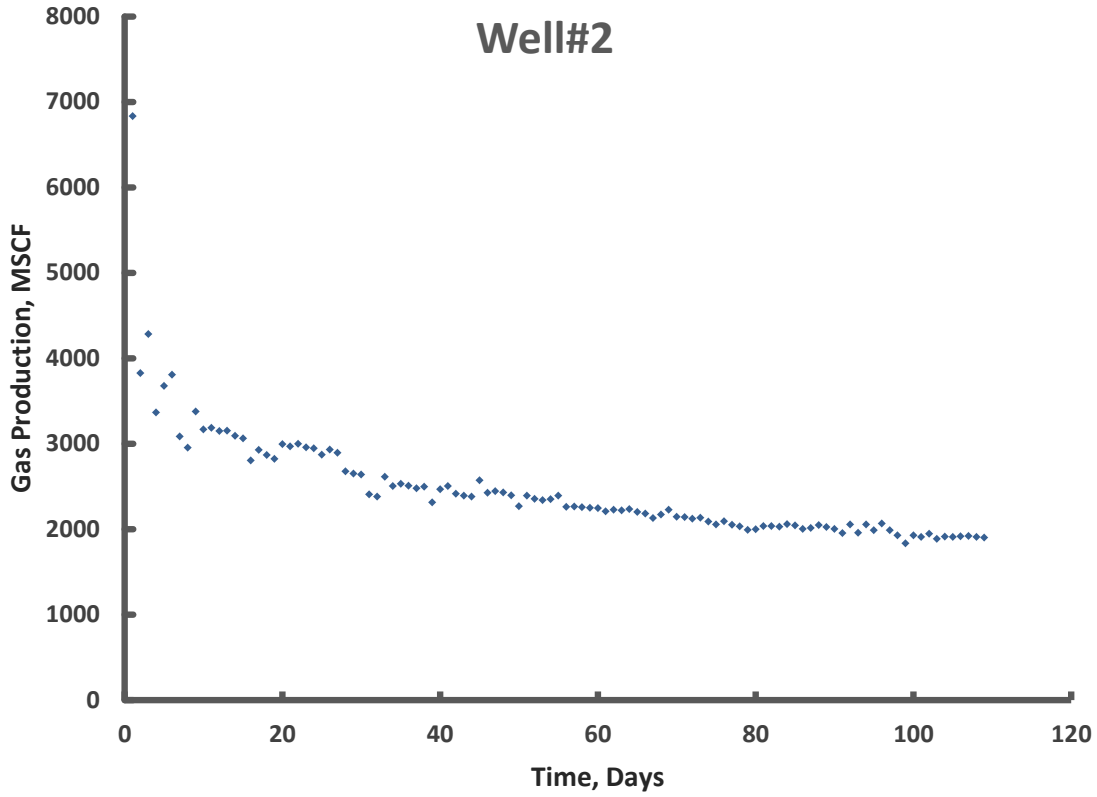
Well#2
Gas Production, MSCF
8000
7000
6000
5000
4000
3000
2000
1000
0
0
20
40
60
80
100
120
Time, Days

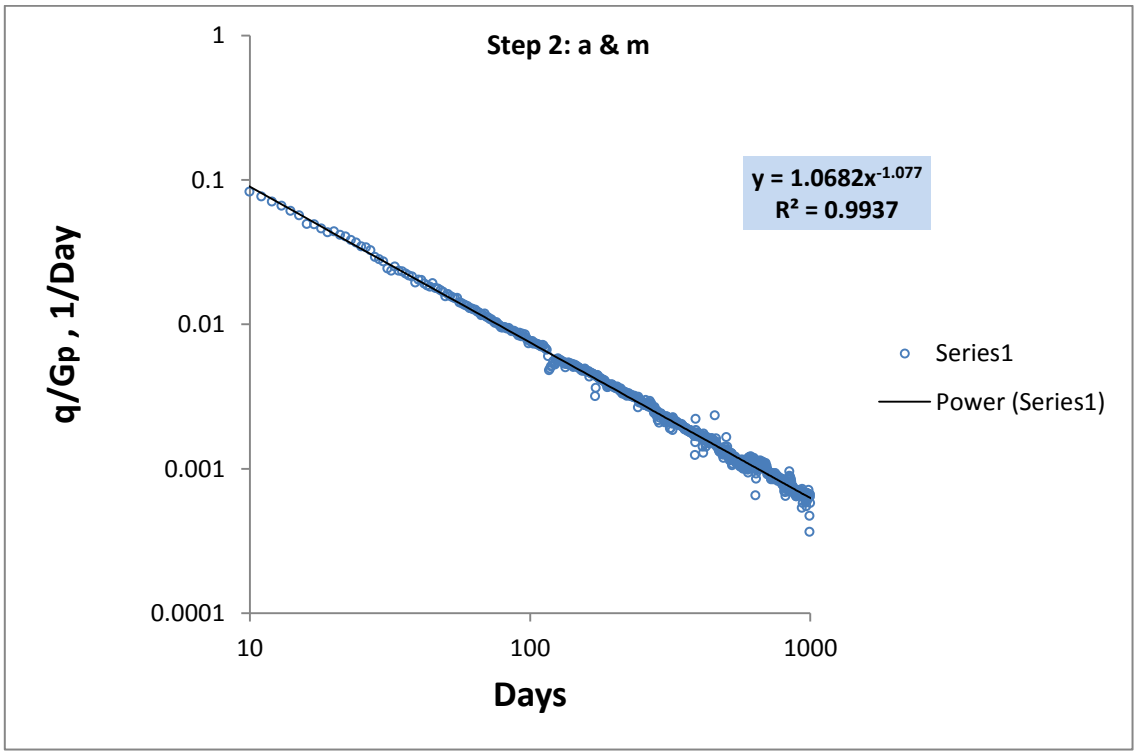
Step 2: a & m
q/Gp , 1/Day
1
0.1
0.01
0.001
0.0001
10
100
1000
Days
y = 1.0682x-1.077
R² = 0.9937
Series1
Power (Series1)

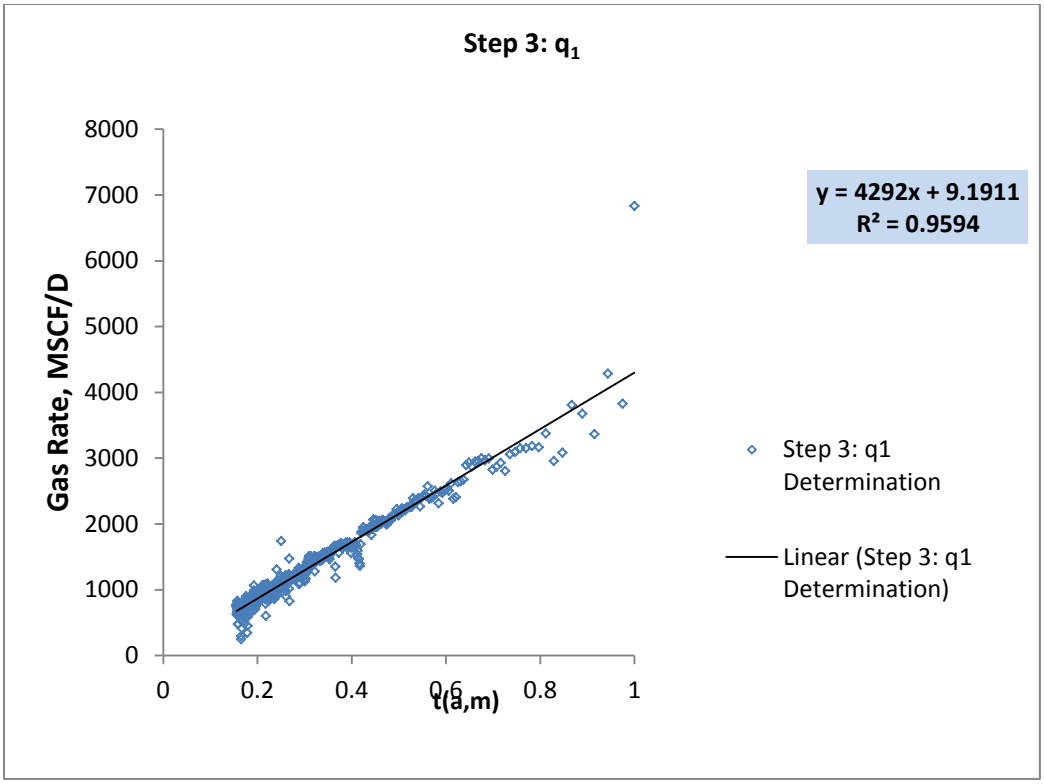
Step 3: q1
8000
7000
6000
5000
4000
3000
2000
1000
0
Gas Rate, MSCF/D
0
0.2
0.4
0.6
0.8
1
t(a,m)
y = 4292x + 9.1911
R² = 0.9594
Step 3: q1 Determination
Linear (Step 3: q1 Determination)

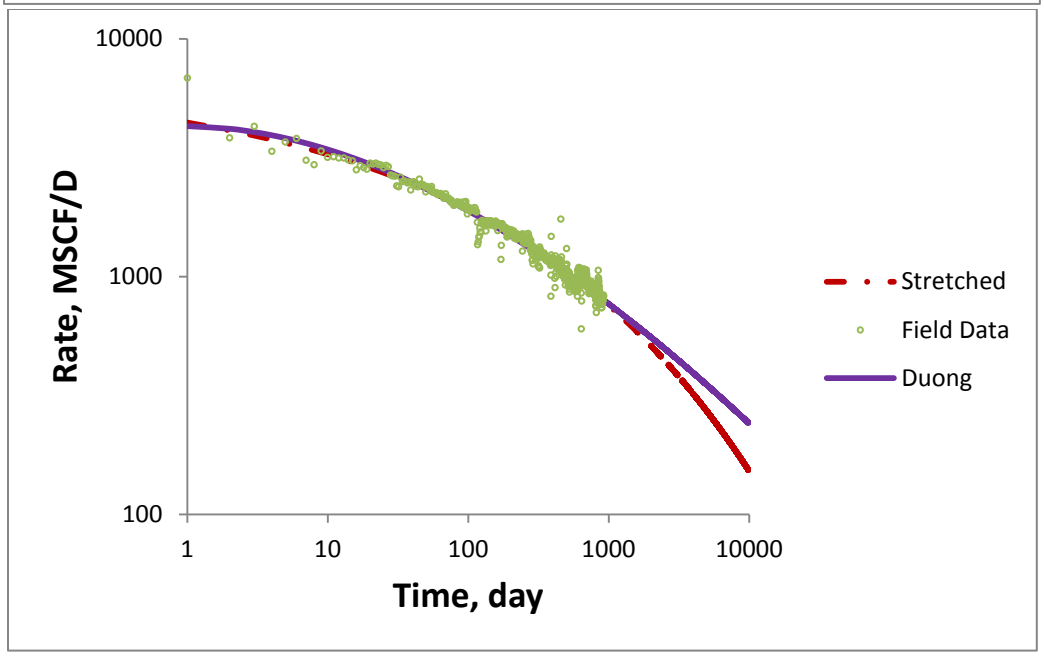
10000
1000
100
Rate, MSCF/D
1
10
100
1000
10000
Time, day
Stretched
Field Data
Duong

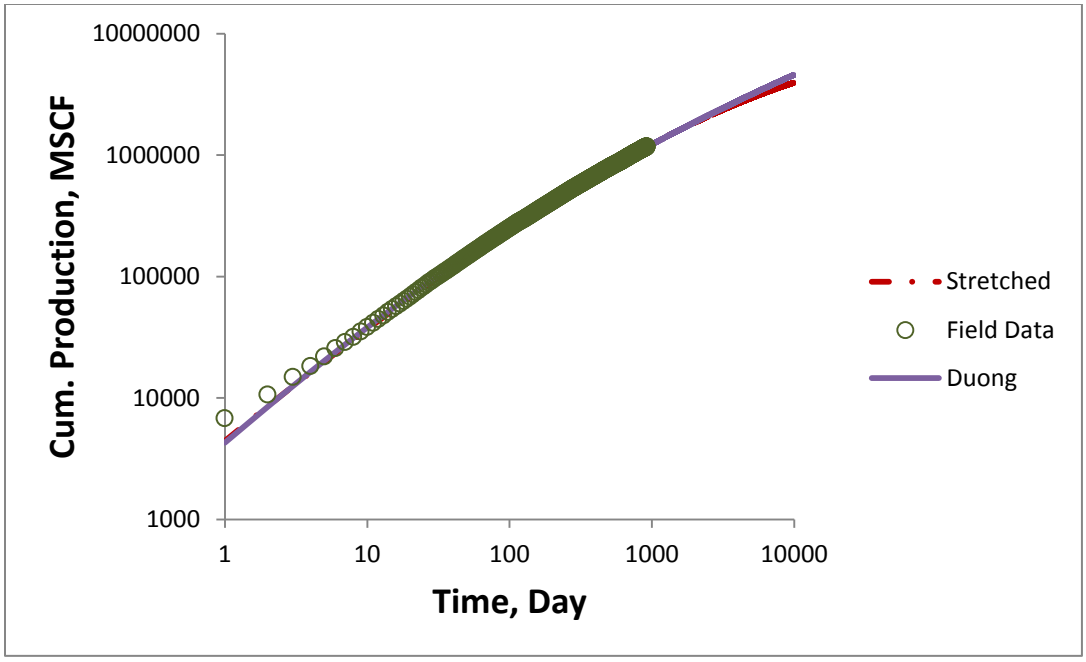
10000000
1000000
100000
10000
1000
Cum. Production, MSCF
1
10
100
1000
10000
Time, Day
Stretched
Field Data
Duong

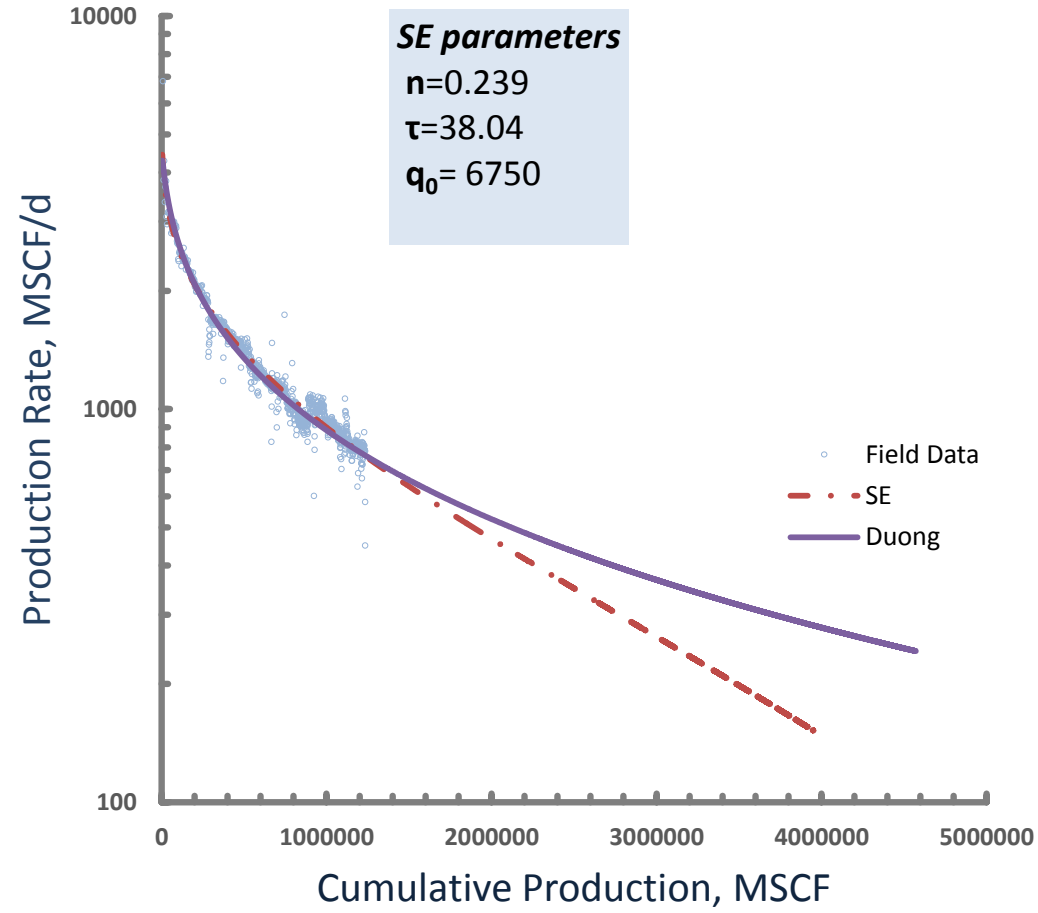
SE parameters
n=0.239
τ=38.04
q0= 6750
10000
1000
100
Production Rate, MSCF/d
0
1000000
2000000
3000000
4000000
5000000
Cumulative Production, MSCF
Field Data
SE
Duong

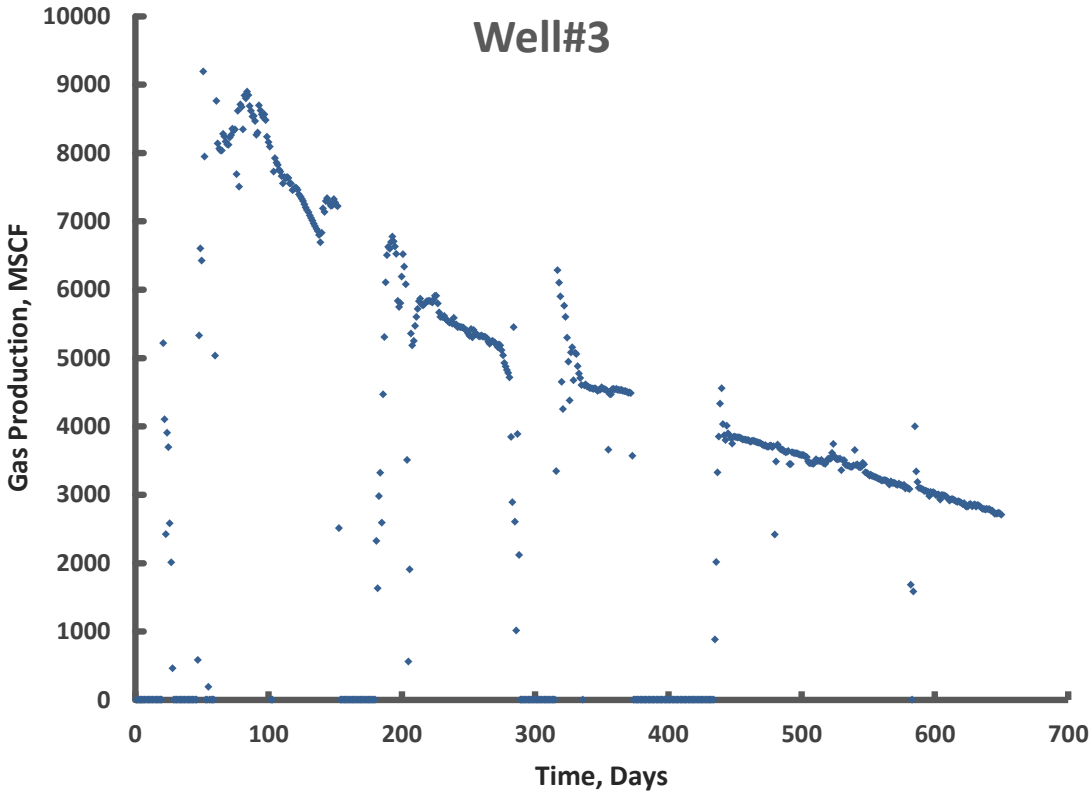
Well#3
Gas Production, MSCF
Time, Days
10000
9000
8000
7000
6000
5000
4000
3000
2000
1000
0
0
100
200
300
400
500
600
700

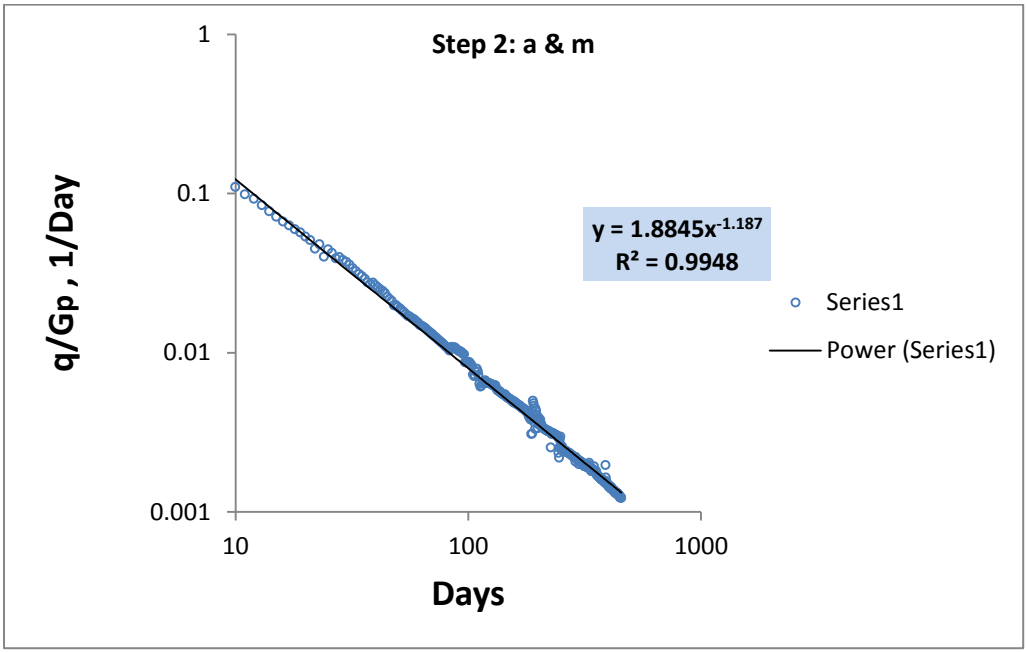
Step 2: a & m
q/Gp , 1/Day
Days
y = 1.8845x-1.187
R² = 0.9948
Series1
Power (Series1)
1
0.1
0.01
0.001
10
100
1000

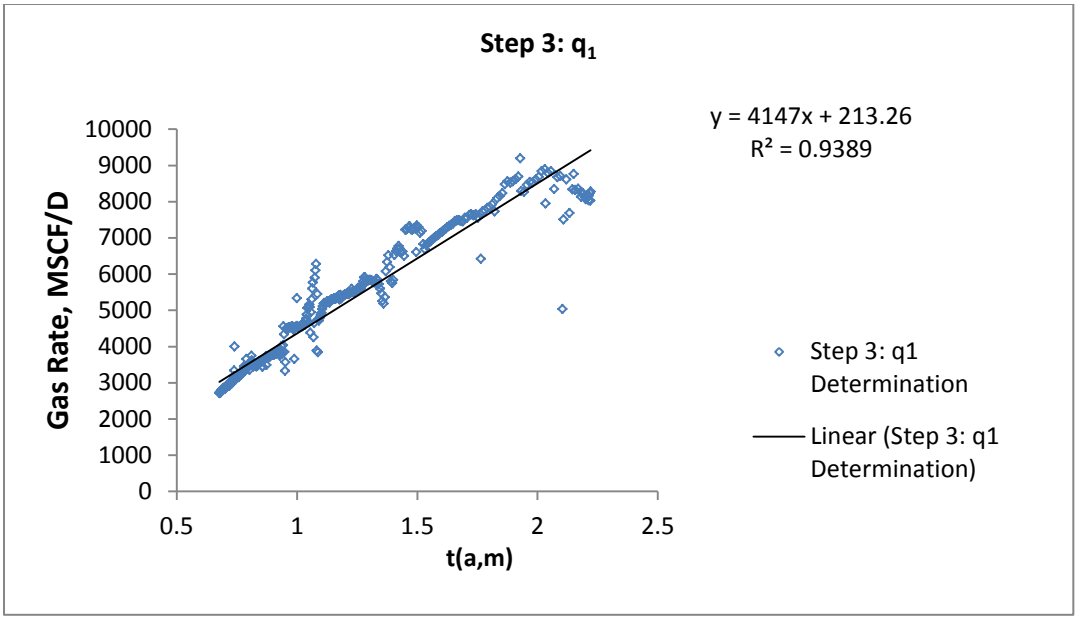
Step 3: q1
y = 4147x + 213.26
R² = 0.9389
Gas Rate, MSCF/D
10000
9000
8000
7000
6000
5000
4000
3000
2000
1000
0
0.5
1
1.5
2
2.5
t(a,m)
Step 3: q1 Determination
Linear (Step 3: q1 Determination)

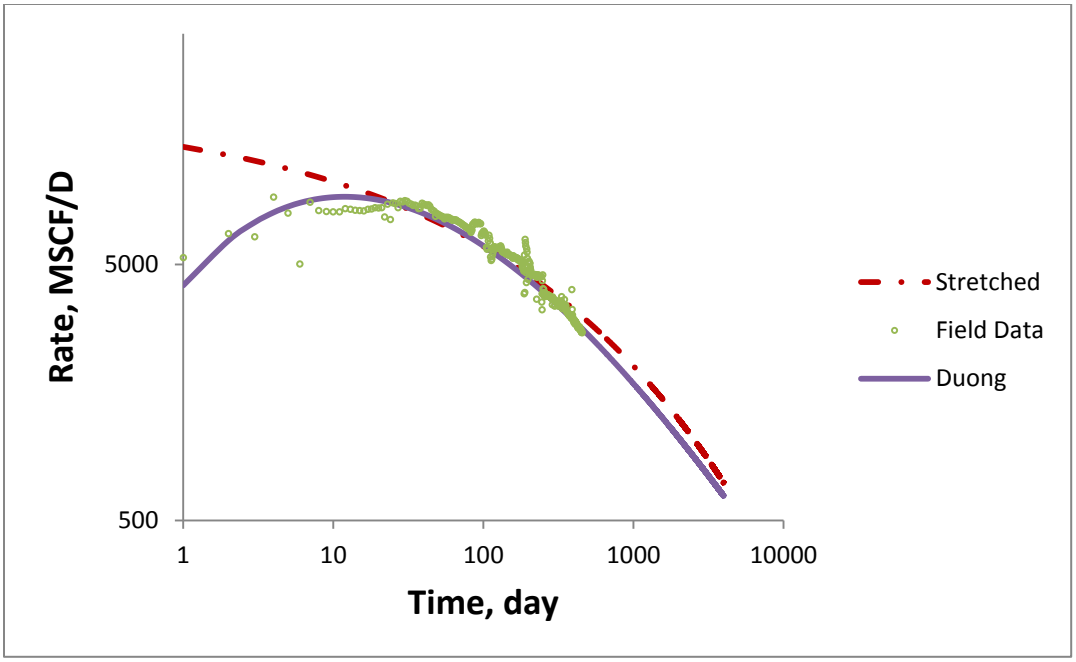
Rate, MSCF/D
5000
500
1
10
100
1000
10000
Time, day
Stretched
Field Data
Duong

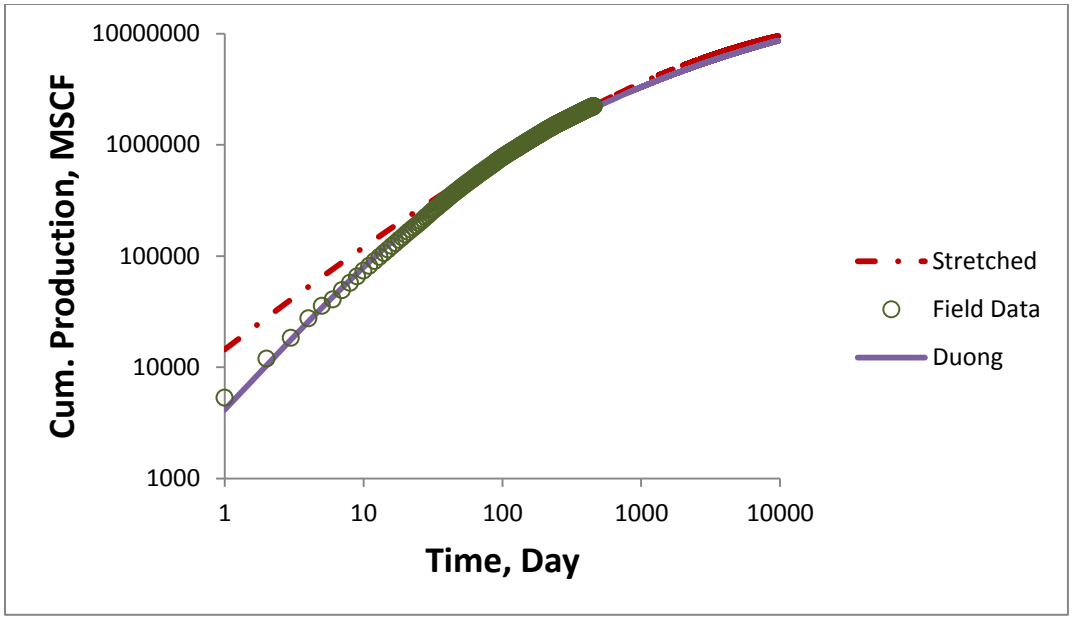
10000000
1000000
100000
10000
1000
Cum. Production, MSCF
1
10
100
1000
10000
Time, Day
Stretched
Field Data
Duong

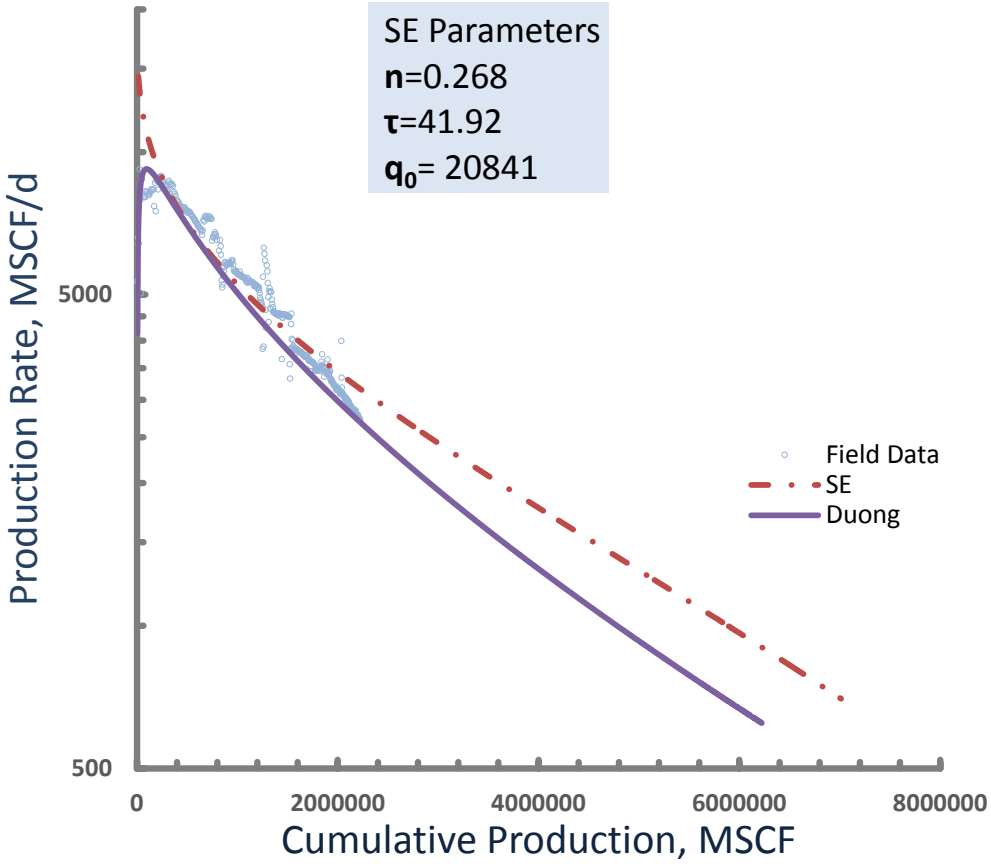
SE Parameters
n=0.268
τ=41.92
q0= 20841
Production Rate, MSCF/d
5000
500
0
2000000
4000000
6000000
8000000
Cumulative Production, MSCF
Field Data
SE
Duong

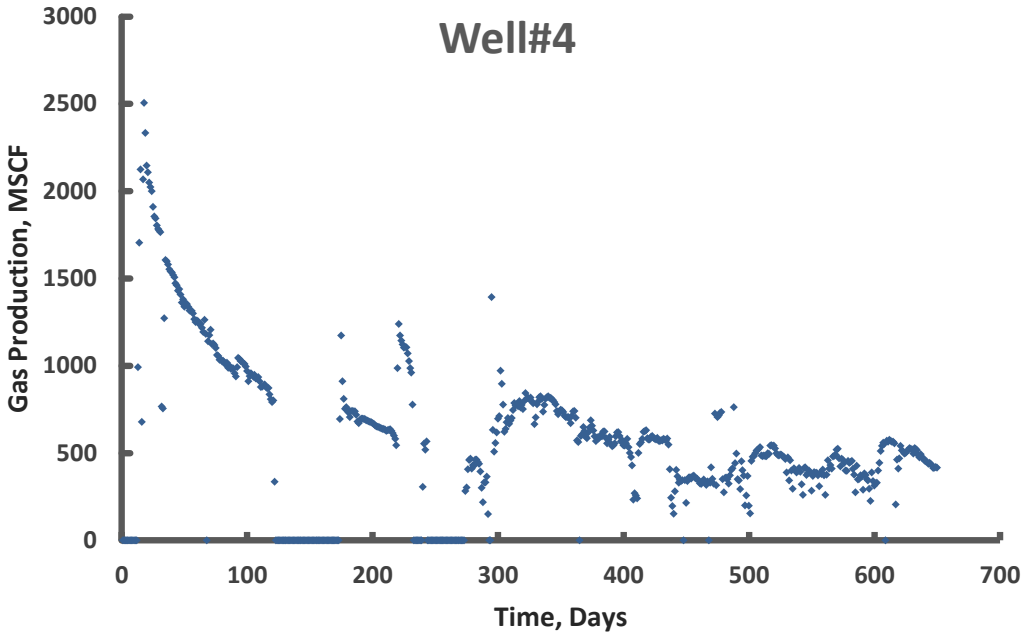
Well#4
Gas Production, MSCF
3000
2500
2000
1500
1000
500
0
0
100
200
300
400
500
600
700
Time, Days

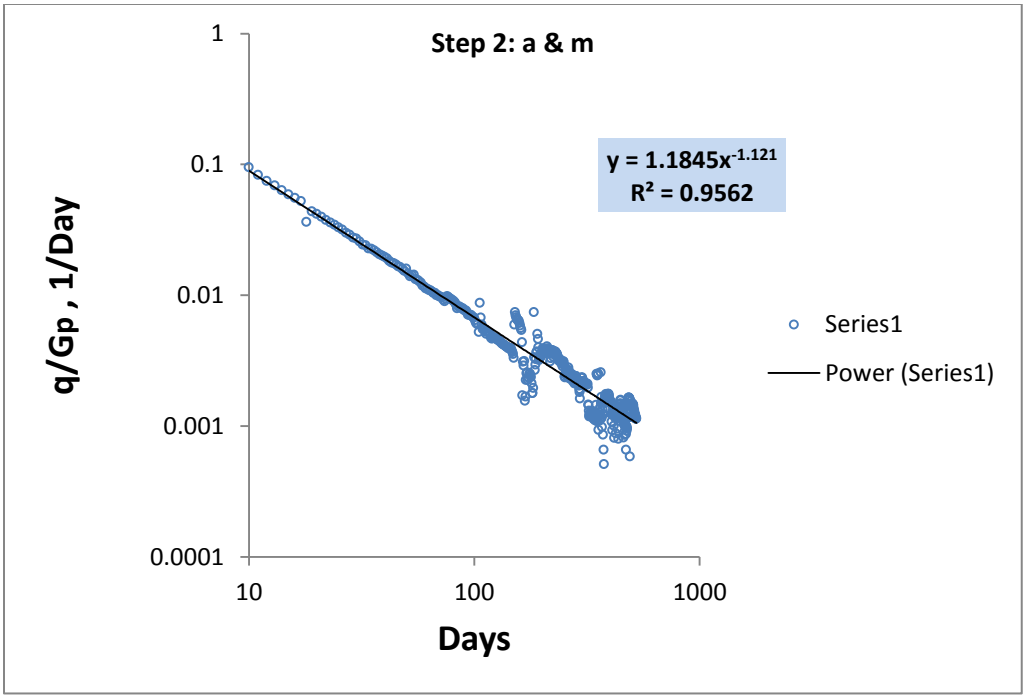
Step 2: a & m
y = 1.1845x-1.121
R² = 0.9562
q/Gp , 1/Day
1
0.1
0.01
0.001
0.0001
10
100
1000
Days
Series1
Power (Series1)

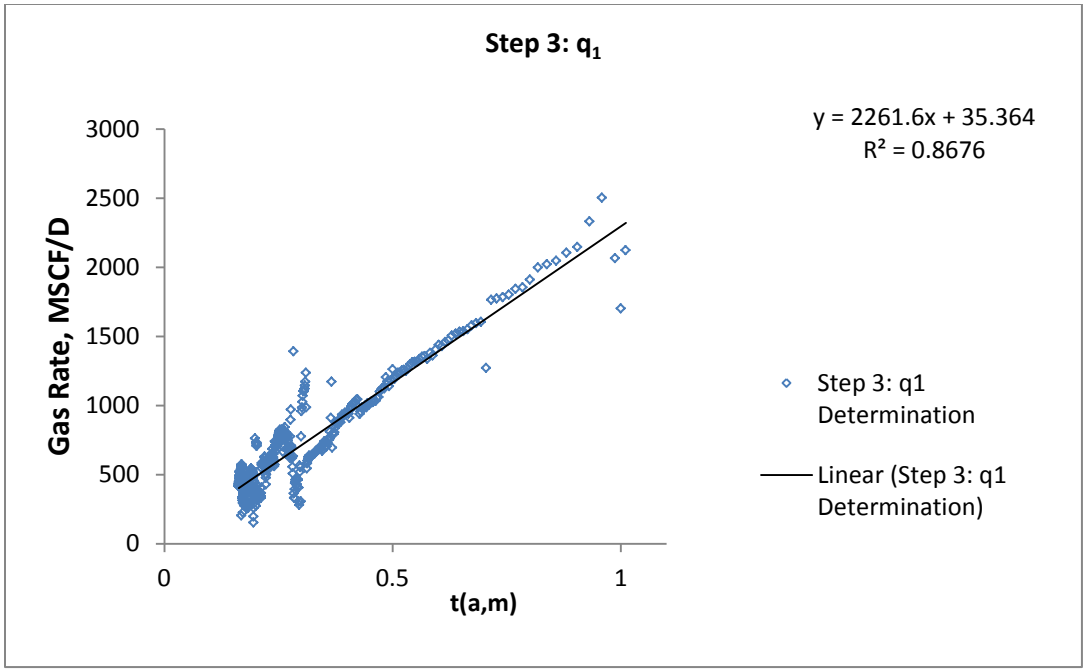
Step 3: q1
y = 2261.6x + 35.364
R² = 0.8676
Gas Rate, MSCF/D
3000
2500
2000
1500
1000
500
0
0
0.5
1
t(a,m)
Step 3: q1 Determination
Linear (Step 3: q1 Determination)

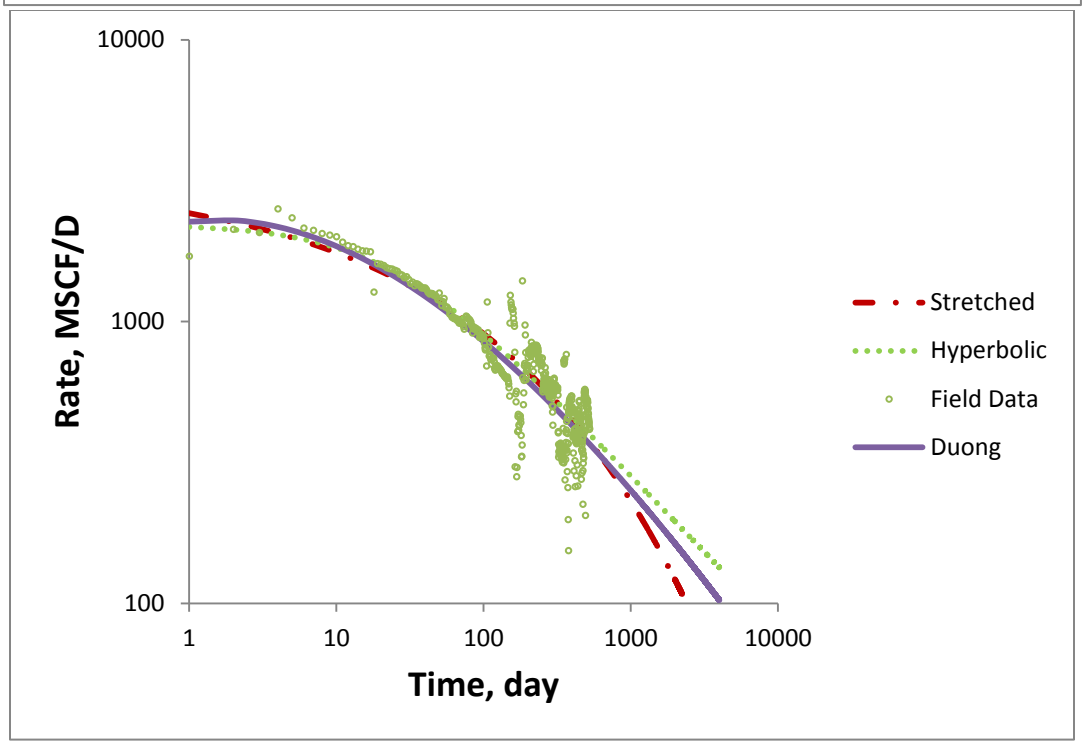
Rate, MSCF/D
10000
1000
100
1
10
100
1000
10000
Time, day
Stretched
Hyperbolic
Field Data
Duong

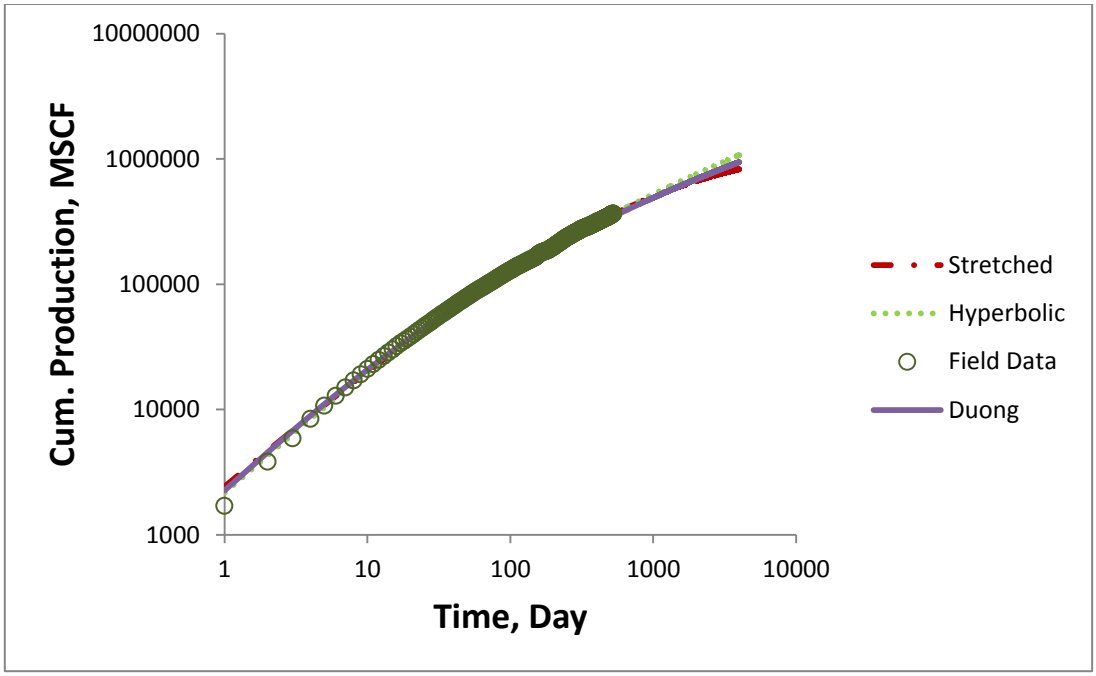
10000000
1000000
100000
10000
1000
Cum. Production, MSCF
1
10
100
1000
10000
Time, Day
Stretched
Hyperbolic
Field Data
Duong

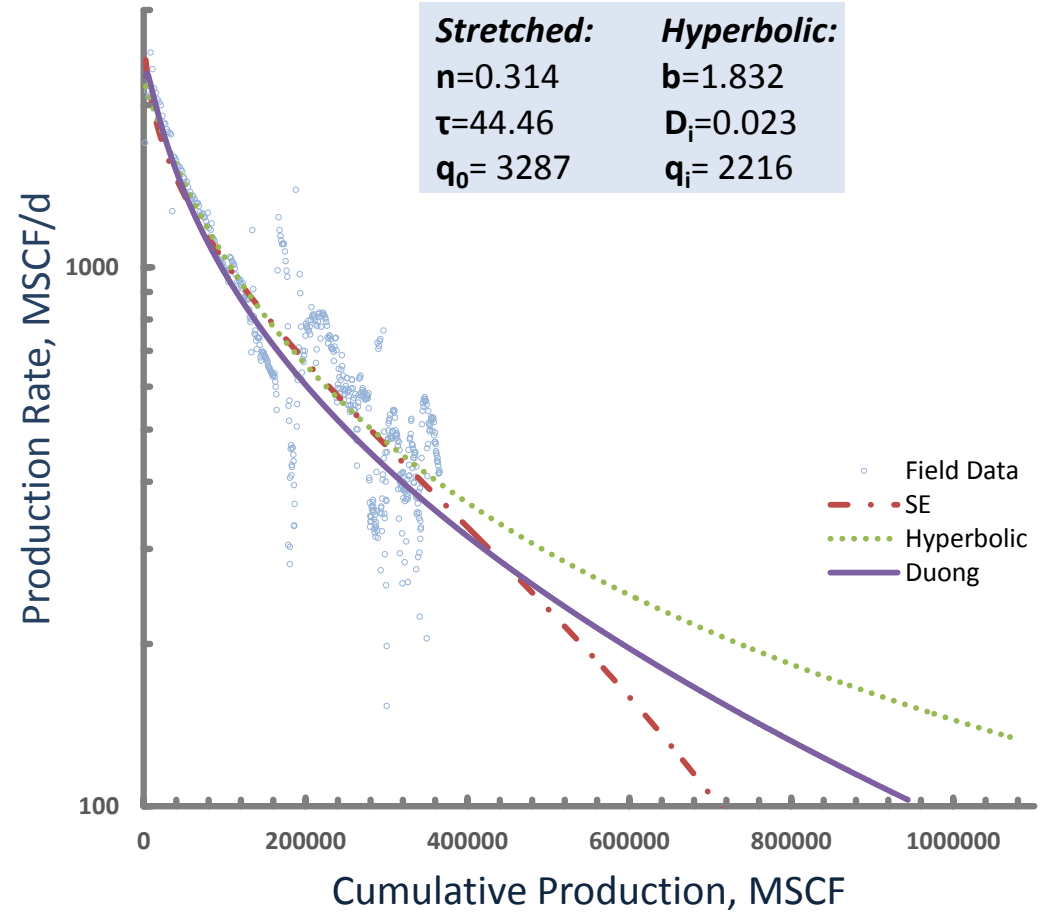
Stretched:
n=0.314
τ=44.46
q0= 3287
Hyperbolic:
b=1.832
Di=0.023
qi= 2216
Production Rate, MSCF/d
1000
100
0
200000
400000
600000
800000
1000000
Cumulative Production, MSCF
Field Data
SE
Hyperbolic
Duong

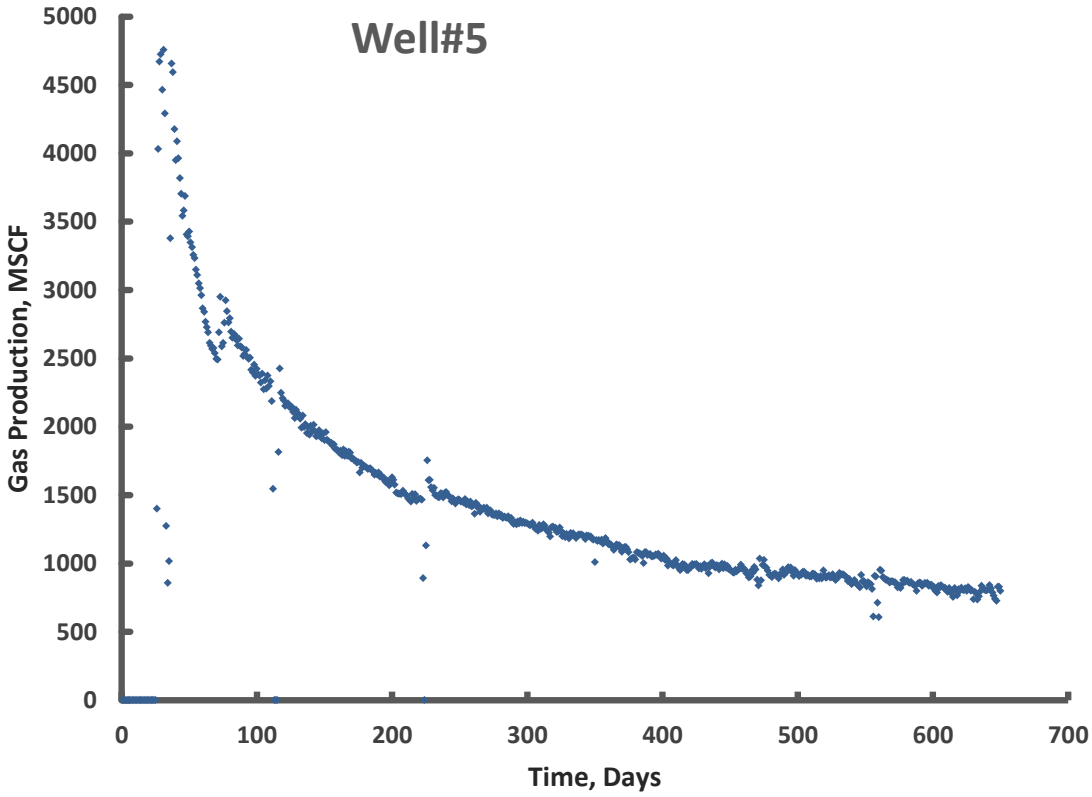
Well#5
Gas Production, MSCF
5000
4500
4000
3500
3000
2500
2000
1500
1000
500
0
0
100
200
300
400
500
600
700
Time, Days

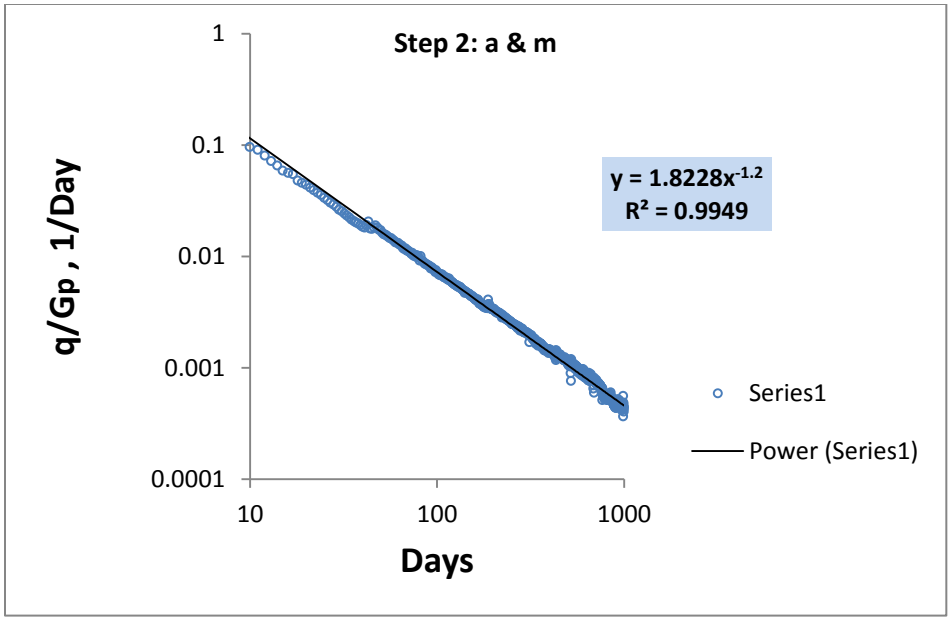
Step 2: a & m
q/Gp , 1/Day
1
0.1
0.01
0.001
0.0001
10
100
1000
Days
y = 1.8228x-1.2
R² = 0.9949
Series1
Power (Series1)

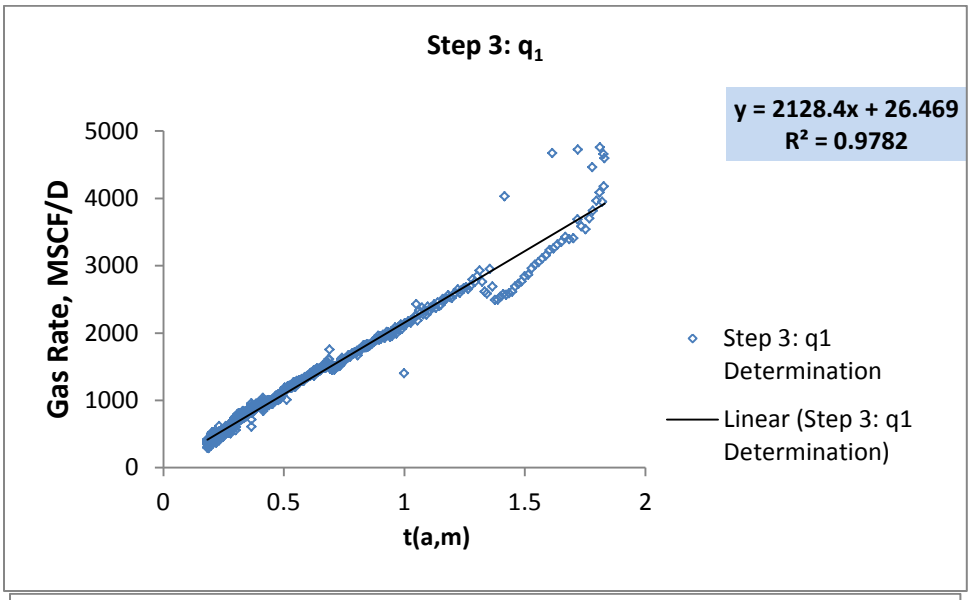
Step 3: q1
y = 2128.4x + 26.469
R² = 0.9782
Gas Rate, MSCF/D
5000
4000
3000
2000
1000
0
0
0.5
1
1.5
2
t(a,m)
Step 3: q1 Determination
Linear (Step 3: q1 Determination)

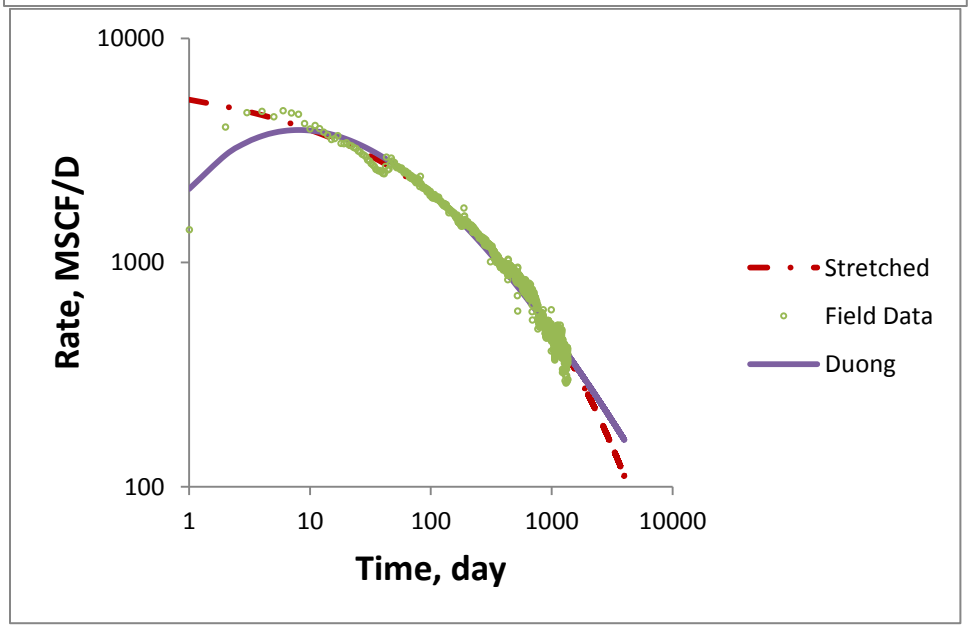
Rate, MSCF/D
10000
1000
100
1
10
100
1000
10000
Time, day
Stretched
Field Data
Duong

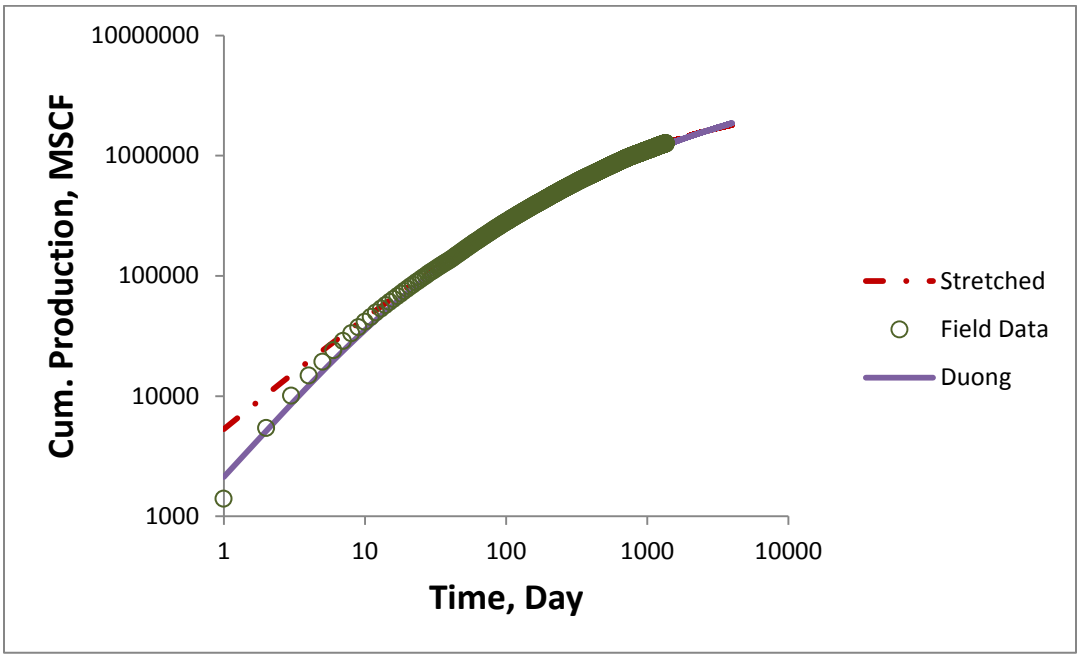
10000000
1000000
100000
10000
1000
Cum. Production, MSCF
1
10
100
1000
10000
Time, Day
Stretched
Field Data
Duong

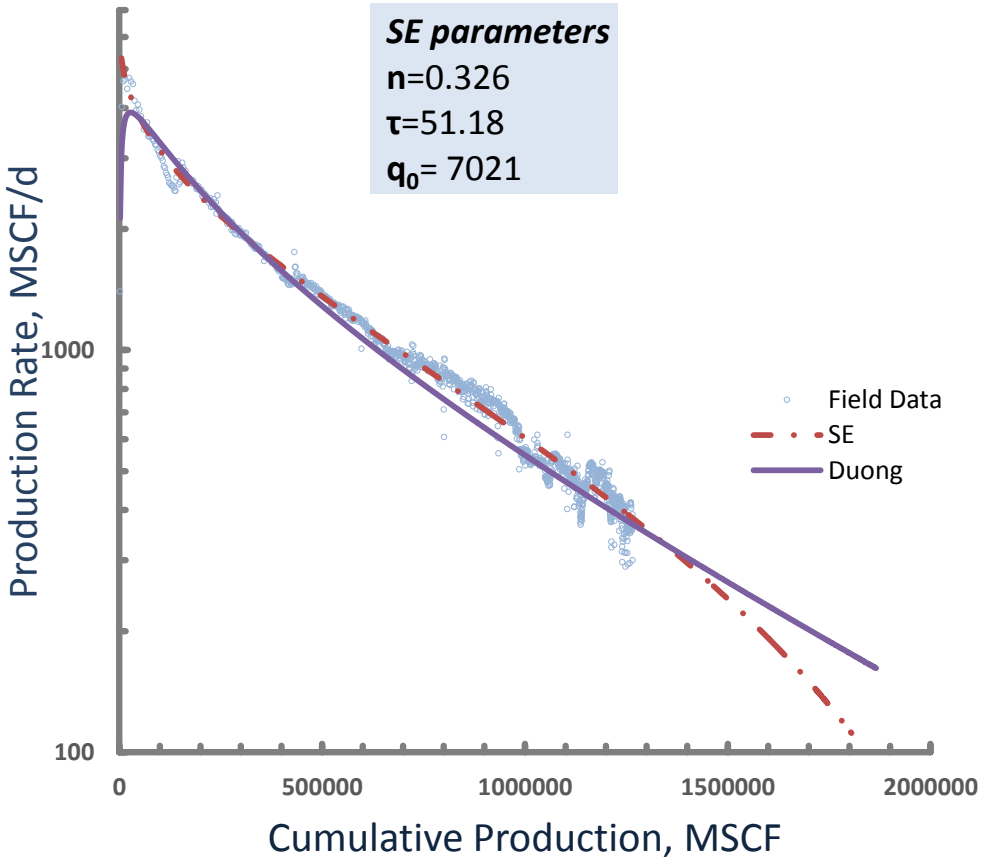
SE parameters
n=0.326
τ=51.18
q0= 7021
Production Rate, MSCF/d
1000
100
0
500000
1000000
1500000
2000000
Cumulative Production, MSCF
Field Data
SE
Duong

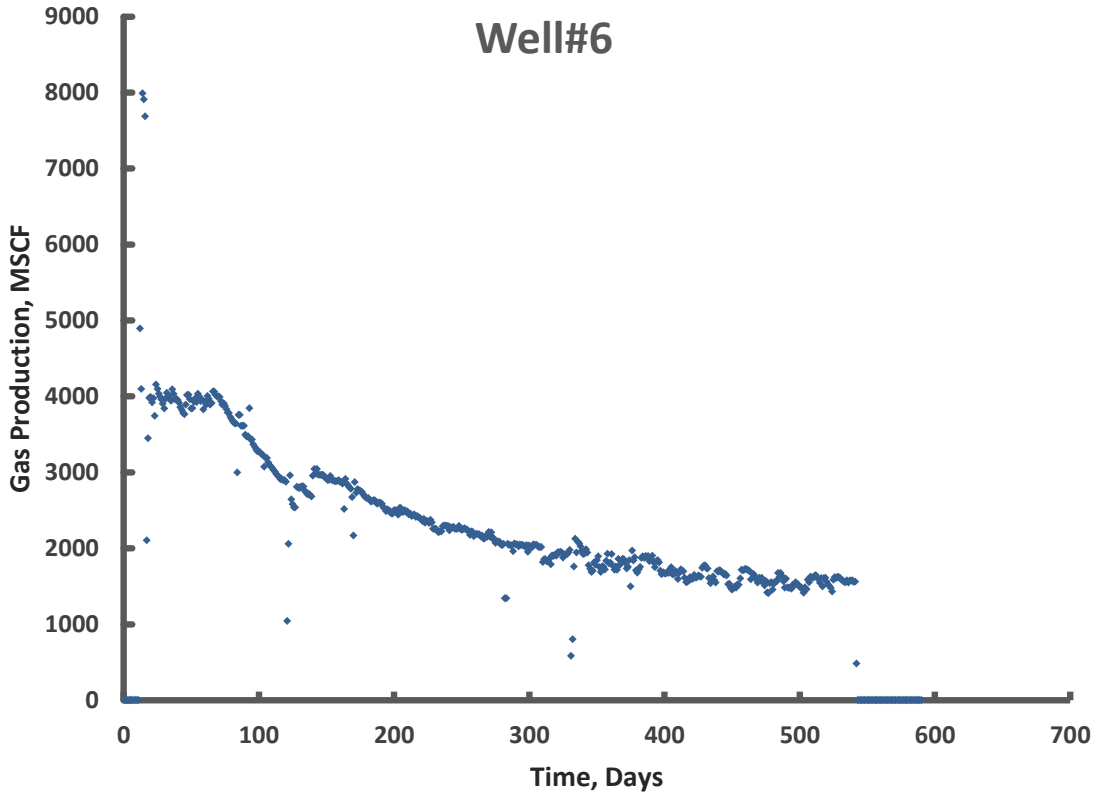
Well#6
Gas Production, MSCF
9000
8000
7000
6000
5000
4000
3000
2000
1000
0
0
100
200
300
400
500
600
700
Time, Days

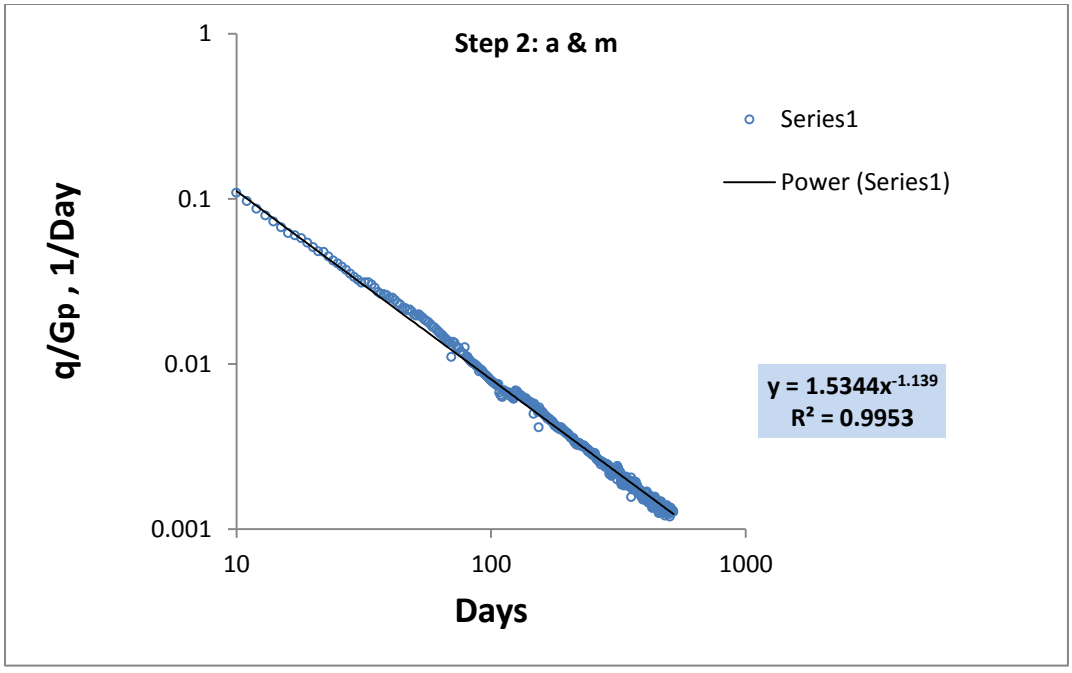
Step 2: a & m
q/Gp , 1/Day
1
0.1
0.01
0.001
10
100
1000
Days
Series1
Power (Series1)
y = 1.5344x-1.139
R² = 0.9953

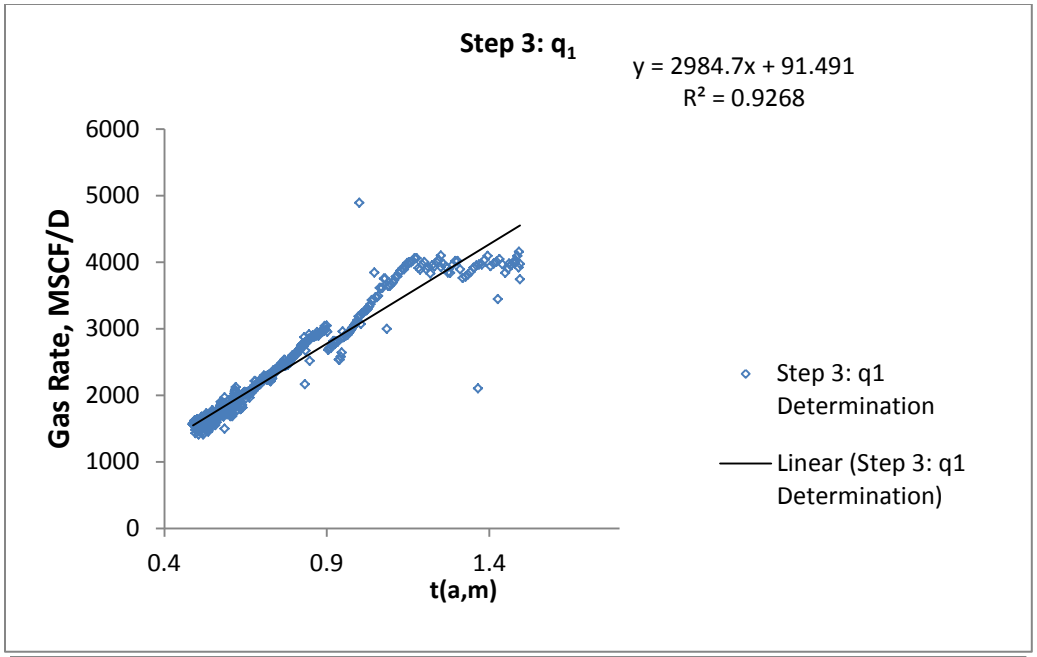
Step 3: q1
y = 2984.7x + 91.491
R² = 0.9268
Gas Rate, MSCF/D
6000
5000
4000
3000
2000
1000
0
0.4
0.9
1.4
t(a,m)
Step 3: q1 Determination
Linear (Step 3: q1 Determination)

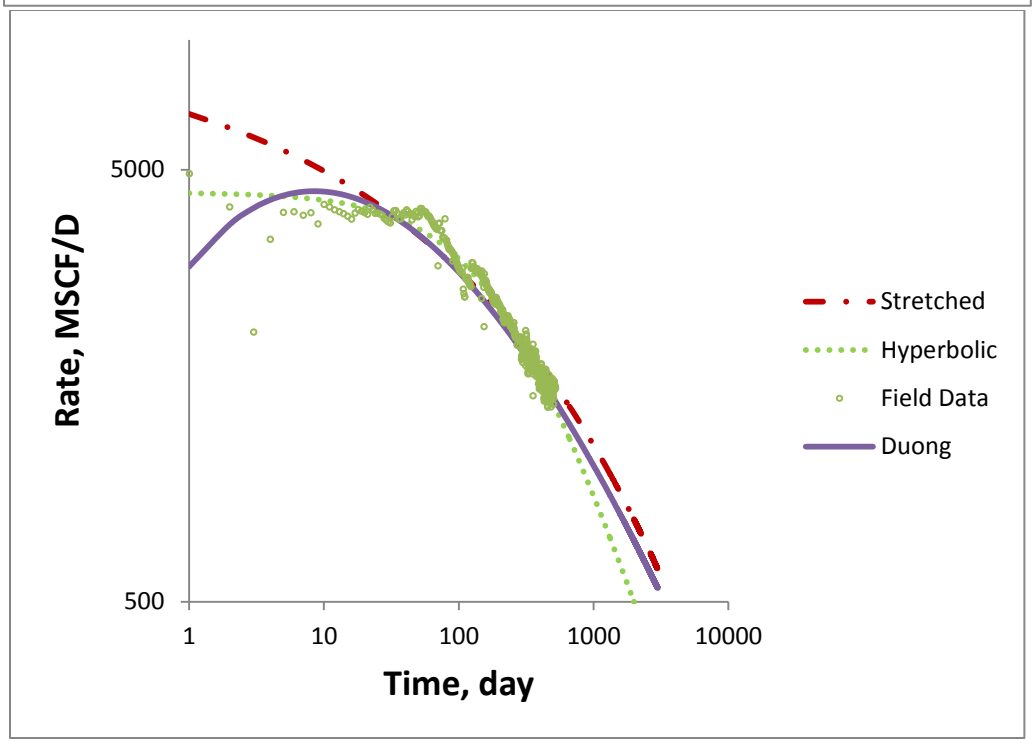
Rate, MSCF/D
5000
500
1
10
100
1000
10000
Time, day
Stretched
Hyperbolic
Field Data
Duong

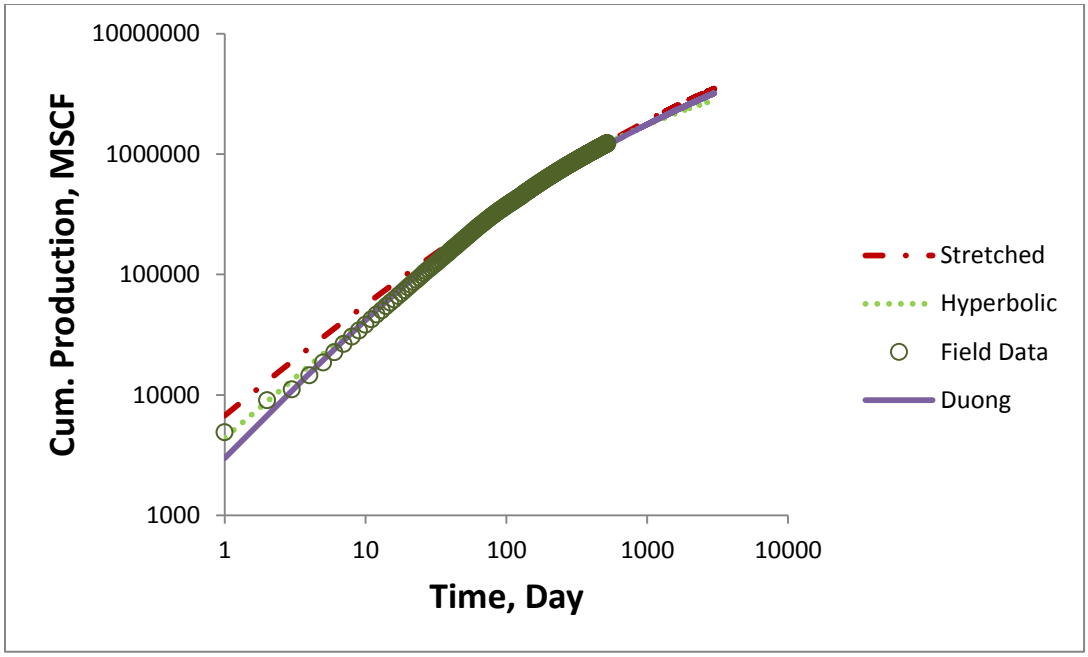
10000000
1000000
100000
10000
1000
Cum. Production, MSCF
1
10
100
1000
10000
Time, Day
Stretched
Hyperbolic
Field Data
Duong

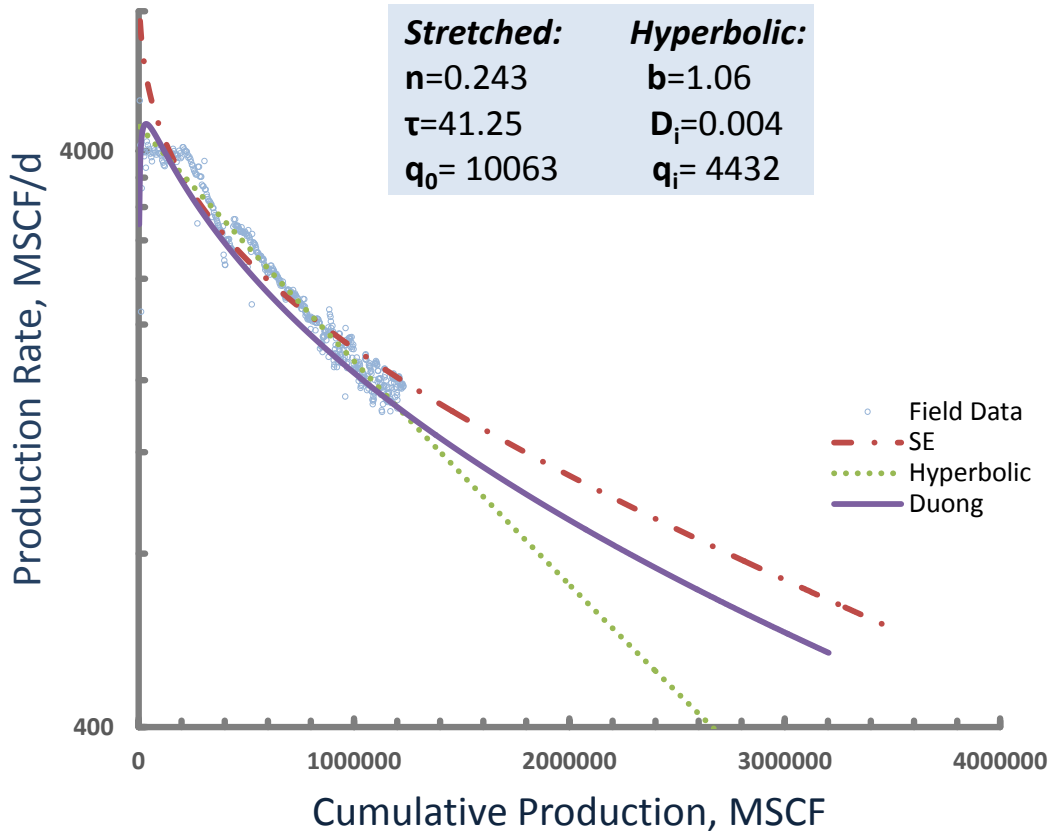
Stretched:
n=0.243
τ=41.25
q0= 10063
Hyperbolic:
b=1.06
Di=0.004
qi= 4432
4000
400
Production Rate, MSCF/d
0
1000000
2000000
3000000
4000000
Cumulative Production, MSCF
Field Data
SE
Hyperbolic
Duong

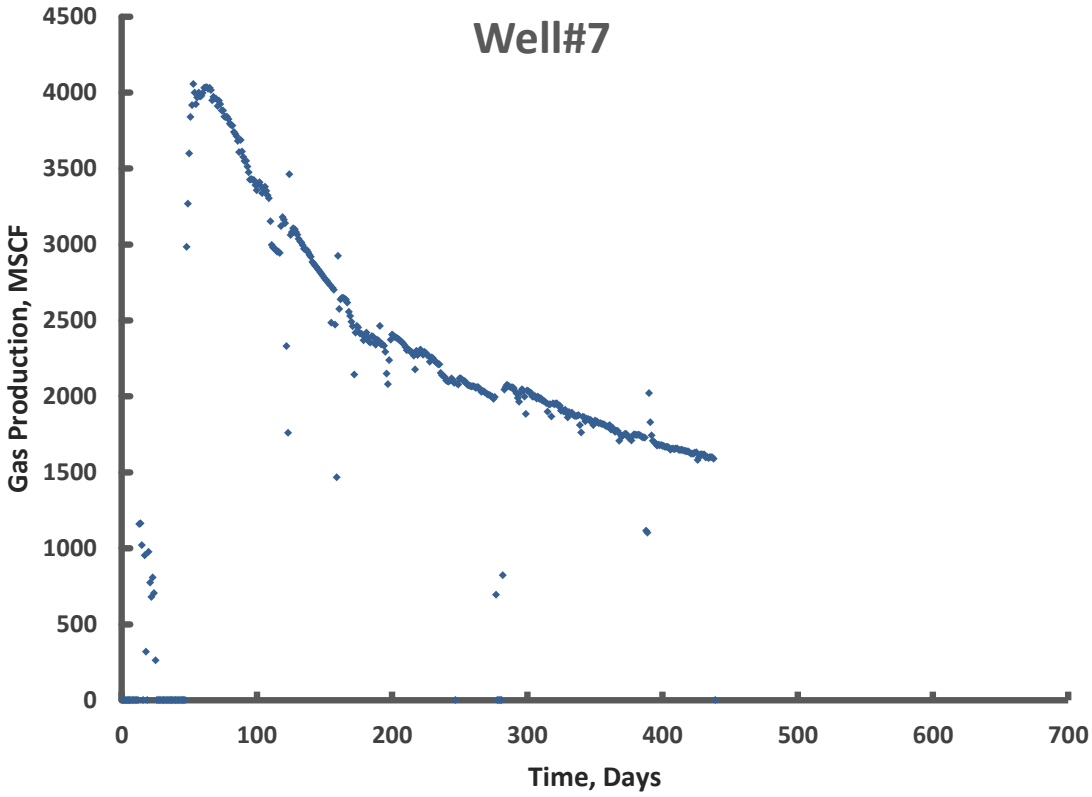
Well#7
Gas Production, MSCF
Time, Days
4500
4000
3500
3000
2500
2000
1500
1000
500
0
0
100
200
300
400
500
600
700

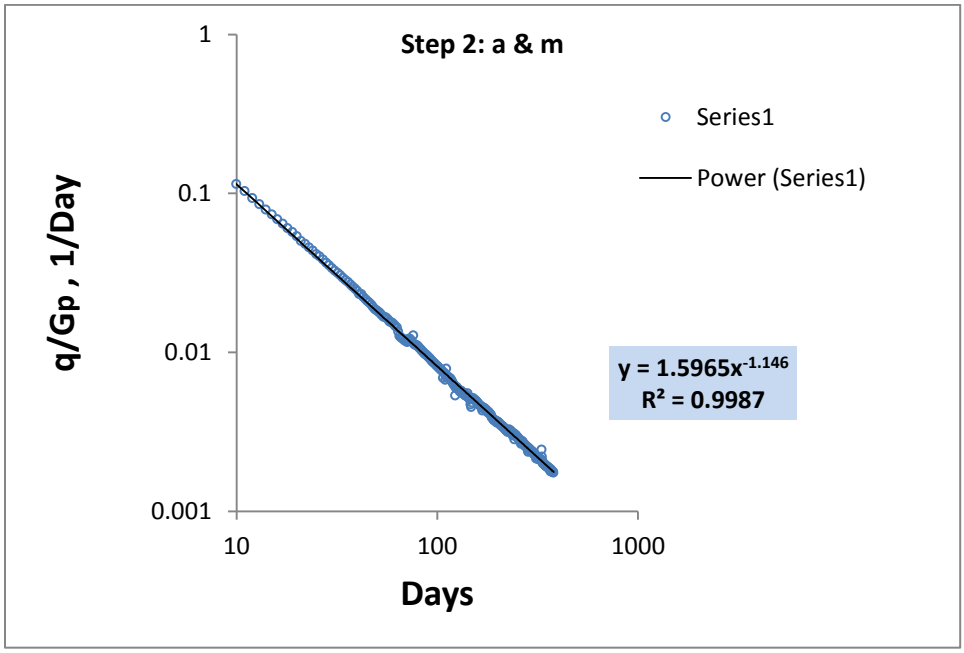
Step 2: a & m
q/Gp , 1/Day
Days
Series1
Power (Series1)
y = 1.5965x-1.146
R² = 0.9987
1
0.1
0.01
0.001
10
100
1000

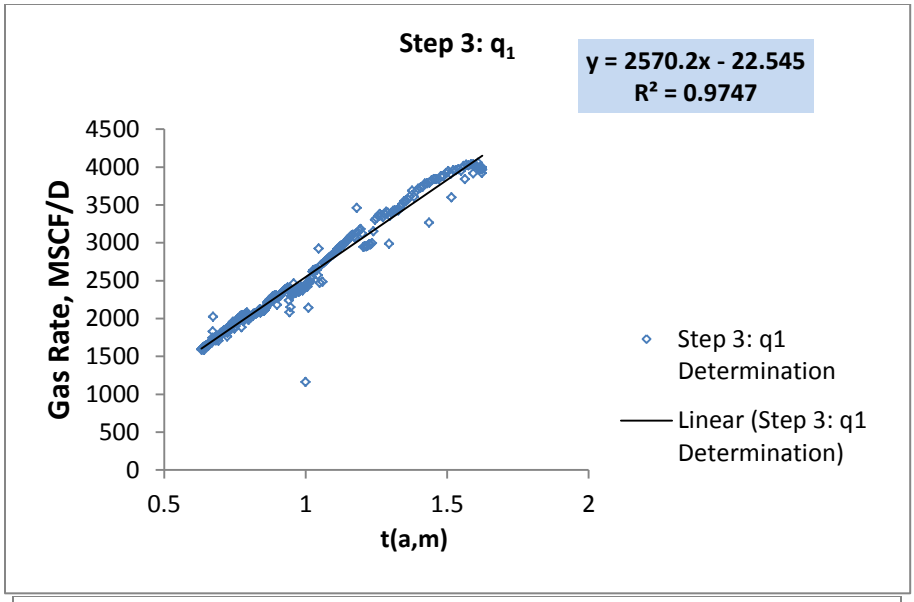
Step 3: q1
y = 2570.2x - 22.545
R² = 0.9747
Gas Rate, MSCF/D
4500
4000
3500
3000
2500
2000
1500
1000
500
0
0.5
1
1.5
2
t(a,m)
Step 3: q1 Determination
Linear (Step 3: q1 Determination)

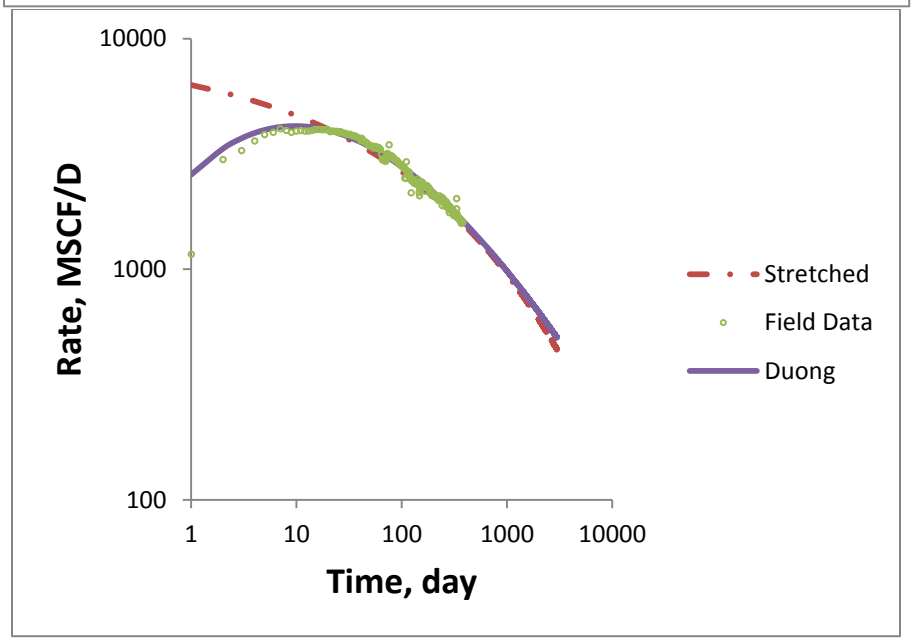
Rate, MSCF/D
10000
1000
100
1
10
100
1000
10000
Time, day
Stretched
Field Data
Duong

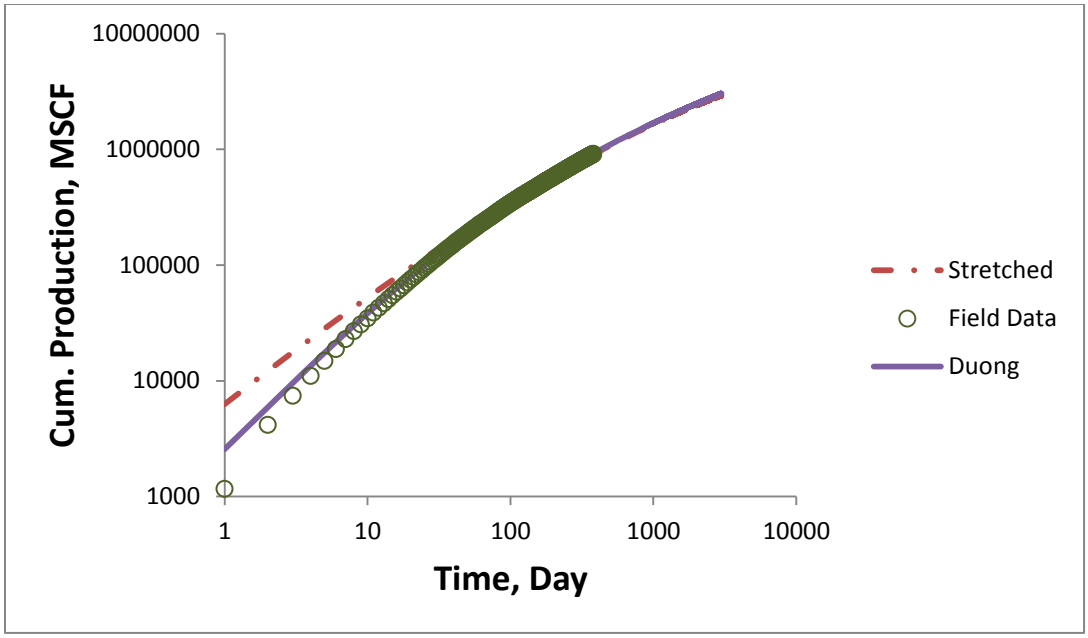
10000000
1000000
100000
10000
1000
Cum. Production, MSCF
1
10
100
1000
10000
Time, Day
Stretched
Field Data
Duong

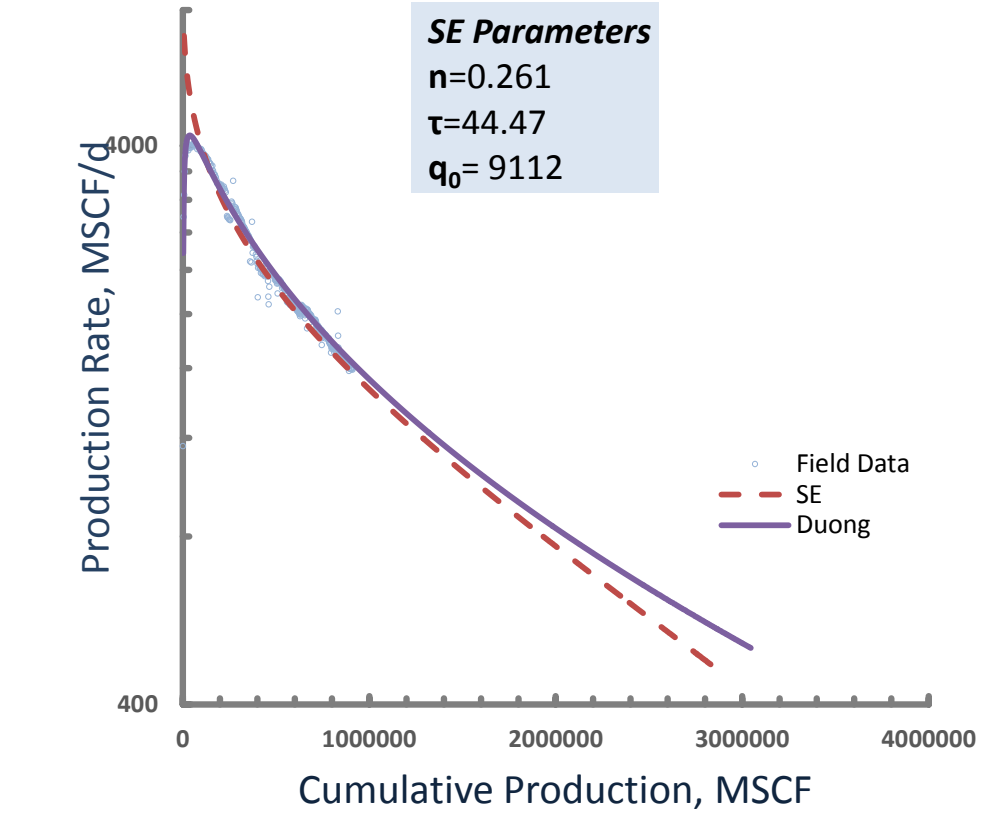
SE Parameters
n=0.261
τ=44.47
q0= 9112
4000
400
Production Rate, MSCF/d
0
1000000
2000000
3000000
4000000
Cumulative Production, MSCF
Field Data
SE
Duong

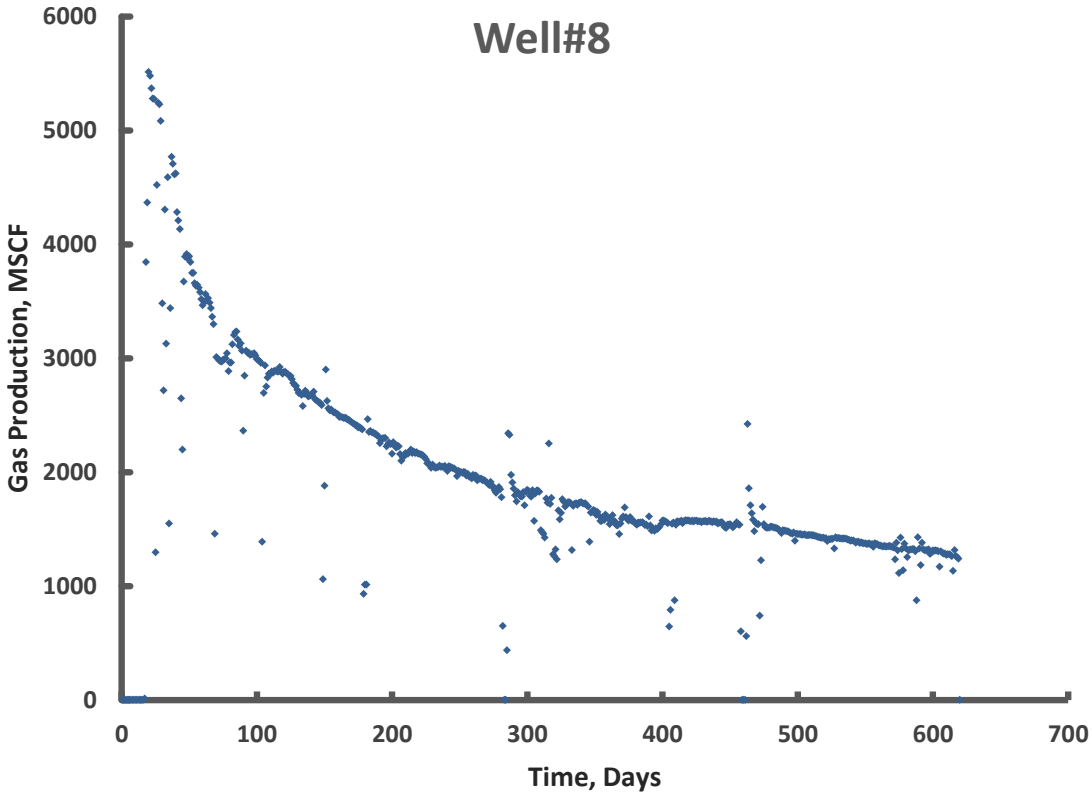
Well#8
Gas Production, MSCF
6000
5000
4000
3000
2000
1000
0
0
100
200
300
400
500
600
700
Time, Days

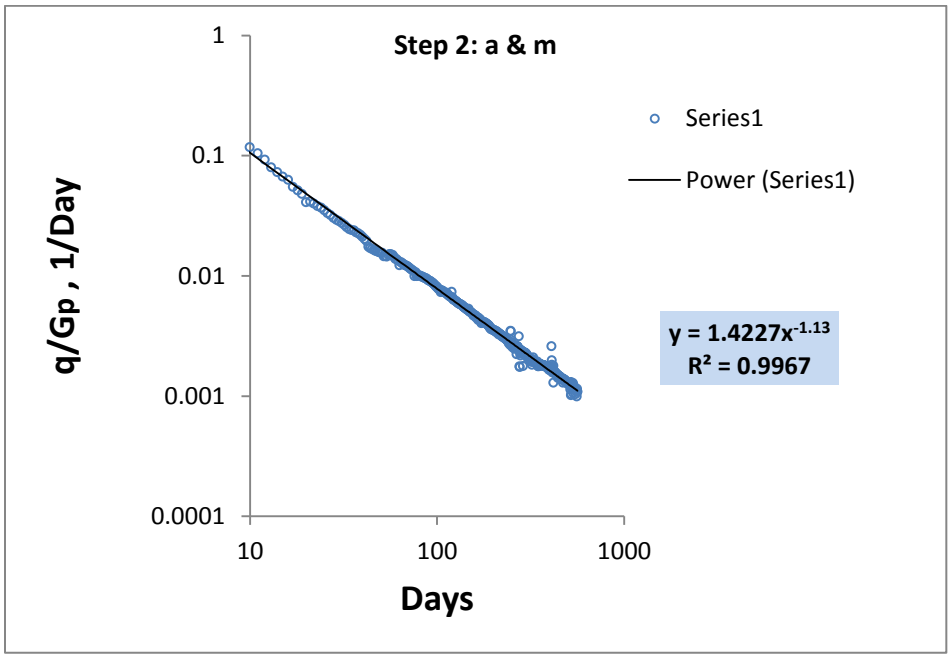
Step 2: a & m
q/Gp , 1/Day
1
0.1
0.01
0.001
0.0001
10
100
1000
Days
Series1
Power (Series1)
y = 1.4227x-1.13
R² = 0.9967

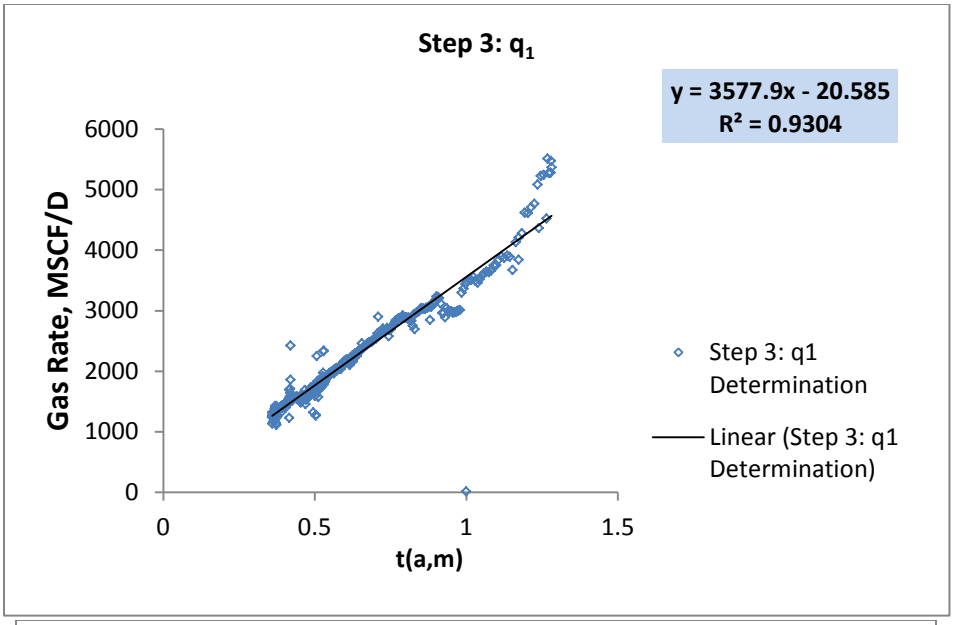
Step 3: q1
y = 3577.9x - 20.585
R² = 0.9304
Gas Rate, MSCF/D
6000
5000
4000
3000
2000
1000
0
0
0.5
1
1.5
t(a,m)
Step 3: q1 Determination
Linear (Step 3: q1 Determination)

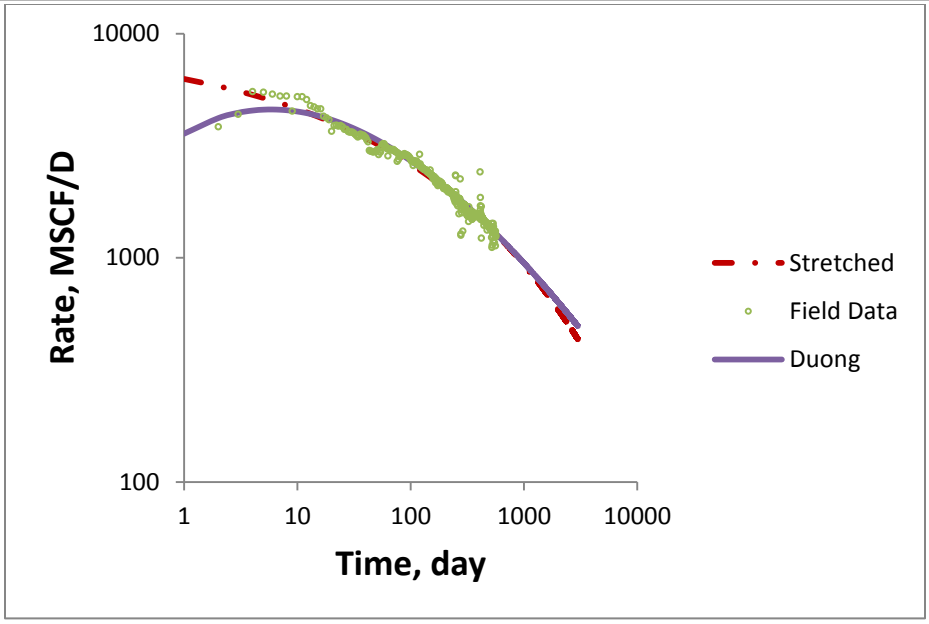
Rate, MSCF/D
10000
1000
100
1
10
100
1000
10000
Time, day
Stretched
Field Data
Duong

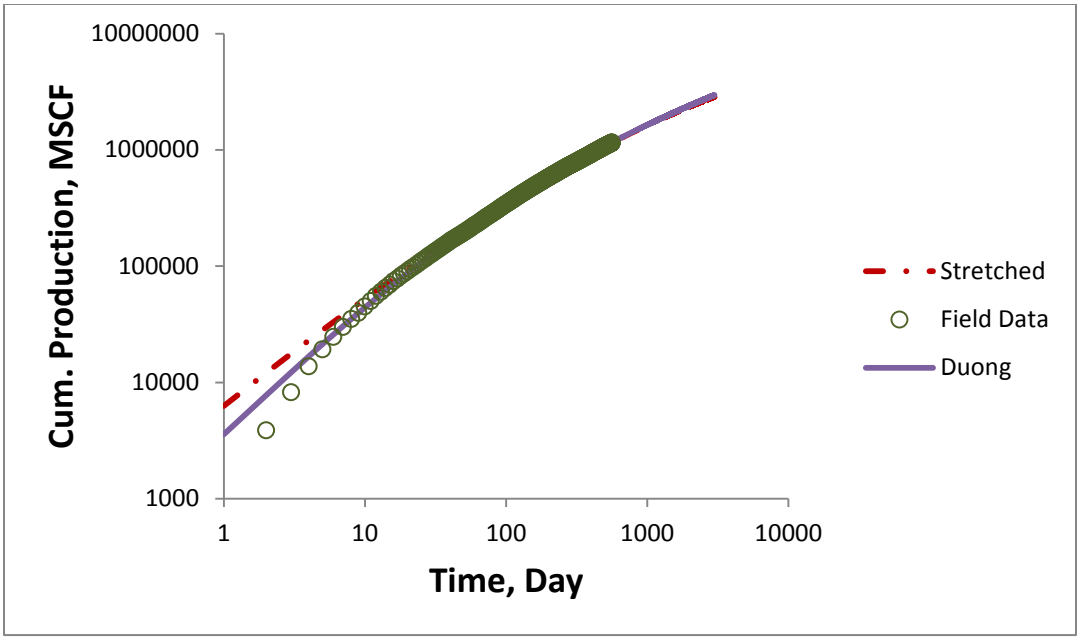
10000000
1000000
100000
10000
1000
Cum. Production, MSCF
1
10
100
1000
10000
Time, Day
Stretched
Field Data
Duong

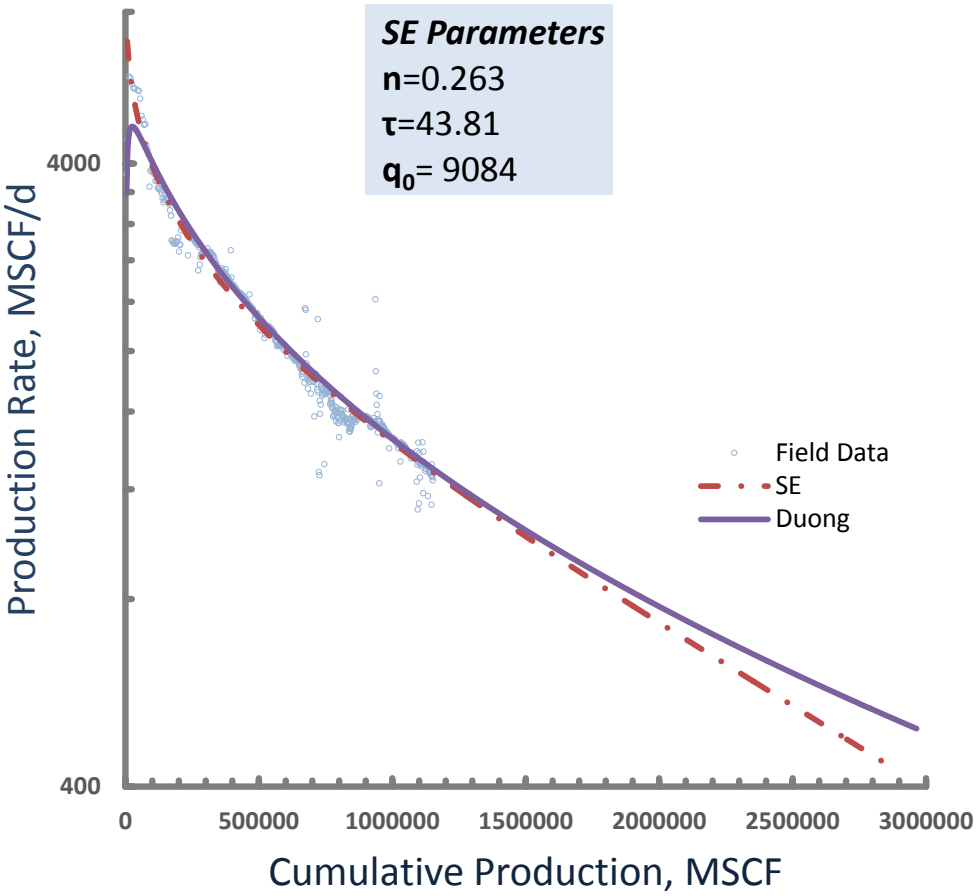
SE Parameters
n=0.263
τ=43.81
q0= 9084
4000
400
Production Rate, MSCF/d
0
500000
1000000
1500000
2000000
2500000
3000000
Cumulative Production, MSCF
Field Data
SE
Duong

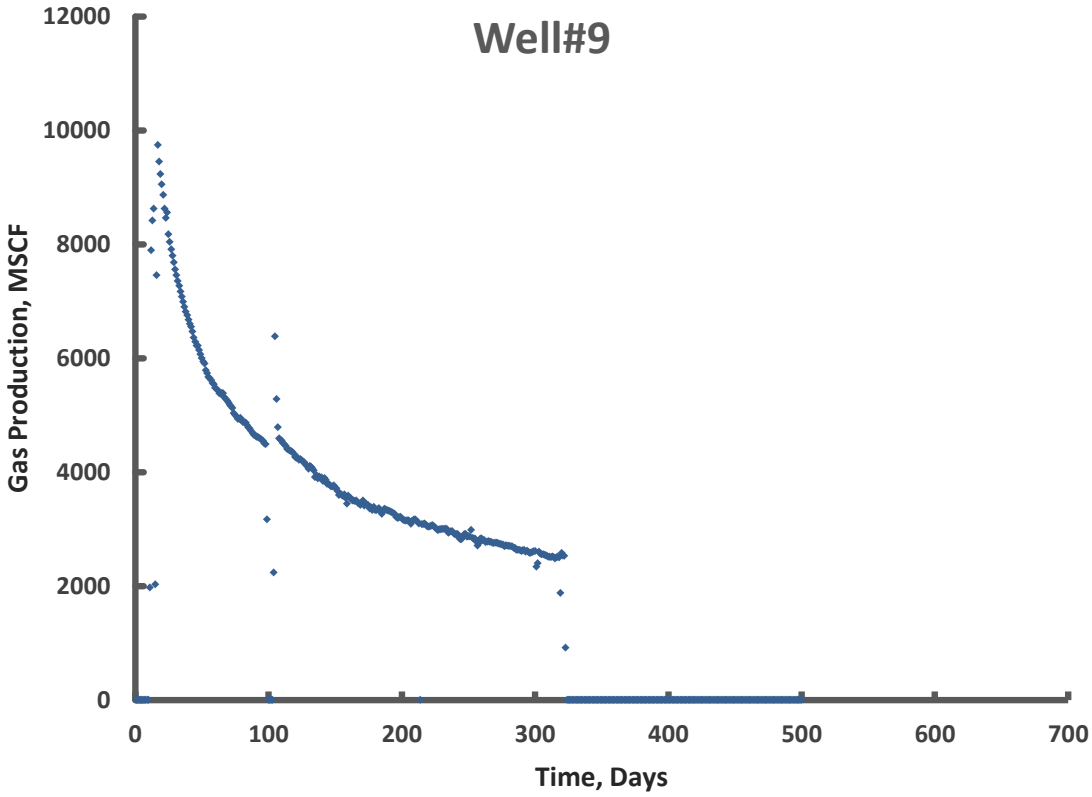
Well#9
Gas Production, MSCF
12000
10000
8000
6000
4000
2000
0
0
100
200
300
400
500
600
700
Time, Days

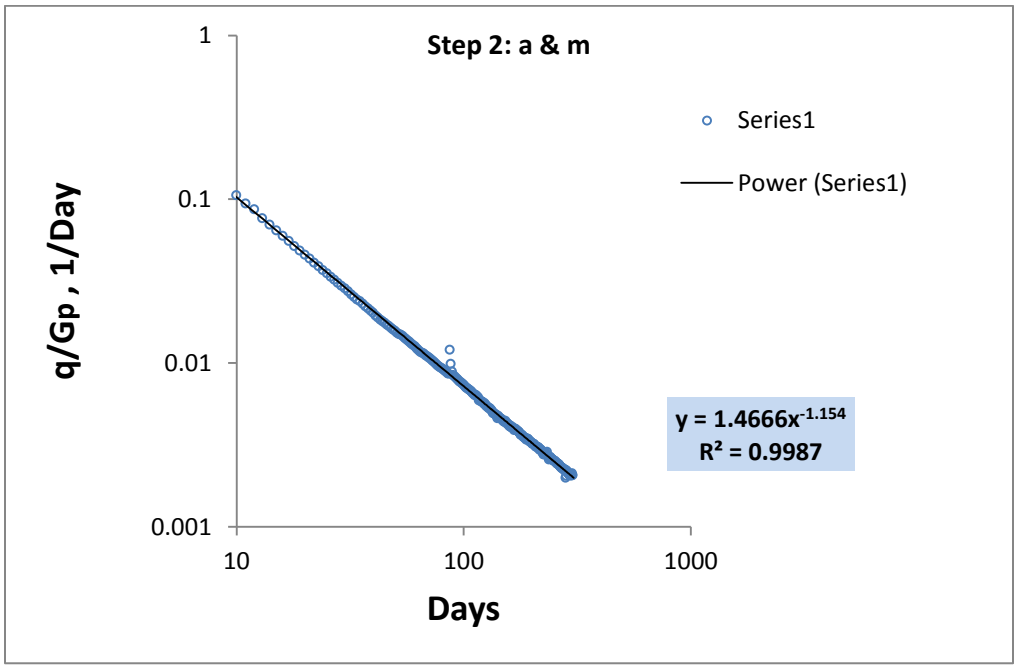
Step 2: a & m
q/Gp , 1/Day
1
0.1
0.01
0.001
10
100
1000
Days
Series1
Power (Series1)
y = 1.4666x-1.154
R² = 0.9987

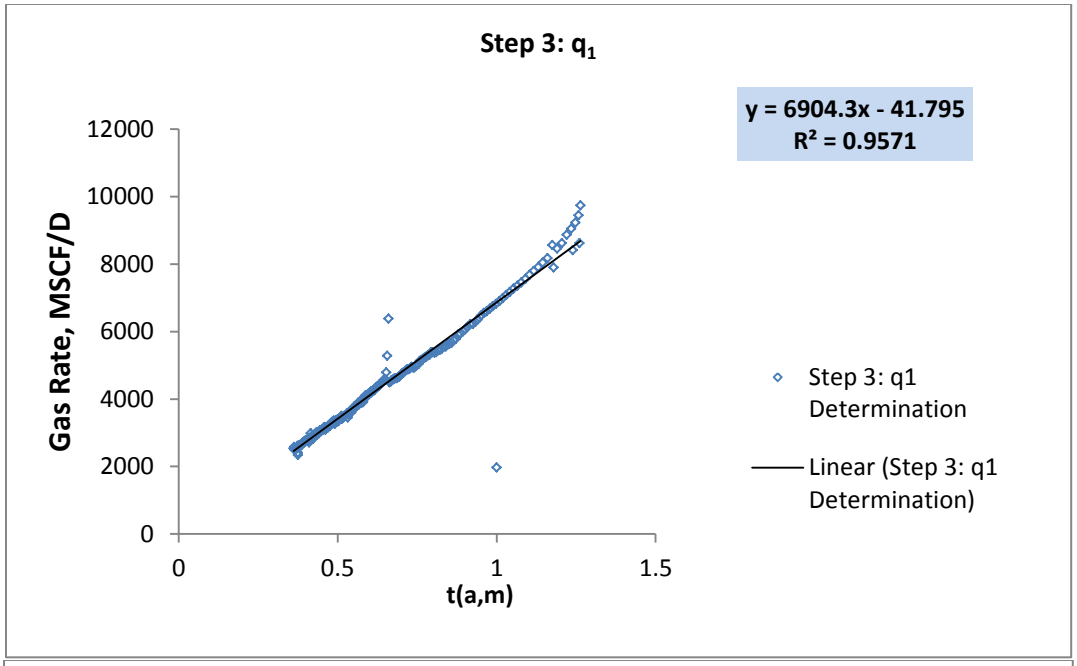
Step 3: q1
y = 6904.3x - 41.795
R² = 0.9571
Gas Rate, MSCF/D
12000
10000
8000
6000
4000
2000
0
0
0.5
1
1.5
t(a,m)
Step 3: q1 Determination
Linear (Step 3: q1 Determination)

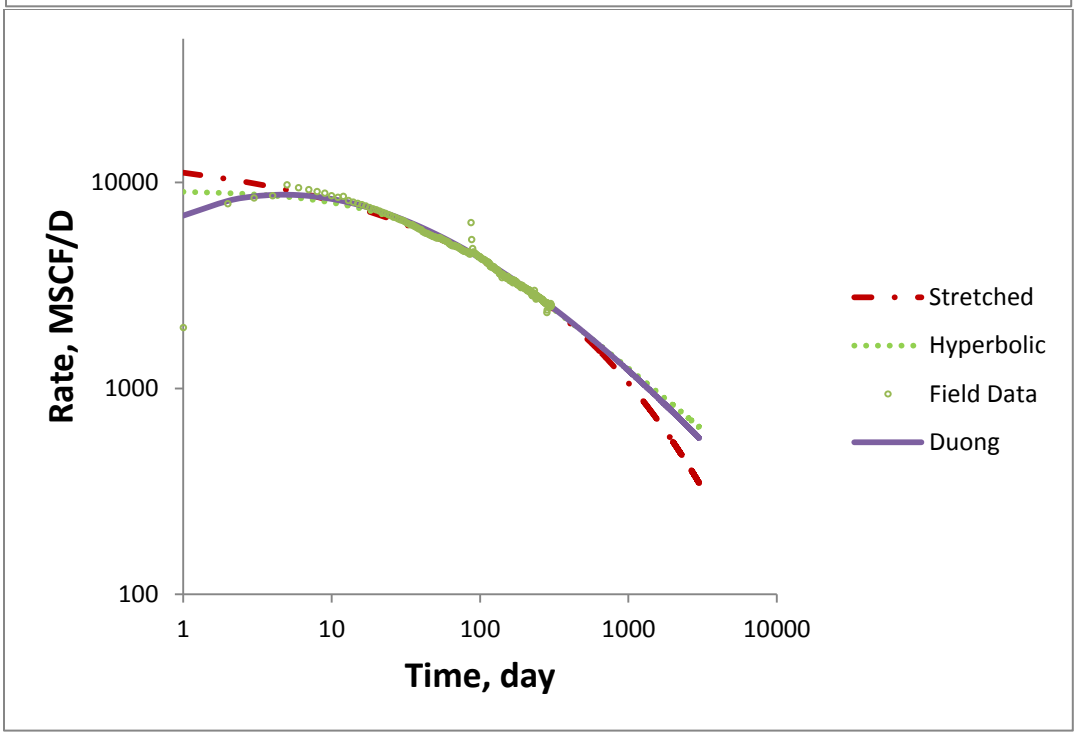
Rate, MSCF/D
10000
1000
100
1
10
100
1000
10000
Time, day
Stretched
Hyperbolic
Field Data
Duong

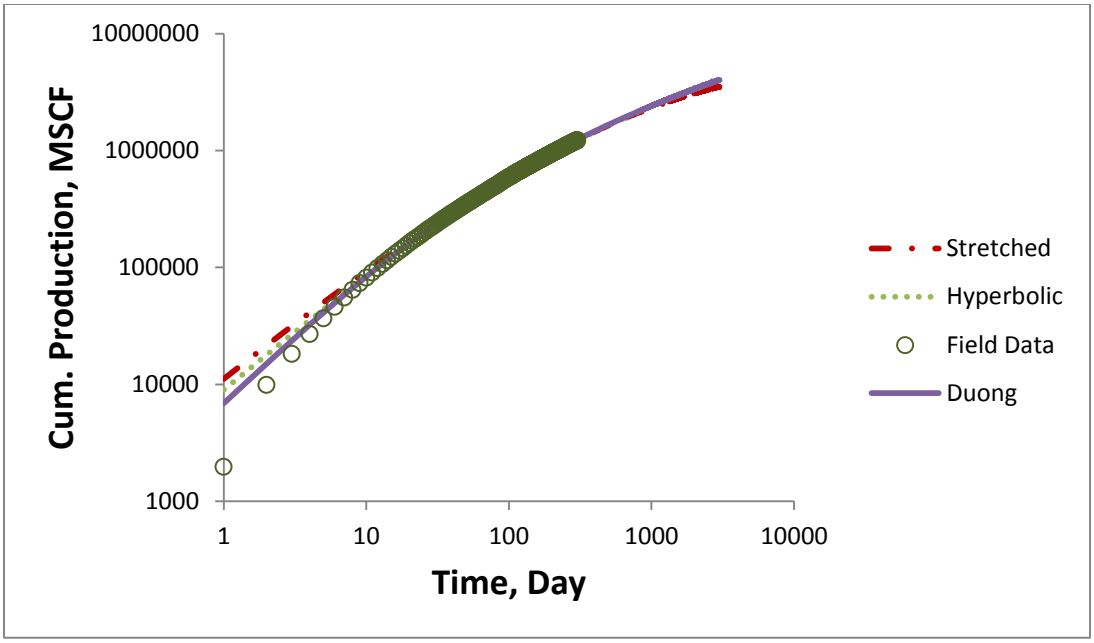
10000000
1000000
100000
10000
1000
Cum. Production, MSCF
1
10
100
1000
10000
Time, Day
Stretched
Hyperbolic
Field Data
Duong

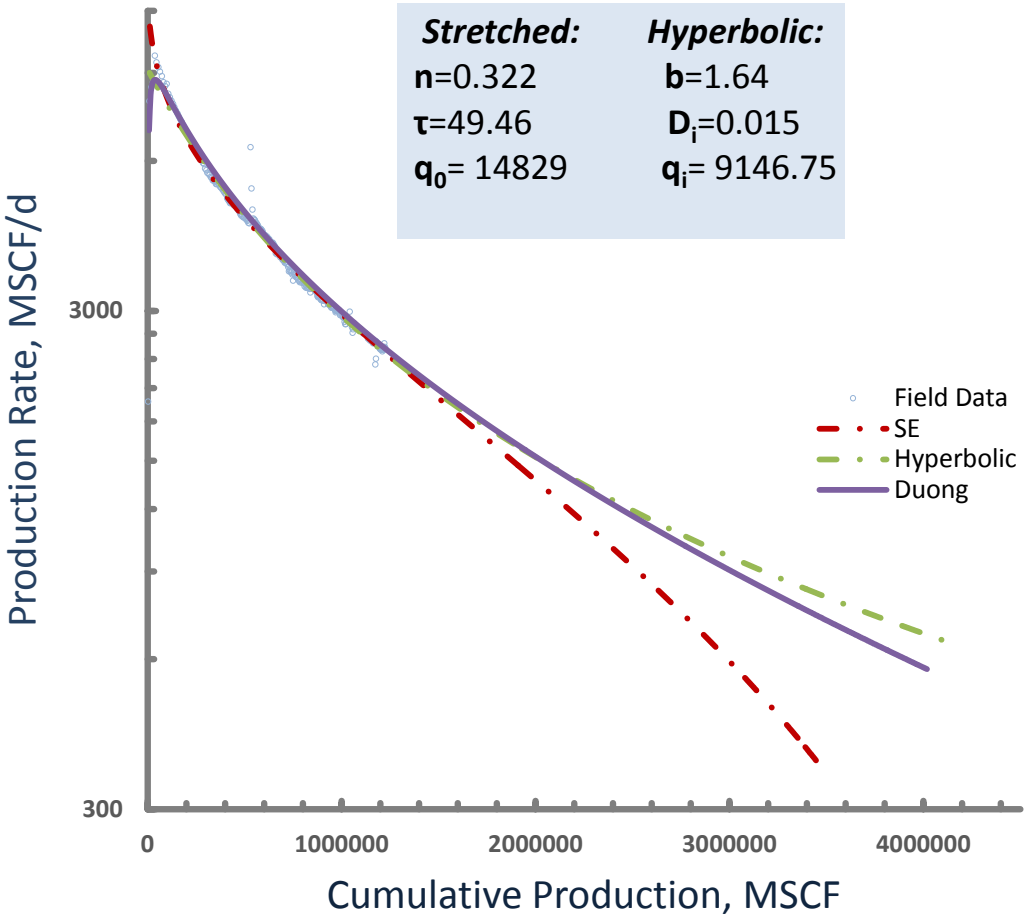
Stretched:
n=0.322
τ=49.46
q0= 14829
Hyperbolic:
b=1.64
Di=0.015
qi= 9146.75
Production Rate, MSCF/d
3000
300
0
1000000
2000000
3000000
4000000
Cumulative Production, MSCF
Field Data
SE
Hyperbolic
Duong

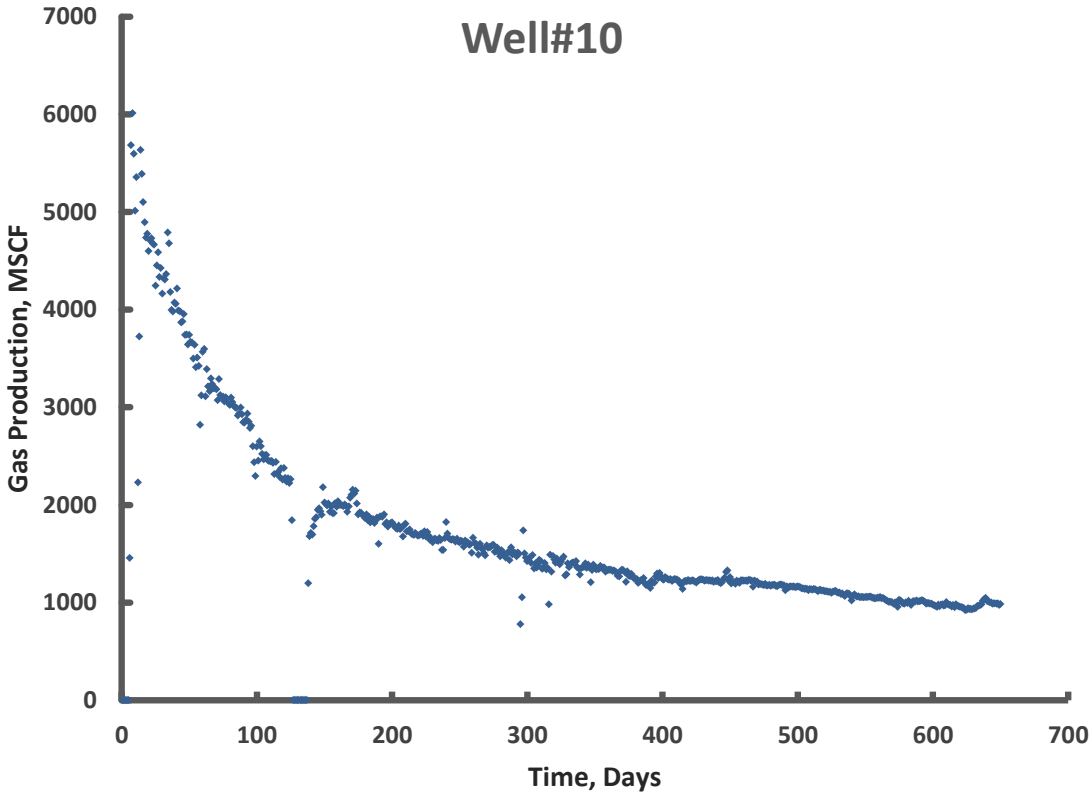
Well#10
Gas Production, MSCF
7000
6000
5000
4000
3000
2000
1000
0
0
100
200
300
400
500
600
700
Time, Days

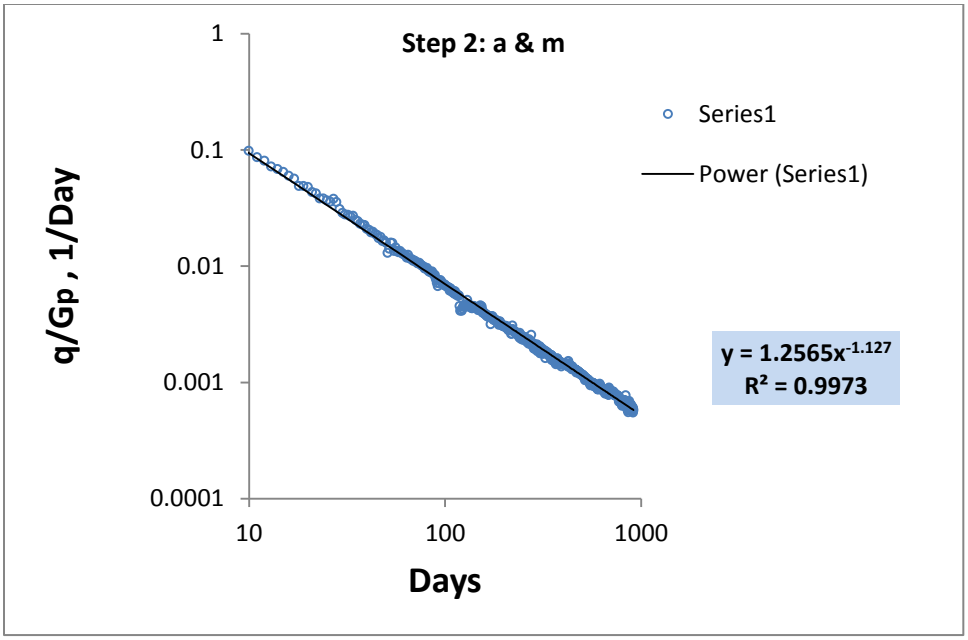
Step 2: a & m
q/Gp , 1/Day
1
0.1
0.01
0.001
0.0001
10
100
1000
Days
Series1
Power (Series1)
y = 1.2565x-1.127
R² = 0.9973

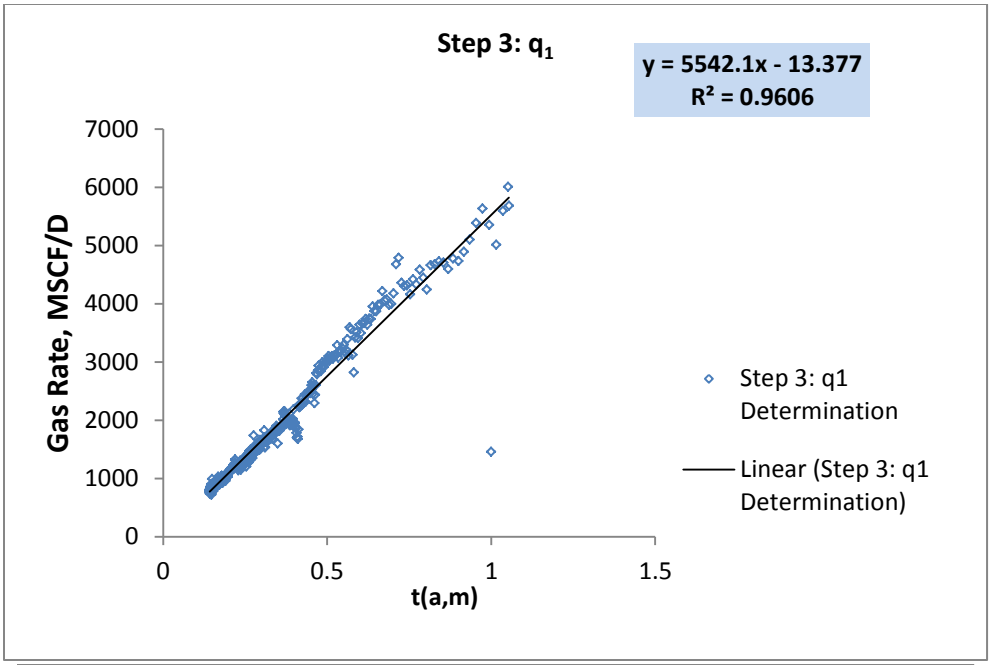
Step 3: q1
y = 5542.1x - 13.377
R² = 0.9606
Gas Rate, MSCF/D
7000
6000
5000
4000
3000
2000
1000
0
0
0.5
1
1.5
t(a,m)
Step 3: q1 Determination
Linear (Step 3: q1 Determination)

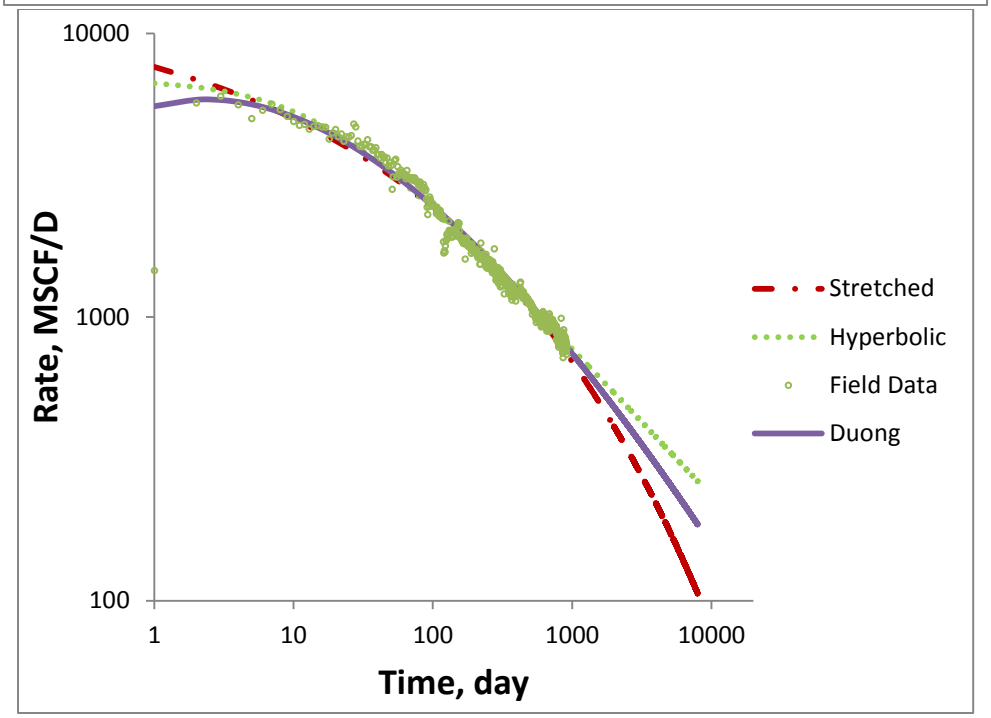
Rate, MSCF/D
10000
1000
100
1
10
100
1000
10000
Time, day
Stretched
Hyperbolic
Field Data
Duong

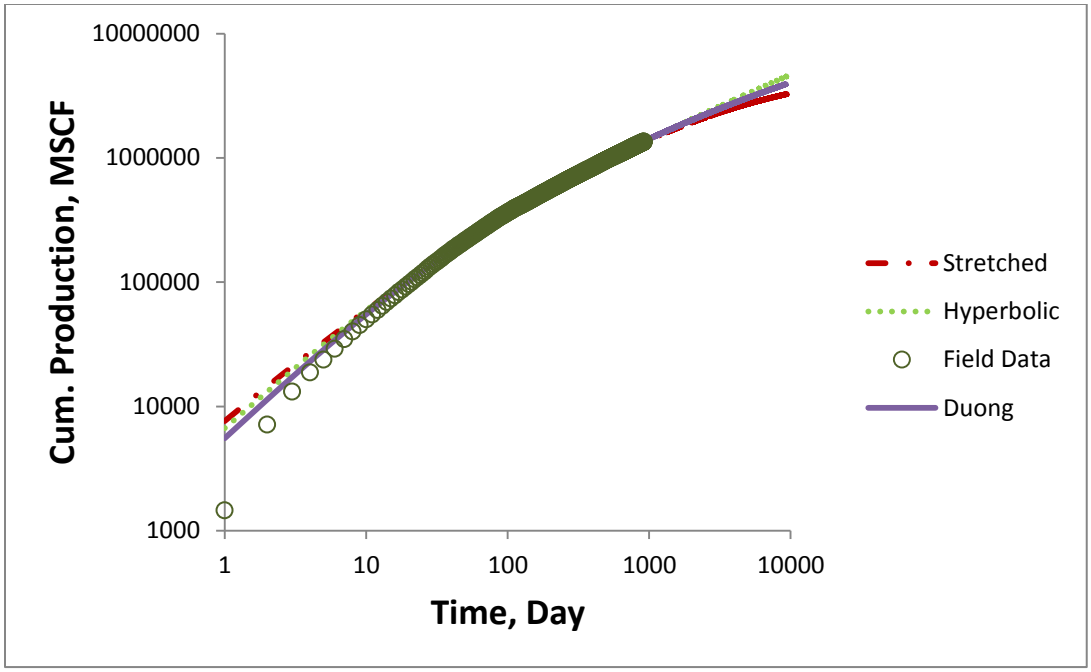
10000000
1000000
100000
10000
1000
Cum. Production, MSCF
1
10
100
1000
10000
Time, Day
Stretched
Hyperbolic
Field Data
Duong

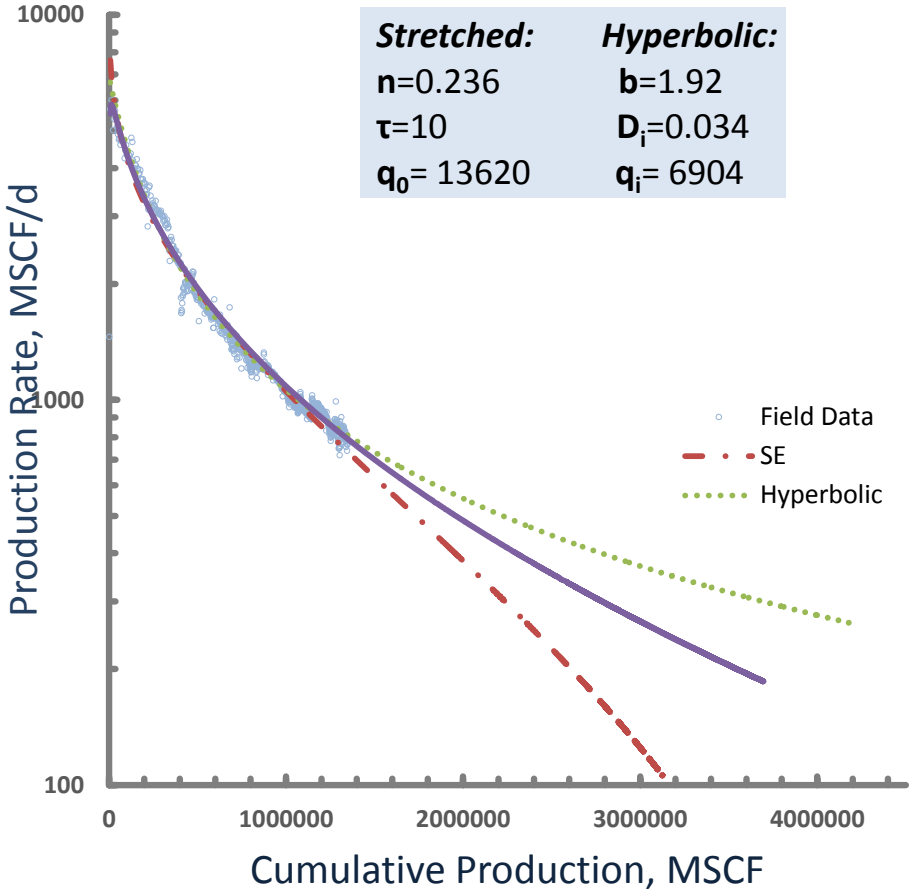
Stretched:
n=0.236
τ=10
q0= 13620
Hyperbolic:
b=1.92
Di=0.034
qi= 6904
10000
1000
100
Production Rate, MSCF/d
0
1000000
2000000
3000000
4000000
Cumulative Production, MSCF
Field Data
SE
Hyperbolic

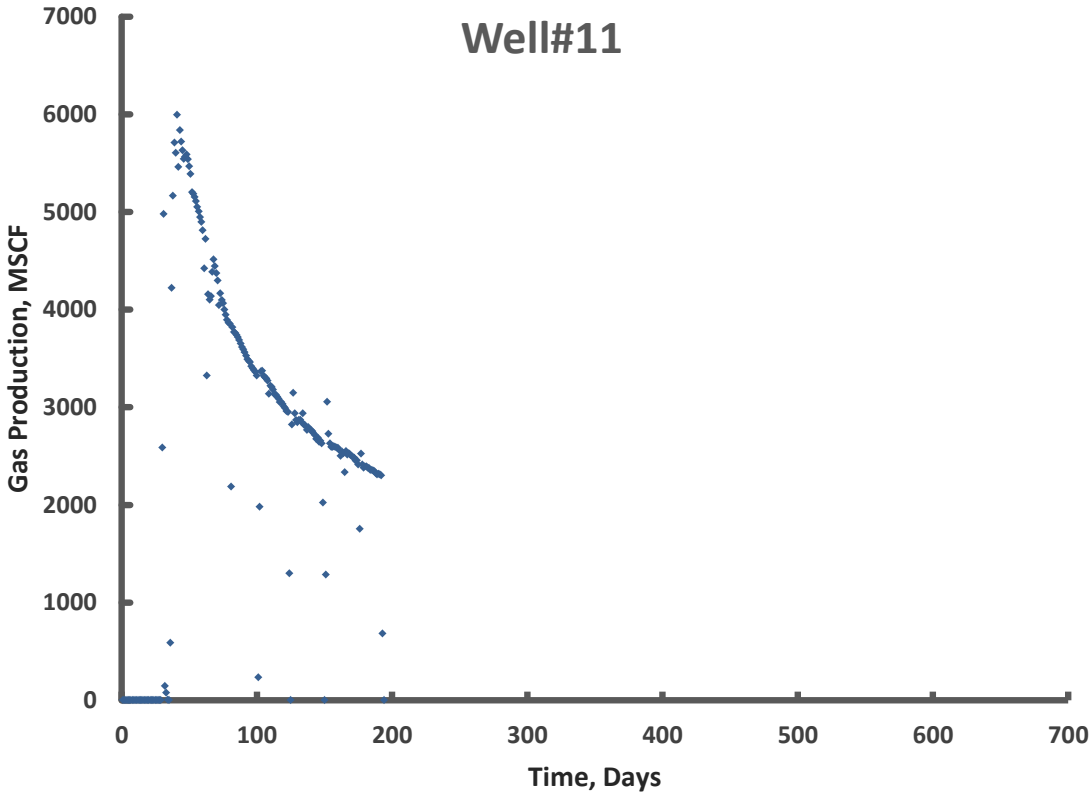
Well#11
Gas Production, MSCF
7000
6000
5000
4000
3000
2000
1000
0
0
100
200
300
400
500
600
700
Time, Days

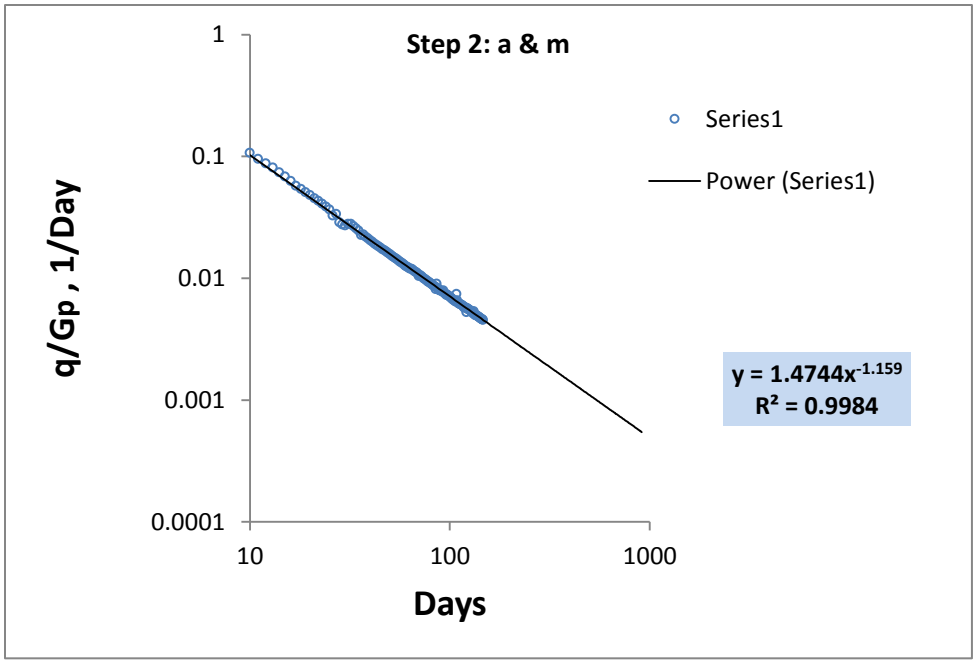
Step 2: a & m
q/Gp , 1/Day
1
0.1
0.01
0.001
0.0001
10
100
1000
Days
Series1
Power (Series1)
y = 1.4744x-1.159
R² = 0.9984

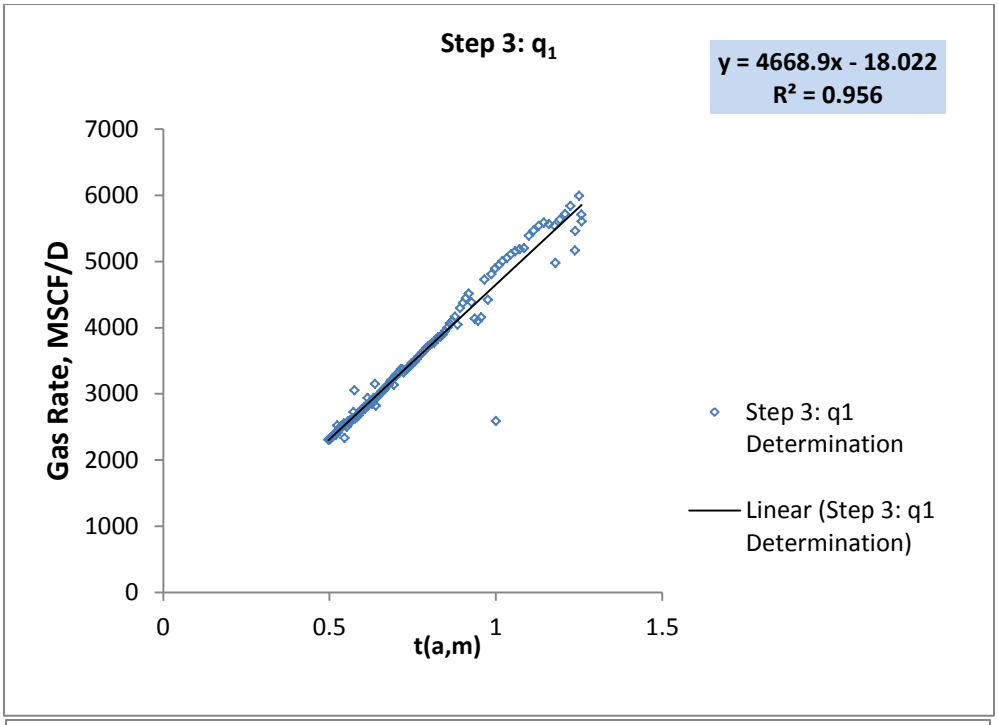
Step 3: q1
y = 4668.9x - 18.022
R² = 0.956
Gas Rate, MSCF/D
7000
6000
5000
4000
3000
2000
1000
0
0
0.5
1
1.5
t(a,m)
Step 3: q1 Determination
Linear (Step 3: q1 Determination)

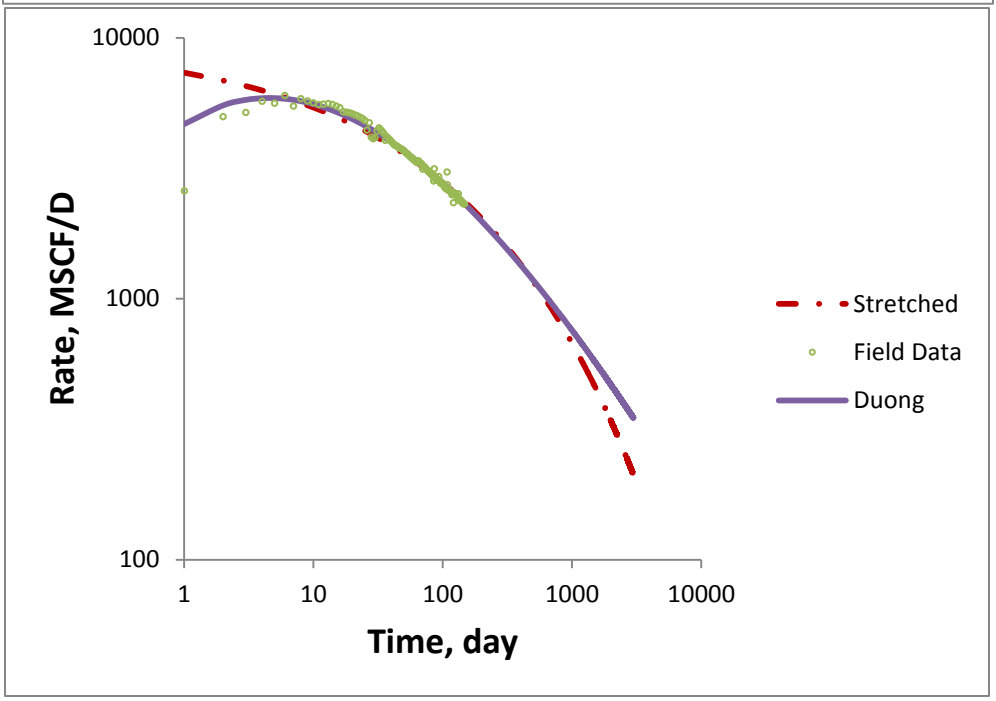
Rate, MSCF/D
10000
1000
100
1
10
100
1000
10000
Time, day
Stretched
Field Data
Duong

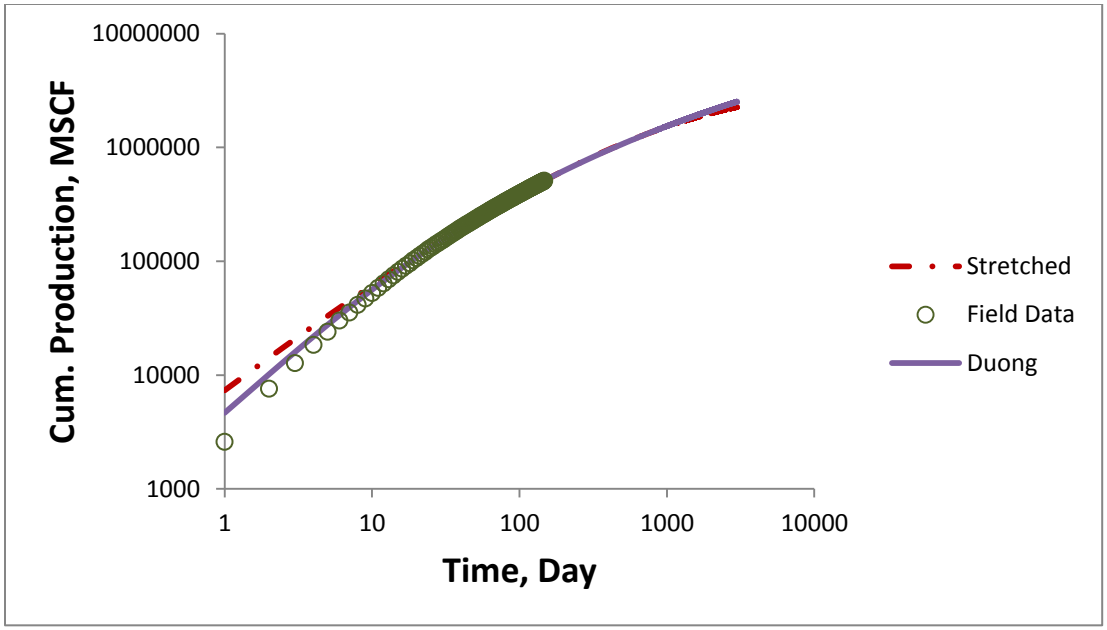
10000000
1000000
100000
10000
1000
Cum. Production, MSCF
1
10
100
1000
10000
Time, Day
Stretched
Field Data
Duong

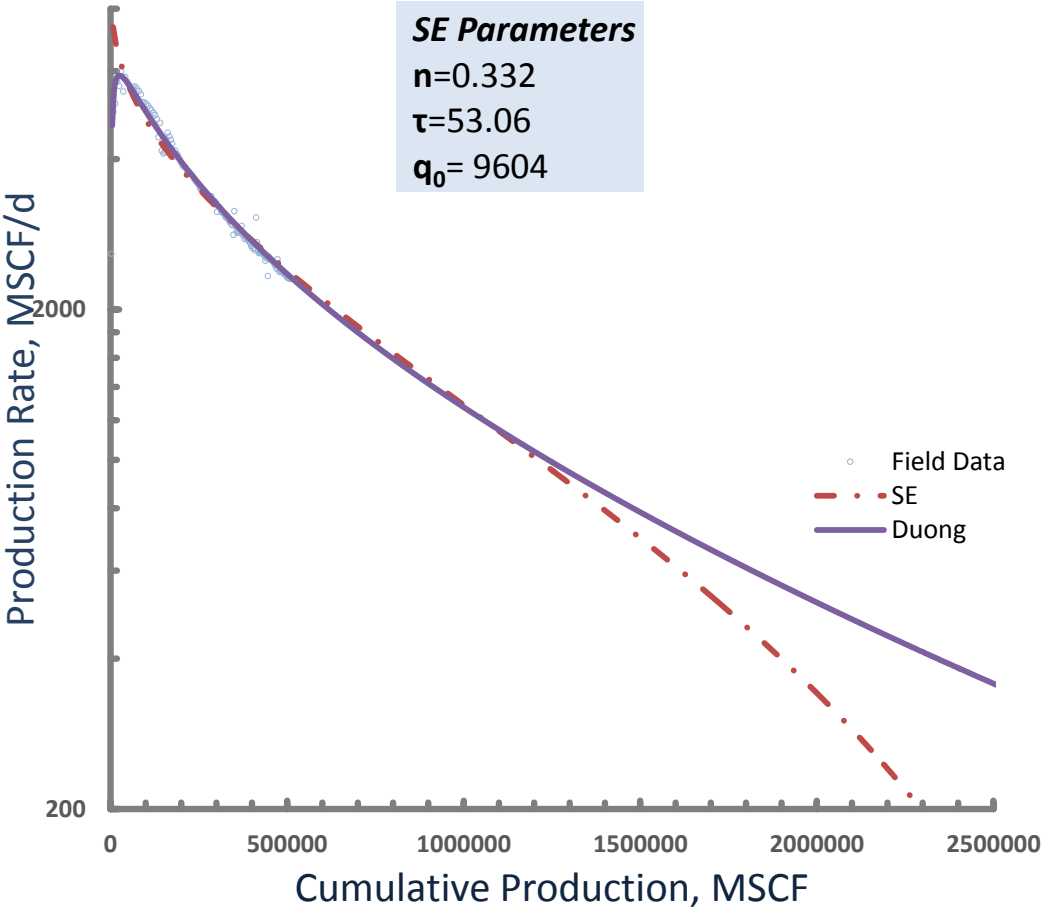
SE Parameters
n=0.332
τ=53.06
q0= 9604
2000
200
Production Rate, MSCF/d
0
500000
1000000
1500000
2000000
2500000
Cumulative Production, MSCF
Field Data
SE
Duong

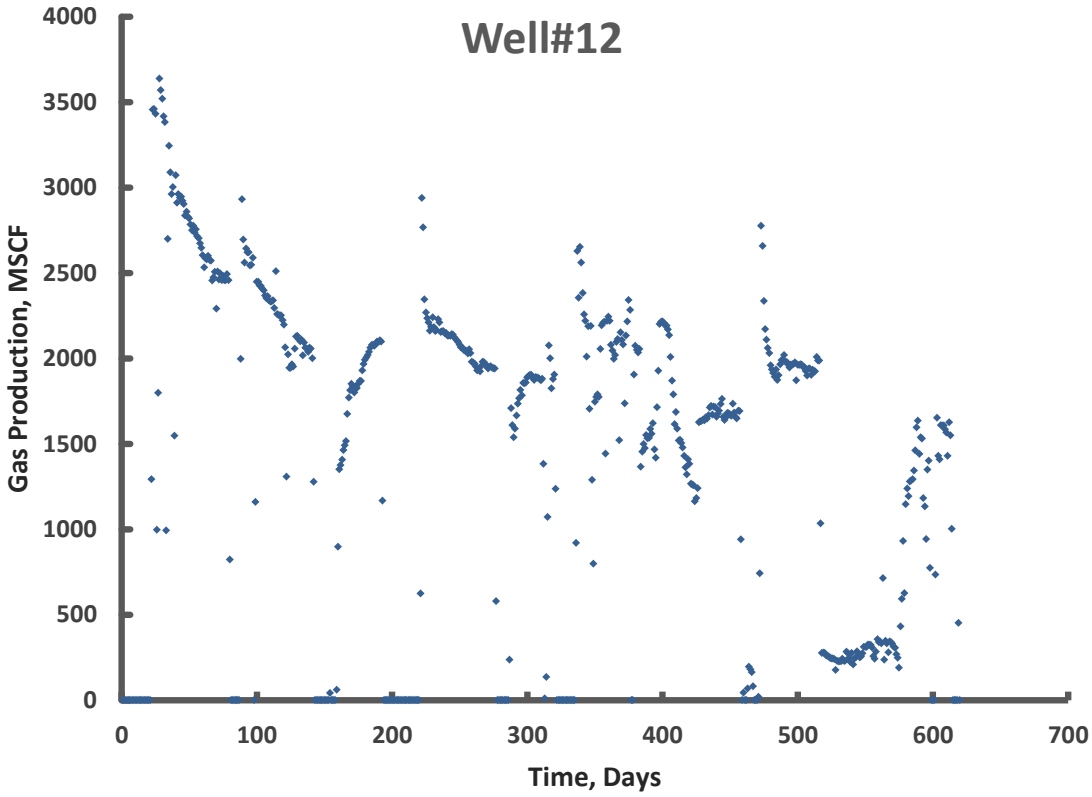
Well#12
Gas Production, MSCF
4000
3500
3000
2500
2000
1500
1000
500
0
0
100
200
300
400
500
600
700
Time, Days

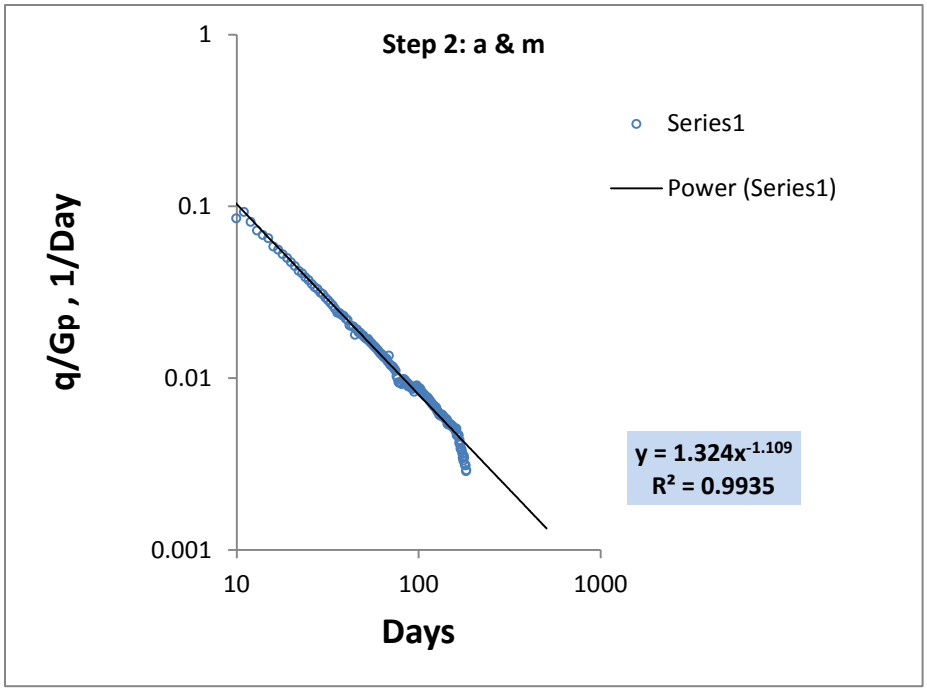
Step 2: a & m
q/Gp , 1/Day
1
0.1
0.01
0.001
10
100
1000
Days
Series1
Power (Series1)
y = 1.324x-1.109
R² = 0.9935

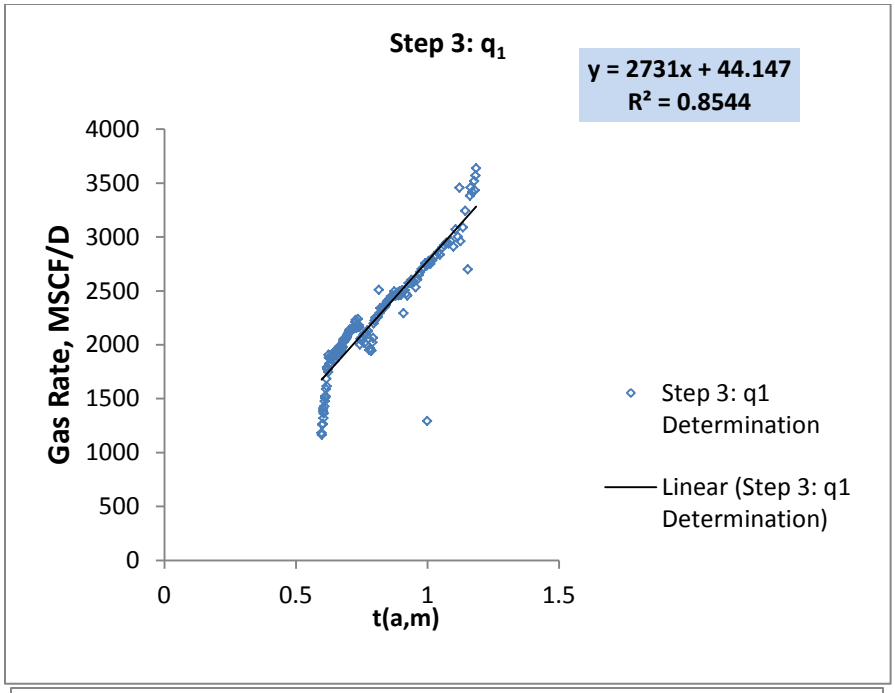
Step 3: q1
y = 2731x + 44.147
R² = 0.8544
Gas Rate, MSCF/D
4000
3500
3000
2500
2000
1500
1000
500
0
0
0.5
1
1.5
t(a,m)
Step 3: q1 Determination
Linear (Step 3: q1 Determination)

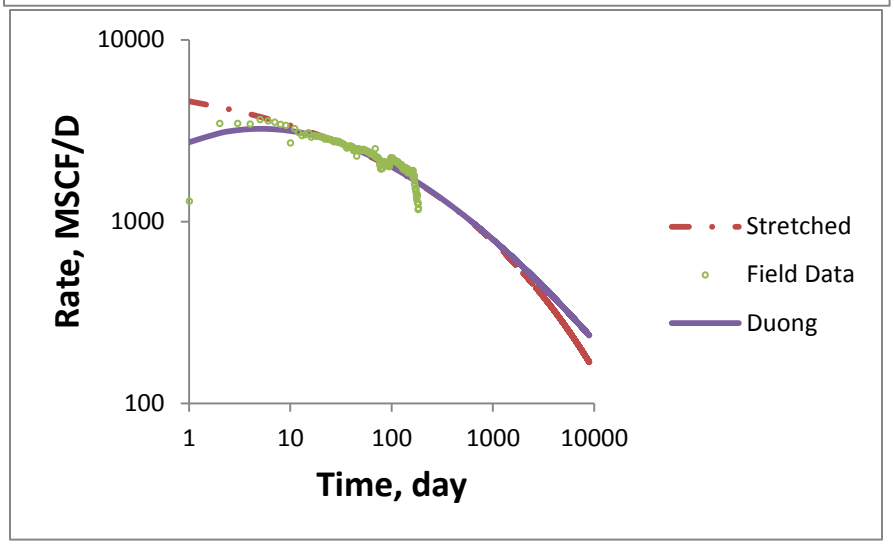
Rate, MSCF/D
10000
1000
100
1
10
100
1000
10000
Time, day
Stretched
Field Data
Duong

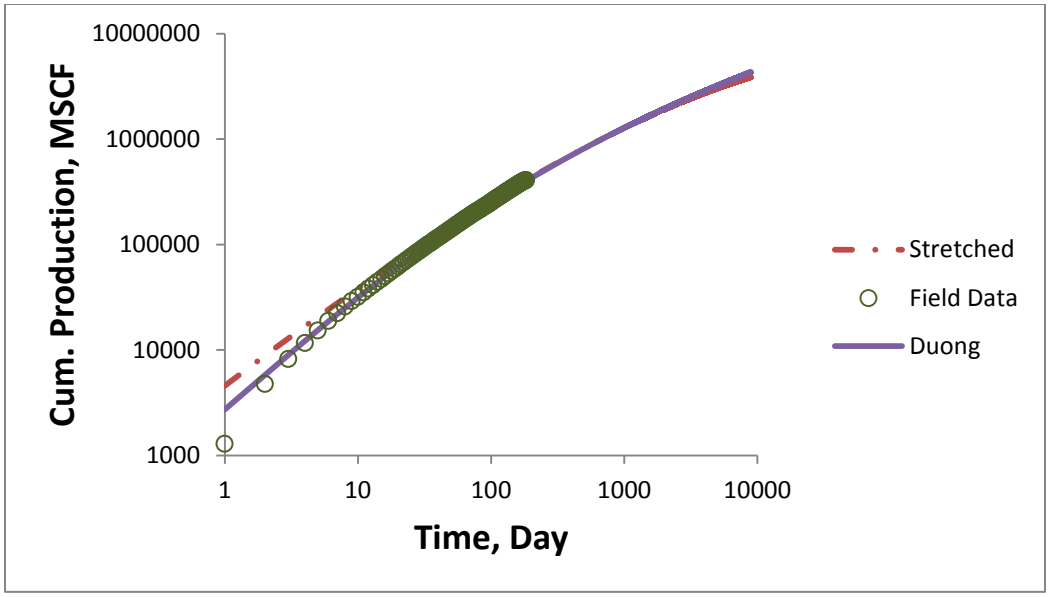
10000000
1000000
100000
10000
1000
Cum. Production, MSCF
1
10
100
1000
10000
Time, Day
Stretched
Field Data
Duong

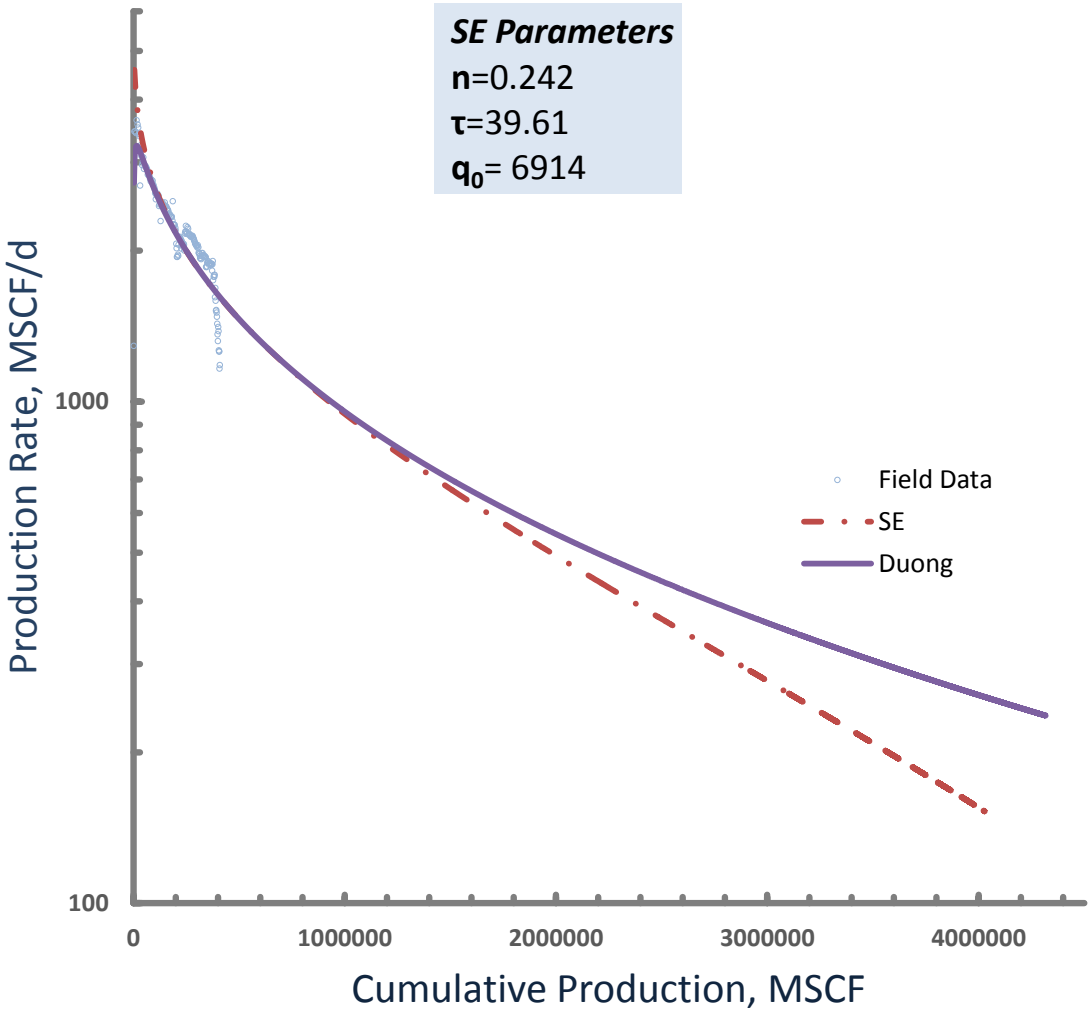
SE Parameters
n=0.242
τ=39.61
q0= 6914
Production Rate, MSCF/d
1000
100
0
1000000
2000000
3000000
4000000
Cumulative Production, MSCF
Field Data
SE
Duong

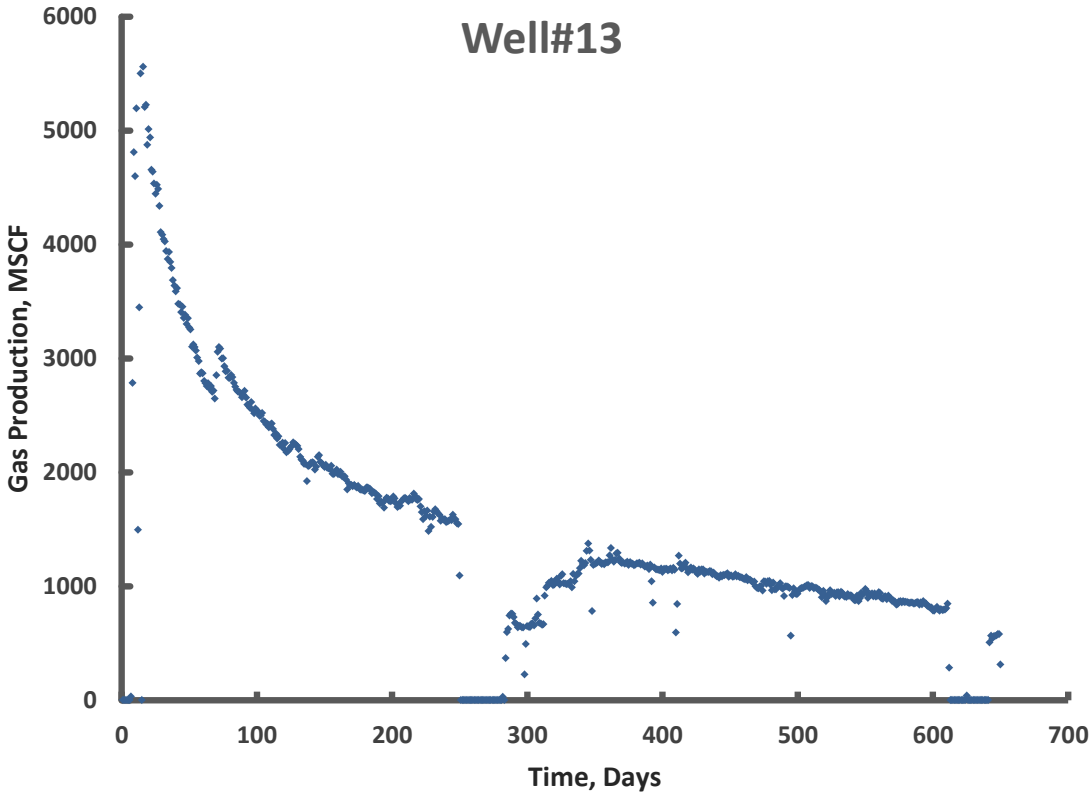
Well#13
Gas Production, MSCF
6000
5000
4000
3000
2000
1000
0
0
100
200
300
400
500
600
700
Time, Days

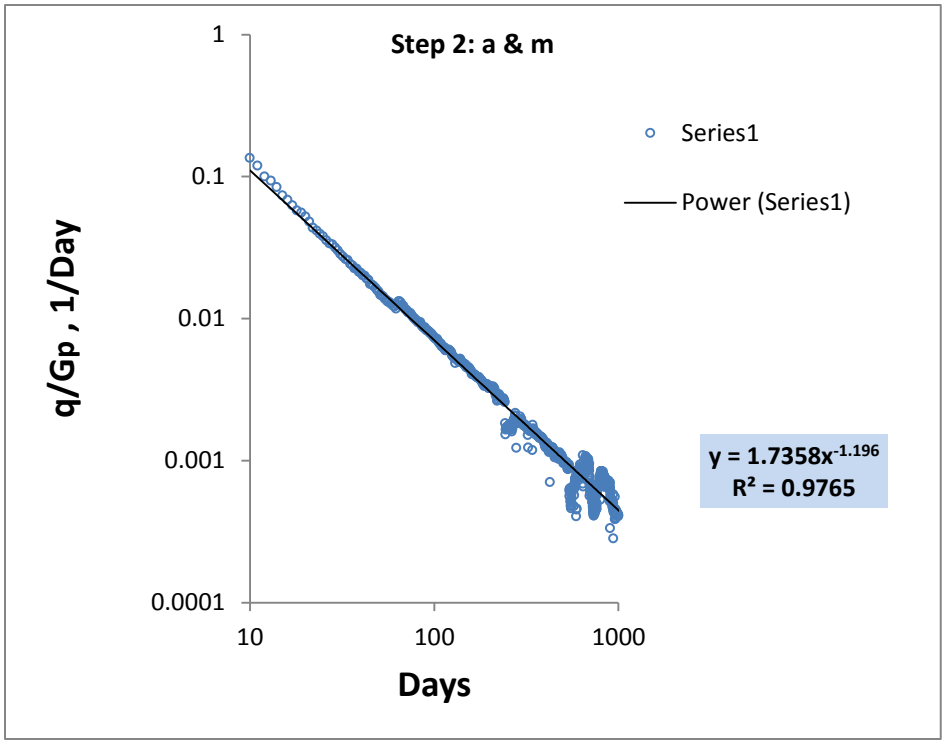
Step 2: a & m
q/Gp , 1/Day
1
0.1
0.01
0.001
0.0001
10
100
1000
Days
Series1
Power (Series1)
y = 1.7358x-1.196
R² = 0.9765

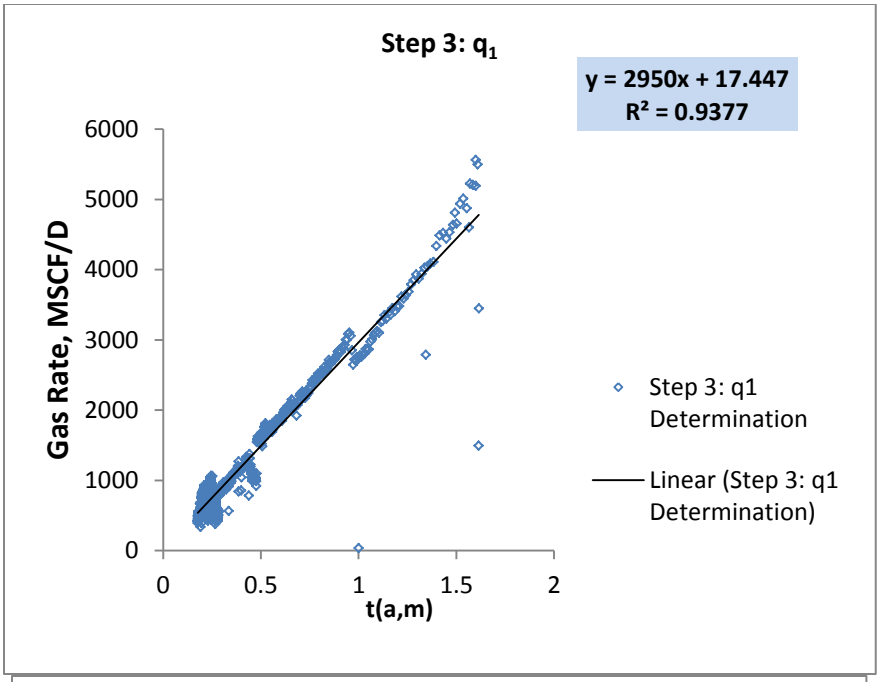
Step 3: q1
y = 2950x + 17.447
R² = 0.9377
Gas Rate, MSCF/D
6000
5000
4000
3000
2000
1000
0
0
0.5
1
1.5
2
t(a,m)
Step 3: q1 Determination
Linear (Step 3: q1 Determination)

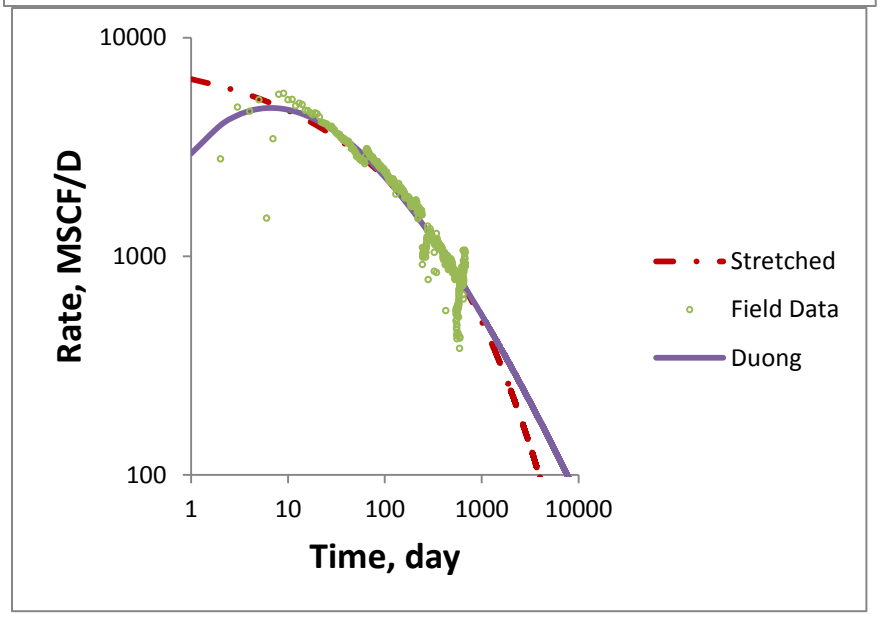
Rate, MSCF/D
10000
1000
100
1
10
100
1000
10000
Time, day
Stretched
Field Data
Duong

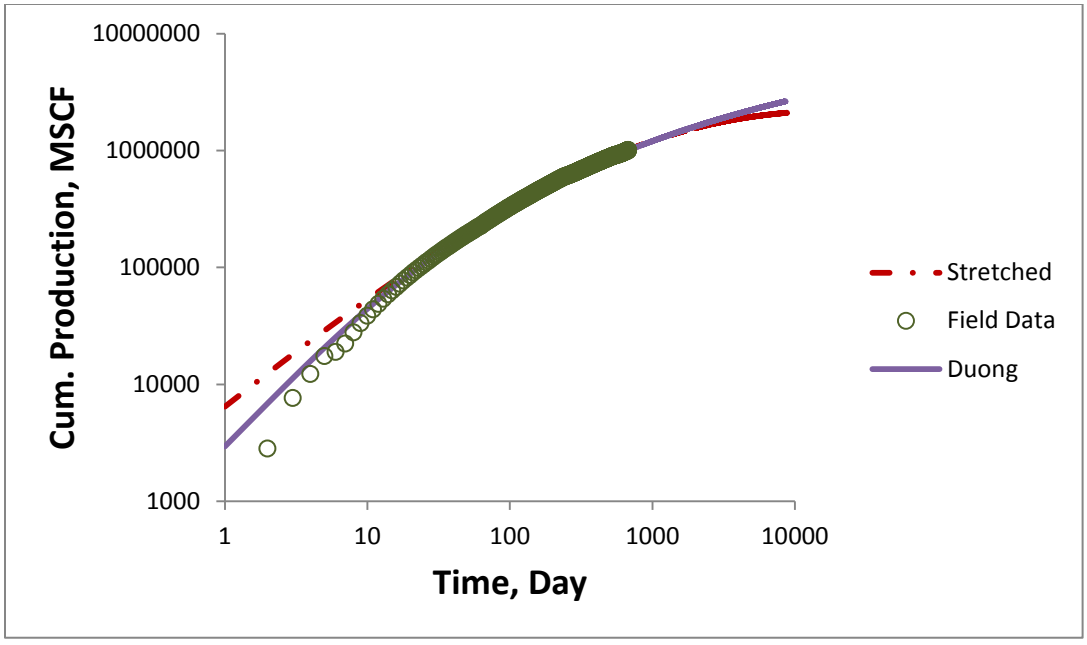
10000000
1000000
100000
10000
1000
Cum. Production, MSCF
1
10
100
1000
10000
Time, Day
Stretched
Field Data
Duong

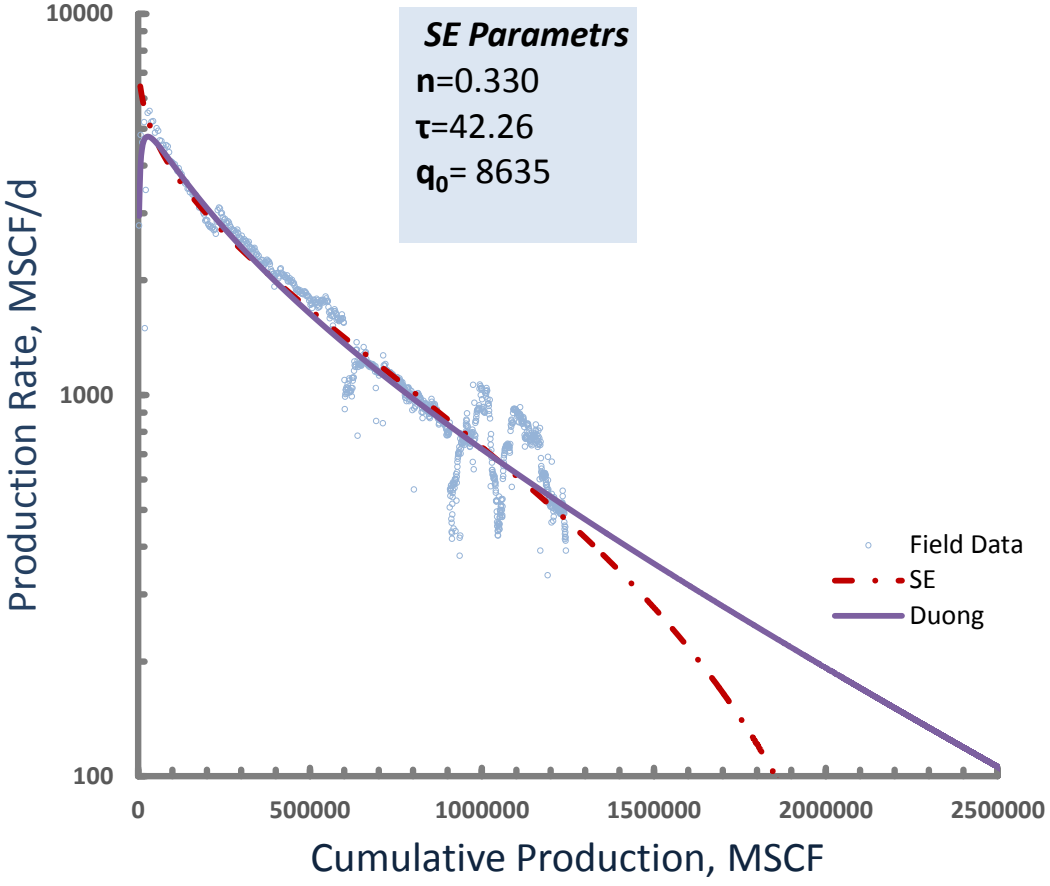
SE Parametrs
n=0.330
τ=42.26
q0= 8635
10000
1000
100
Production Rate, MSCF/d
0
500000
1000000
1500000
2000000
2500000
Cumulative Production, MSCF
Field Data
SE
Duong

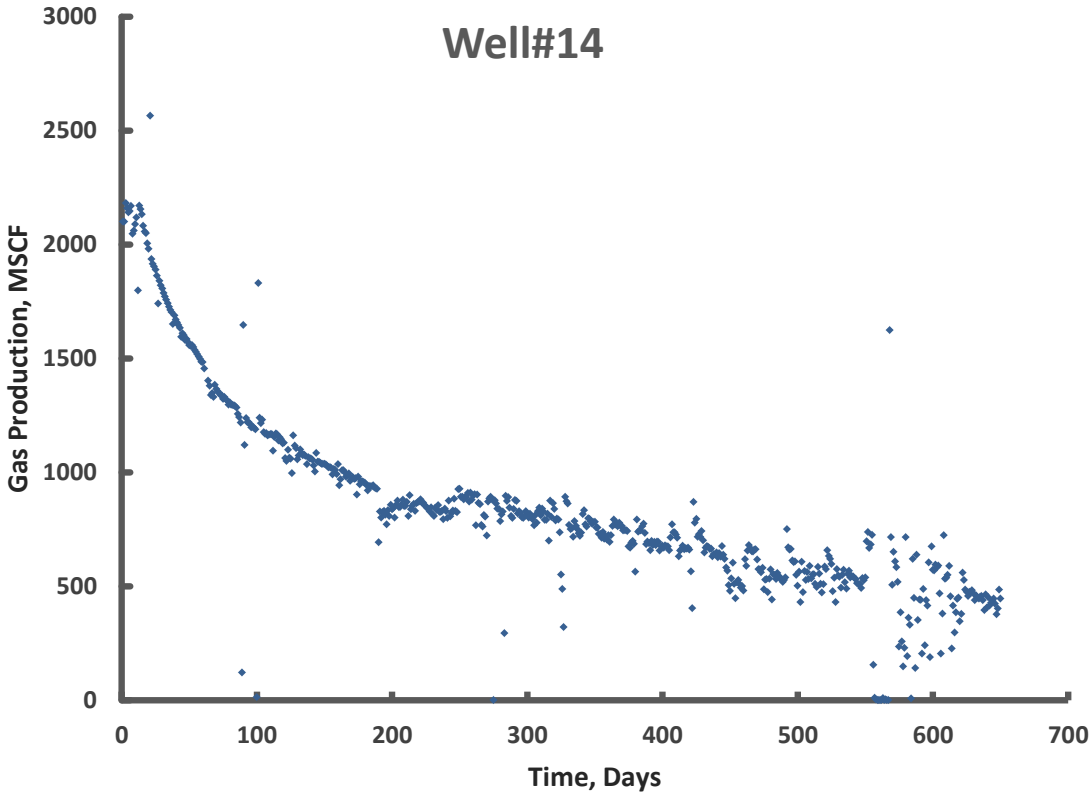
Well#14
Gas Production, MSCF
Time, Days
3000
2500
2000
1500
1000
500
0
0
100
200
300
400
500
600
700

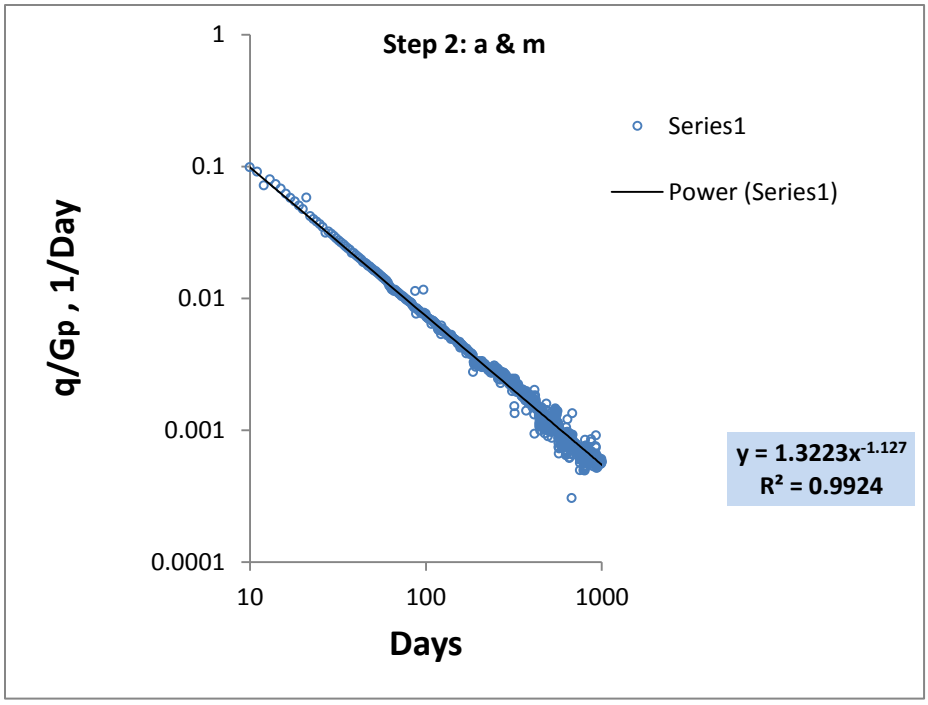
Step 2: a & m
q/Gp , 1/Day
Days
Series1
Power (Series1)
y = 1.3223x-1.127
R² = 0.9924
1
0.1
0.01
0.001
0.0001
10
100
1000

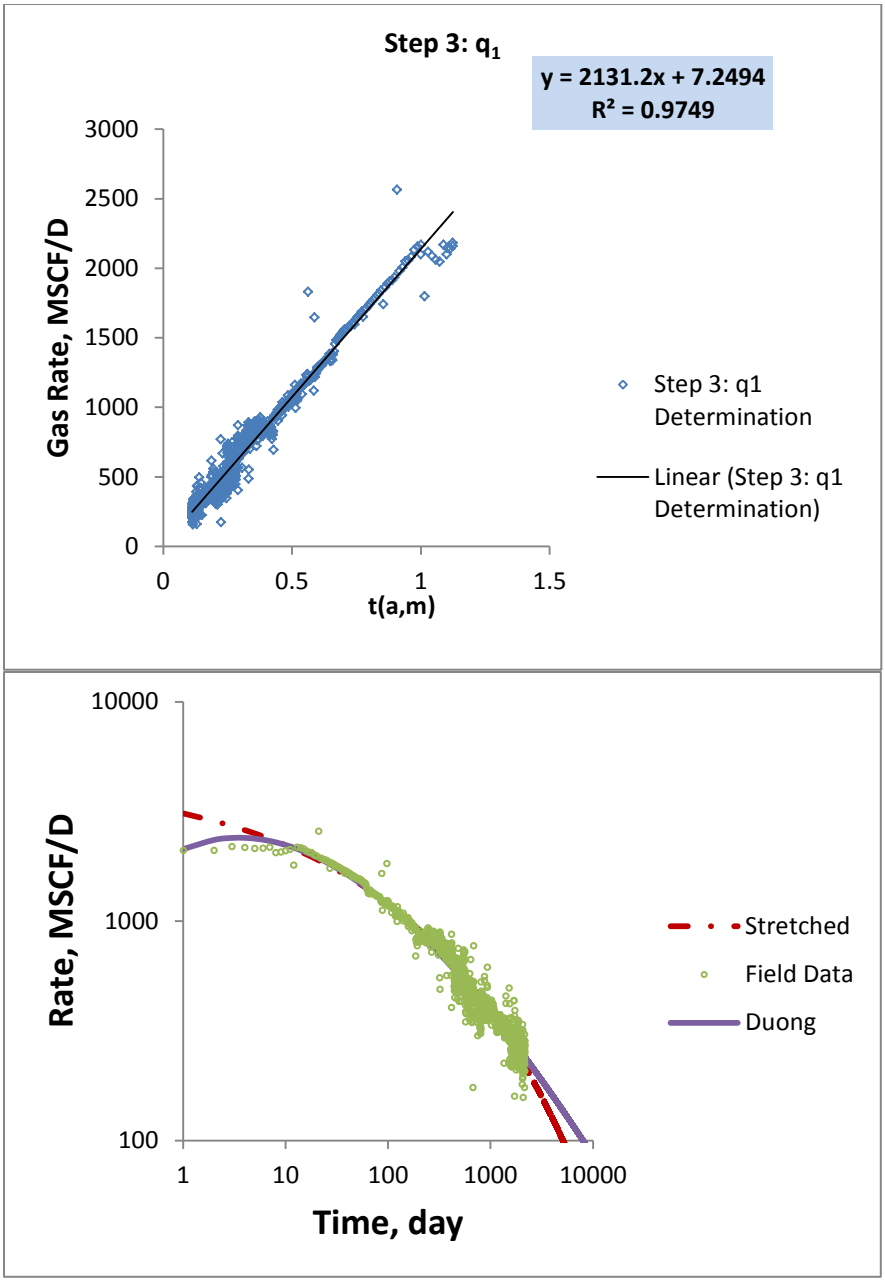
Step 3: q1
y = 2131.2x + 7.2494
R² = 0.9749
Gas Rate, MSCF/D
3000
2500
2000
1500
1000
500
0
0
0.5
1
1.5
t(a,m)
Step 3: q1 Determination
Linear (Step 3: q1 Determination)
Rate, MSCF/D
10000
1000
100
1
10
100
1000
10000
Time, day
Stretched
Field Data
Duong

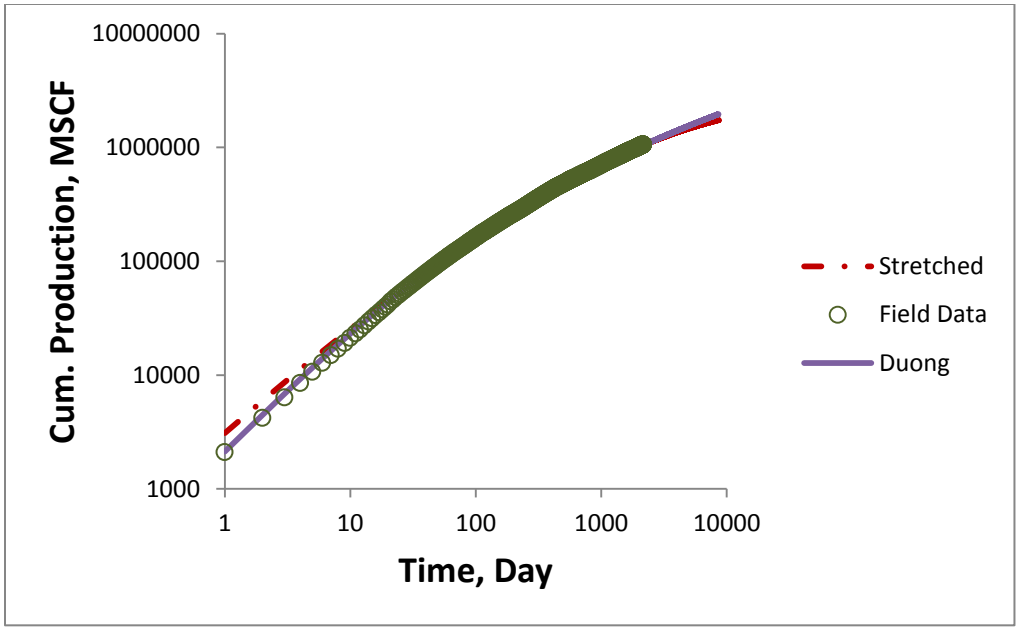
10000000
1000000
100000
10000
1000
Cum. Production, MSCF
1
10
100
1000
10000
Time, Day
Stretched
Field Data
Duong

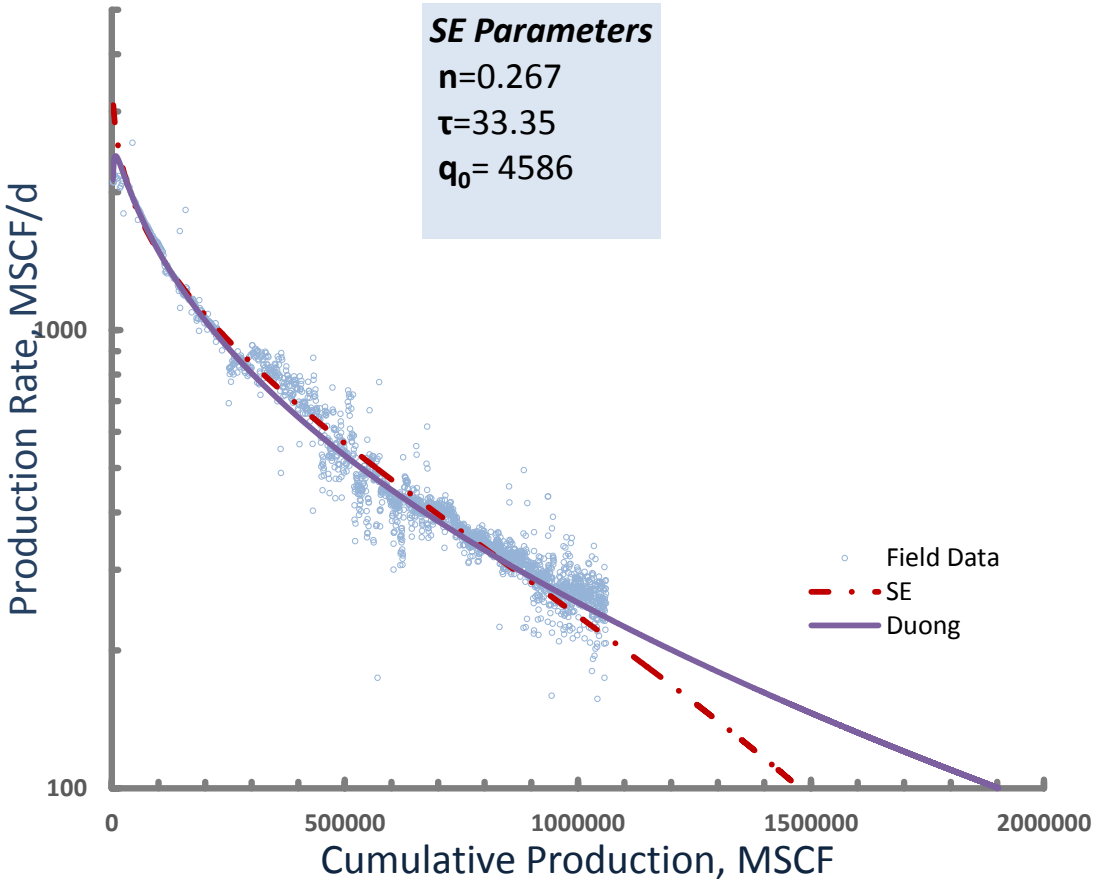
SE Parameters
n=0.267
τ=33.35
q0= 4586
Production Rate, MSCF/d
1000
100
0
500000
1000000
1500000
2000000
Cumulative Production, MSCF
Field Data
SE
Duong

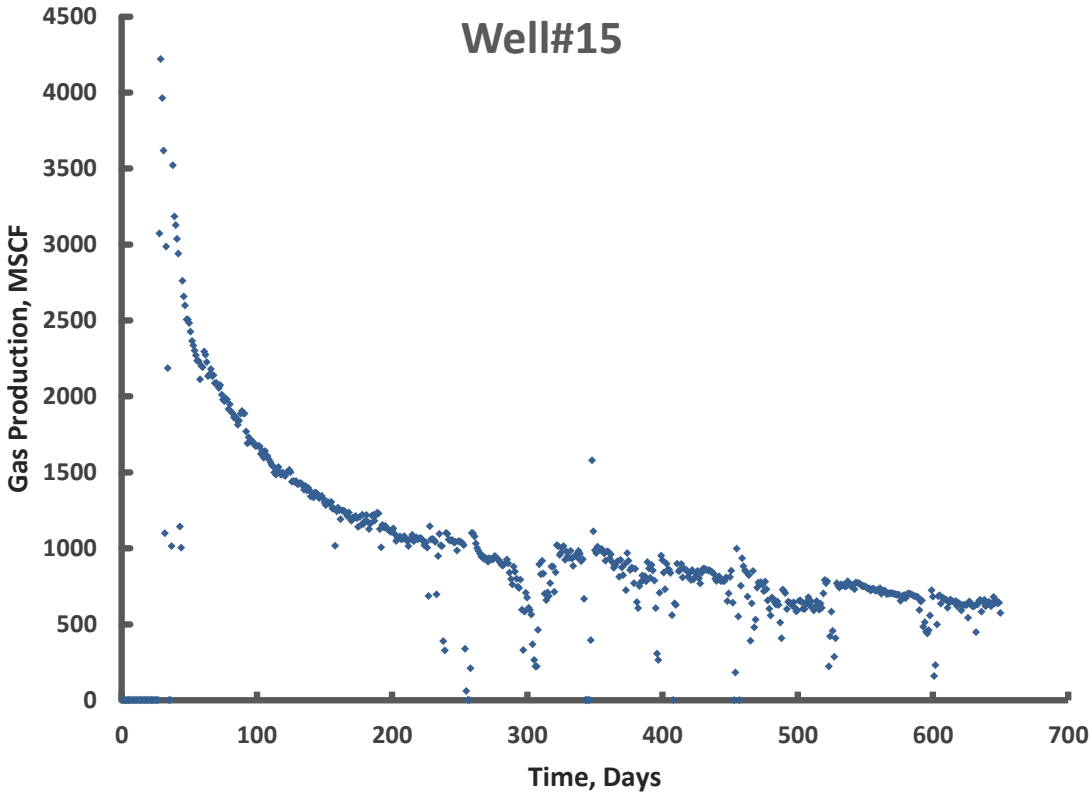
Well#15
Gas Production, MSCF
4500
4000
3500
3000
2500
2000
1500
1000
500
0
0
100
200
300
400
500
600
700
Time, Days

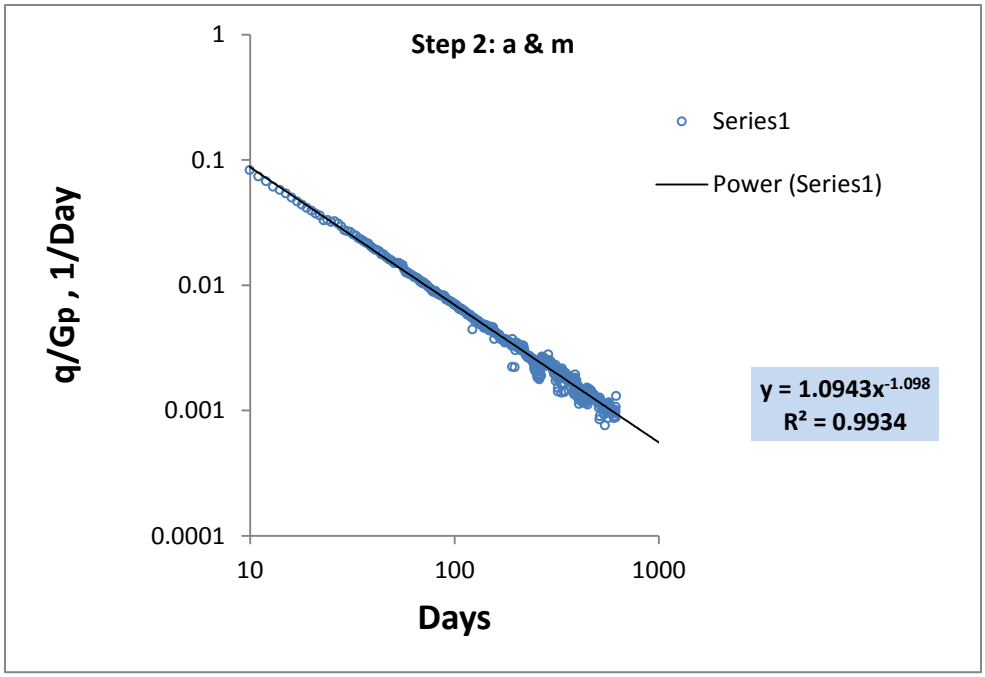
Step 2: a & m
q/Gp , 1/Day
1
0.1
0.01
0.001
0.0001
10
100
1000
Days
Series1
Power (Series1)
y = 1.0943x-1.098
R² = 0.9934

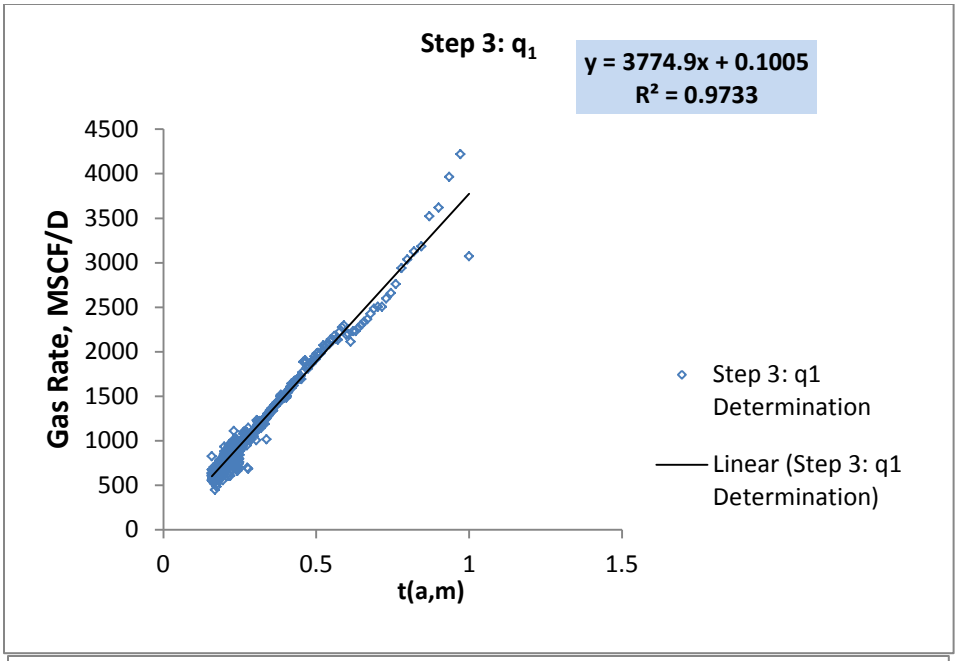
Step 3: q1
y = 3774.9x + 0.1005
R² = 0.9733
Gas Rate, MSCF/D
4500
4000
3500
3000
2500
2000
1500
1000
500
0
0
0.5
1
1.5
t(a,m)
Step 3: q1 Determination
Linear (Step 3: q1 Determination)

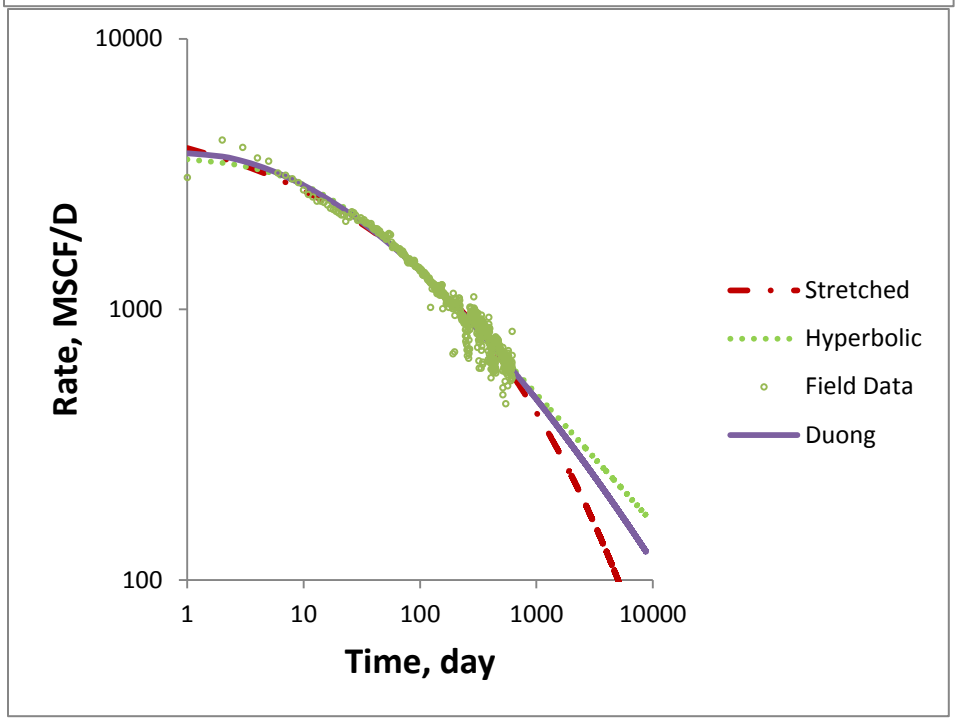
Rate, MSCF/D
10000
1000
100
1
10
100
1000
10000
Time, day
Stretched
Hyperbolic
Field Data
Duong

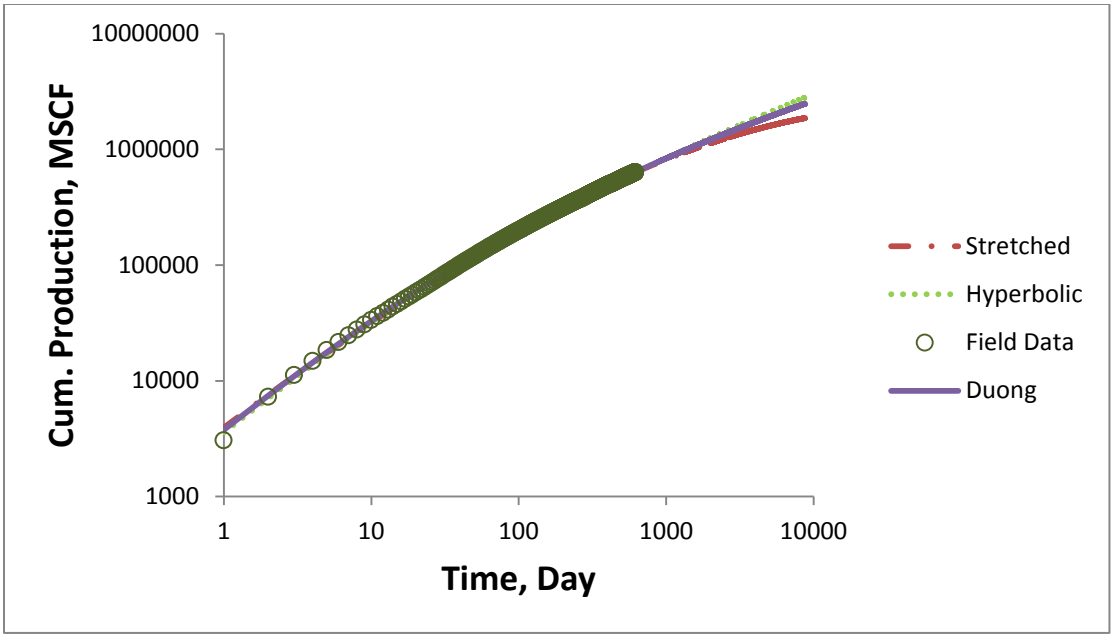
Cum. Production, MSCF
10000000
1000000
100000
10000
1000
1
10
100
1000
10000
Time, Day
Stretched
Hyperbolic
Field Data
Duong

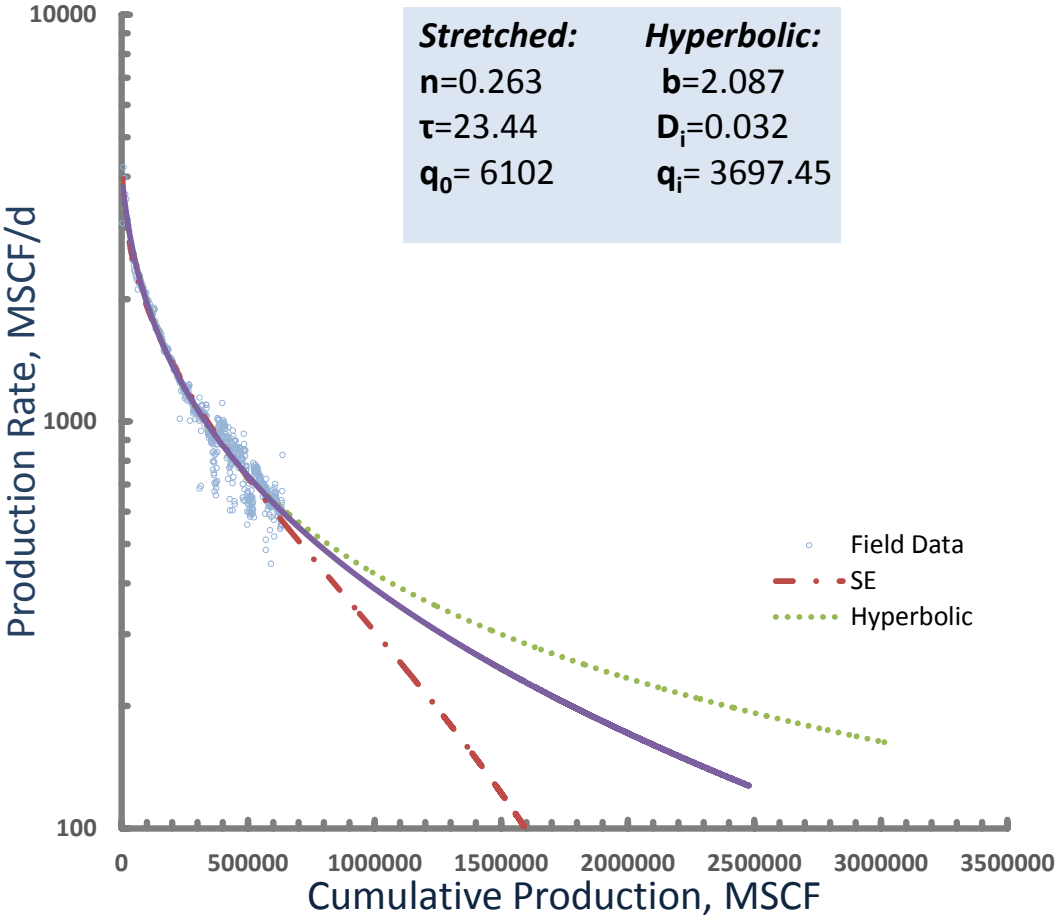
Stretched:
n=0.263
τ=23.44
q0= 6102
Hyperbolic:
b=2.087
Di=0.032
qi= 3697.45
Production Rate, MSCF/d
10000
1000
100
0
500000
1000000
1500000
2000000
2500000
3000000
3500000
Cumulative Production, MSCF
Field Data
SE
Hyperbolic

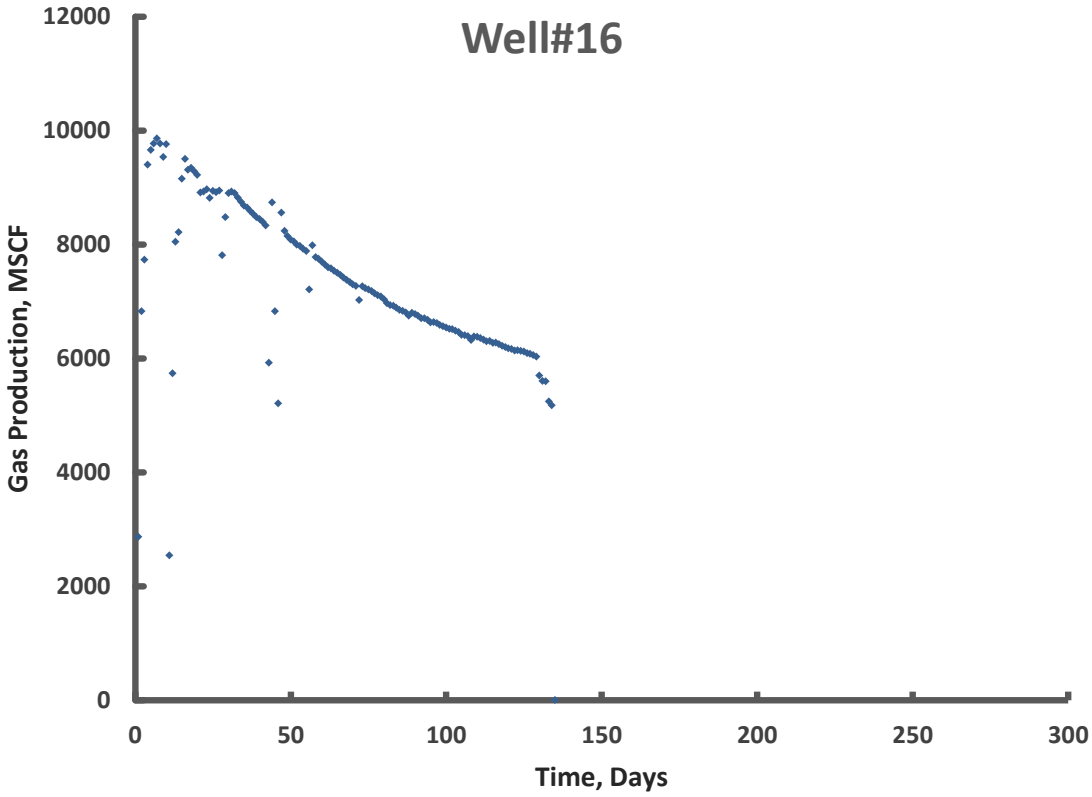
Well#16
Gas Production, MSCF
12000
10000
8000
6000
4000
2000
0
0
50
100
150
200
250
300
Time, Days

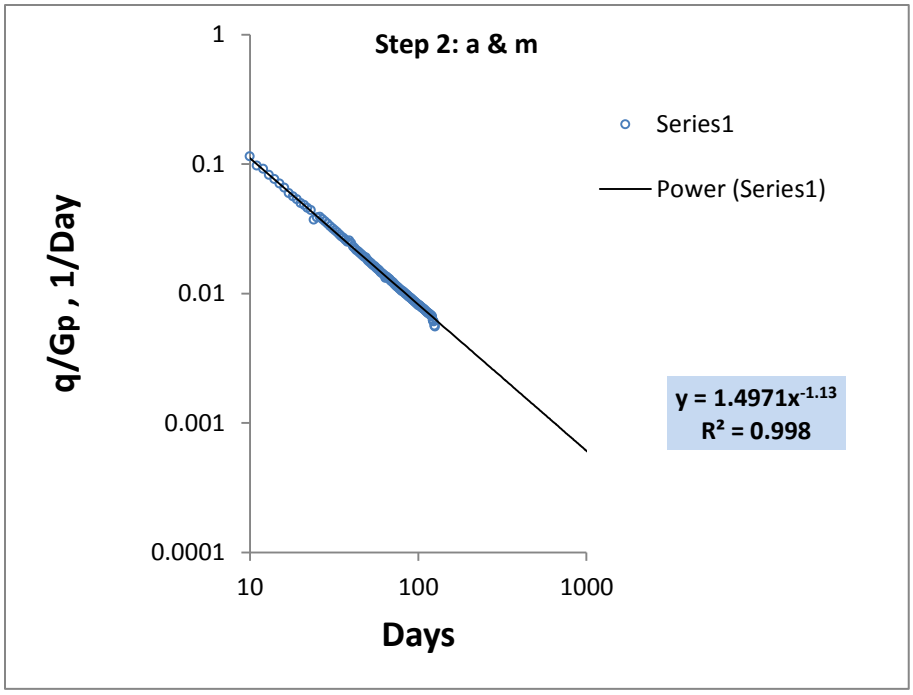
Step 2: a & m
q/Gp , 1/Day
1
0.1
0.01
0.001
0.0001
10
100
1000
Days
Series1
Power (Series1)
y = 1.4971x-1.13
R² = 0.998

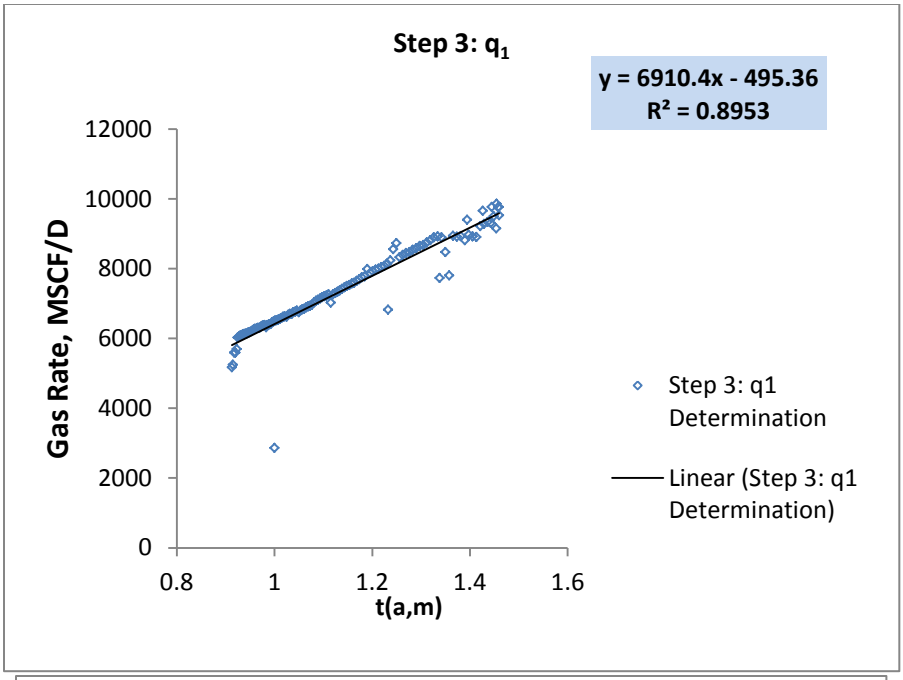
Step 3: q1
y = 6910.4x - 495.36
R² = 0.8953
Gas Rate, MSCF/D
12000
10000
8000
6000
4000
2000
0
0.8
1
1.2
1.4
1.6
t(a,m)
Step 3: q1 Determination
Linear (Step 3: q1 Determination)

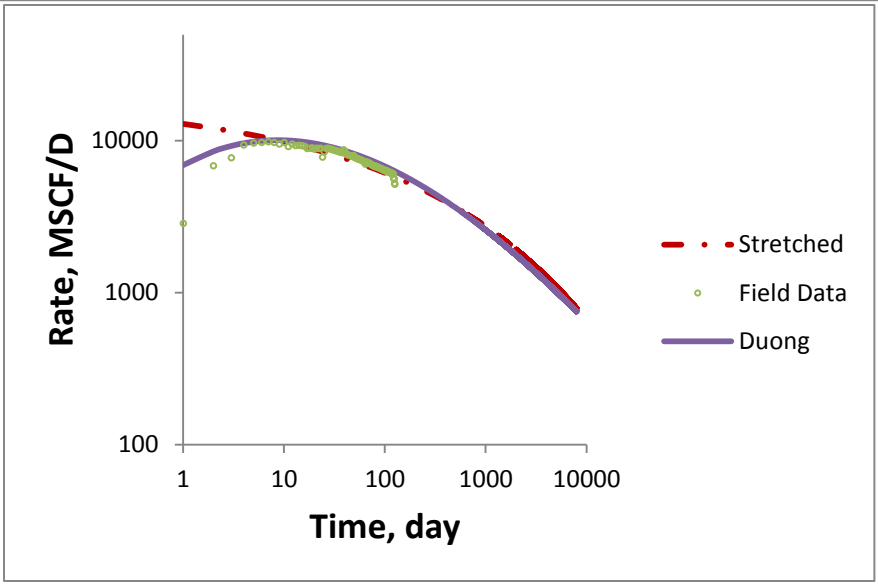
Rate, MSCF/D
10000
1000
100
1
10
100
1000
10000
Time, day
Stretched
Field Data
Duong

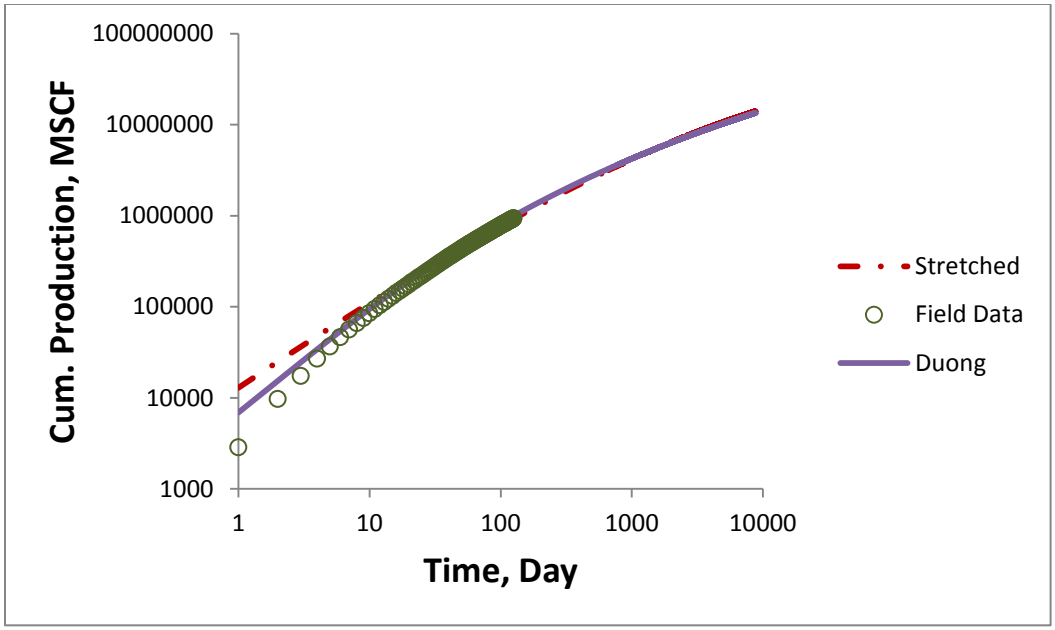
100000000
10000000
1000000
100000
10000
1000
Cum. Production, MSCF
1
10
100
1000
10000
Time, Day
Stretched
Field Data
Duong

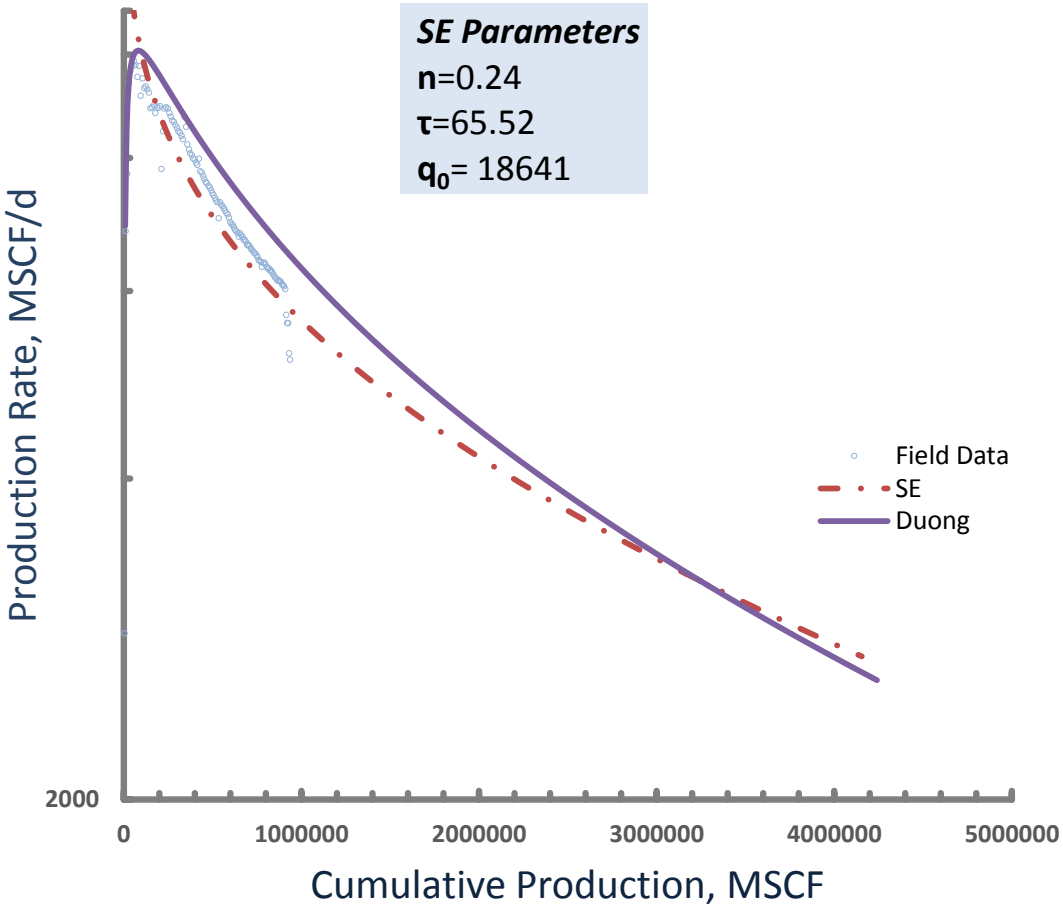
SE Parameters
n=0.24
τ=65.52
q0= 18641
Production Rate, MSCF/d
2000
0
1000000
2000000
3000000
4000000
5000000
Cumulative Production, MSCF
Field Data
SE
Duong

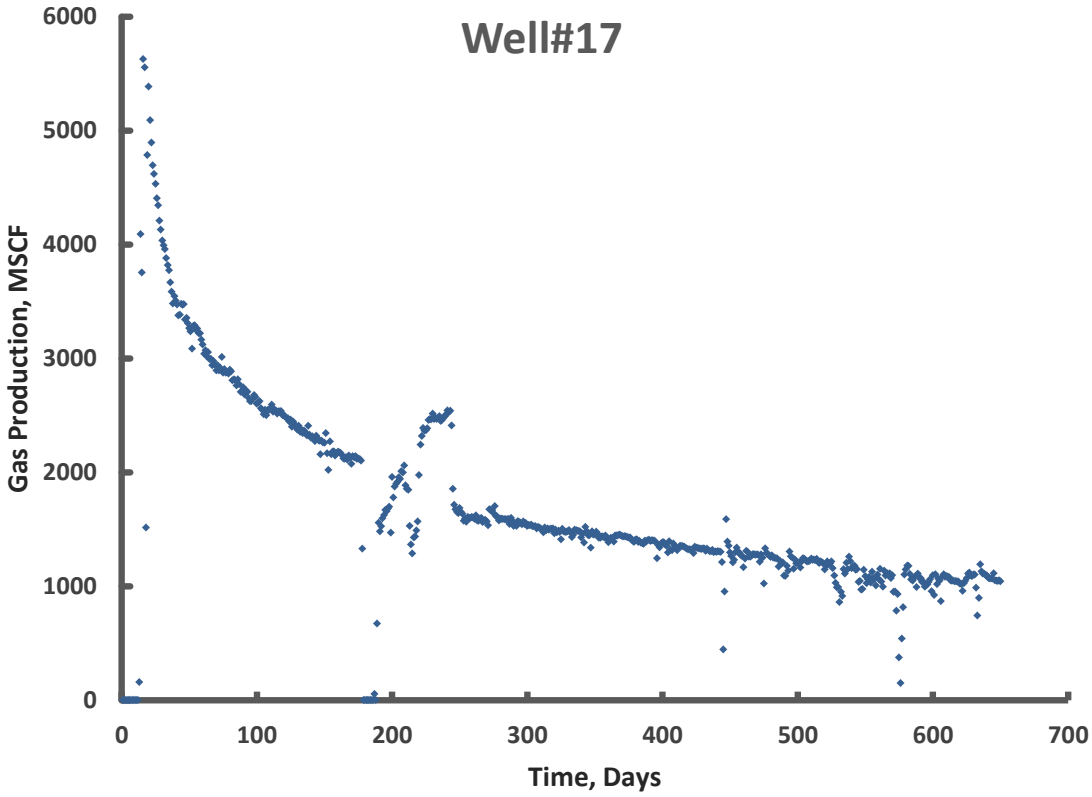
Well#17
Gas Production, MSCF
6000
5000
4000
3000
2000
1000
0
0
100
200
300
400
500
600
700
Time, Days

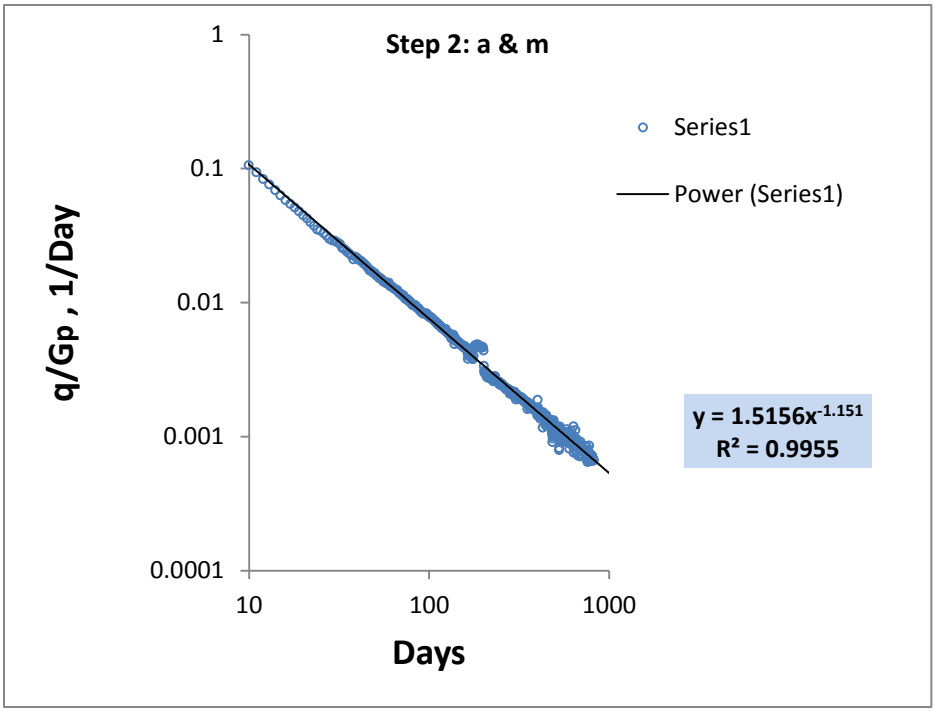
Step 2: a & m
q/Gp , 1/Day
1
0.1
0.01
0.001
0.0001
10
100
1000
Days
Series1
Power (Series1)
y = 1.5156x-1.151
R² = 0.9955

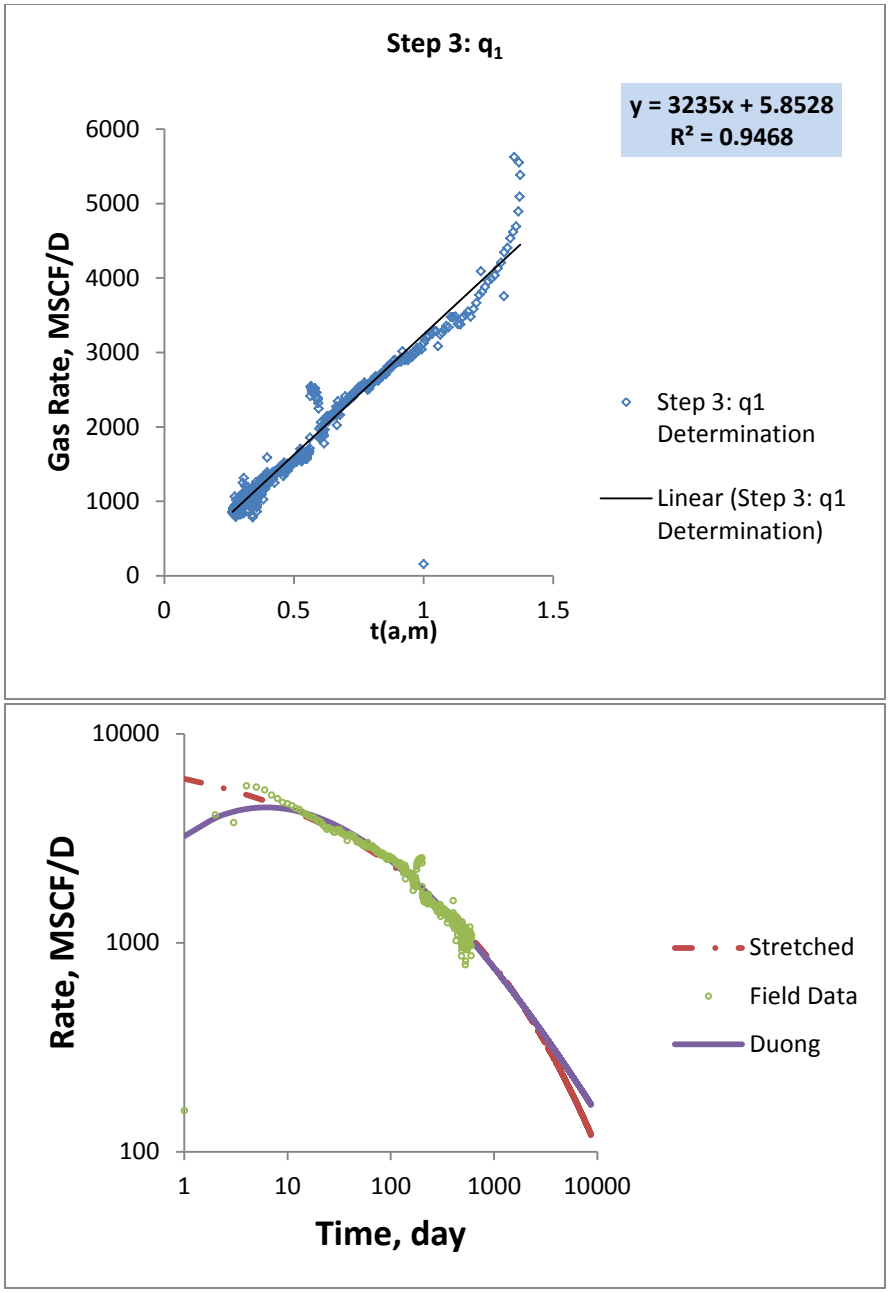
Step 3: q1
y = 3235x + 5.8528
R² = 0.9468
Gas Rate, MSCF/D
6000
5000
4000
3000
2000
1000
0
0
0.5
1
1.5
t(a,m)
Step 3: q1 Determination
Linear (Step 3: q1 Determination)
Rate, MSCF/D
10000
1000
100
1
10
100
1000
10000
Time, day
Stretched
Field Data
Duong

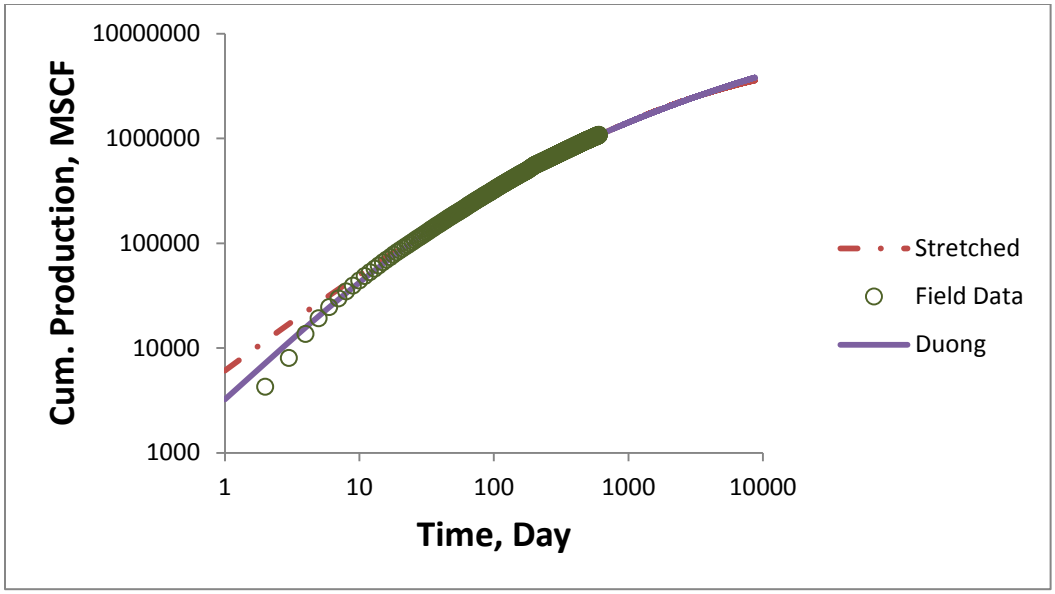
Cum. Production, MSCF
10000000
1000000
100000
10000
1000
1
10
100
1000
10000
Time, Day
Stretched
Field Data
Duong

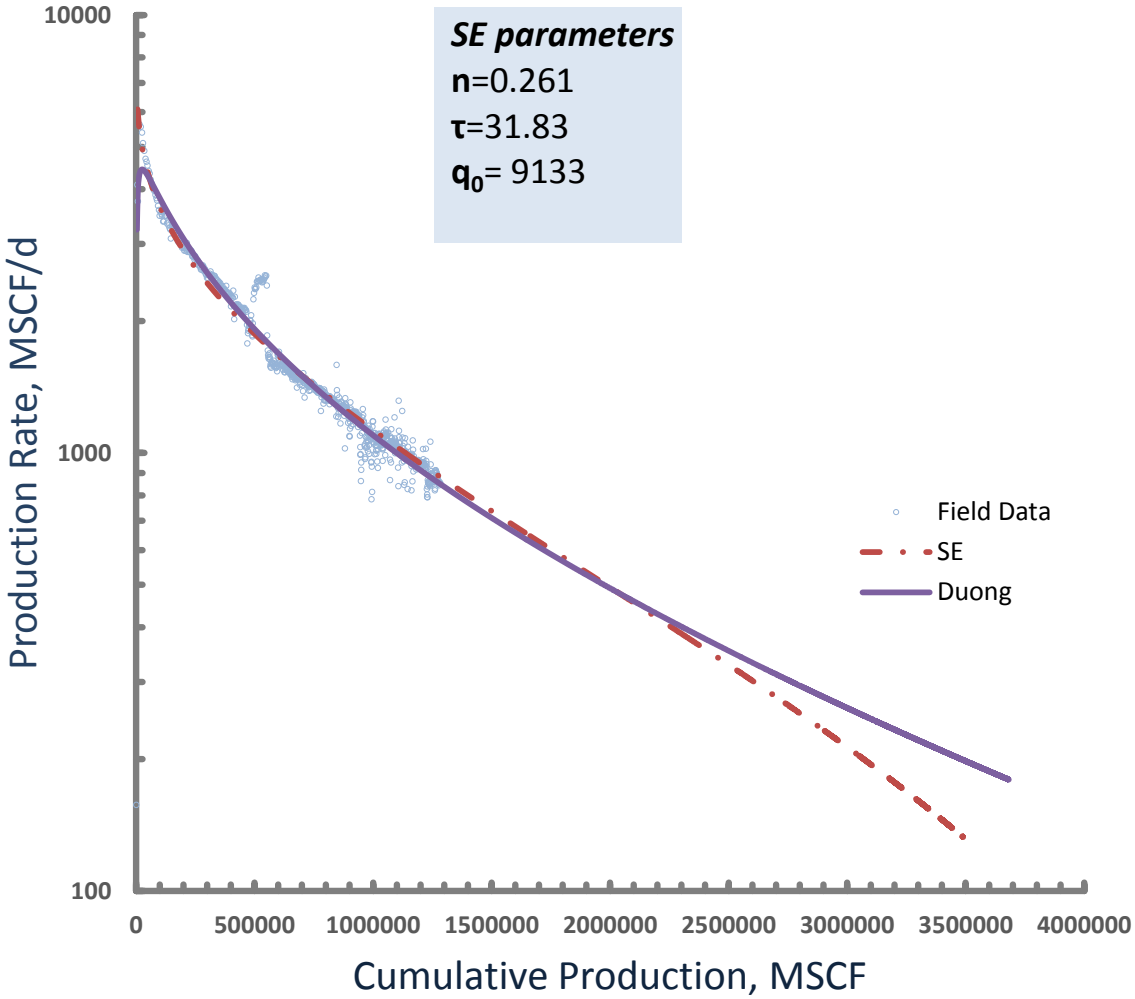
SE parameters
n=0.261
τ=31.83
q0= 9133
Production Rate, MSCF/d
10000
1000
100
0
500000
1000000
1500000
2000000
2500000
3000000
3500000
4000000
Cumulative Production, MSCF
Field Data
SE
Duong

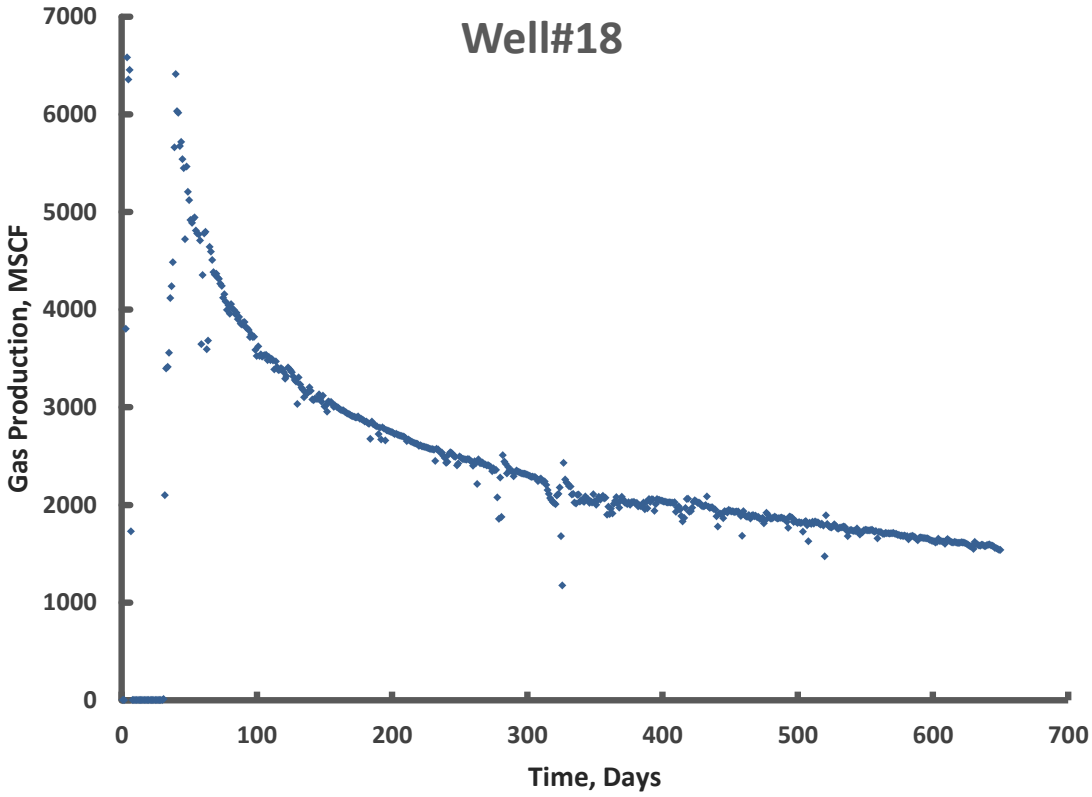
Well#18
Gas Production, MSCF
7000
6000
5000
4000
3000
2000
1000
0
0
100
200
300
400
500
600
700
Time, Days

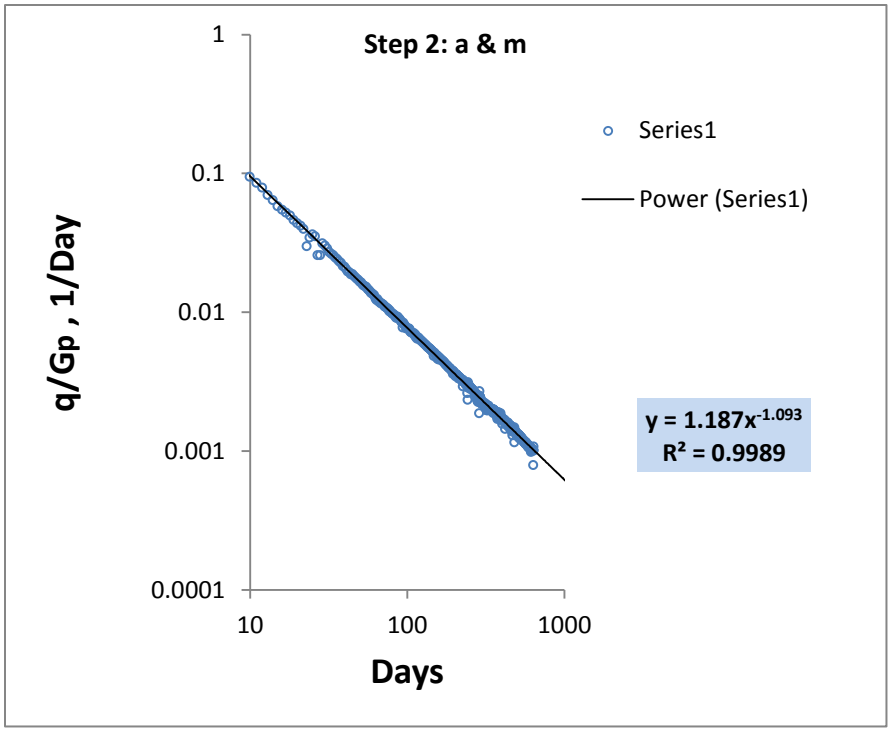
Step 2: a & m
q/Gp , 1/Day
1
0.1
0.01
0.001
0.0001
10
100
1000
Days
Series1
Power (Series1)
y = 1.187x-1.093
R² = 0.9989

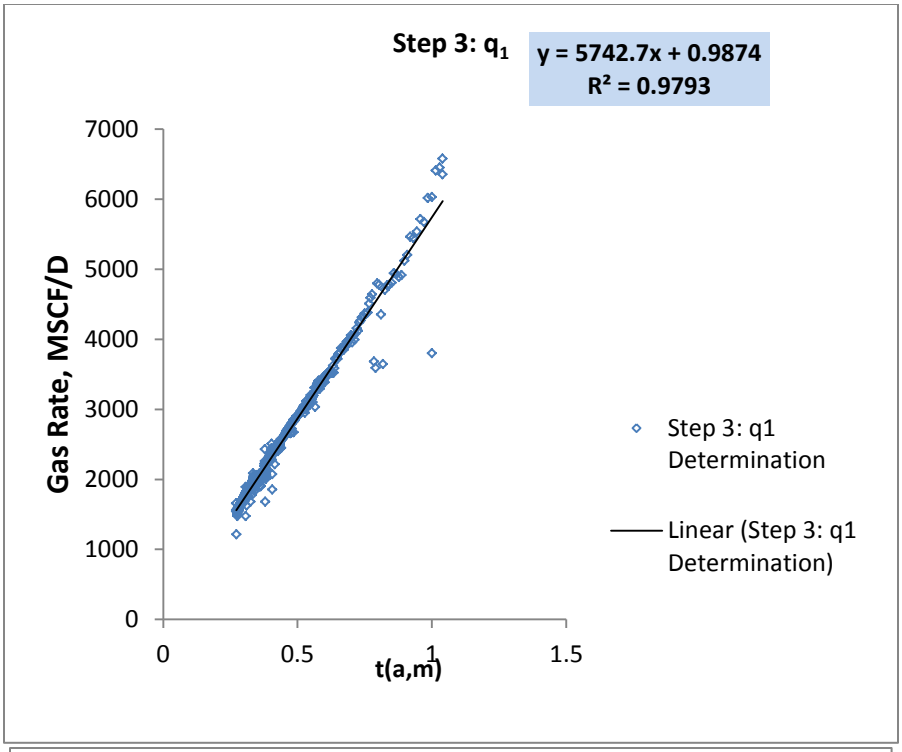
Step 3: q1
y = 5742.7x + 0.9874
R² = 0.9793
Gas Rate, MSCF/D
7000
6000
5000
4000
3000
2000
1000
0
0
0.5
1
1.5
t(a,m)
Step 3: q1 Determination
Linear (Step 3: q1 Determination)

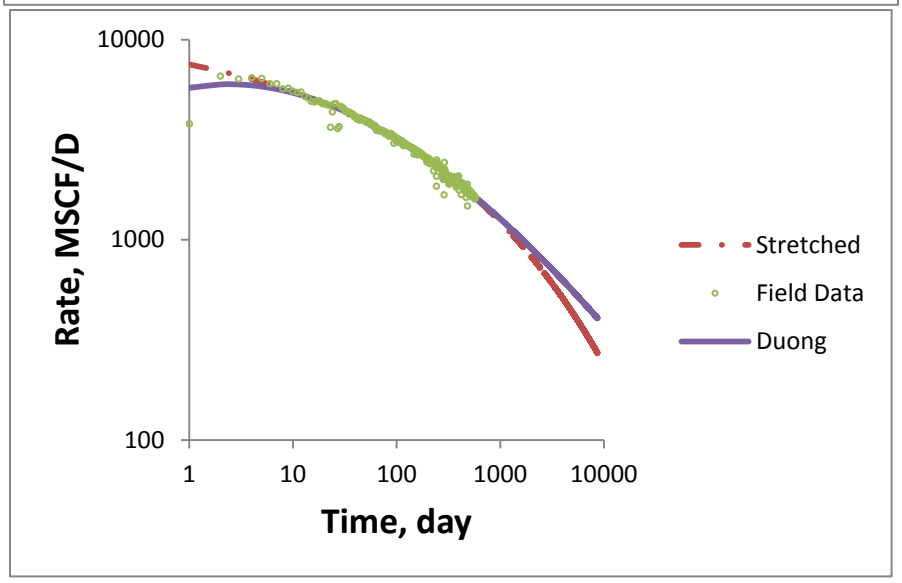
Rate, MSCF/D
10000
1000
100
1
10
100
1000
10000
Time, day
Stretched
Field Data
Duong

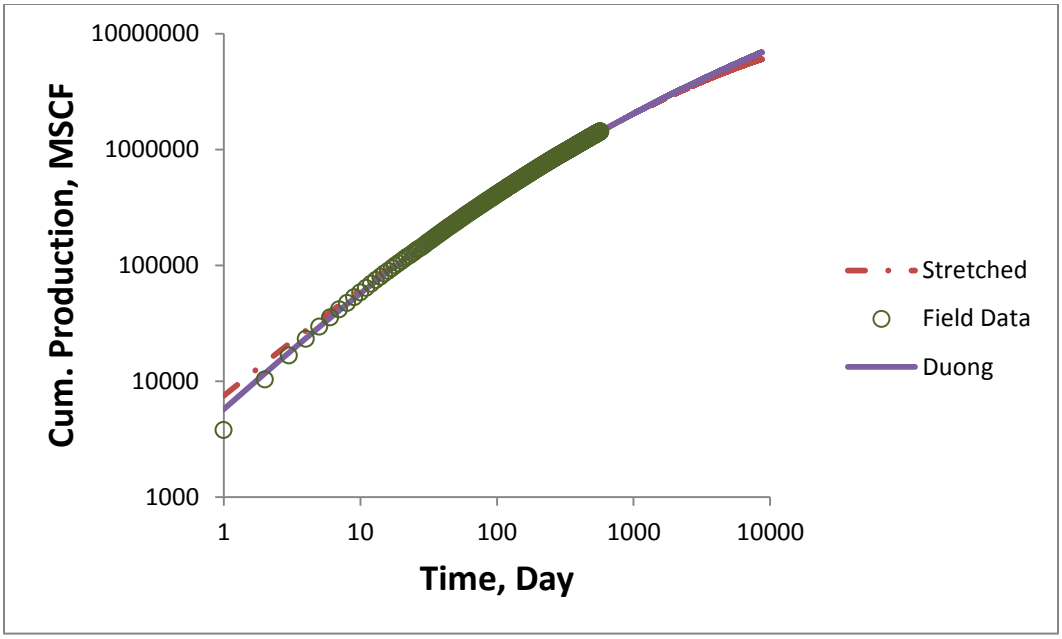
10000000
1000000
100000
10000
1000
Cum. Production, MSCF
1
10
100
1000
10000
Time, Day
Stretched
Field Data
Duong

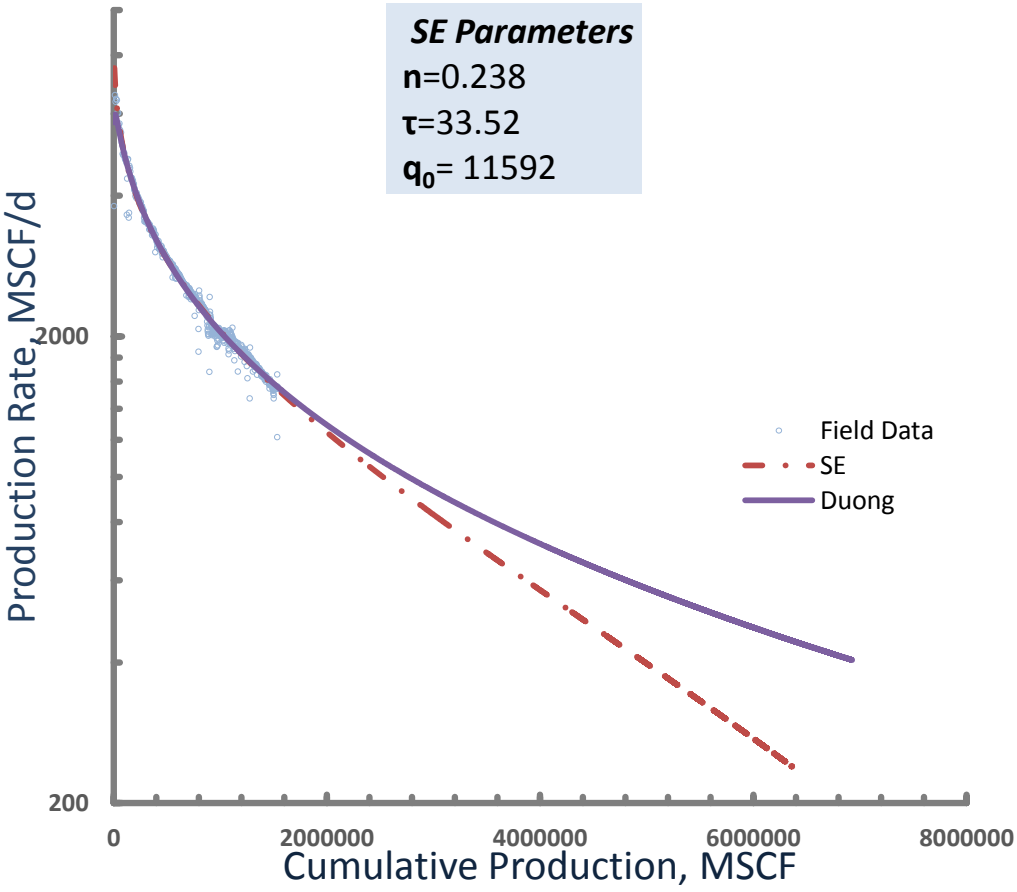
SE Parameters
n=0.238
τ=33.52
q0= 11592
Production Rate, MSCF/d
2000
200
0
2000000
4000000
6000000
8000000
Cumulative Production, MSCF
Field Data
SE
Duong

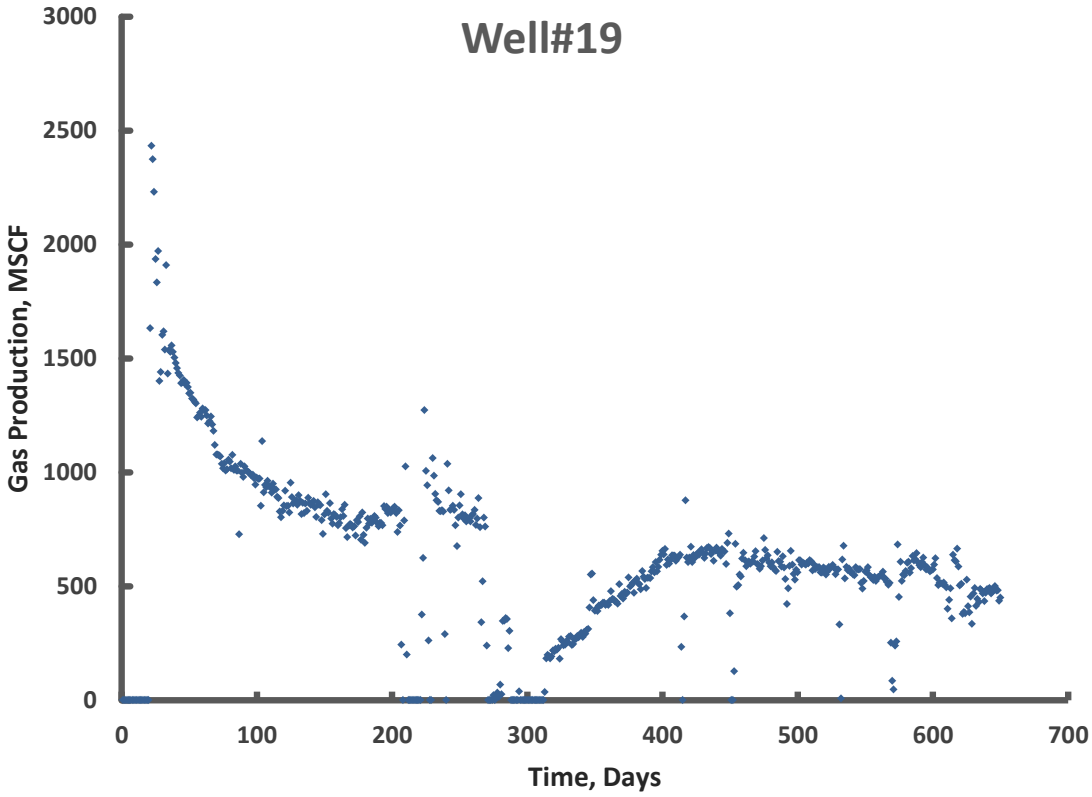
Well#19
Gas Production, MSCF
3000
2500
2000
1500
1000
500
0
0
100
200
300
400
500
600
700
Time, Days

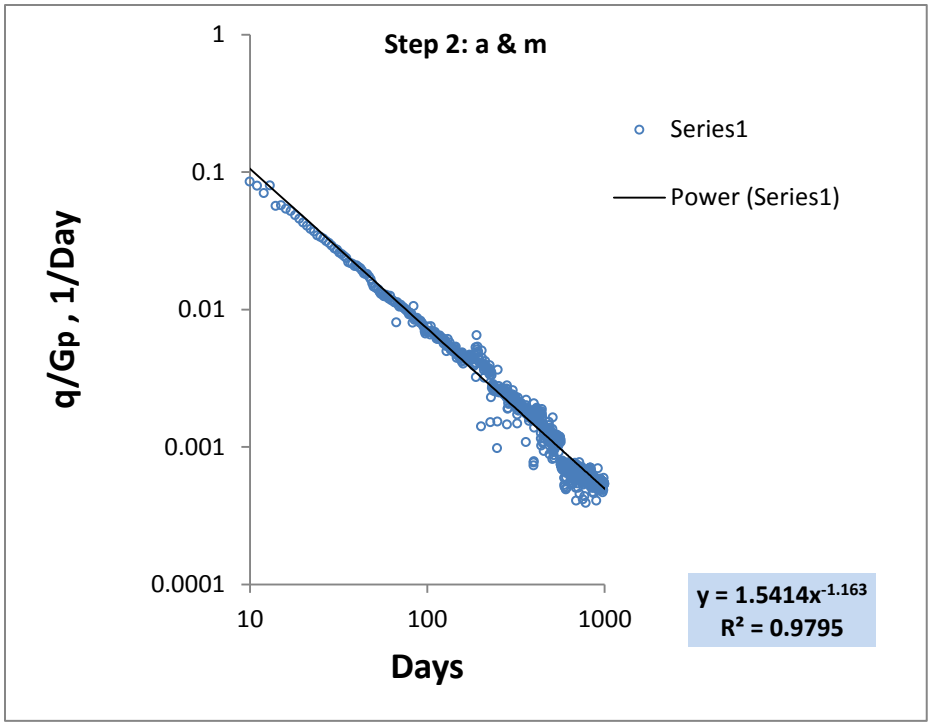
Step 2: a & m
q/Gp , 1/Day
1
0.1
0.01
0.001
0.0001
10
100
1000
Days
Series1
Power (Series1)
y = 1.5414x-1.163
R² = 0.9795

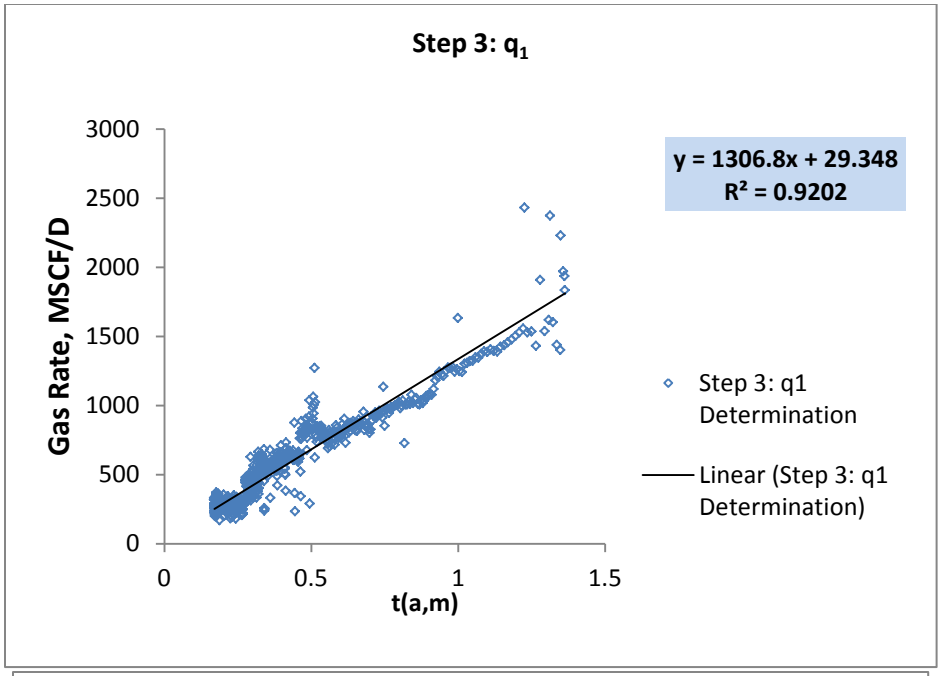
Step 3: q1
Gas Rate, MSCF/D
t(a,m)
y = 1306.8x + 29.348
R² = 0.9202
Step 3: q1 Determination
Linear (Step 3: q1 Determination)

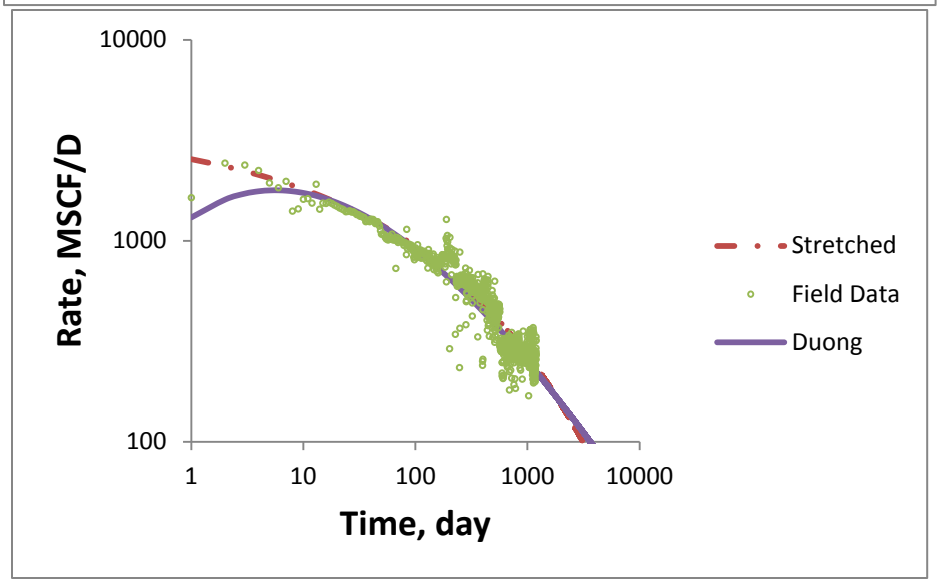
Rate, MSCF/D
Time, day
Stretched
Field Data
Duong

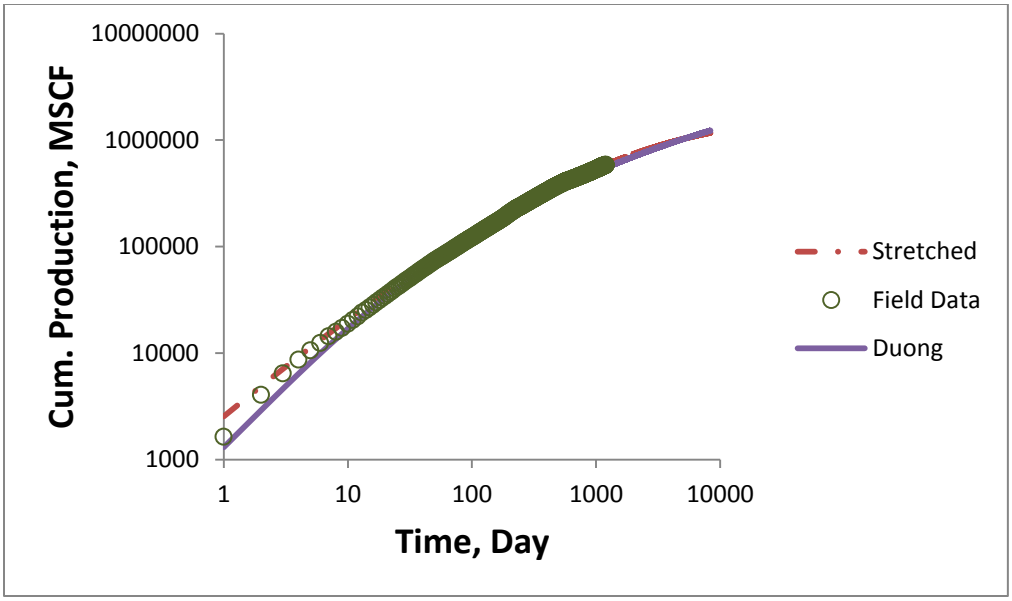
Cum. Production, MSCF
10000000
1000000
100000
10000
1000
1
10
100
1000
10000
Time, Day
Stretched
Field Data
Duong

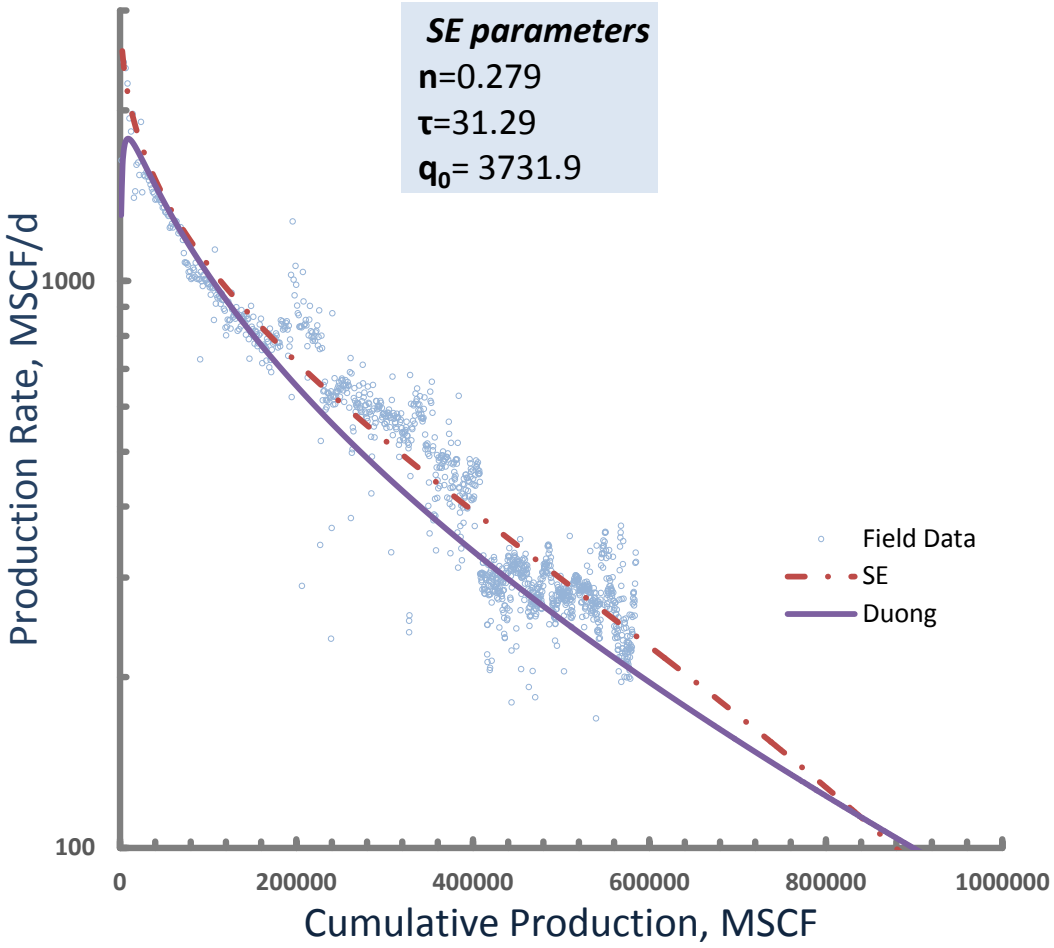
SE parameters
n=0.279
τ=31.29
q0= 3731.9
Production Rate, MSCF/d
1000
100
0
200000
400000
600000
800000
1000000
Cumulative Production, MSCF
Field Data
SE
Duong

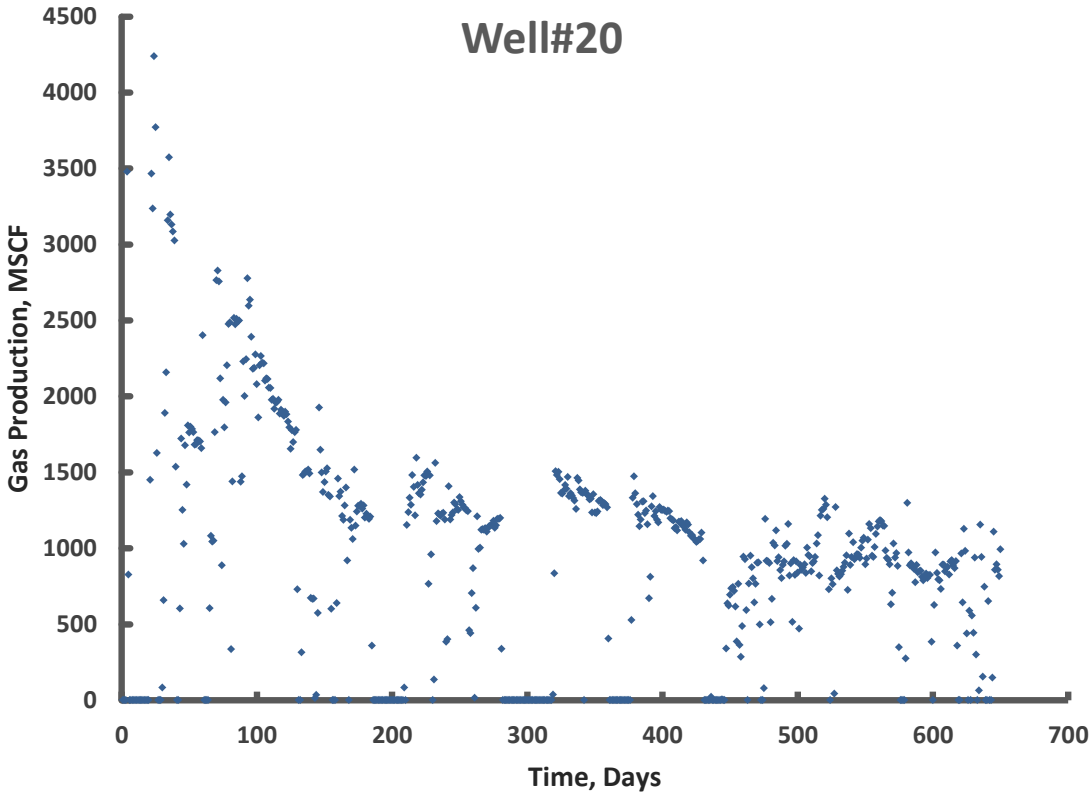
Well#20
Gas Production, MSCF
4500
4000
3500
3000
2500
2000
1500
1000
500
0
0
100
200
300
400
500
600
700
Time, Days

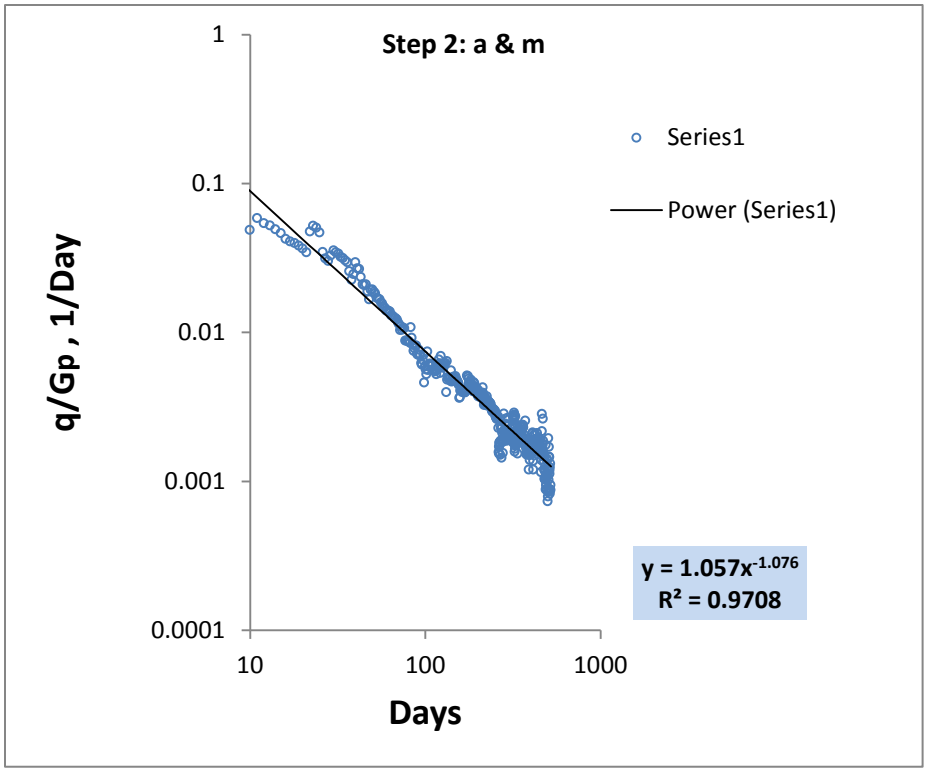
Step 2: a & m
q/Gp , 1/Day
1
0.1
0.01
0.001
0.0001
10
100
1000
Days
Series1
Power (Series1)
y = 1.057x-1.076
R² = 0.9708

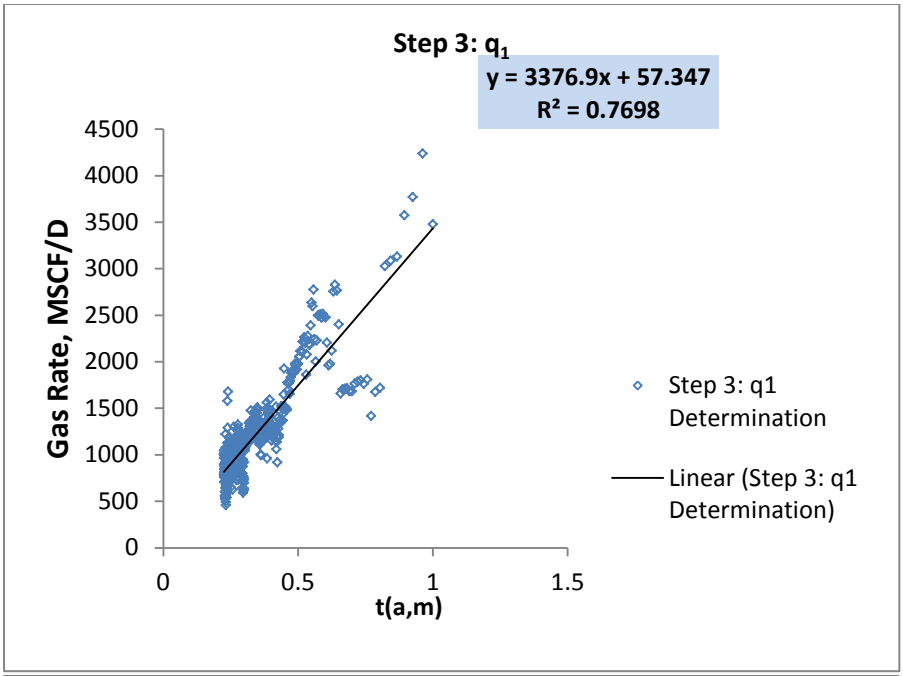
Step 3: q1
y = 3376.9x + 57.347
R² = 0.7698
Gas Rate, MSCF/D
4500
4000
3500
3000
2500
2000
1500
1000
500
0
0
0.5
1
1.5
t(a,m)
Step 3: q1 Determination
Linear (Step 3: q1 Determination)

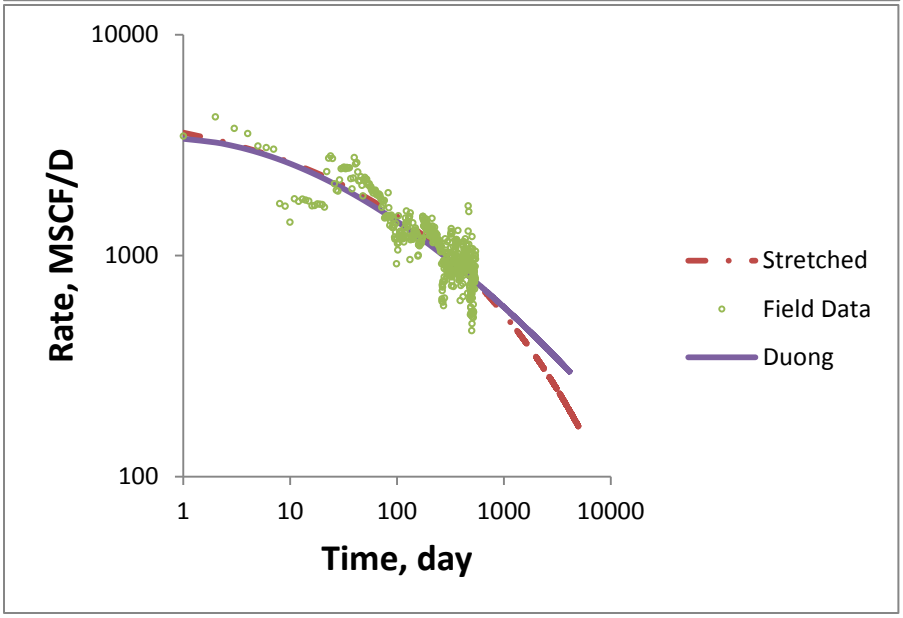
Rate, MSCF/D
10000
1000
100
1
10
100
1000
10000
Time, day
Stretched
Field Data
Duong

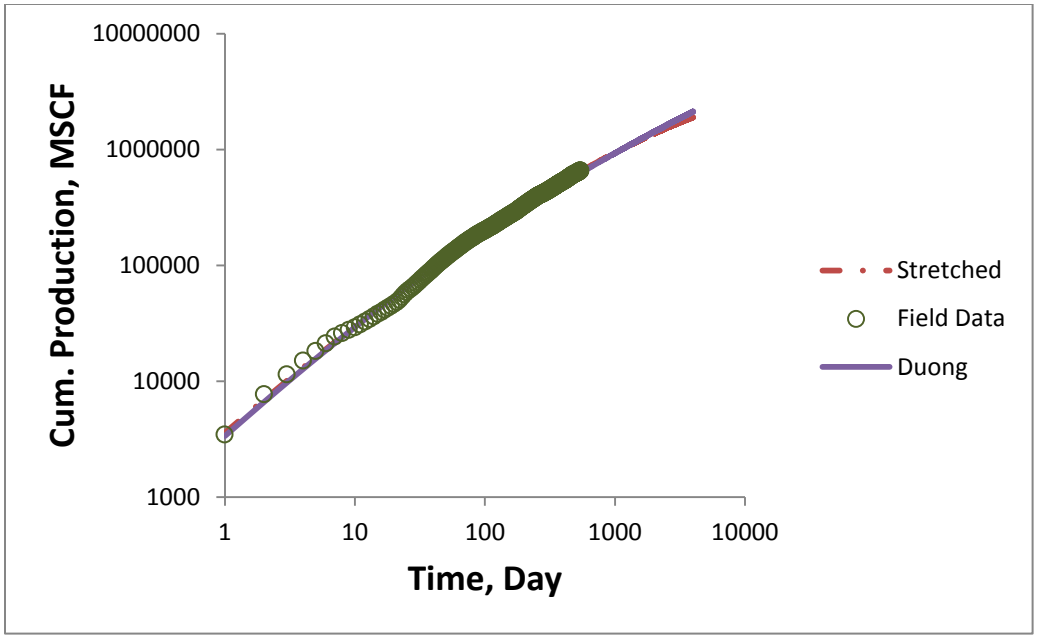
10000000
1000000
100000
10000
1000
Cum. Production, MSCF
1
10
100
1000
10000
Time, Day
Stretched
Field Data
Duong

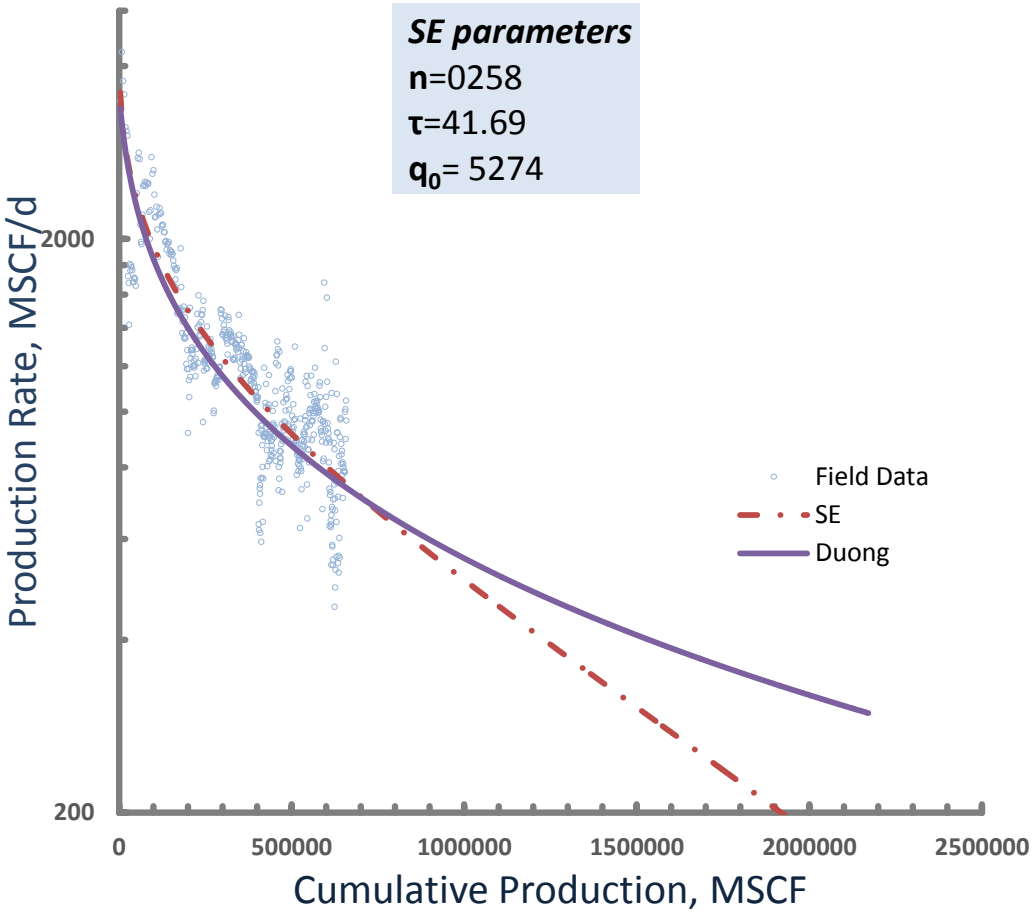
SE parameters
n=0258
τ=41.69
q0= 5274
2000
200
Production Rate, MSCF/d
0
500000
1000000
1500000
2000000
2500000
Cumulative Production, MSCF
Field Data
SE
Duong

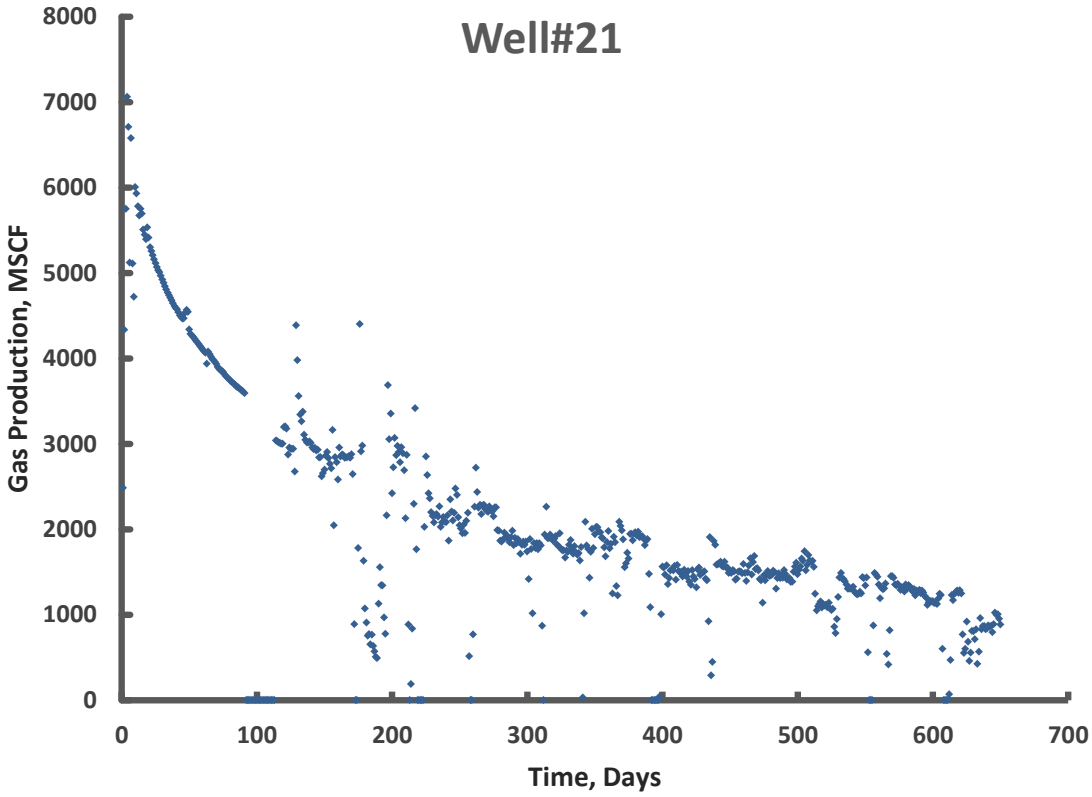
Well#21
Gas Production, MSCF
8000
7000
6000
5000
4000
3000
2000
1000
0
0
100
200
300
400
500
600
700
Time, Days

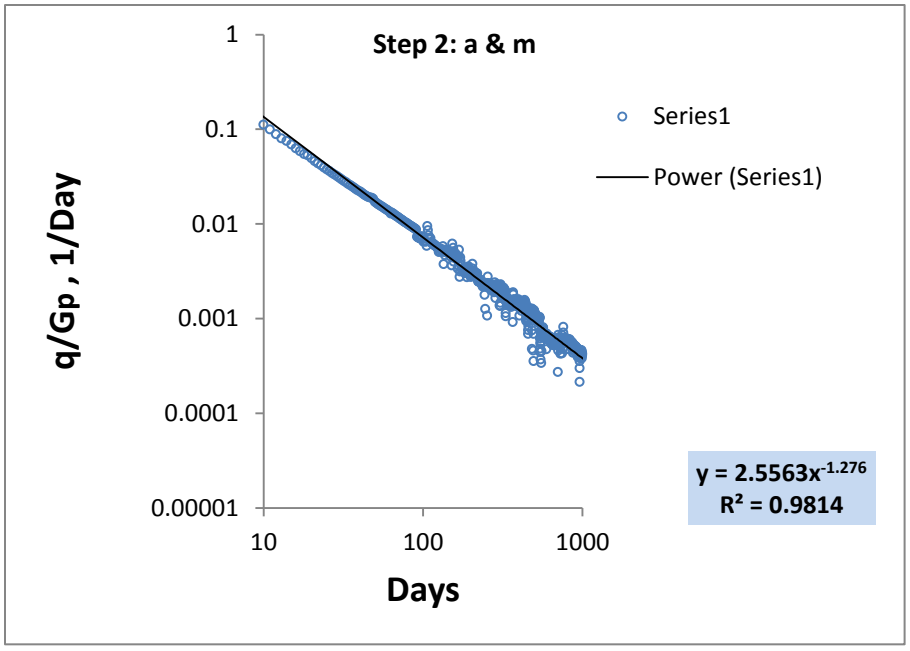
Step 2: a & m
q/Gp , 1/Day
1
0.1
0.01
0.001
0.0001
0.00001
10
100
1000
Days
Series1
Power (Series1)
y = 2.5563x-1.276
R² = 0.9814

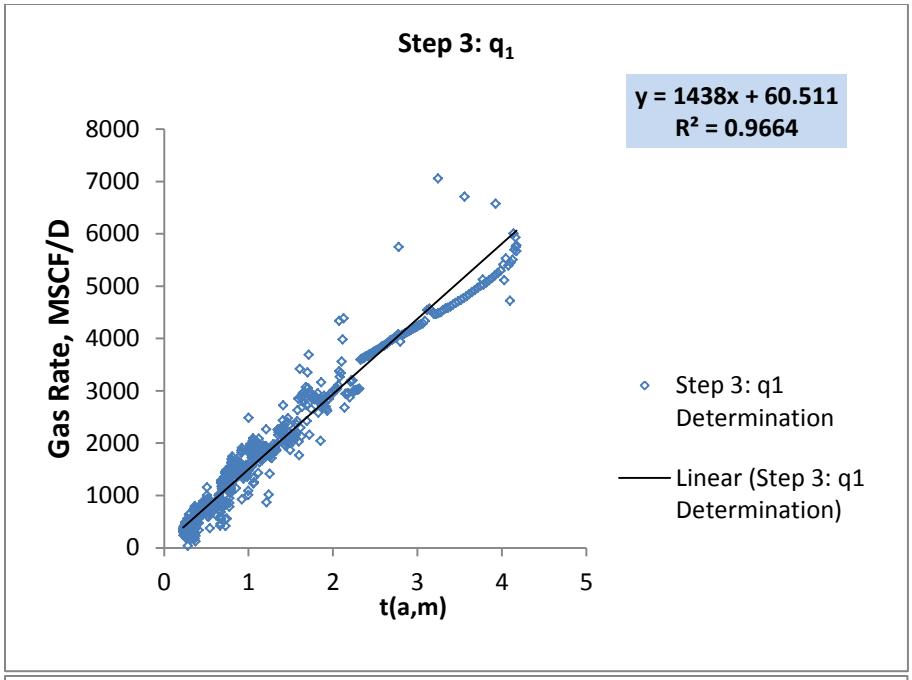
Step 3: q1
y = 1438x + 60.511
R² = 0.9664
Gas Rate, MSCF/D
8000
7000
6000
5000
4000
3000
2000
1000
0
0
1
2
3
4
5
t(a,m)
Step 3: q1 Determination
Linear (Step 3: q1 Determination)

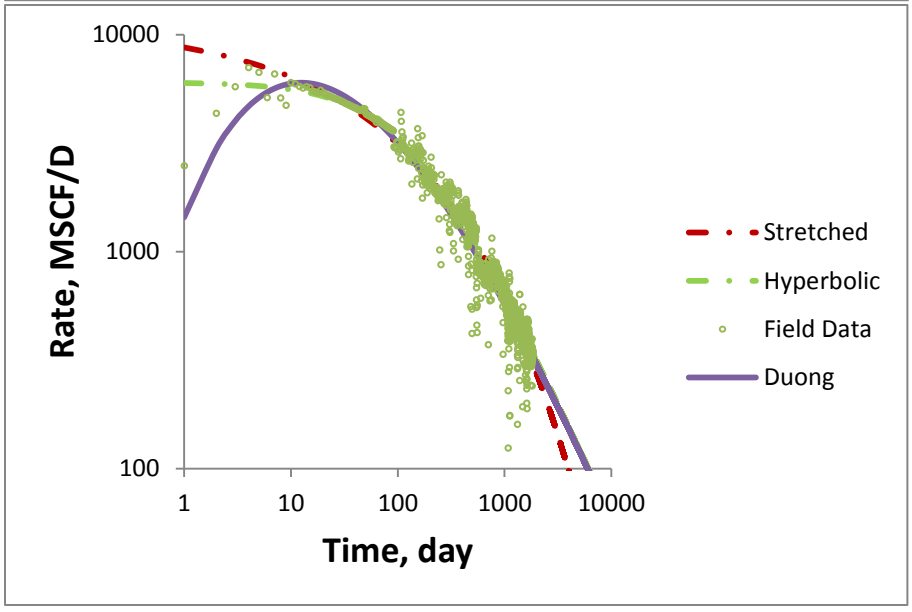
Rate, MSCF/D
10000
1000
100
1
10
100
1000
10000
Time, day
Stretched
Hyperbolic
Field Data
Duong

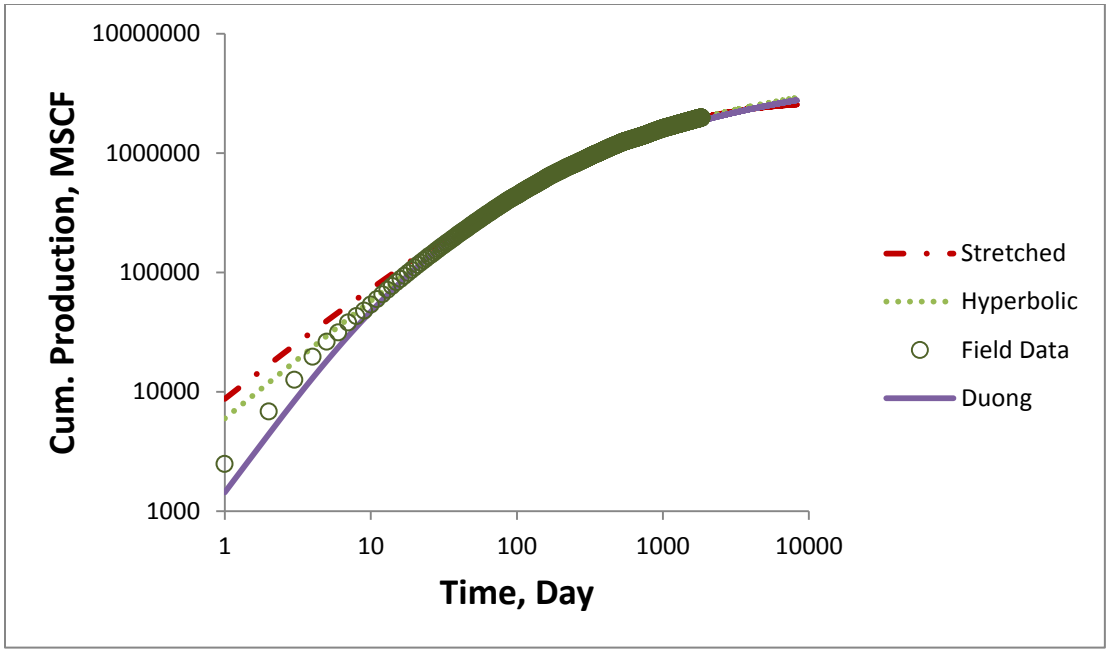
10000000
1000000
100000
10000
1000
Cum. Production, MSCF
1
10
100
1000
10000
Time, Day
Stretched
Hyperbolic
Field Data
Duong

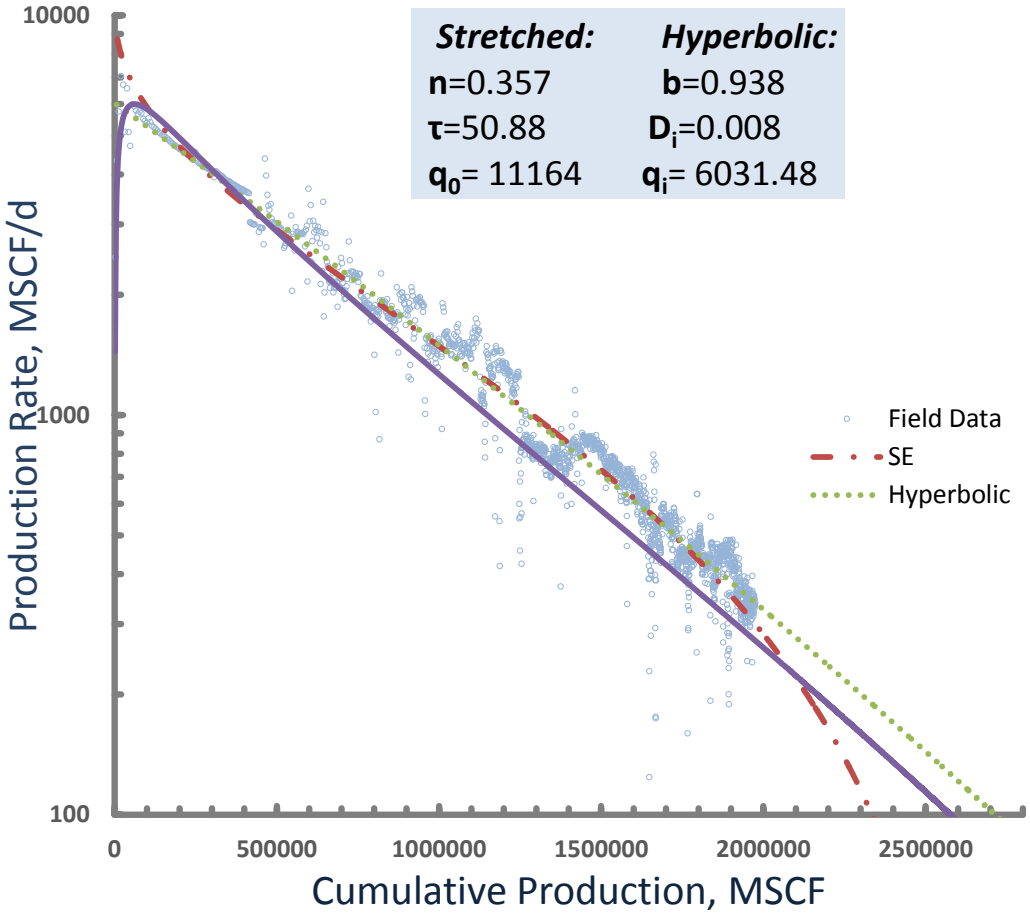
Stretched:
Hyperbolic:
n=0.357
b=0.938
τ=50.88
Di=0.008
q0= 11164
qi= 6031.48
10000
1000
100
Production Rate, MSCF/d
0
500000
1000000
1500000
2000000
2500000
Cumulative Production, MSCF
Field Data
SE
Hyperbolic

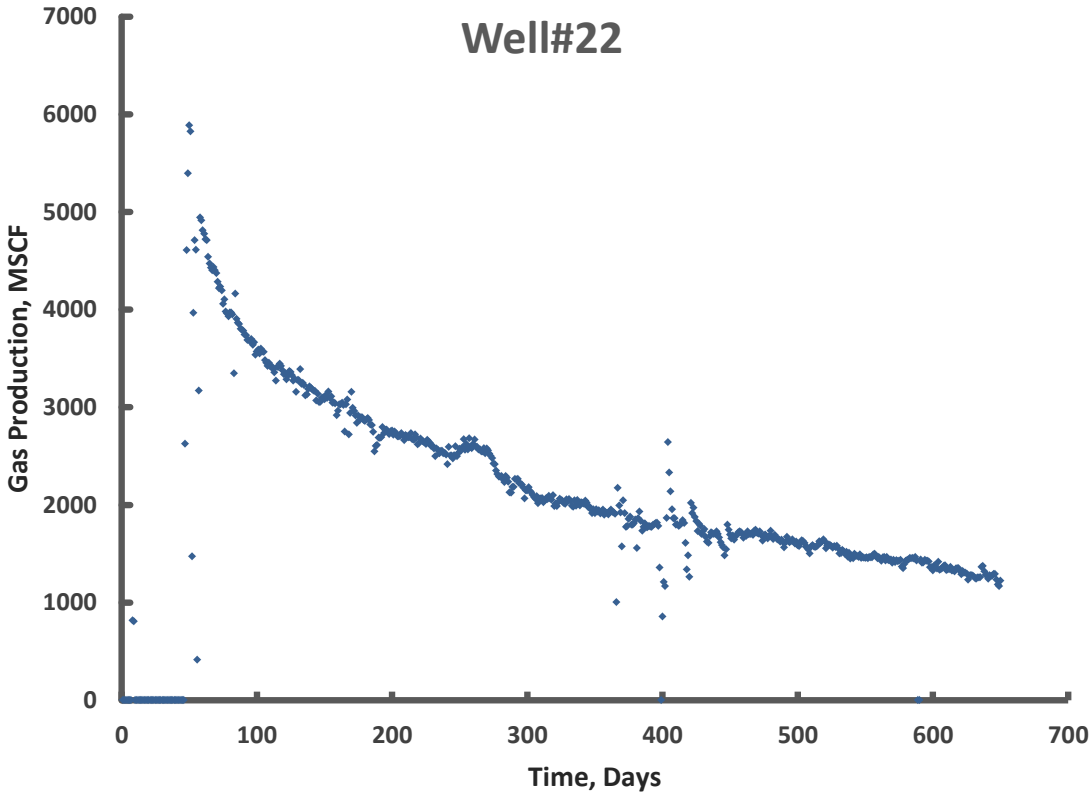
Well#22
Gas Production, MSCF
7000
6000
5000
4000
3000
2000
1000
0
0
100
200
300
400
500
600
700
Time, Days

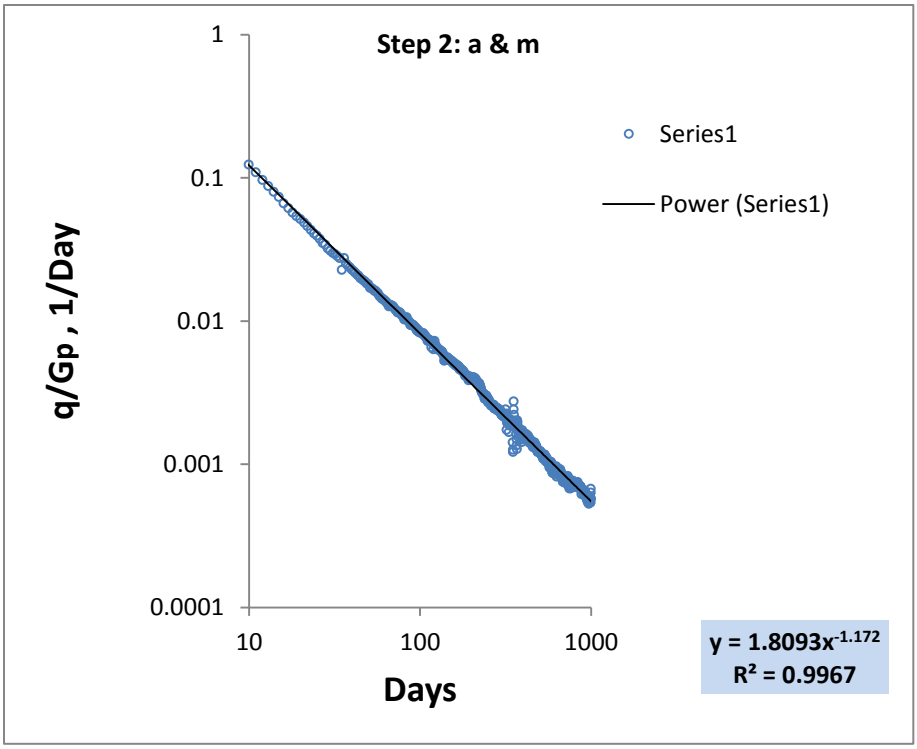
Step 2: a & m
q/Gp , 1/Day
1
0.1
0.01
0.001
0.0001
10
100
1000
Days
Series1
Power (Series1)
y = 1.8093x-1.172
R² = 0.9967

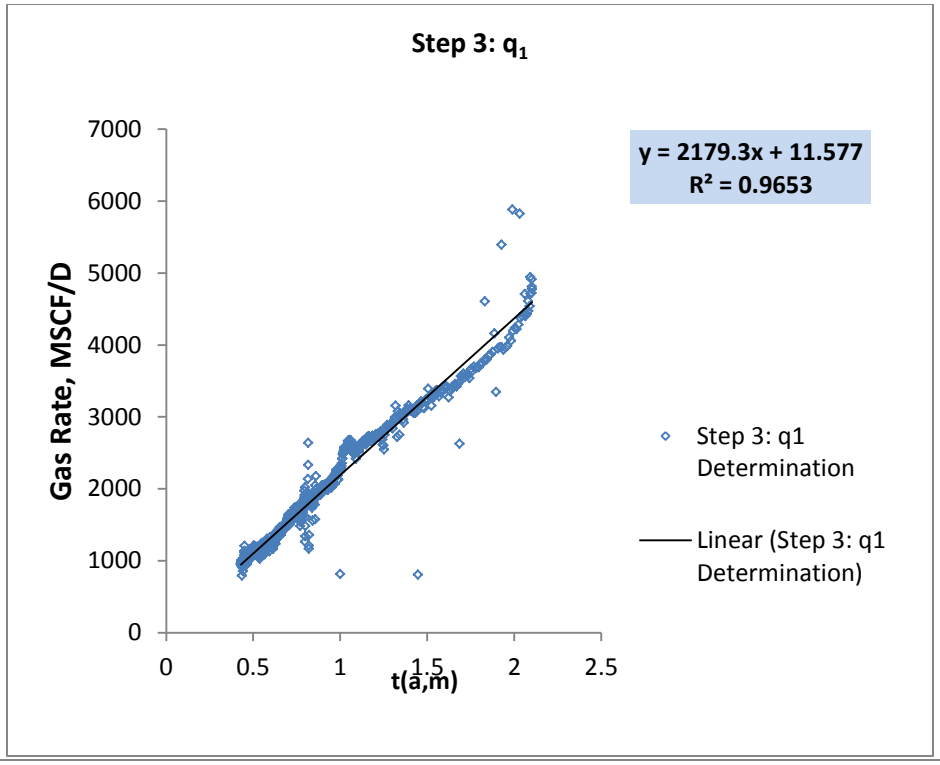
Step 3: q1
y = 2179.3x + 11.577
R² = 0.9653
Gas Rate, MSCF/D
7000
6000
5000
4000
3000
2000
1000
0
0
0.5
1
1.5
2
2.5
t(a,m)
Step 3: q1 Determination
Linear (Step 3: q1 Determination)

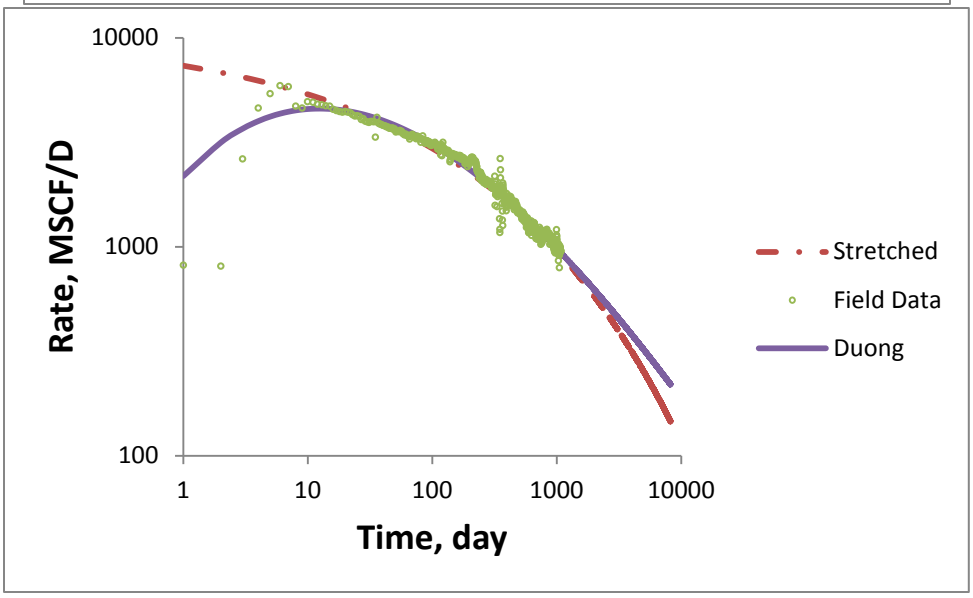
Rate, MSCF/D
10000
1000
100
1
10
100
1000
10000
Time, day
Stretched
Field Data
Duong

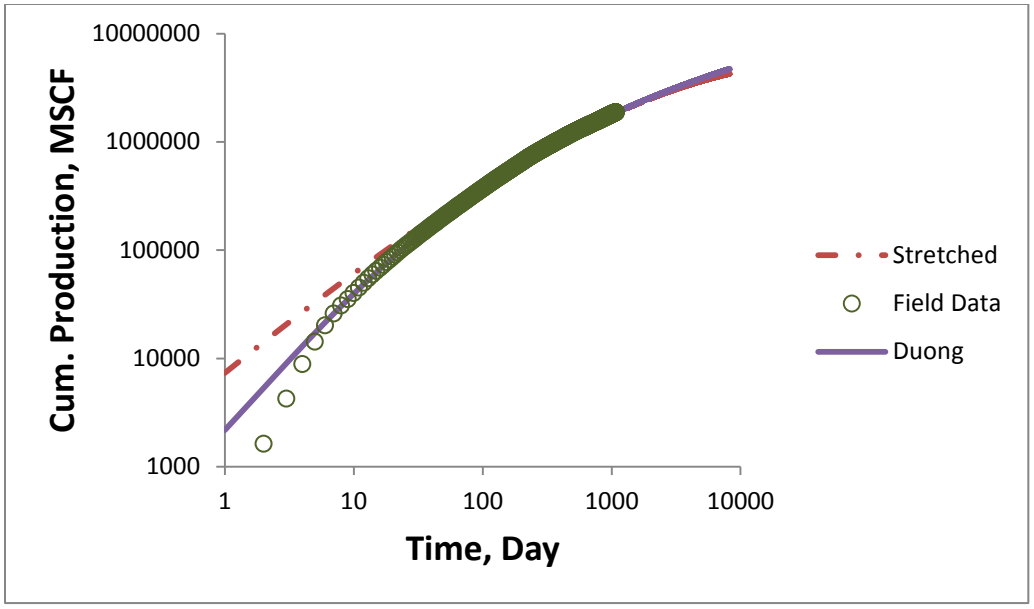
10000000
1000000
100000
10000
1000
Cum. Production, MSCF
1
10
100
1000
10000
Time, Day
Stretched
Field Data
Duong

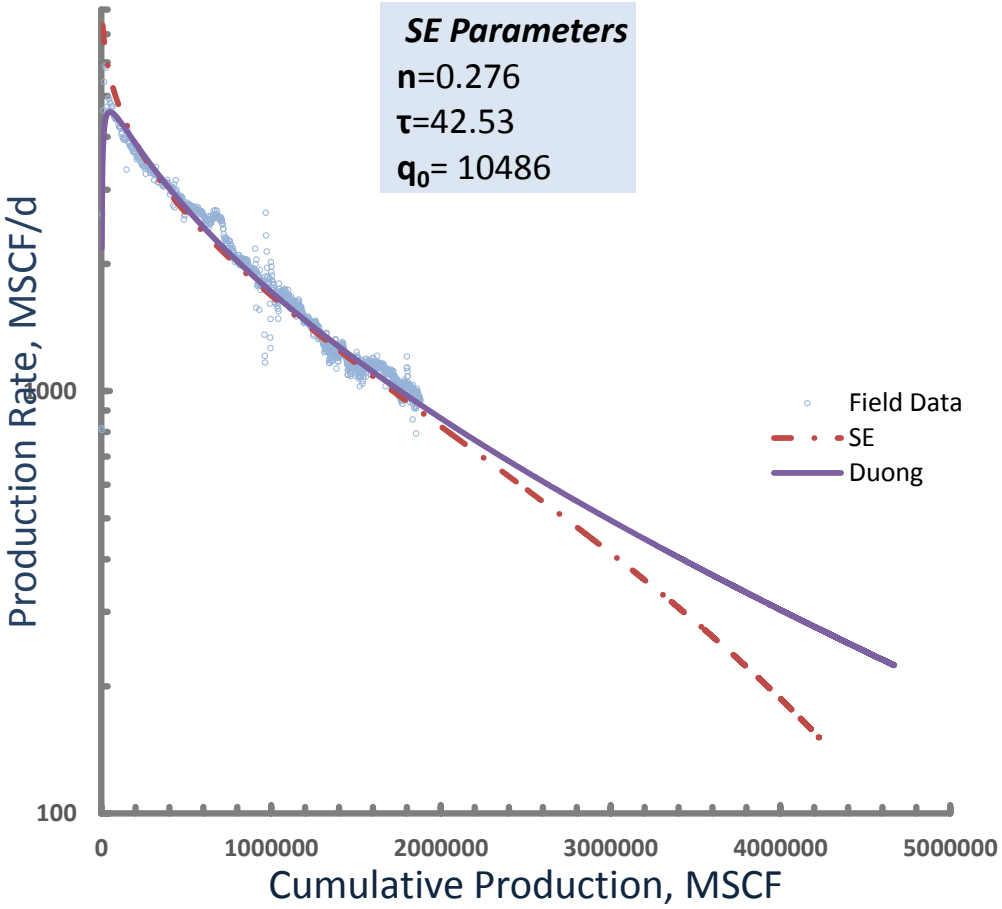
SE Parameters
n=0.276
τ=42.53
q0= 10486
Production Rate, MSCF/d
1000
100
0
1000000
2000000
3000000
4000000
5000000
Cumulative Production, MSCF
Field Data
SE
Duong

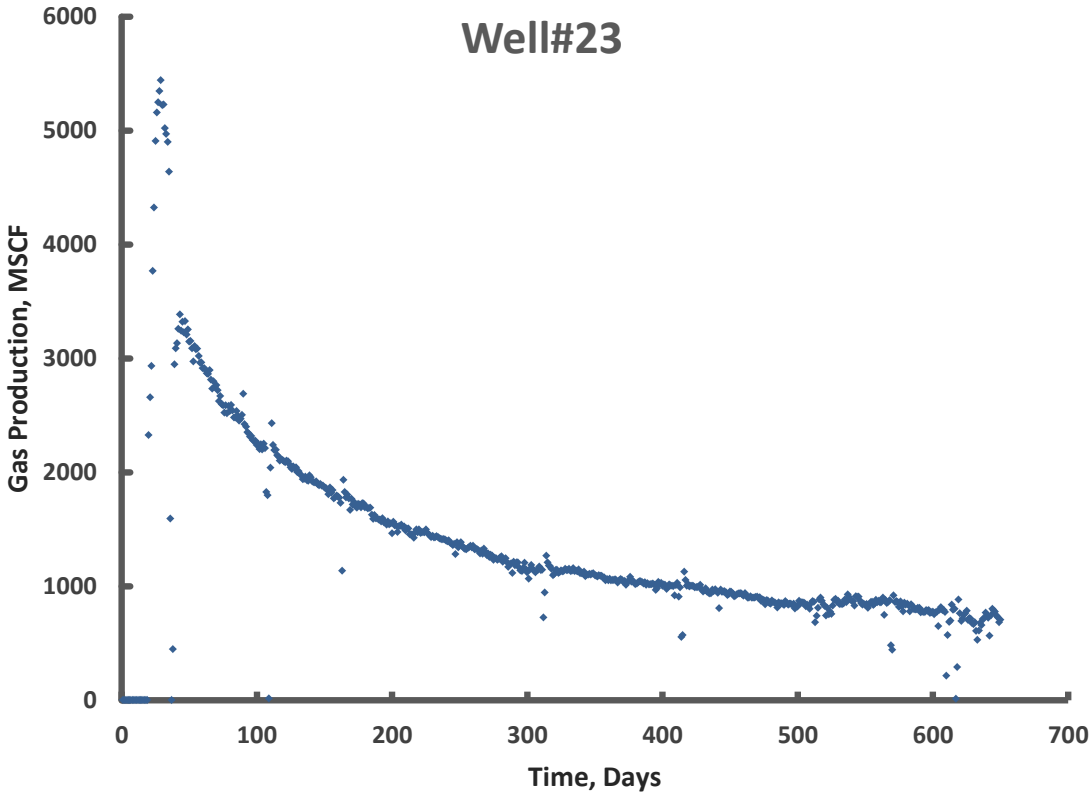
Well#23
Gas Production, MSCF
6000
5000
4000
3000
2000
1000
0
0
100
200
300
400
500
600
700
Time, Days

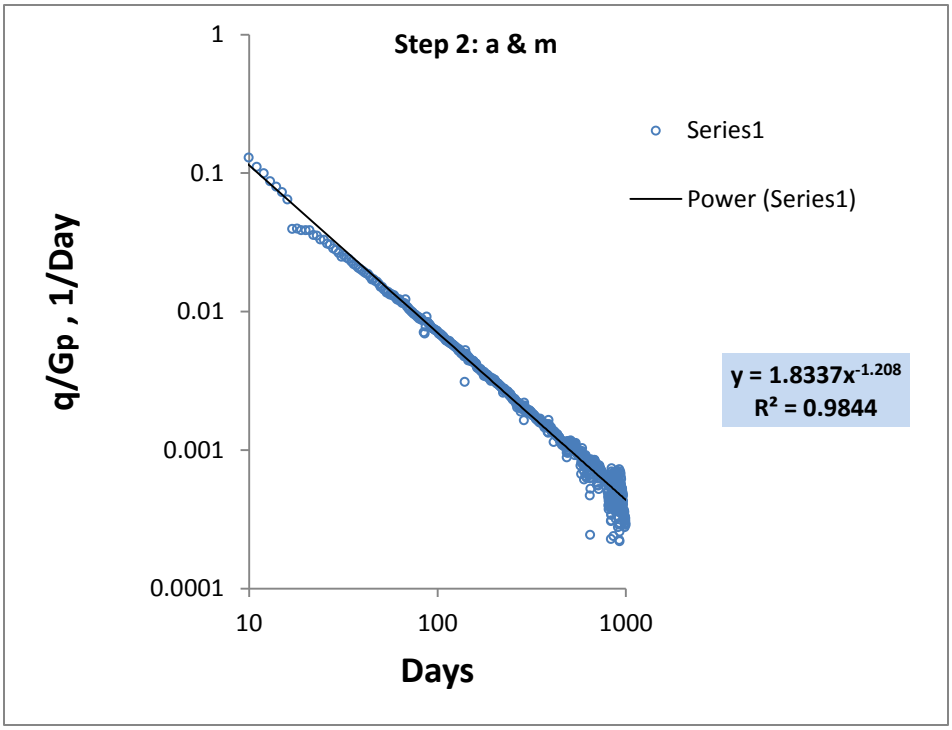
Step 2: a & m
q/Gp , 1/Day
1
0.1
0.01
0.001
0.0001
10
100
1000
Days
Series1
Power (Series1)
y = 1.8337x-1.208
R² = 0.9844

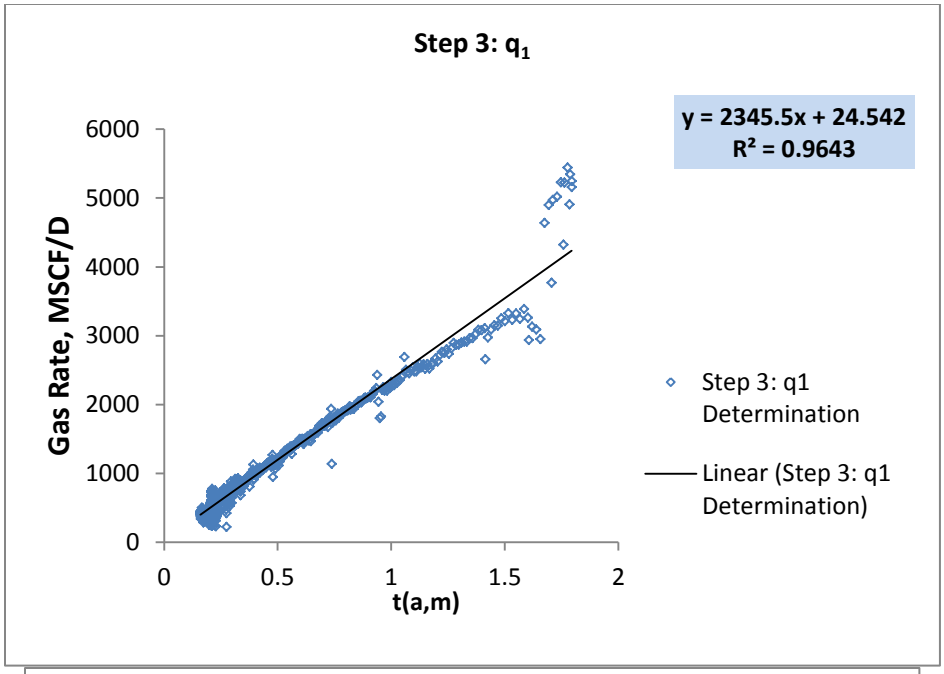
Step 3: q1
y = 2345.5x + 24.542
R² = 0.9643
Gas Rate, MSCF/D
6000
5000
4000
3000
2000
1000
0
0
0.5
1
1.5
2
t(a,m)
Step 3: q1 Determination
Linear (Step 3: q1 Determination)

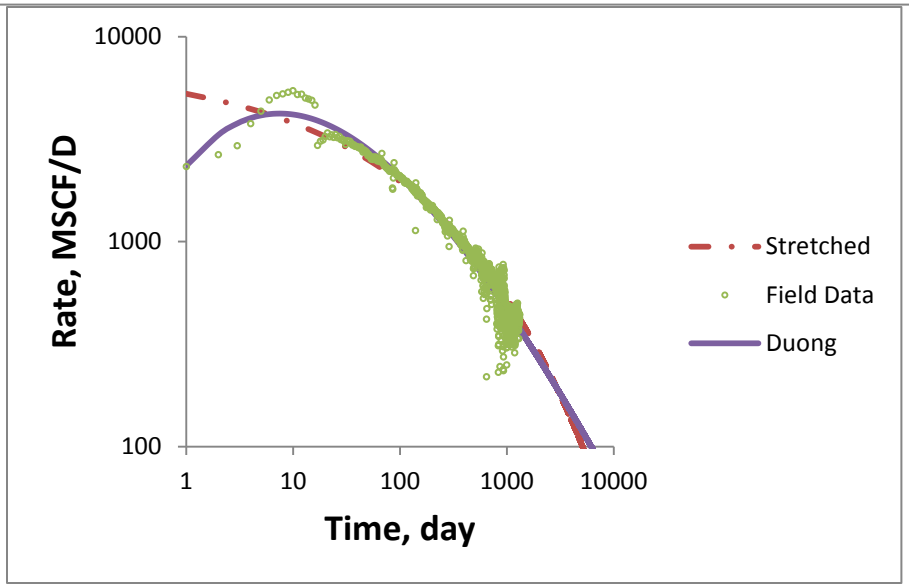
Rate, MSCF/D
10000
1000
100
1
10
100
1000
10000
Time, day
Stretched
Field Data
Duong

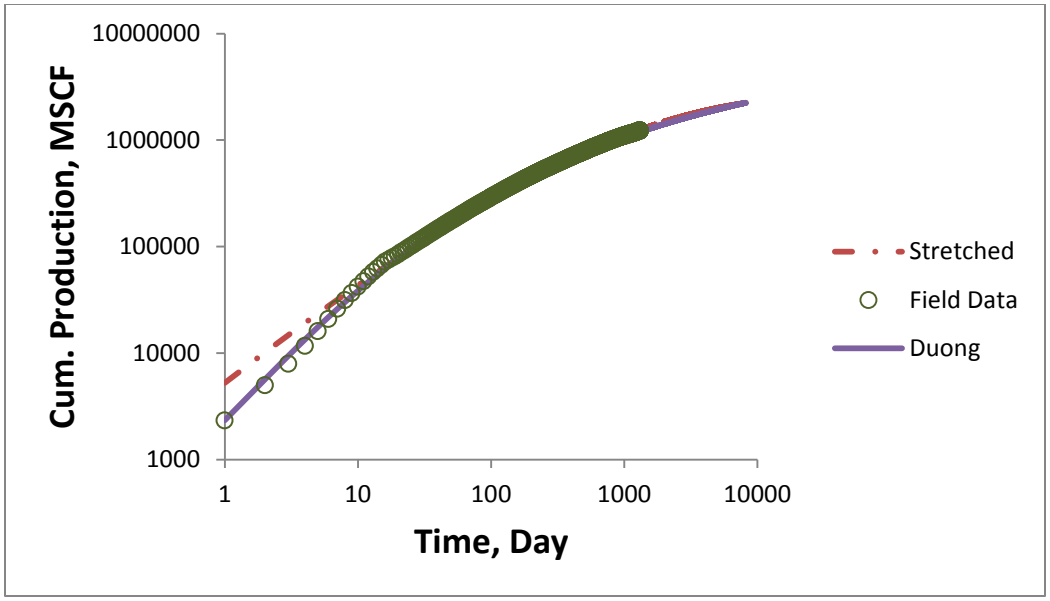
10000000
1000000
100000
10000
1000
Cum. Production, MSCF
1
10
100
1000
10000
Time, Day
Stretched
Field Data
Duong

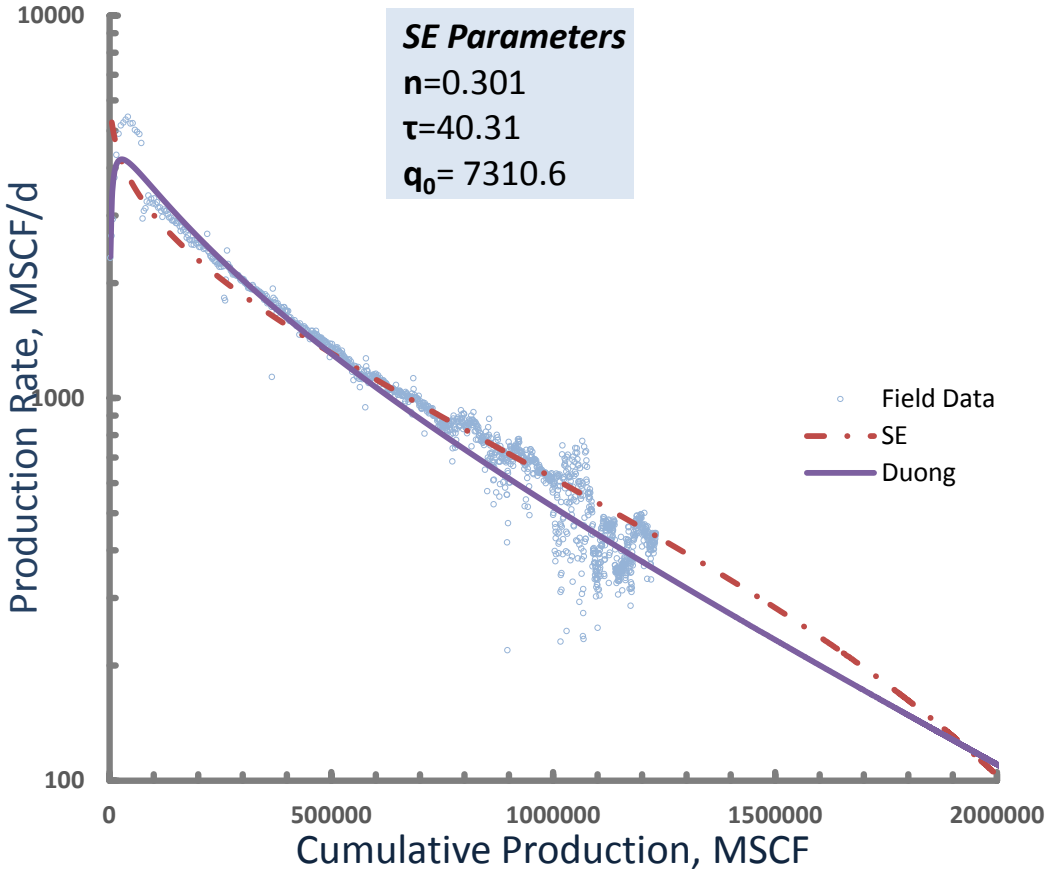
SE Parameters
n=0.301
τ=40.31
q0= 7310.6
10000
1000
100
Production Rate, MSCF/d
0
500000
1000000
1500000
2000000
Cumulative Production, MSCF
Field Data
SE
Duong

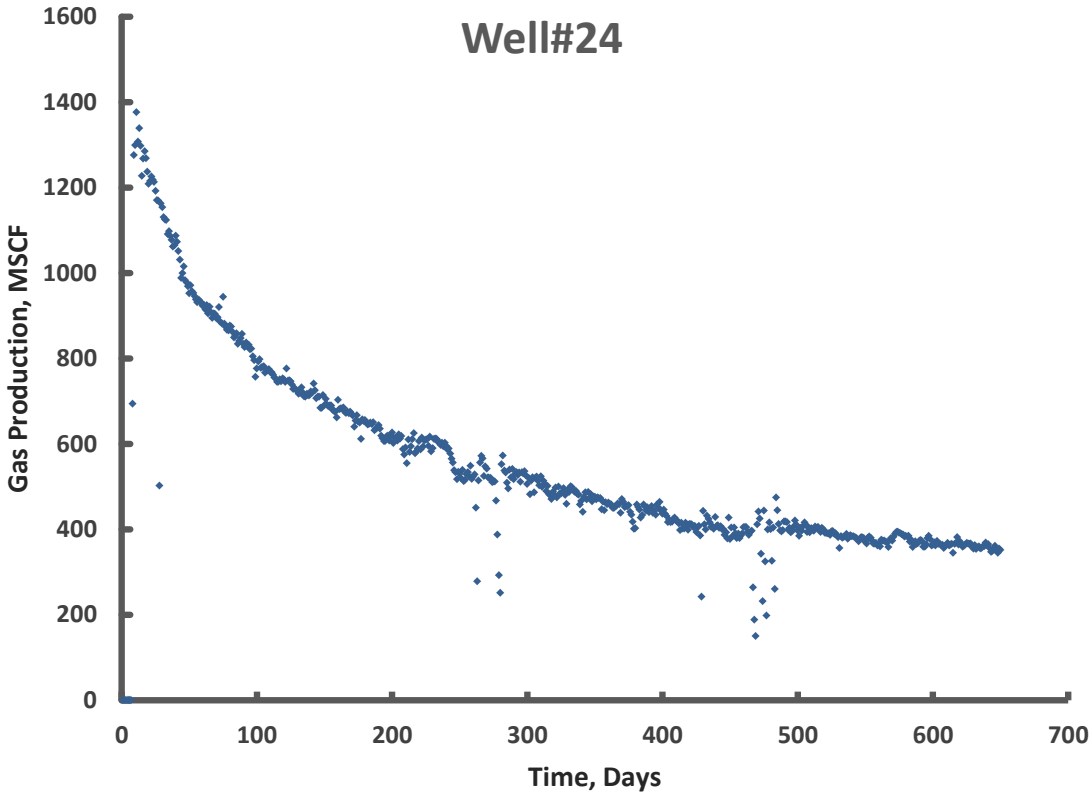
Well#24
Gas Production, MSCF
Time, Days
1600
1400
1200
1000
800
600
400
200
0
0
100
200
300
400
500
600
700

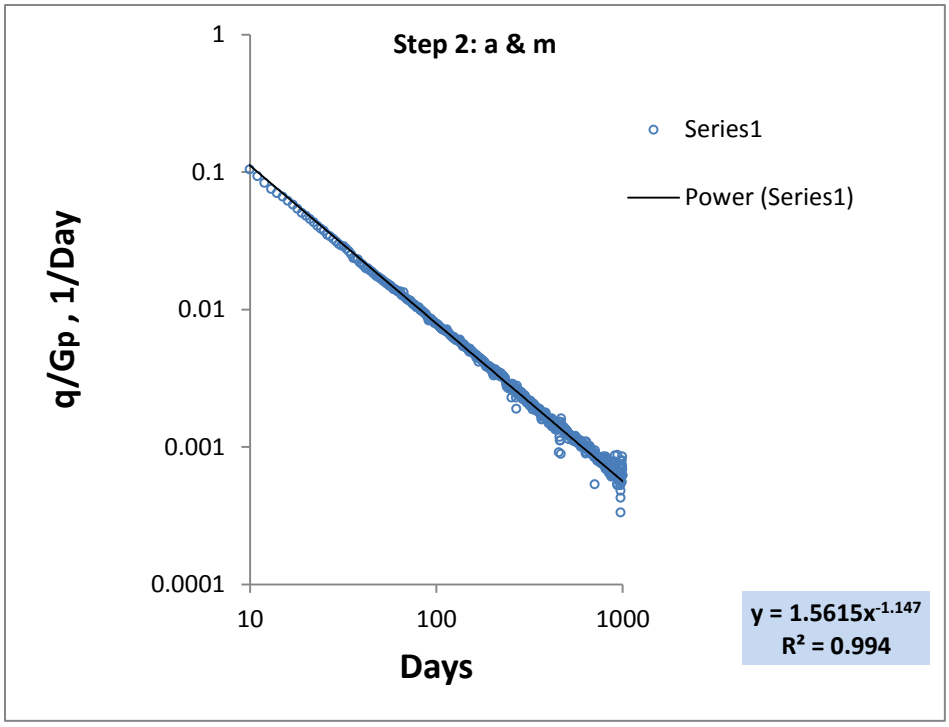
Step 2: a & m
q/Gp , 1/Day
Days
Series1
Power (Series1)
1
0.1
0.01
0.001
0.0001
10
100
1000
y = 1.5615x-1.147
R² = 0.994

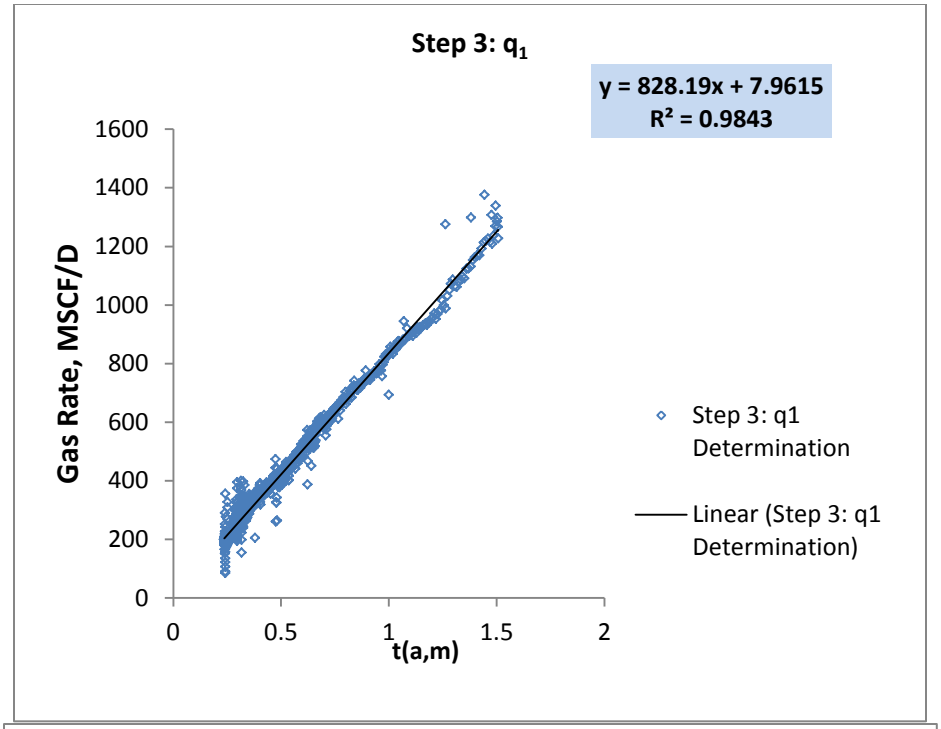
Step 3: q1
y = 828.19x + 7.9615
R² = 0.9843
Gas Rate, MSCF/D
1600
1400
1200
1000
800
600
400
200
0
0
0.5
1
1.5
2
t(a,m)
Step 3: q1 Determination
Linear (Step 3: q1 Determination)

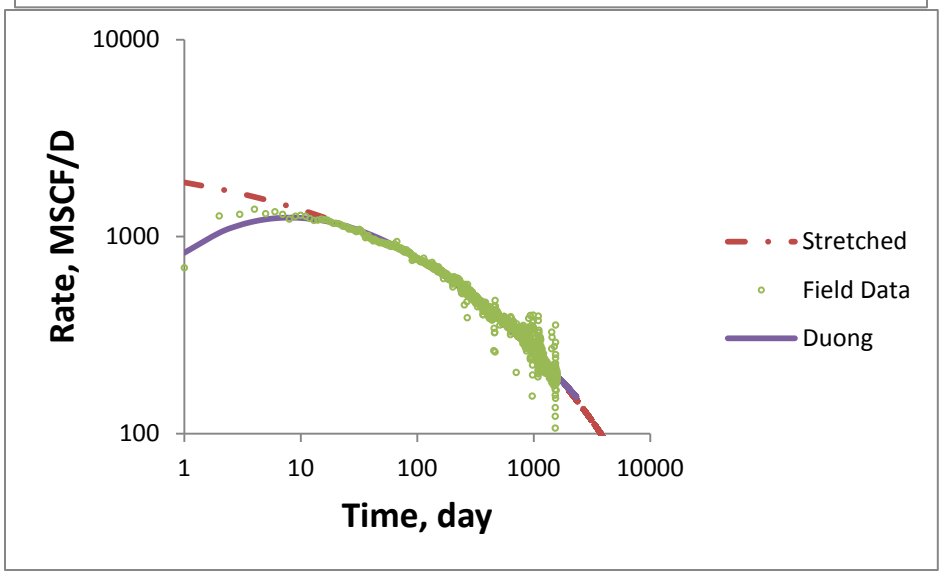
Rate, MSCF/D
10000
1000
100
1
10
100
1000
10000
Time, day
Stretched
Field Data
Duong

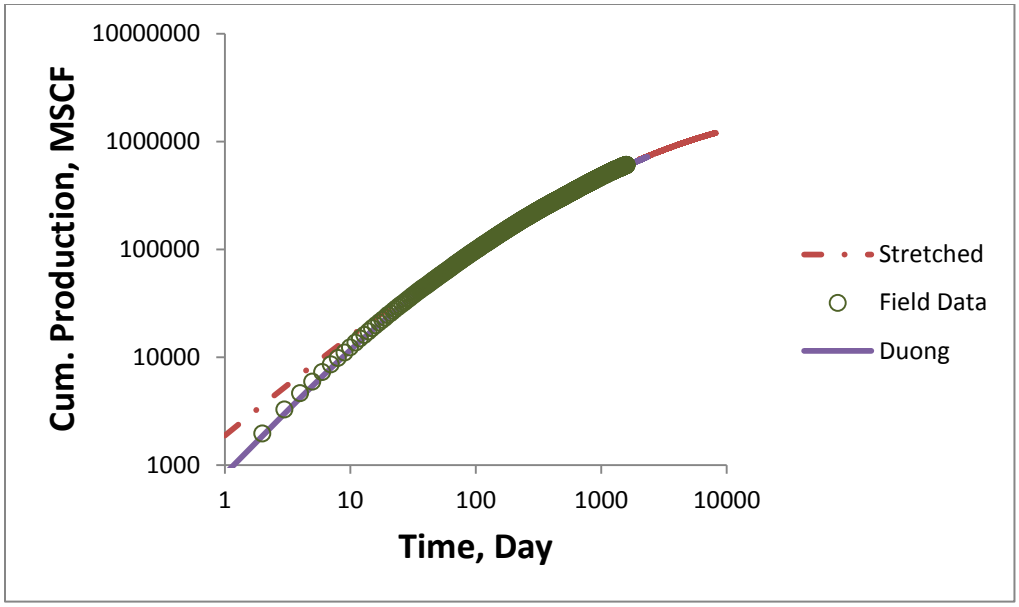
Cum. Production, MSCF
10000000
1000000
100000
10000
1000
1
10
100
1000
10000
Time, Day
Stretched
Field Data
Duong

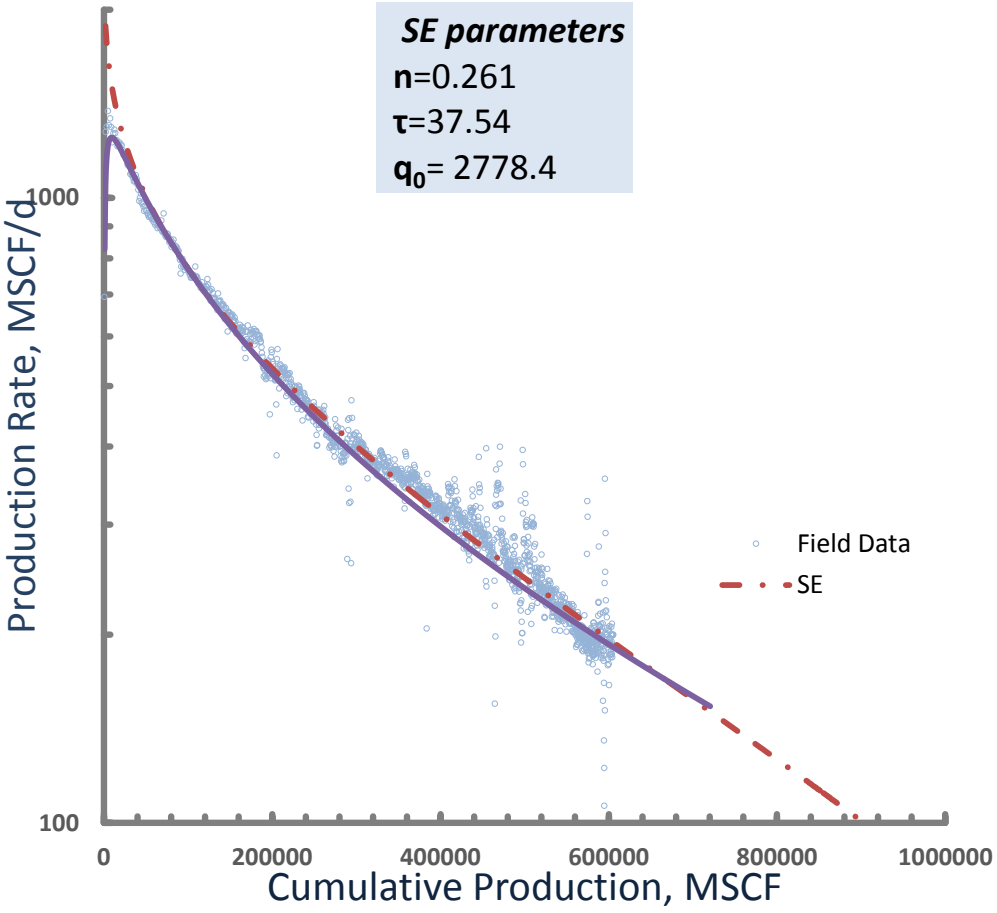
SE parameters
n=0.261
τ=37.54
q0= 2778.4
Production Rate, MSCF/d
1000
100
0
200000
400000
600000
800000
1000000
Cumulative Production, MSCF
Field Data
SE

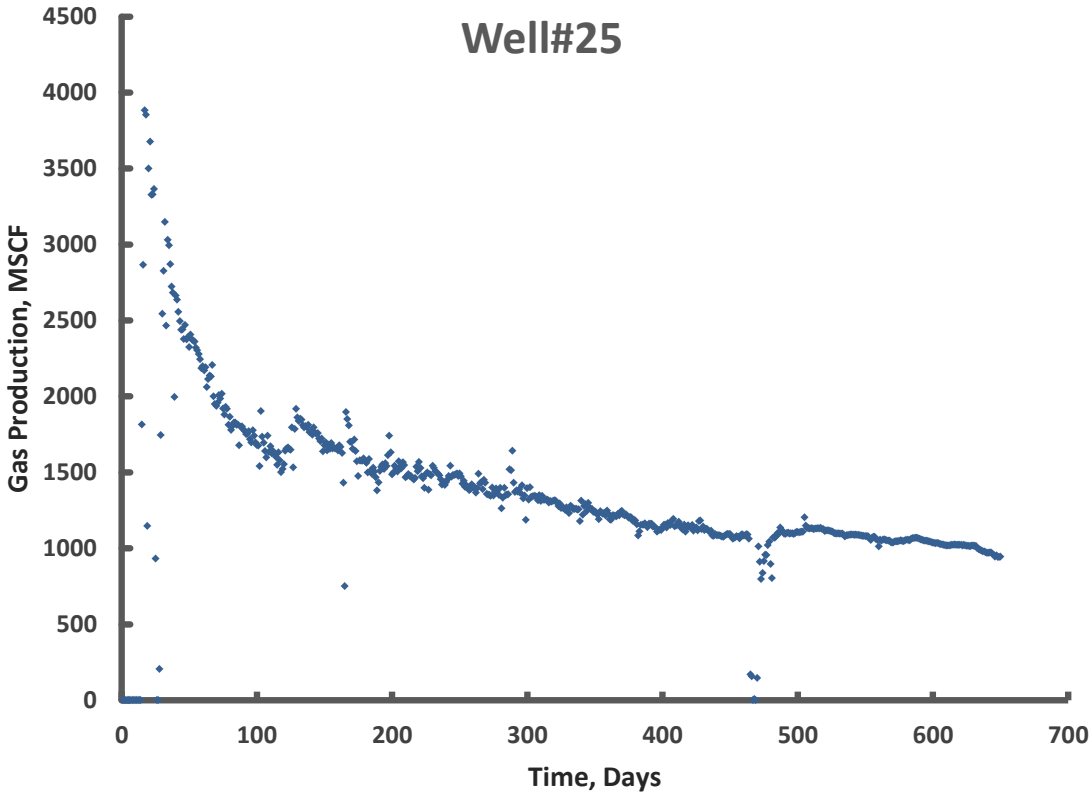
Well#25
Gas Production, MSCF
4500
4000
3500
3000
2500
2000
1500
1000
500
0
0
100
200
300
400
500
600
700
Time, Days

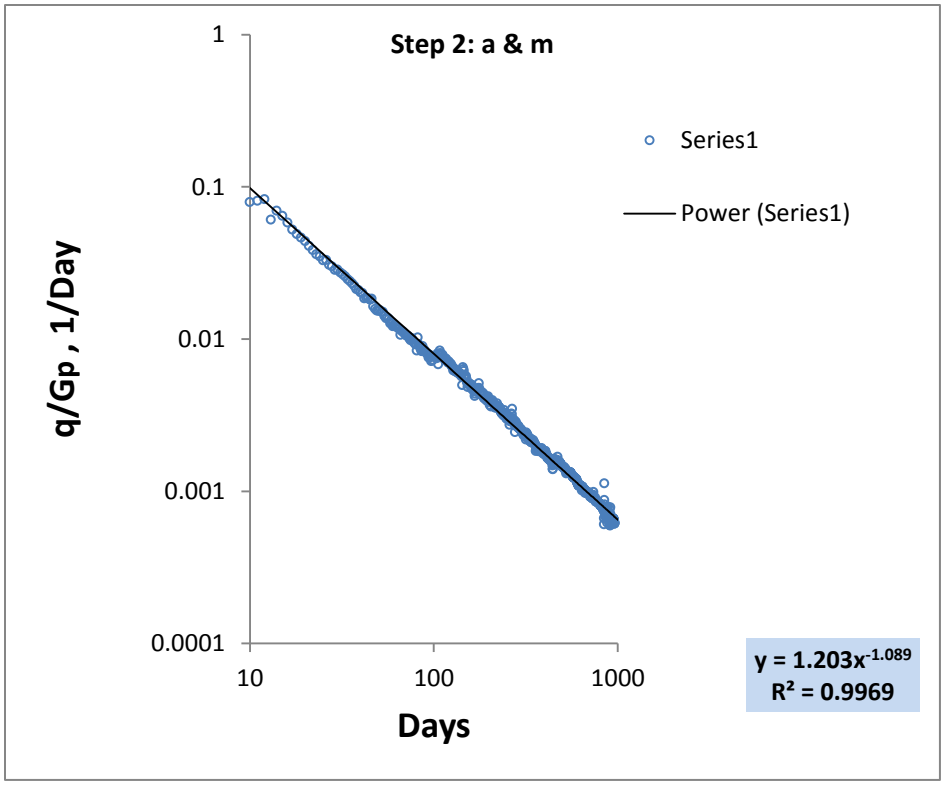
Step 2: a & m
q/Gp , 1/Day
1
0.1
0.01
0.001
0.0001
10
100
1000
Days
Series1
Power (Series1)
y = 1.203x-1.089
R² = 0.9969

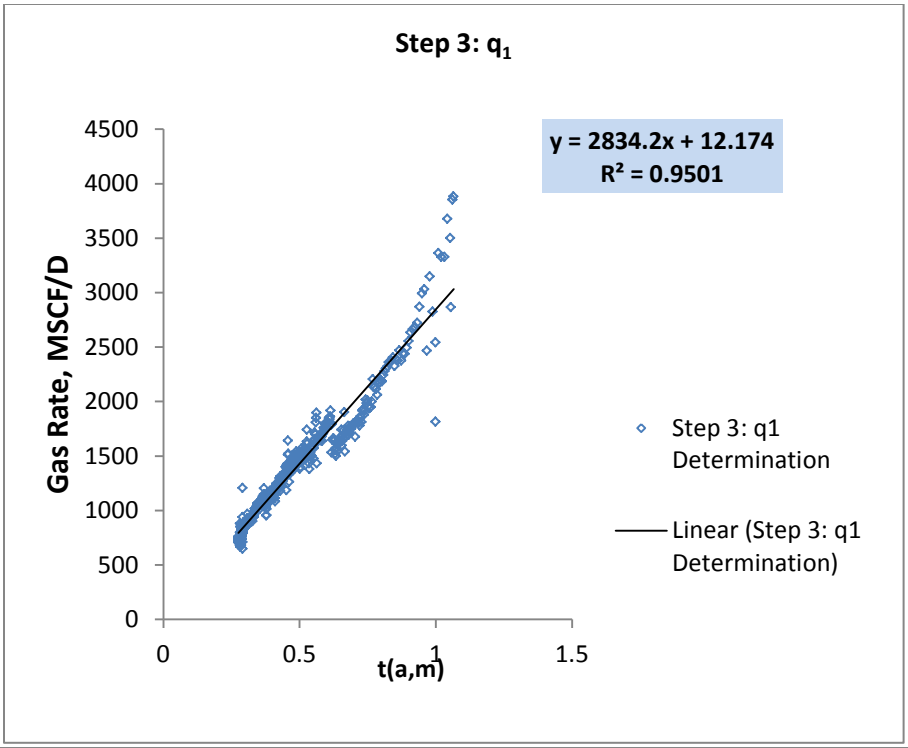
Step 3: q1
y = 2834.2x + 12.174
R² = 0.9501
Gas Rate, MSCF/D
4500
4000
3500
3000
2500
2000
1500
1000
500
0
0
0.5
1
1.5
t(a,m)
Step 3: q1 Determination
Linear (Step 3: q1 Determination)

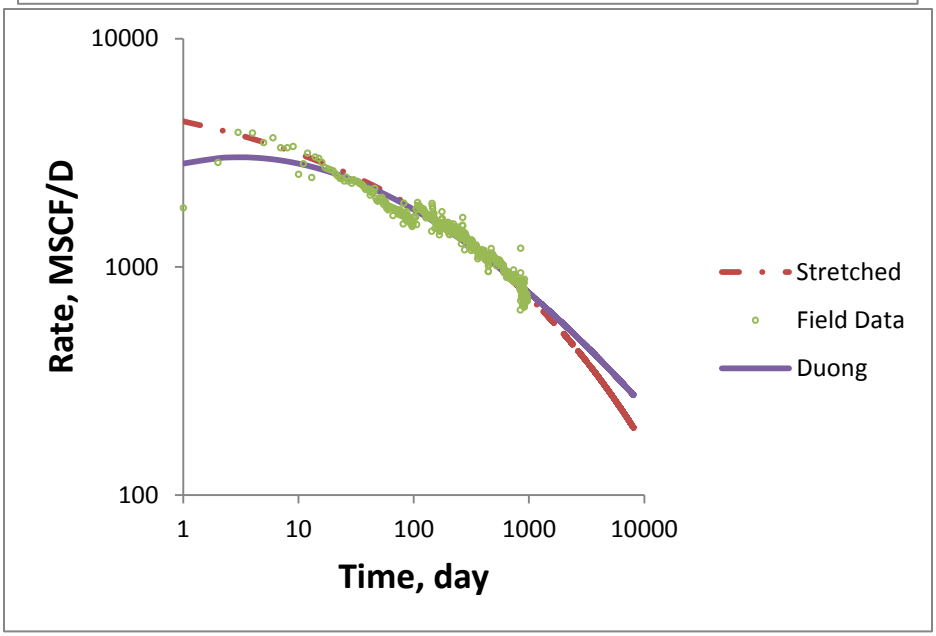
Rate, MSCF/D
10000
1000
100
1
10
100
1000
10000
Time, day
Stretched
Field Data
Duong

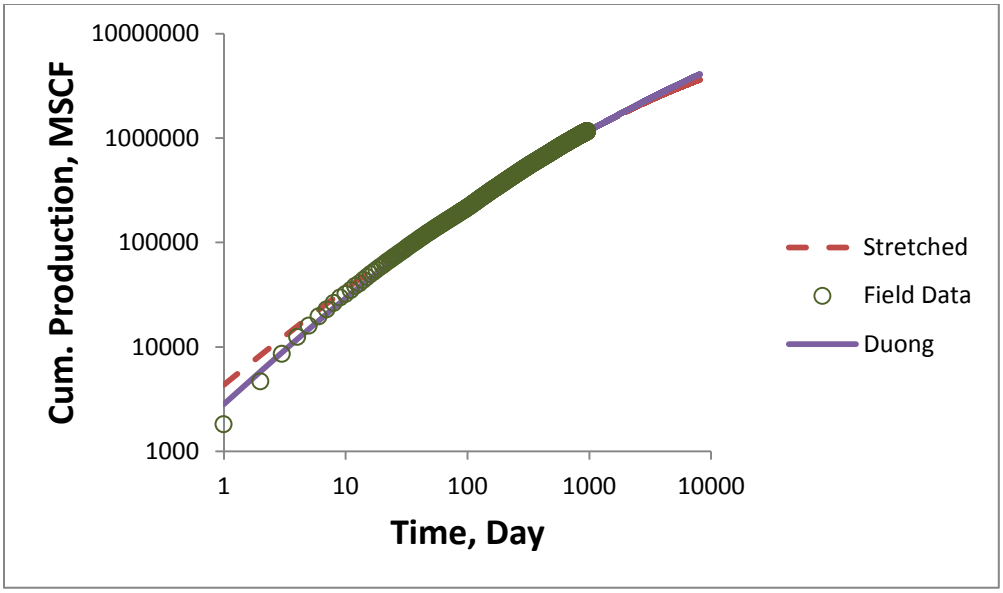
Cum. Production, MSCF
10000000
1000000
100000
10000
1000
1
10
100
1000
10000
Time, Day
Stretched
Field Data
Duong

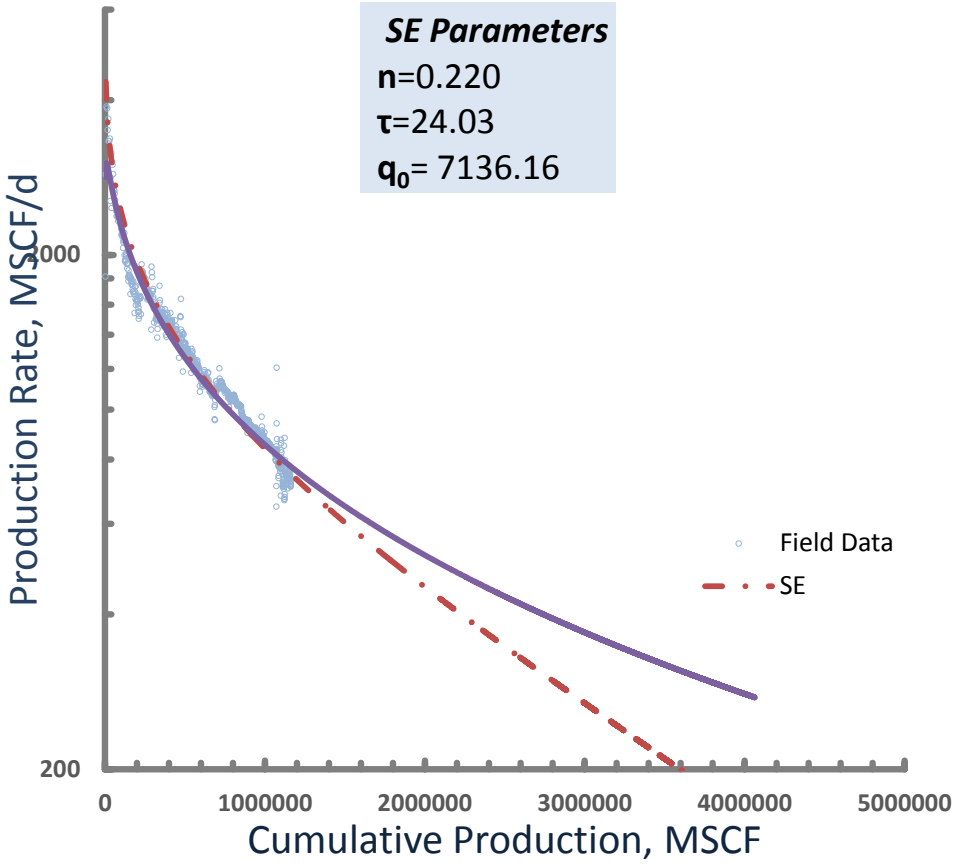
SE Parameters
n=0.220
τ=24.03
q0= 7136.16
Production Rate, MSCF/d
3000
200
0
1000000
2000000
3000000
4000000
5000000
Cumulative Production, MSCF
Field Data
SE

APPENDIX B

This section contains the results of our proposed conditioned SEDM parameter estimation procedure for SEDM for all of the previously investigated 25 wells in Barnett Shale in Newark East Field. In this new approach only two parameters (n and τ) are needed to be searched, and the third parameter (q_0) can be obtained using the critical gas rate based on Turner's equations. The advantage of this 2-variable search over the 3-variable search (Appendix A) is that it leads to a unique set of parameters (i.e. avoids the non-uniqueness) while it still provides enough flexibility to fit the actual data. These plots compares the SEDM based on the best 3-variable search and new conditioned 2-variable search based on Turner's critical gas rate for each individual well.

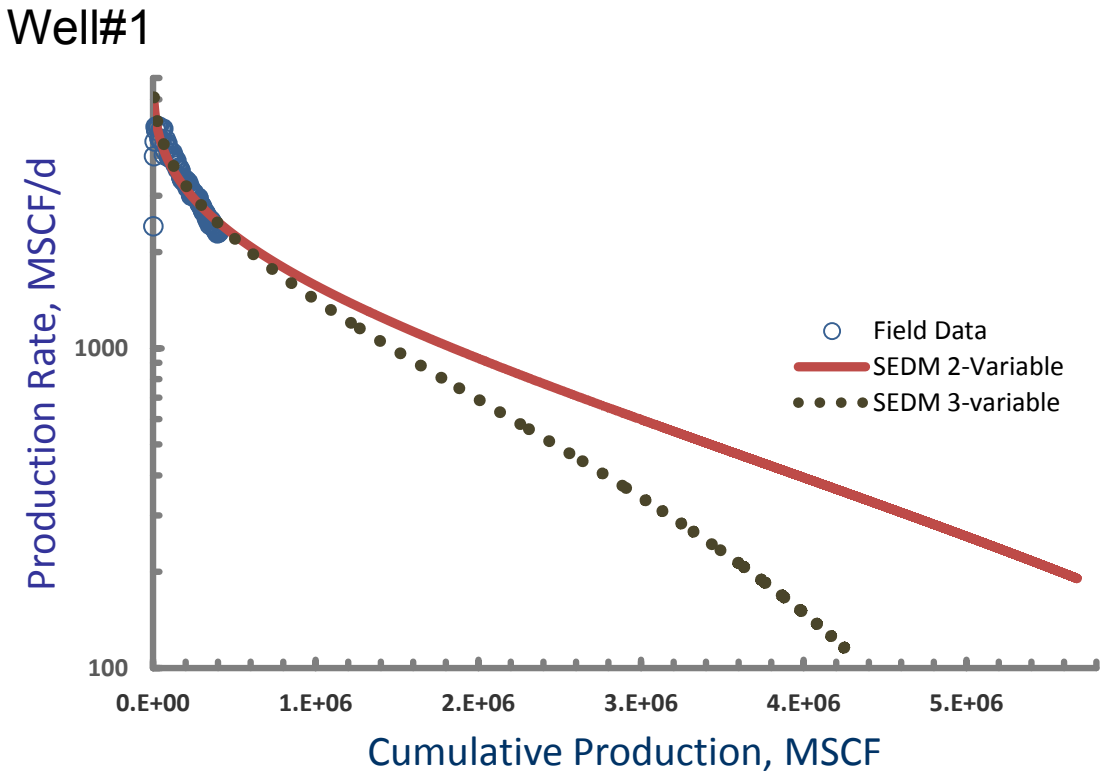
Well#1
Production Rate, MSCF/d
1000
100
0.E+00
1.E+06
2.E+06
3.E+06
4.E+06
5.E+06
Cumulative Production, MSCF
Field Data
SEDM 2-Variable
SEDM 3-variable

Well#2

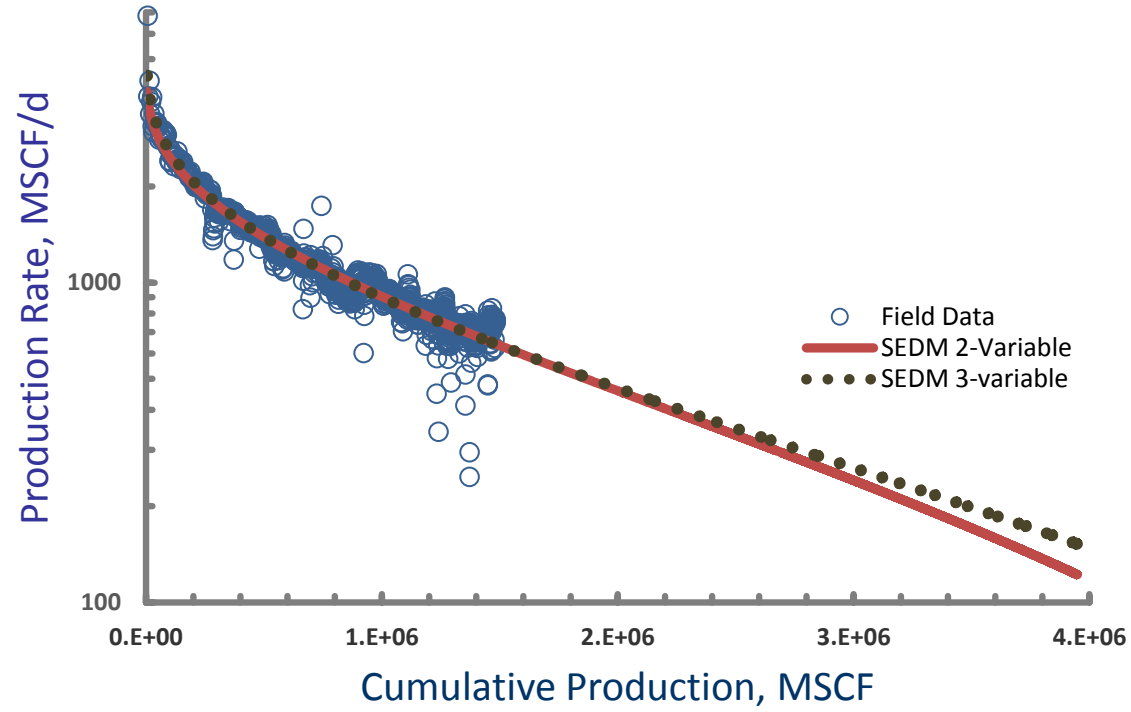
Production Rate, MSCF/d
1000
100
0.E+00
1.E+06
2.E+06
3.E+06
4.E+06
Cumulative Production, MSCF
Field Data
SEDM 2-Variable
SEDM 3-variable

Well#3

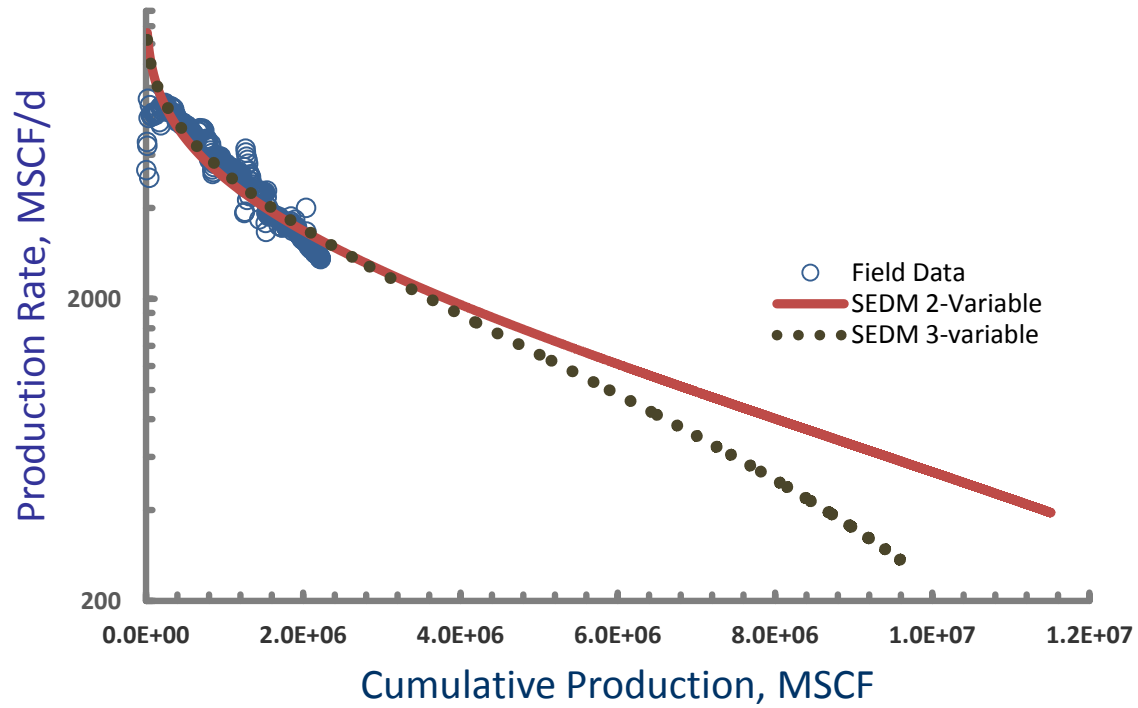
Production Rate, MSCF/d
2000
200
0.0E+00
2.0E+06
4.0E+06
6.0E+06
8.0E+06
1.0E+07
1.2E+07
Cumulative Production, MSCF
Field Data
SEDM 2-Variable
SEDM 3-variable

Well#4

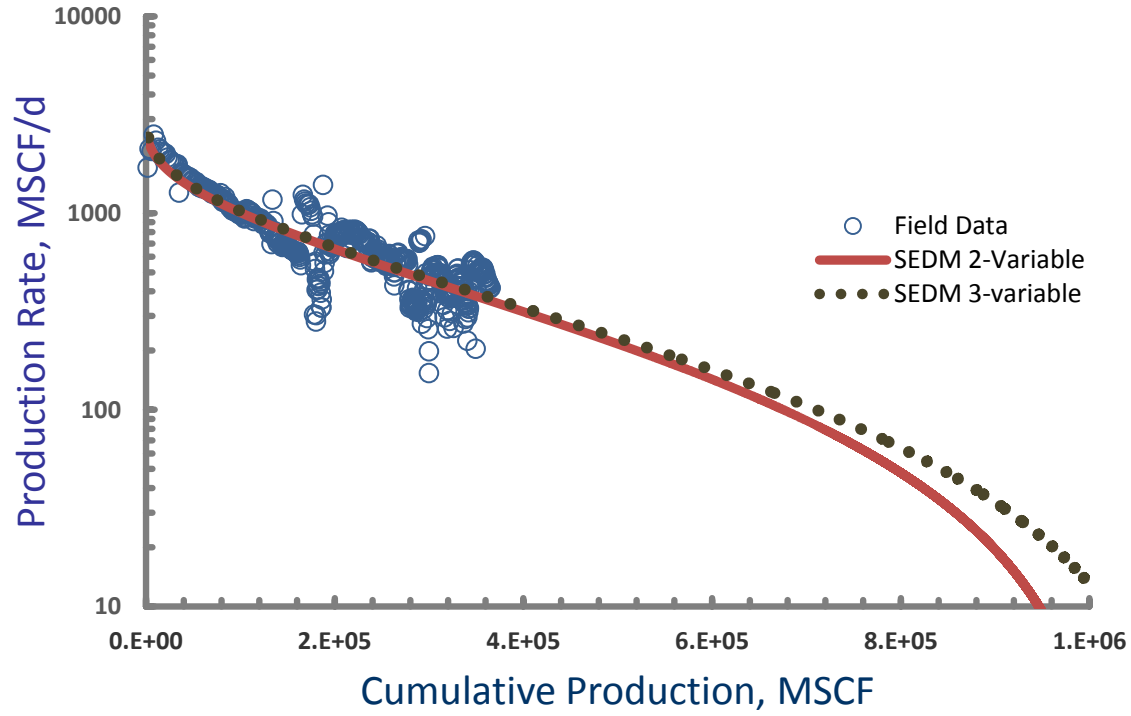
10000
1000
100
10
Production Rate, MSCF/d
0.E+00
2.E+05
4.E+05
6.E+05
8.E+05
1.E+06
Cumulative Production, MSCF
Field Data
SEDM 2-Variable
SEDM 3-variable

Well#5

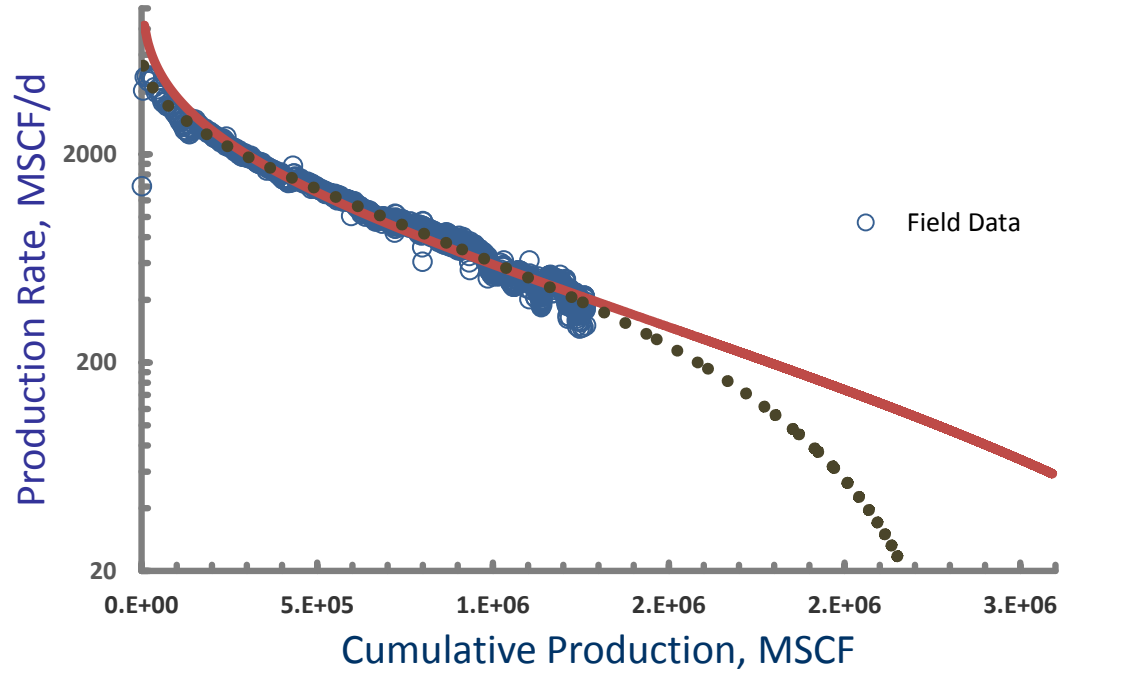
2000
200
20
Production Rate, MSCF/d
0.E+00
5.E+05
1.E+06
2.E+06
2.E+06
3.E+06
Cumulative Production, MSCF
Field Data

Well#6

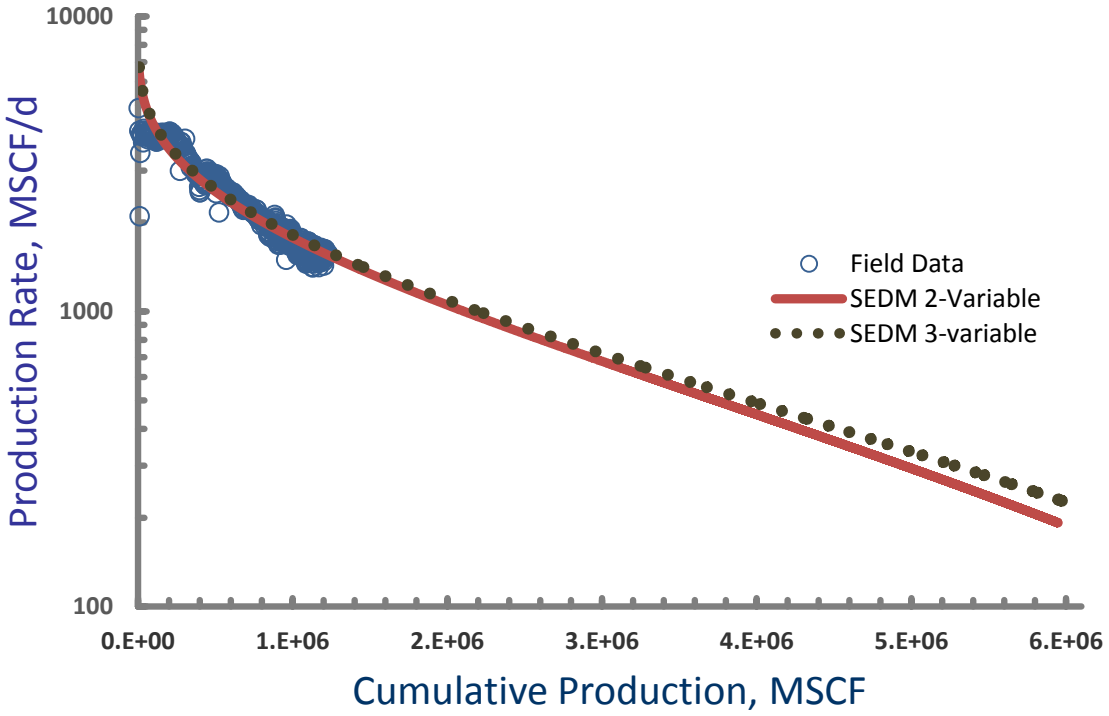
10000
1000
100
Production Rate, MSCF/d
0.E+00
1.E+06
2.E+06
3.E+06
4.E+06
5.E+06
6.E+06
Cumulative Production, MSCF
Field Data
SEDM 2-Variable
SEDM 3-variable

Well#7

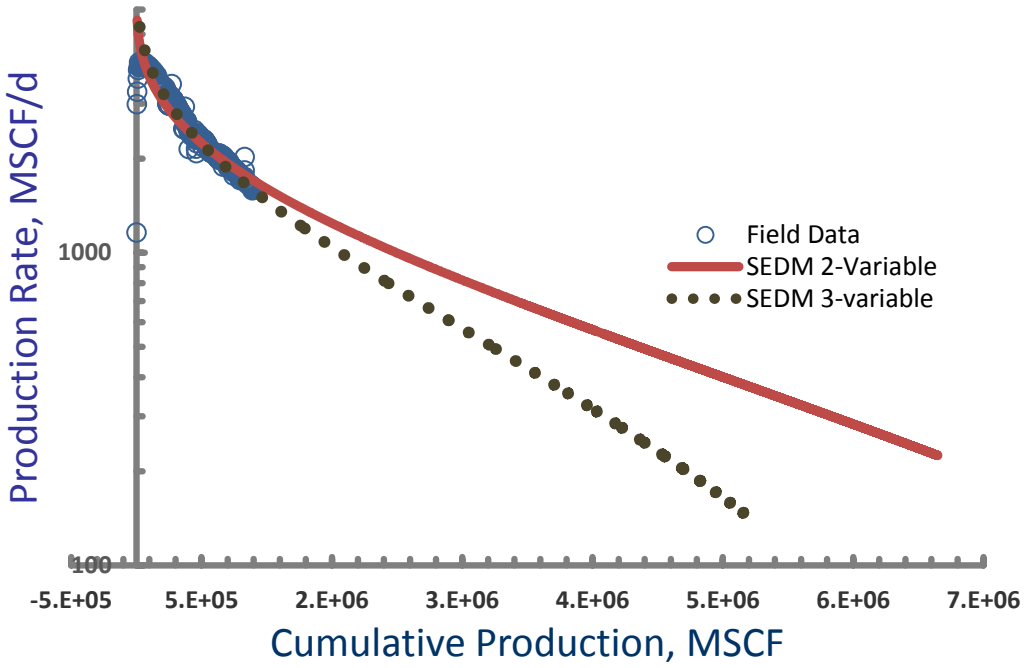
1000
100
Production Rate, MSCF/d
-5.E+05
5.E+05
2.E+06
3.E+06
4.E+06
5.E+06
6.E+06
7.E+06
Cumulative Production, MSCF
Field Data
SEDM 2-Variable
SEDM 3-variable

Well#8

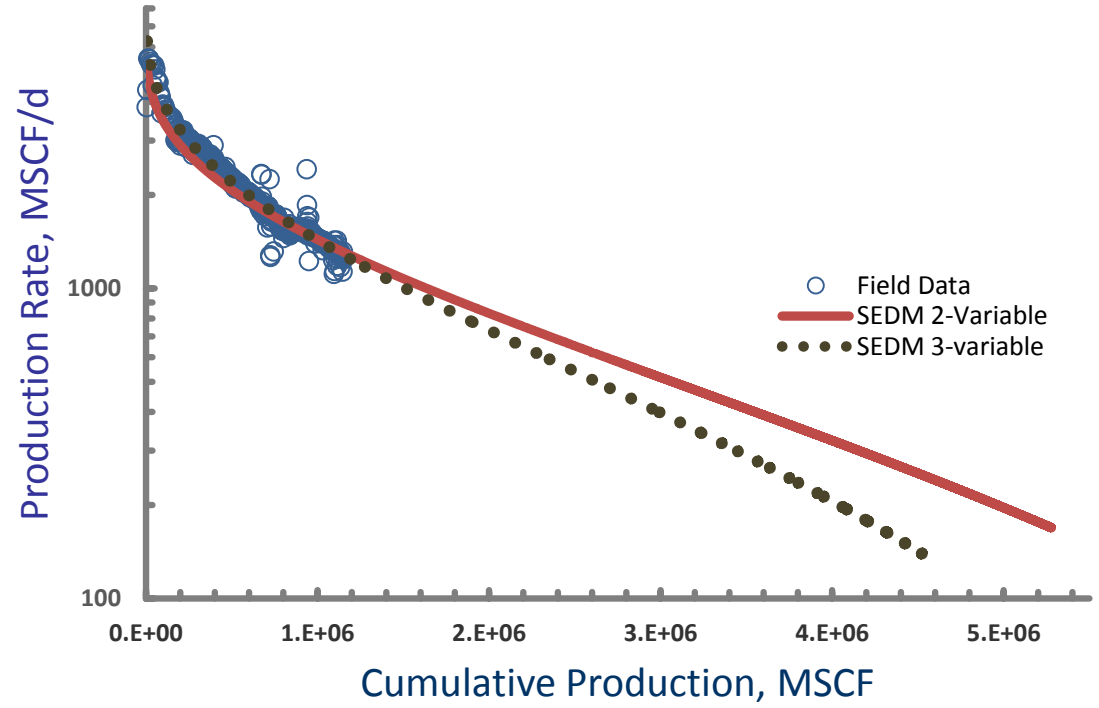
Production Rate, MSCF/d
1000
100
0.E+00
1.E+06
2.E+06
3.E+06
4.E+06
5.E+06
Cumulative Production, MSCF
Field Data
SEDM 2-Variable
SEDM 3-variable

Well#9

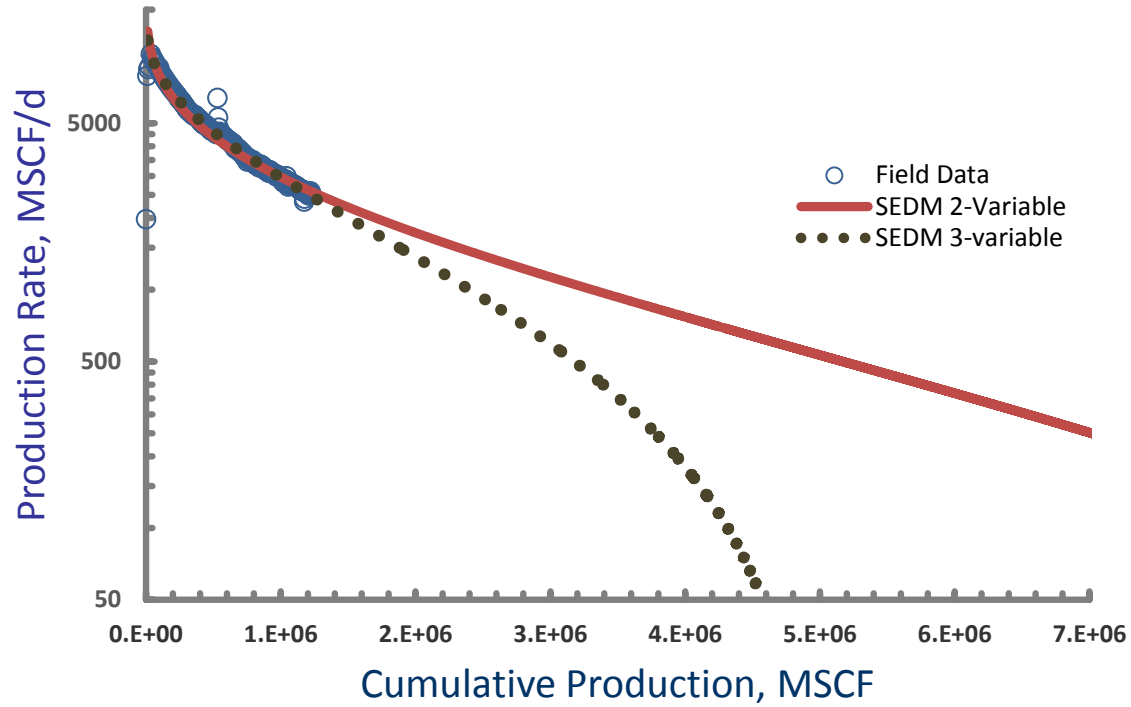
Production Rate, MSCF/d
5000
500
50
0.E+00
1.E+06
2.E+06
3.E+06
4.E+06
5.E+06
6.E+06
7.E+06
Cumulative Production, MSCF
Field Data
SEDM 2-Variable
SEDM 3-variable

Well#10

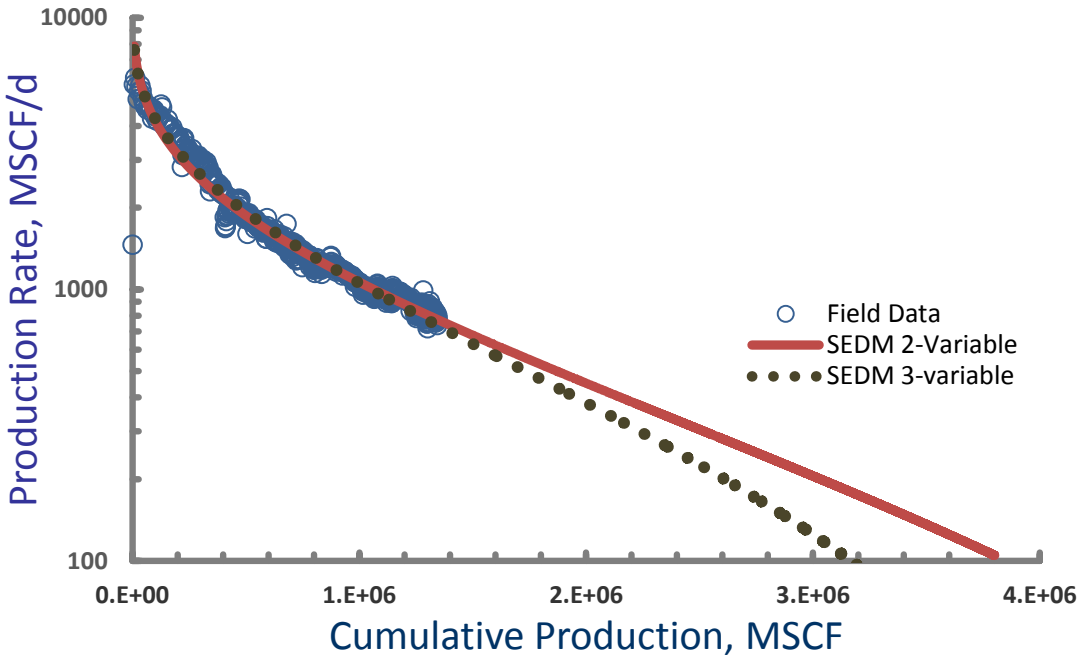

Well#11

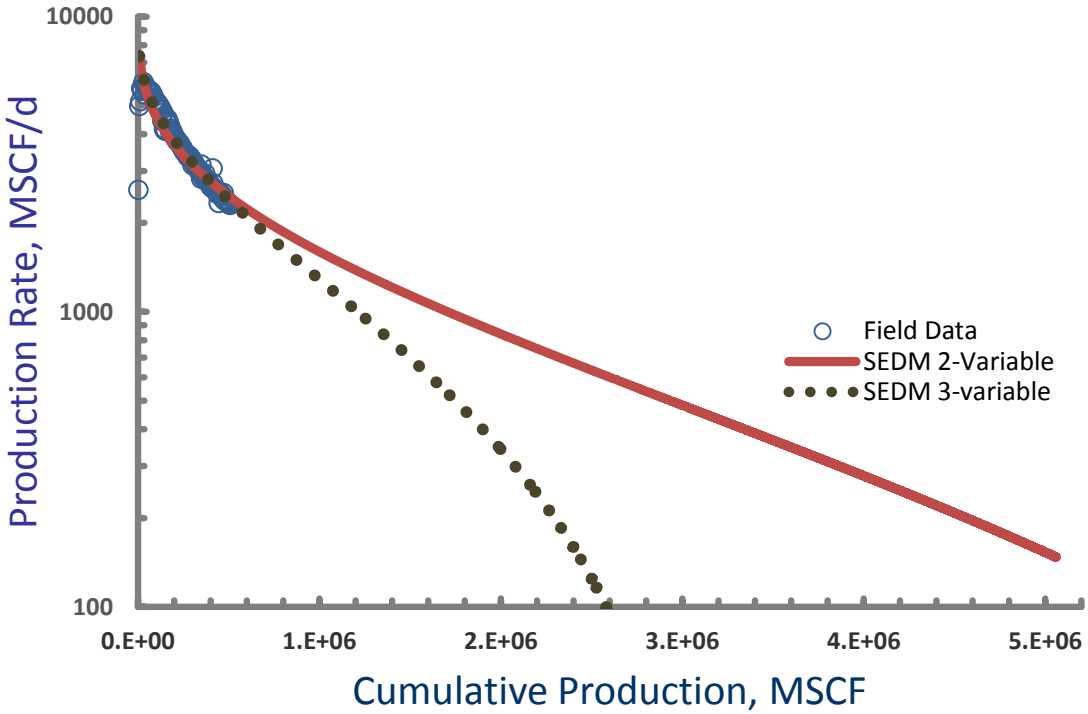

Well#12

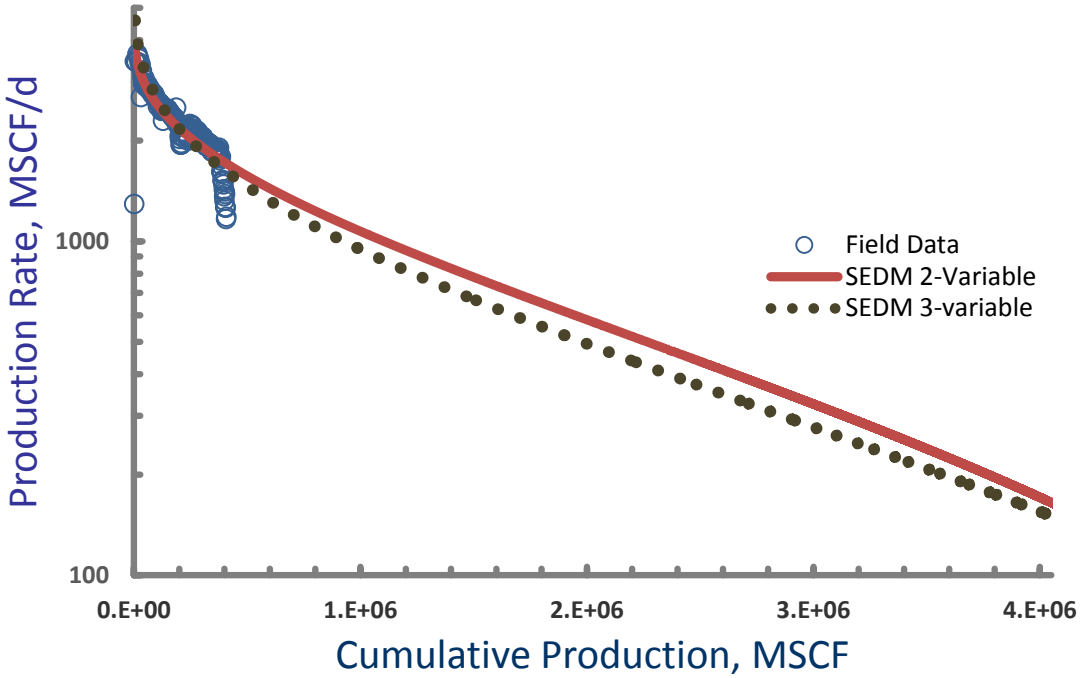

Well#13

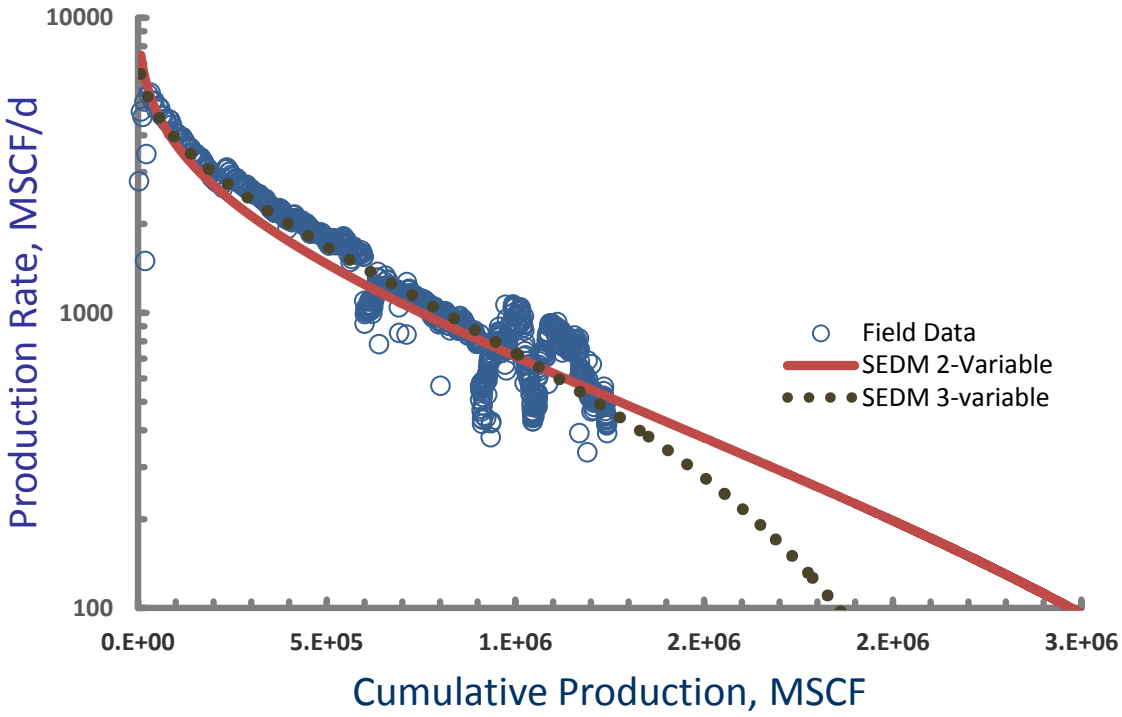

Well#14

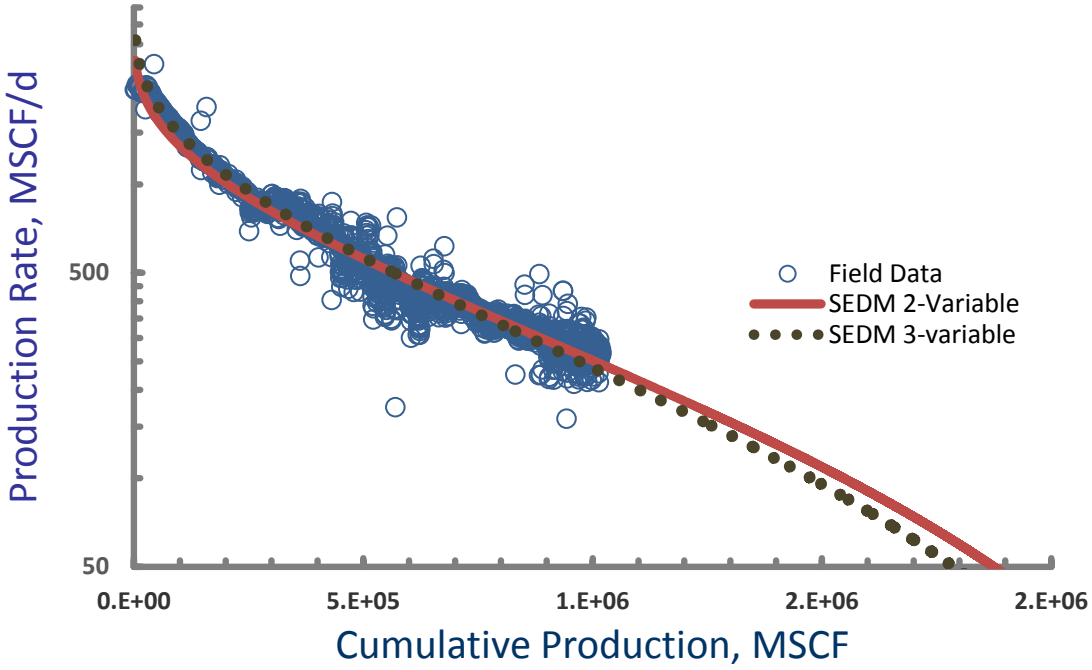

Well#15

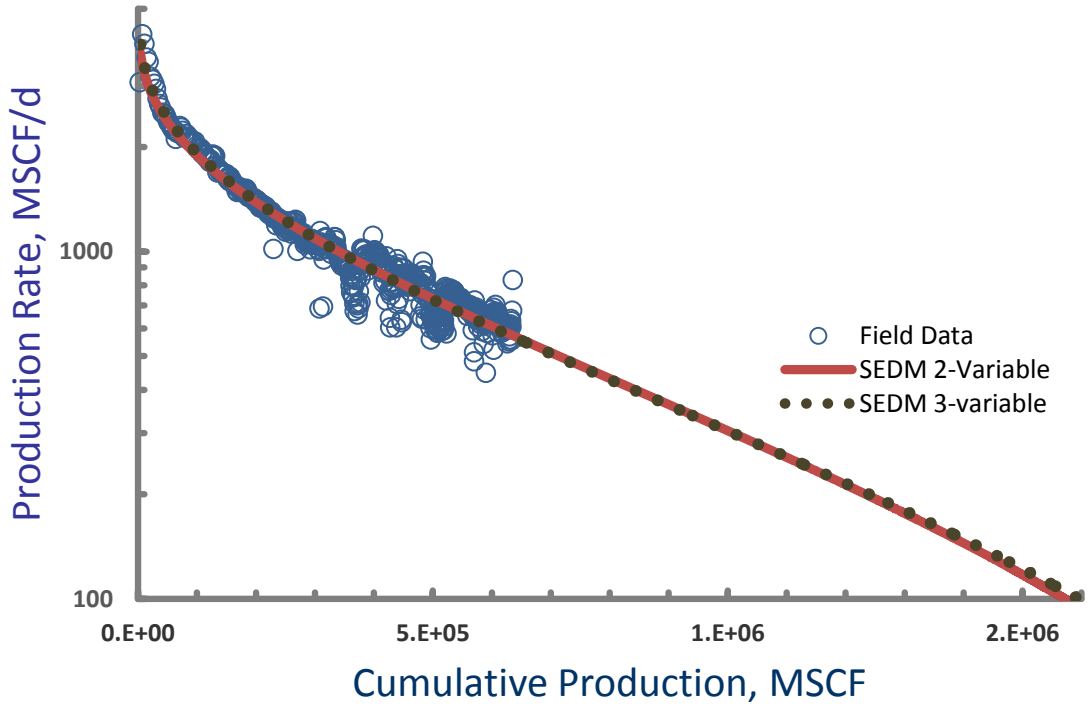

Well#16

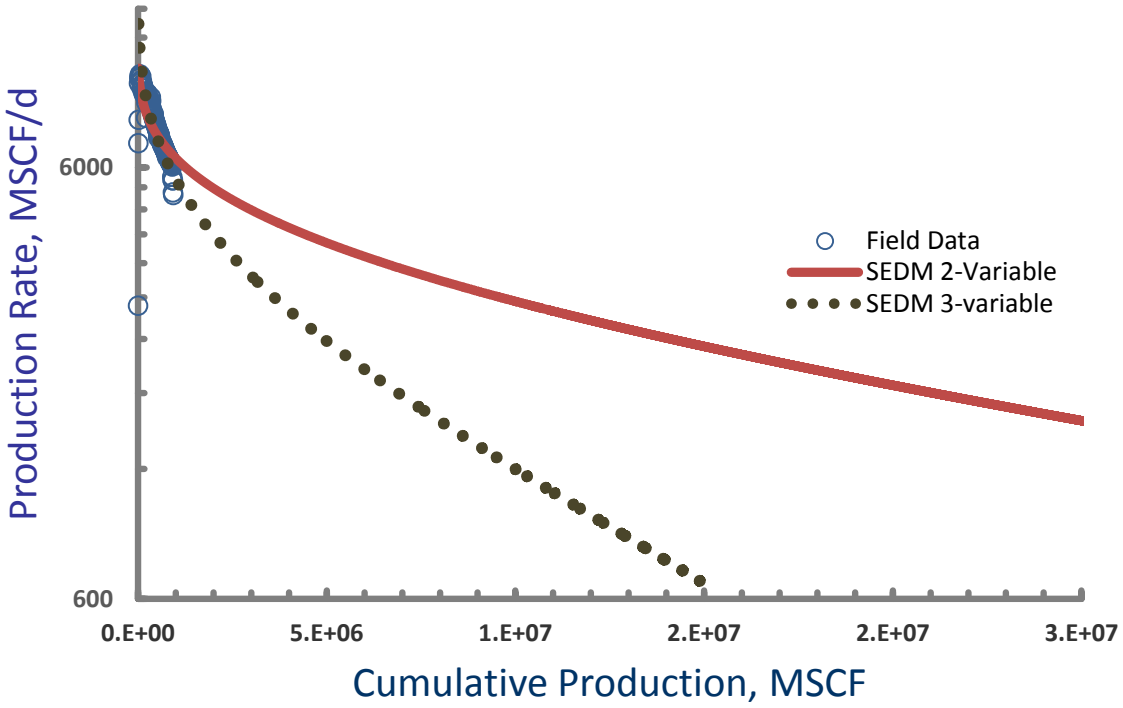

Well#17

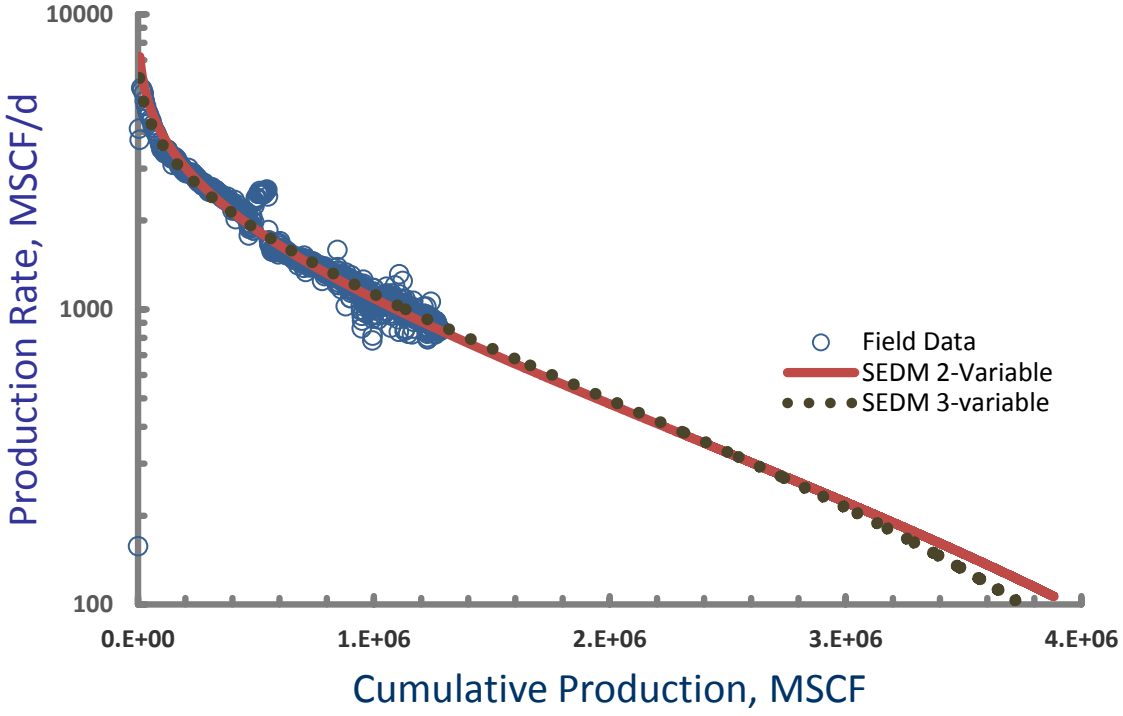

Well#18

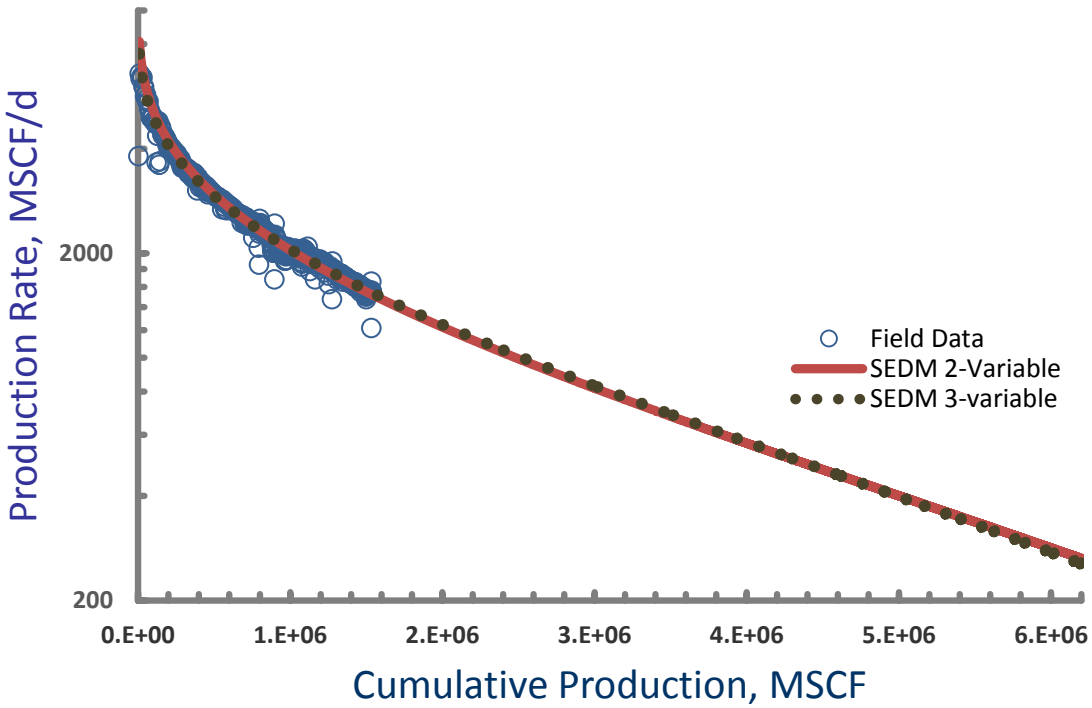

Well#19

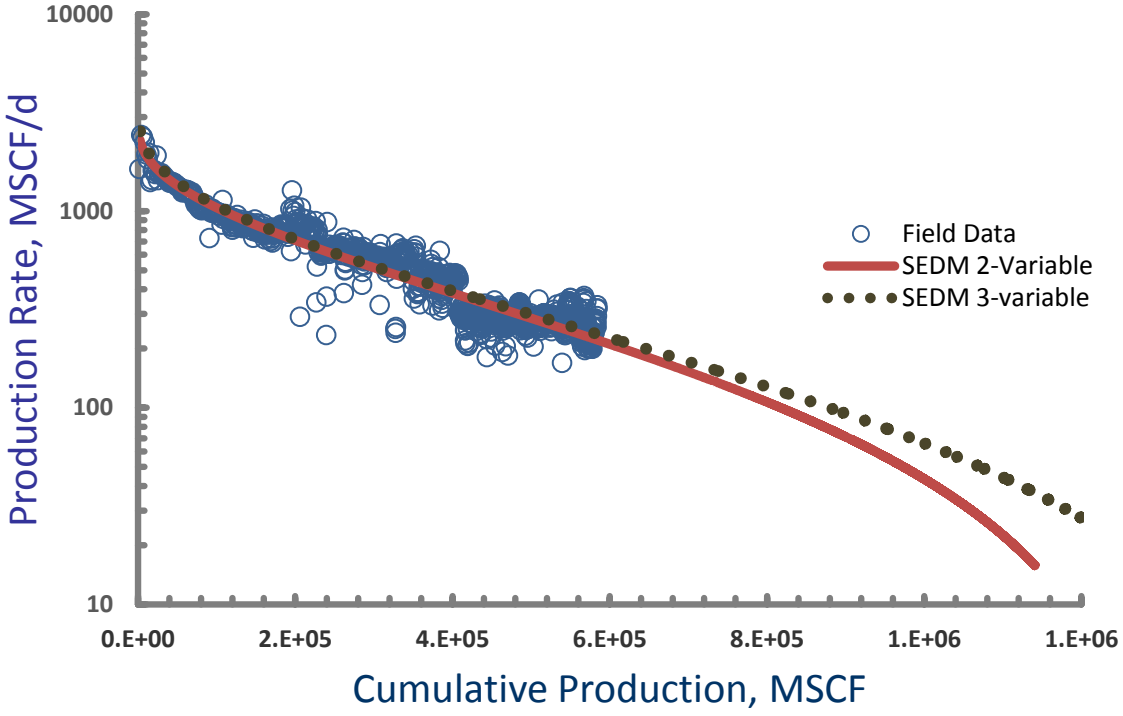
10000
1000
100
10
Production Rate, MSCF/d
0.E+00
2.E+05
4.E+05
6.E+05
8.E+05
1.E+06
1.E+06
Cumulative Production, MSCF
Field Data
SEDM 2-Variable
SEDM 3-variable

Well#20

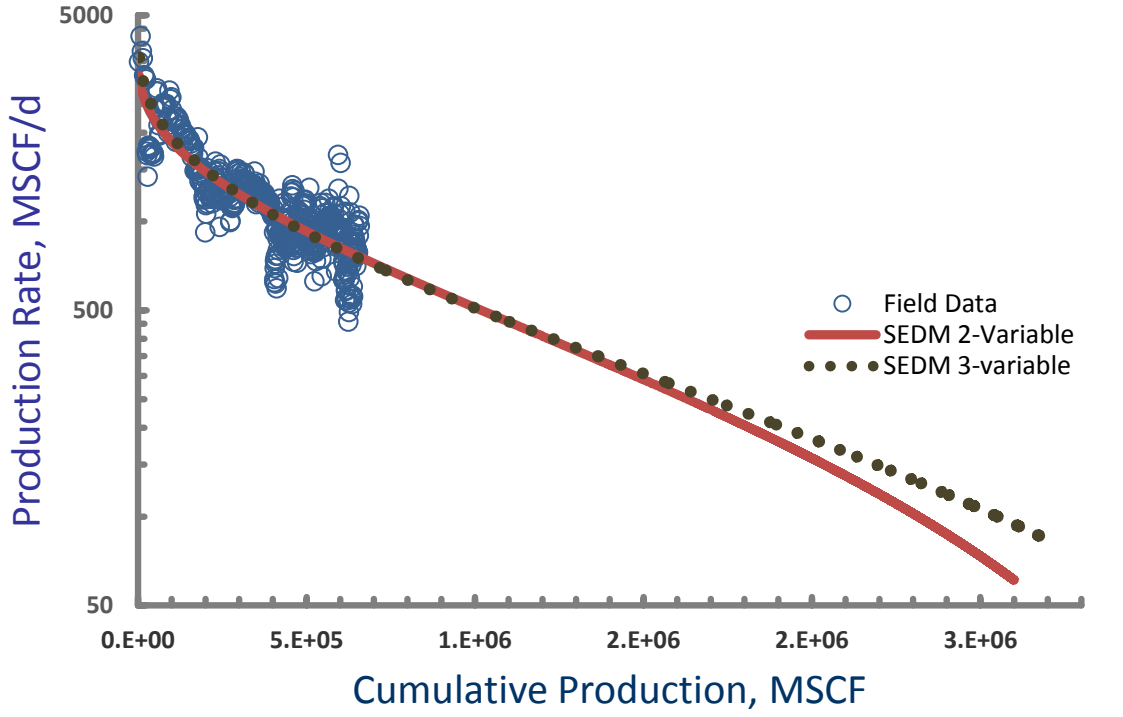
5000
500
50
Production Rate, MSCF/d
0.E+00
5.E+05
1.E+06
2.E+06
2.E+06
3.E+06
Cumulative Production, MSCF
Field Data
SEDM 2-Variable
SEDM 3-variable

Well#21

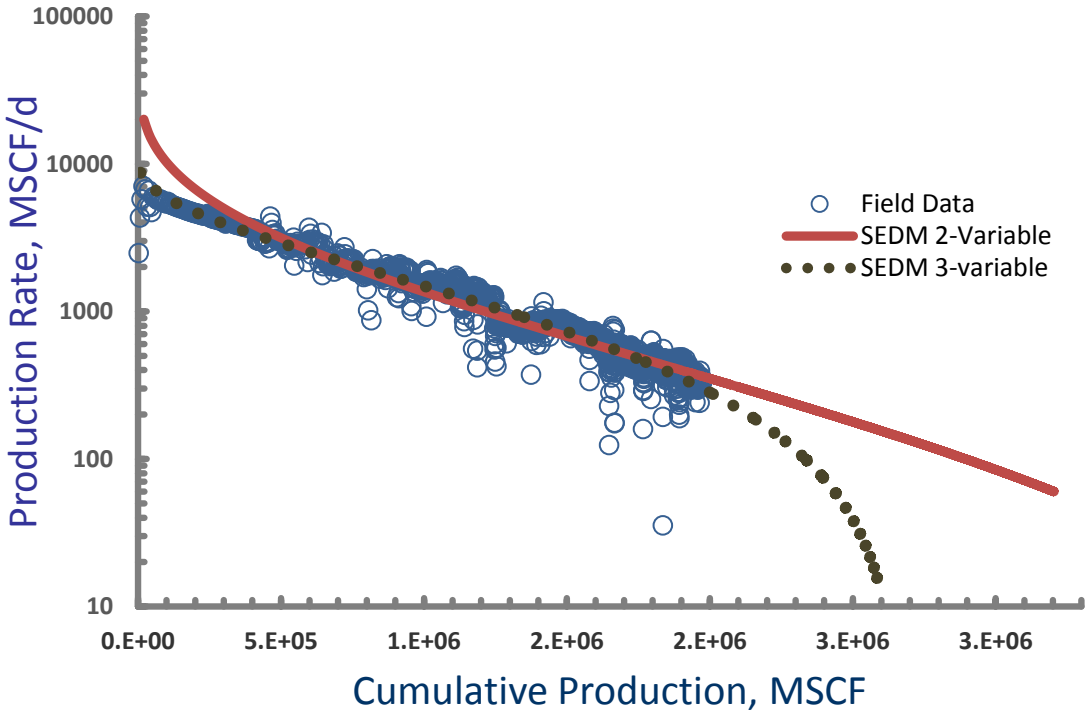

Well#22

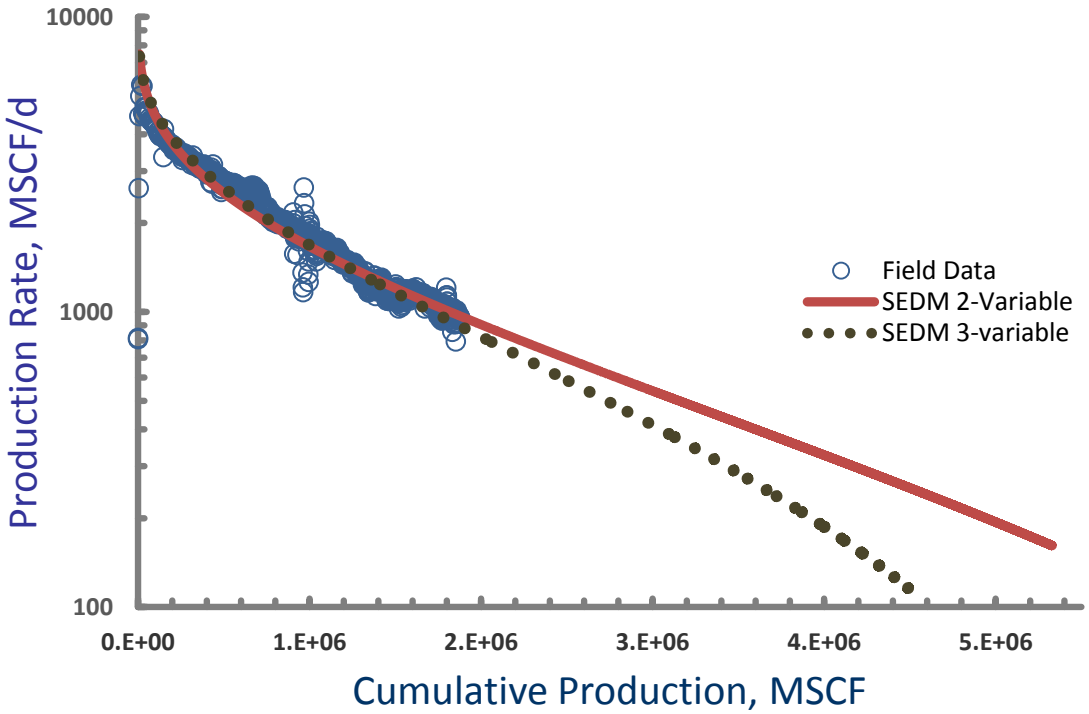

Well#23

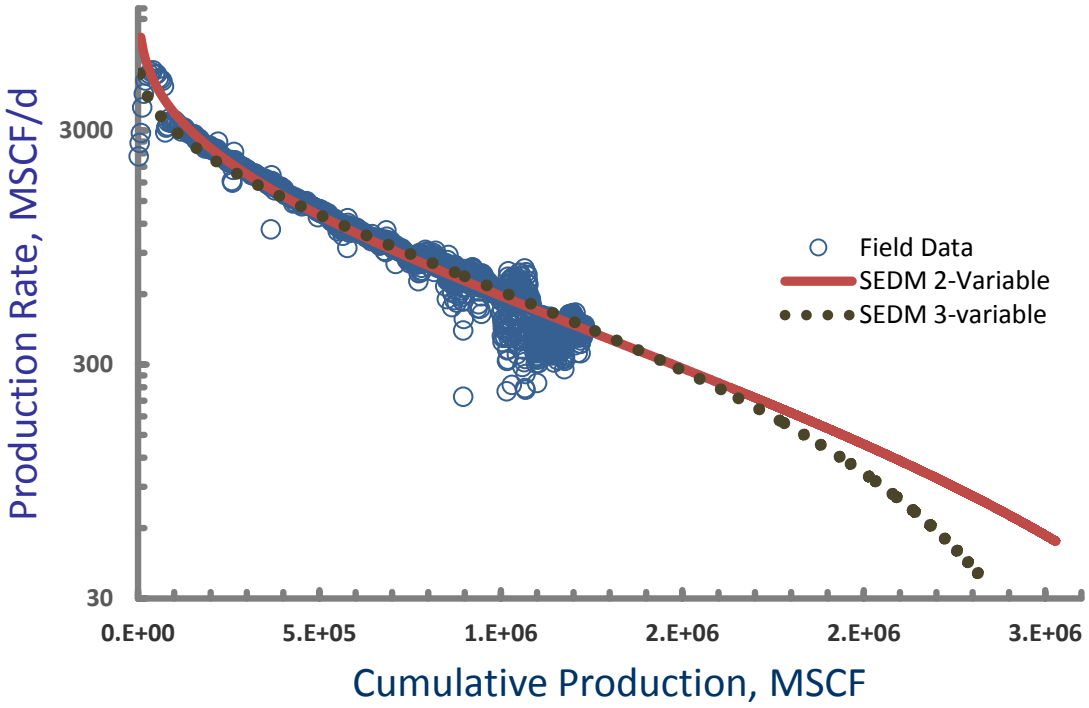

Well#24

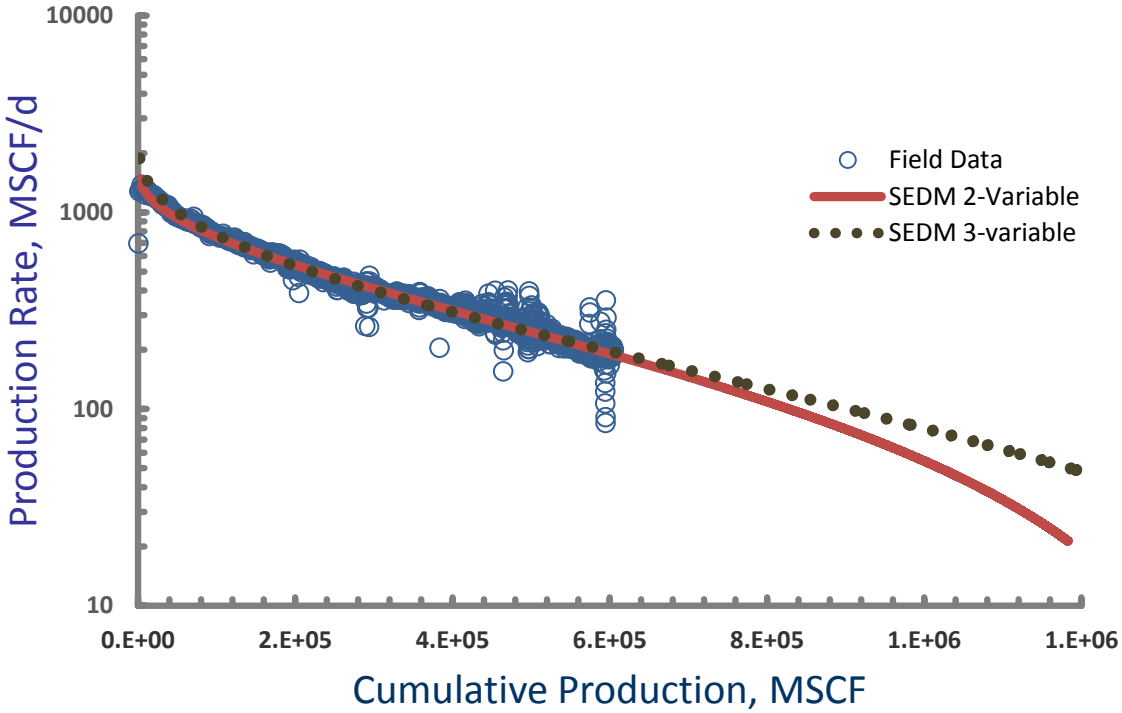

Well#25

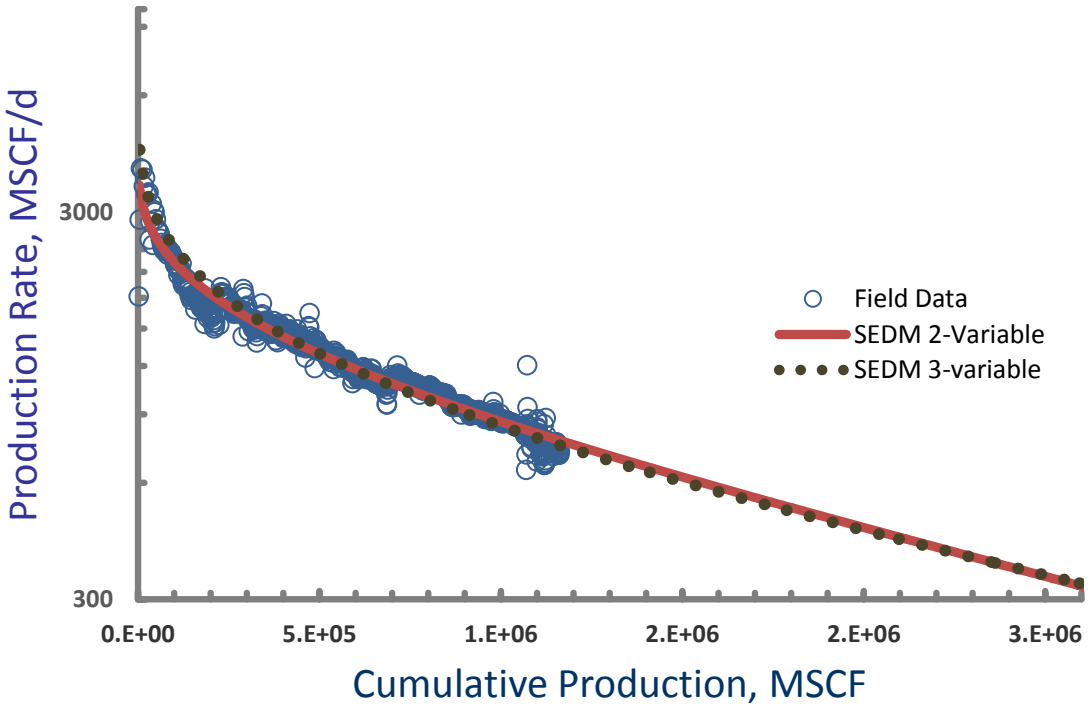
Production Rate, MSCF/d
3000
300
0.E+00
5.E+05
1.E+06
2.E+06
2.E+06
3.E+06
Cumulative Production, MSCF
Field Data
SEDM 2-Variable
SEDM 3-variable

APPENDIX C

The most expected SEDM parameter "n" and "$t_{infl.}$" for Barnett Shale gas (Table 6.1) were used to calculate initial rate (q_0) values related to P_{10}, P_{50}, and P_{90} for each individual well. Then these SEDM parameters were used to determine the decline behavior of each individual shale gas well for P_{10}, P_{50}, and P_{90} cases.

This section contains plots of rate *vs.* time and *log (q) vs.* cumulative of each individual well from the sample of 25 wells for P_{10}, P_{50}, and P_{90} cases and the deterministic SEDM decline behavior that previously was calculated for each well.

.

Well#1

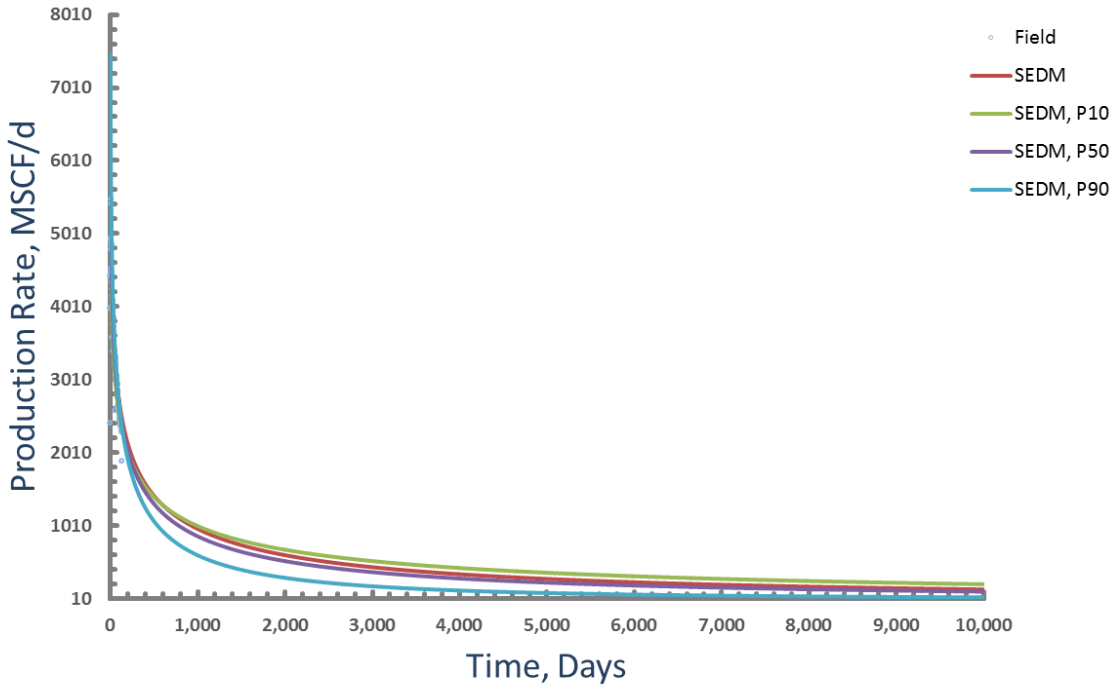
8010
7010
6010
5010
4010
3010
2010
1010
10
Production Rate, MSCF/d
0
1,000
2,000
3,000
4,000
5,000
6,000
7,000
8,000
9,000
10,000
Time, Days
Field
SEDM
SEDM, P10
SEDM, P50
SEDM, P90

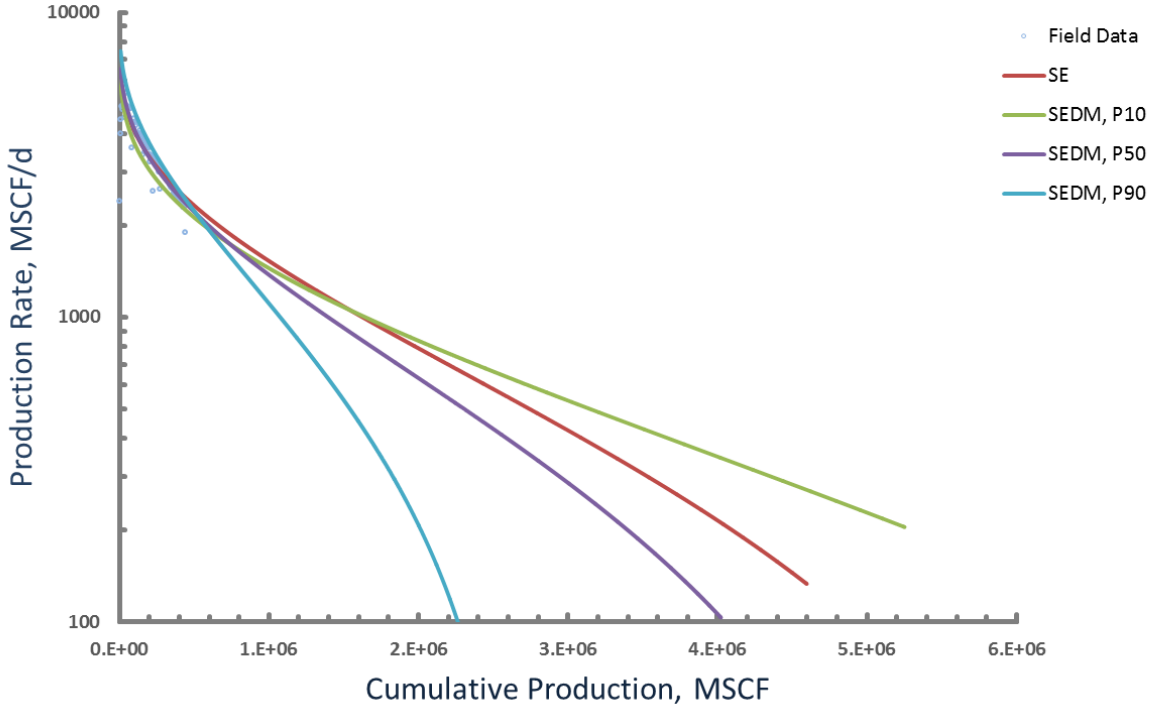
10000
1000
100
Production Rate, MSCF/d
0.E+00
1.E+06
2.E+06
3.E+06
4.E+06
5.E+06
6.E+06
Cumulative Production, MSCF
Field Data
SE
SEDM, P10
SEDM, P50
SEDM, P90

Well#2

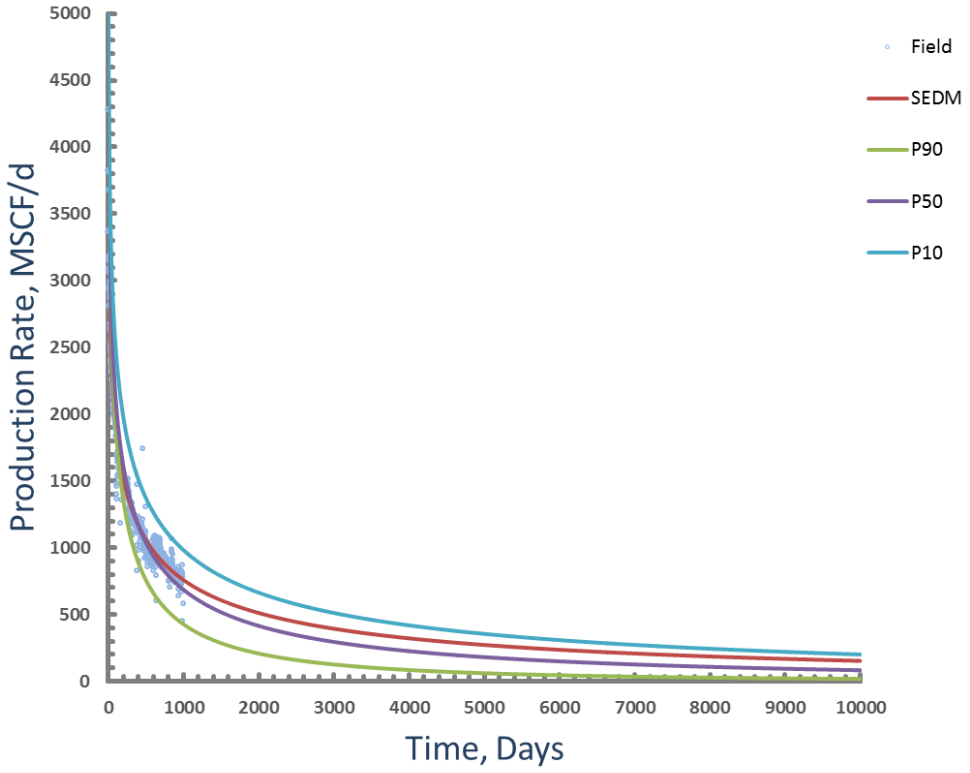
Production Rate, MSCF/d
Time, Days
Field
SEDM
P90
P50
P10
5000
4500
4000
3500
3000
2500
2000
1500
1000
500
0
0
1000
2000
3000
4000
5000
6000
7000
8000
9000
10000

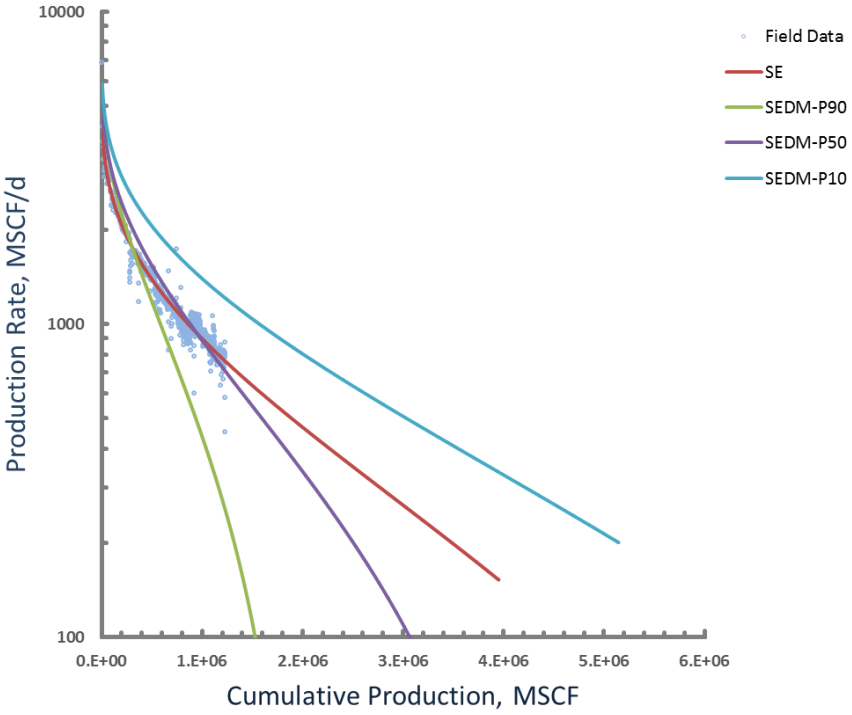
Production Rate, MSCF/d
Cumulative Production, MSCF
Field Data
SE
SEDM-P90
SEDM-P50
SEDM-P10
10000
1000
100
0.E+00
1.E+06
2.E+06
3.E+06
4.E+06
5.E+06
6.E+06

Well#3

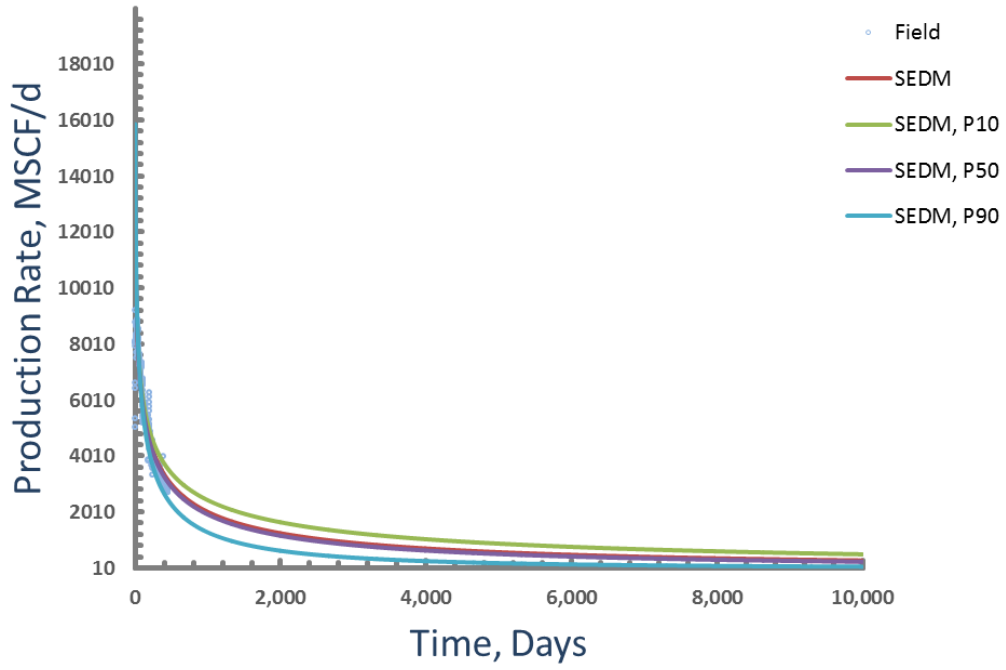
Field
SEDM
SEDM, P10
SEDM, P50
SEDM, P90
Production Rate, MSCF/d
18010
16010
14010
12010
10010
8010
6010
4010
2010
10
0
2,000
4,000
6,000
8,000
10,000
Time, Days

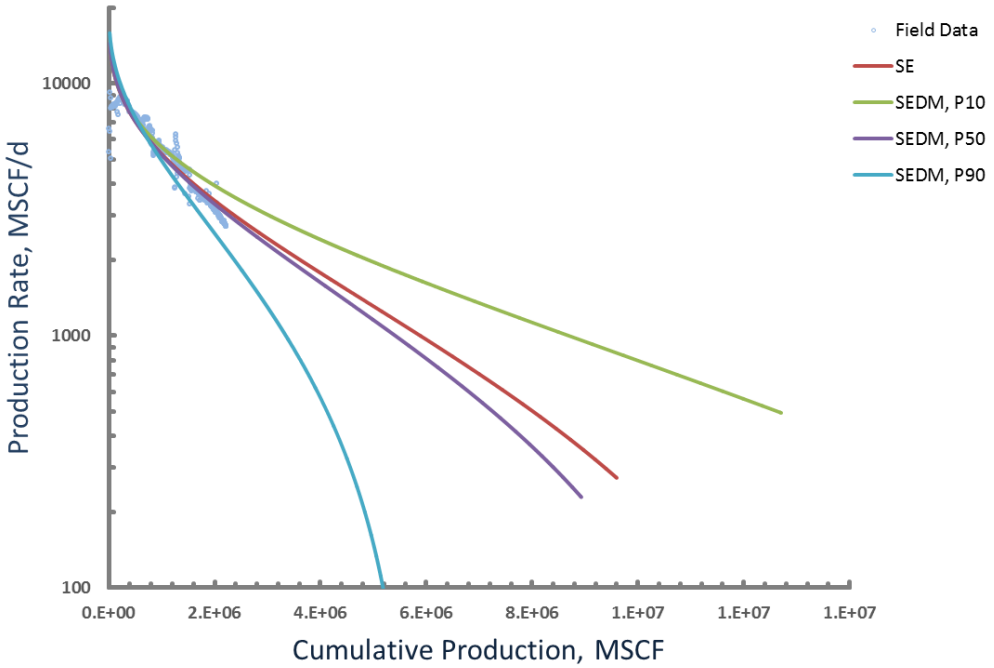
Field Data
SE
SEDM, P10
SEDM, P50
SEDM, P90
Production Rate, MSCF/d
10000
1000
100
0.E+00
2.E+06
4.E+06
6.E+06
8.E+06
1.E+07
1.E+07
1.E+07
Cumulative Production, MSCF

Well#4

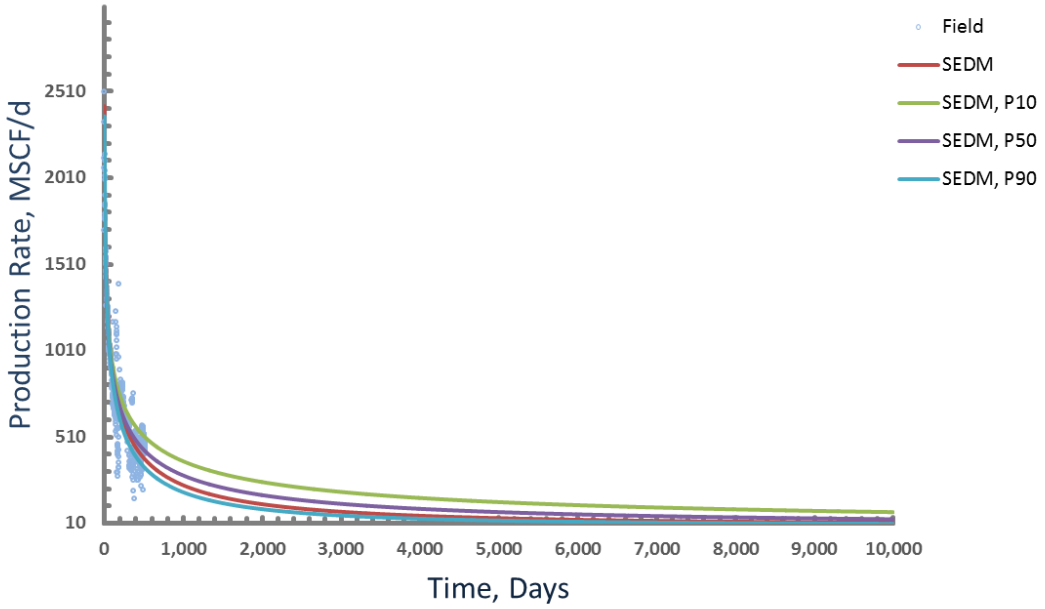
Field
SEDM
SEDM, P10
SEDM, P50
SEDM, P90
Production Rate, MSCF/d
2510
2010
1510
1010
510
10
0
1,000
2,000
3,000
4,000
5,000
6,000
7,000
8,000
9,000
10,000
Time, Days

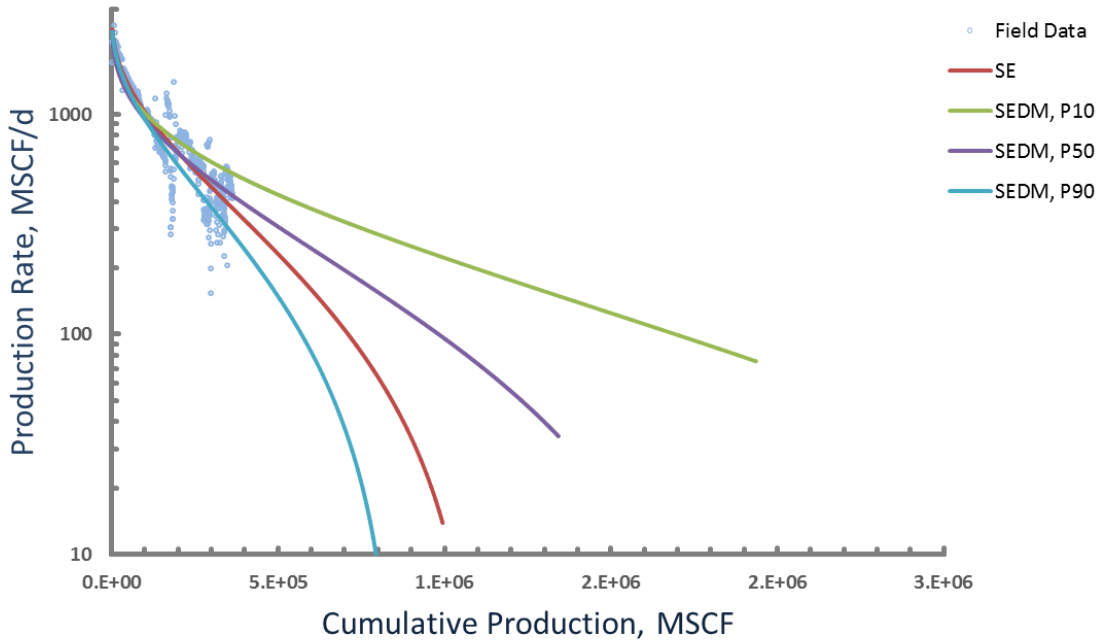
Field Data
SE
SEDM, P10
SEDM, P50
SEDM, P90
Production Rate, MSCF/d
1000
100
10
0.E+00
5.E+05
1.E+06
2.E+06
2.E+06
3.E+06
Cumulative Production, MSCF

Well#5

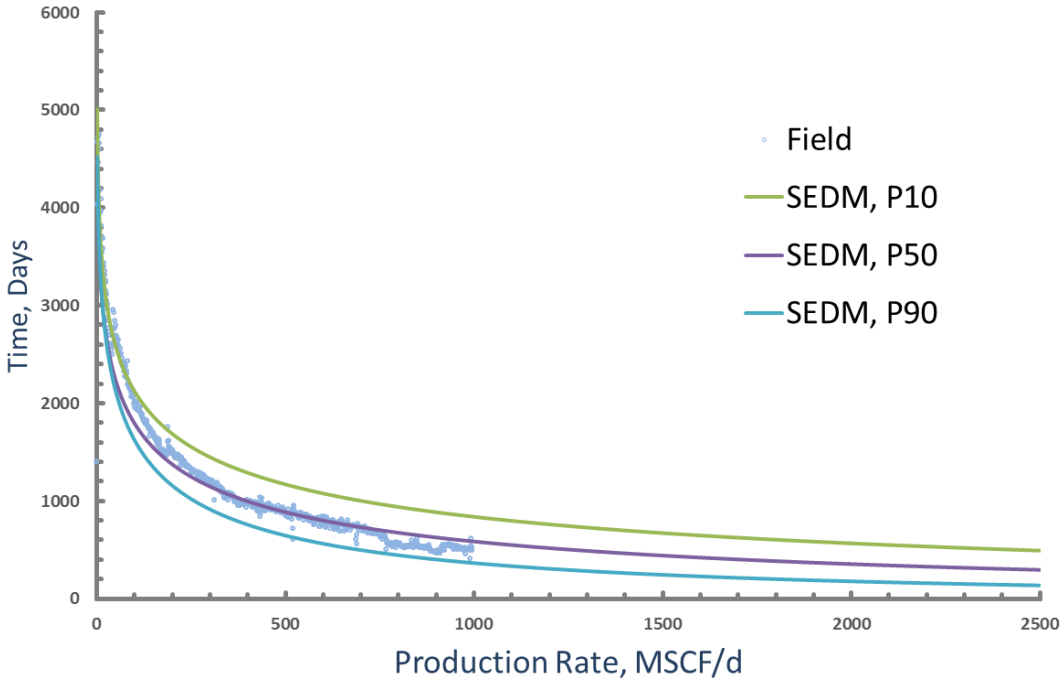
6000
5000
4000
3000
2000
1000
0
Time, Days
0
500
1000
1500
2000
2500
Production Rate, MSCF/d
Field
SEDM, P10
SEDM, P50
SEDM, P90

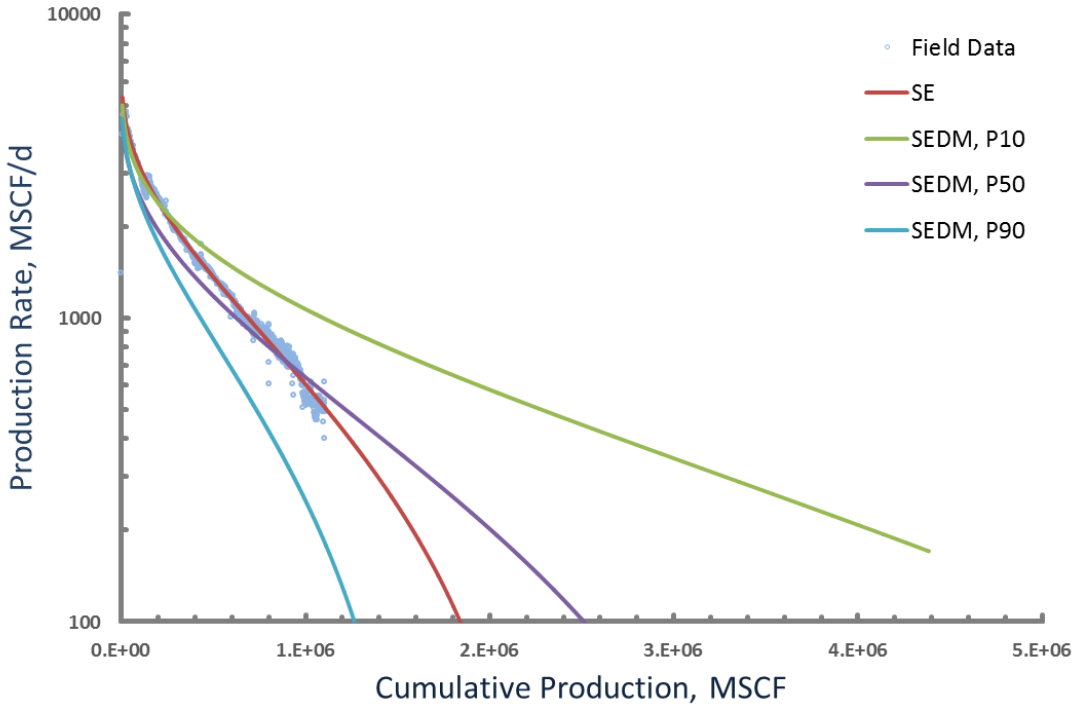
10000
1000
100
Production Rate, MSCF/d
0.E+00
1.E+06
2.E+06
3.E+06
4.E+06
5.E+06
Cumulative Production, MSCF
Field Data
SE
SEDM, P10
SEDM, P50
SEDM, P90

Well#6

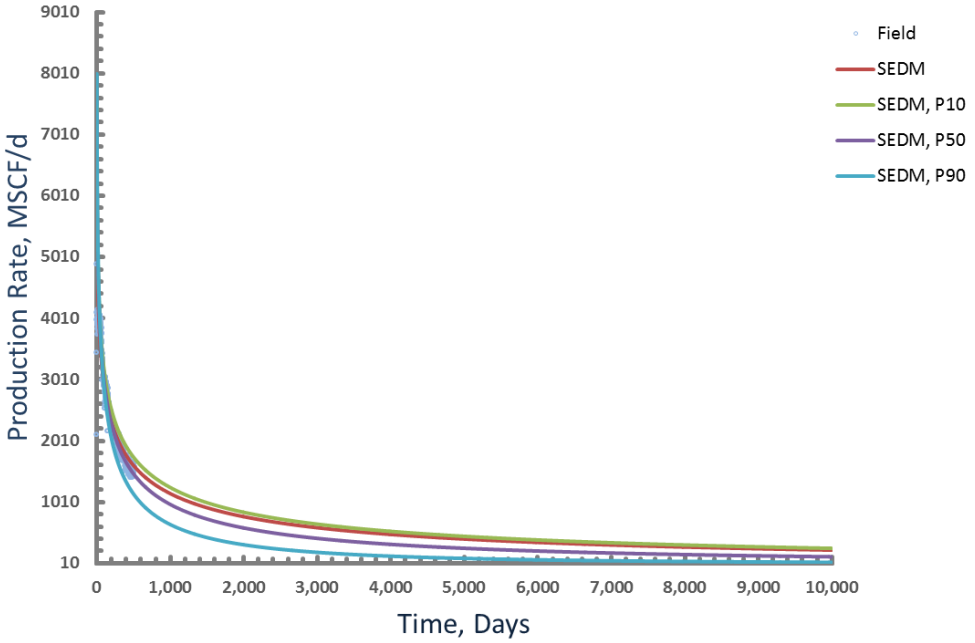
9010
8010
7010
6010
5010
4010
3010
2010
1010
10
Production Rate, MSCF/d
0
1,000
2,000
3,000
4,000
5,000
6,000
7,000
8,000
9,000
10,000
Time, Days
Field
SEDM
SEDM, P10
SEDM, P50
SEDM, P90

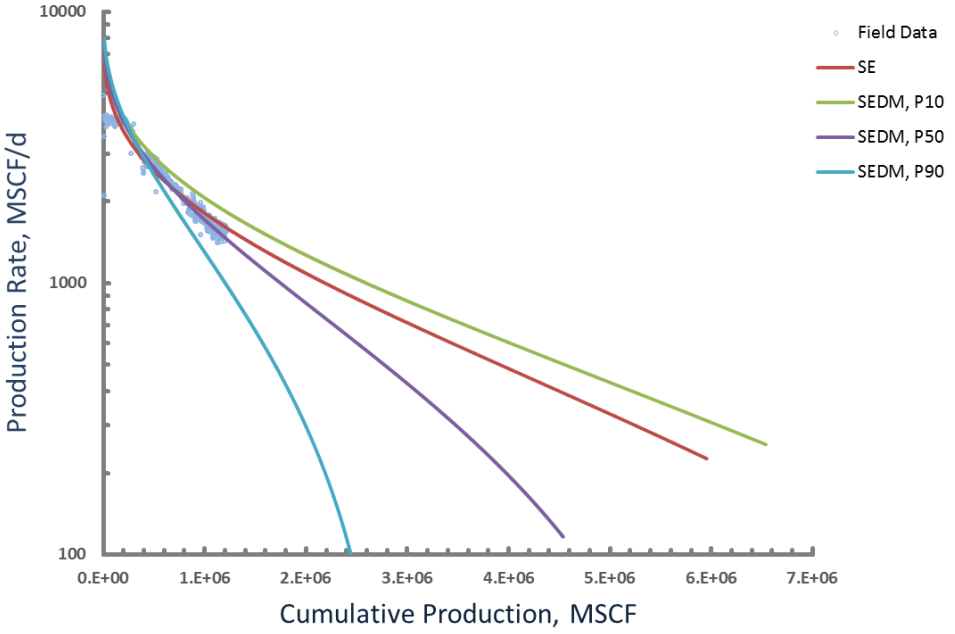
10000
1000
100
Production Rate, MSCF/d
0.E+00
1.E+06
2.E+06
3.E+06
4.E+06
5.E+06
6.E+06
7.E+06
Cumulative Production, MSCF
Field Data
SE
SEDM, P10
SEDM, P50
SEDM, P90

Well#7

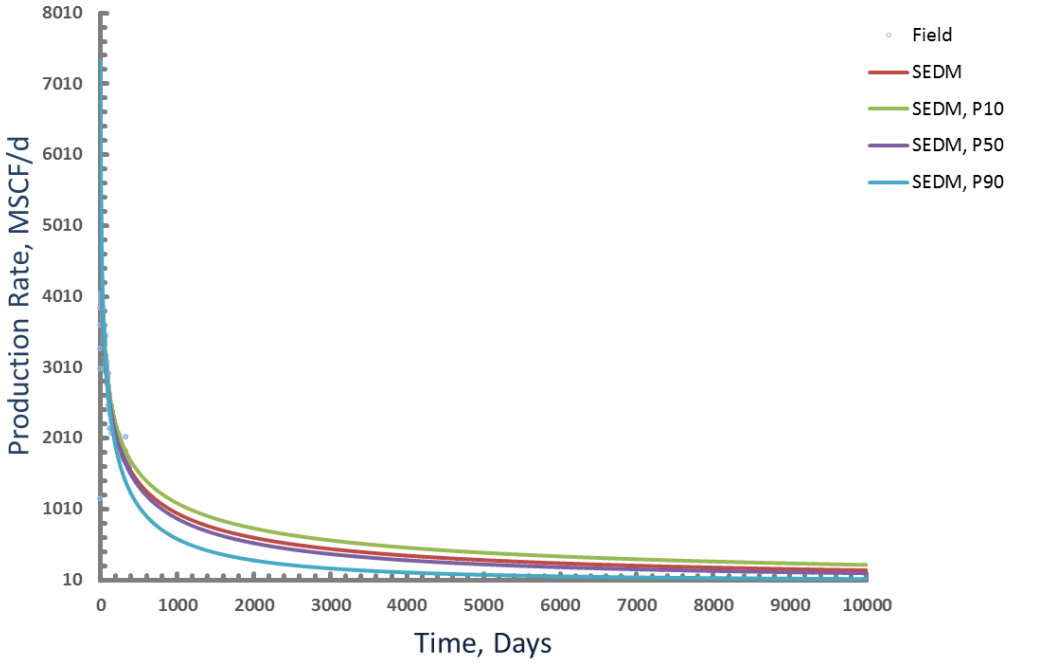
8010
7010
6010
5010
4010
3010
2010
1010
10
Production Rate, MSCF/d
0
1000
2000
3000
4000
5000
6000
7000
8000
9000
10000
Time, Days
Field
SEDM
SEDM, P10
SEDM, P50
SEDM, P90

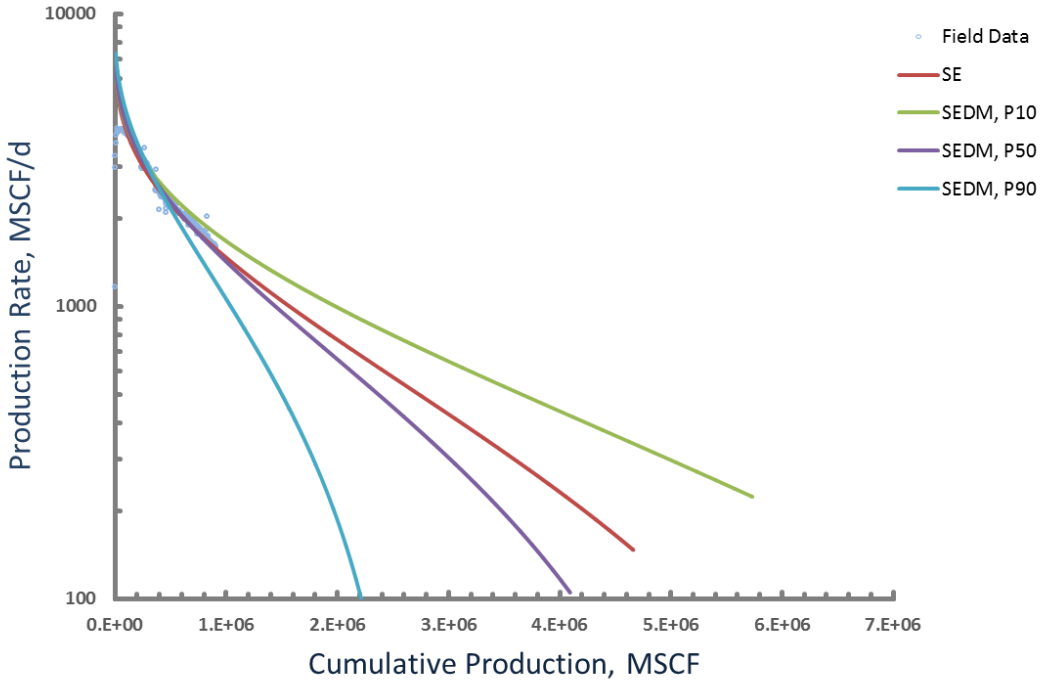
10000
1000
100
Production Rate, MSCF/d
0.E+00
1.E+06
2.E+06
3.E+06
4.E+06
5.E+06
6.E+06
7.E+06
Cumulative Production, MSCF
Field Data
SE
SEDM, P10
SEDM, P50
SEDM, P90

Well#8

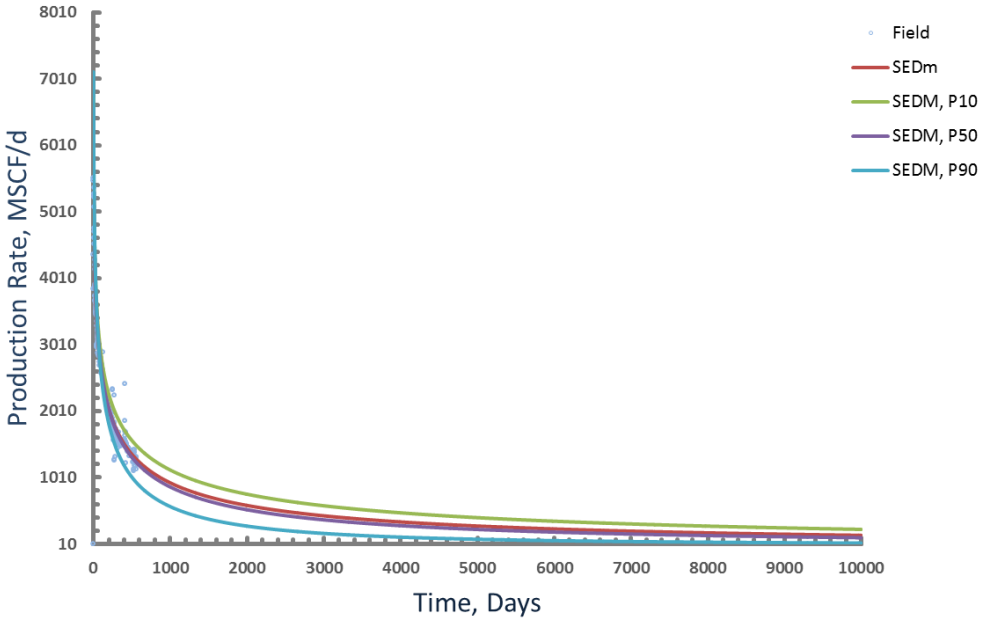
8010
7010
6010
5010
4010
3010
2010
1010
10
Production Rate, MSCF/d
0
1000
2000
3000
4000
5000
6000
7000
8000
9000
10000
Time, Days
Field
SEDm
SEDM, P10
SEDM, P50
SEDM, P90

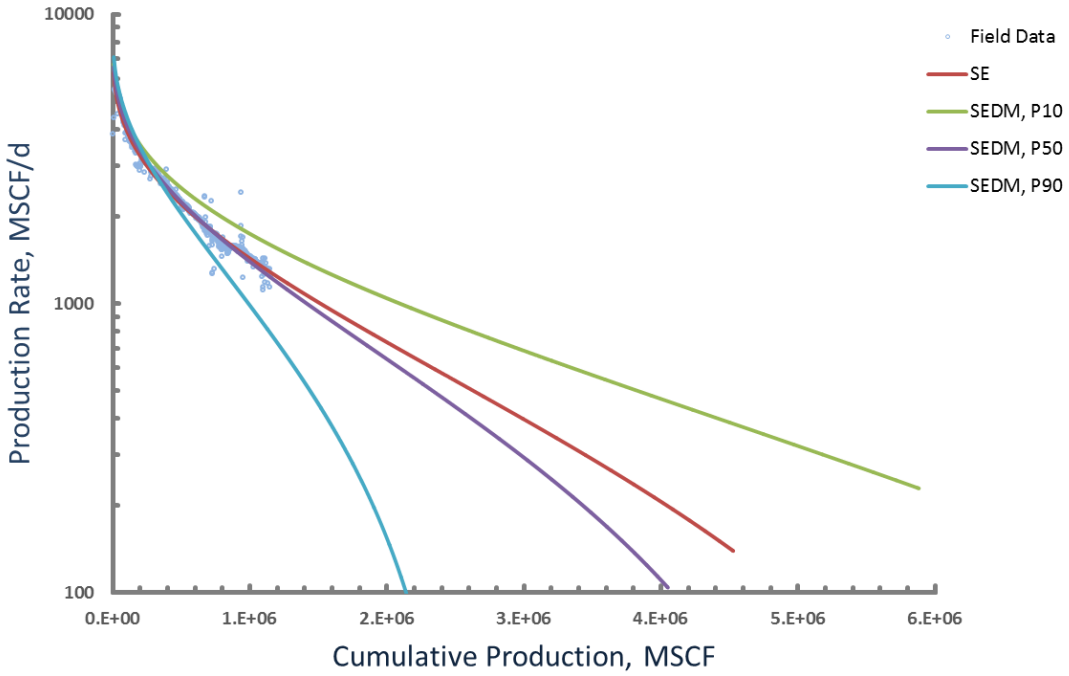
10000
1000
100
Production Rate, MSCF/d
0.E+00
1.E+06
2.E+06
3.E+06
4.E+06
5.E+06
6.E+06
Cumulative Production, MSCF
Field Data
SE
SEDM, P10
SEDM, P50
SEDM, P90

Well#9

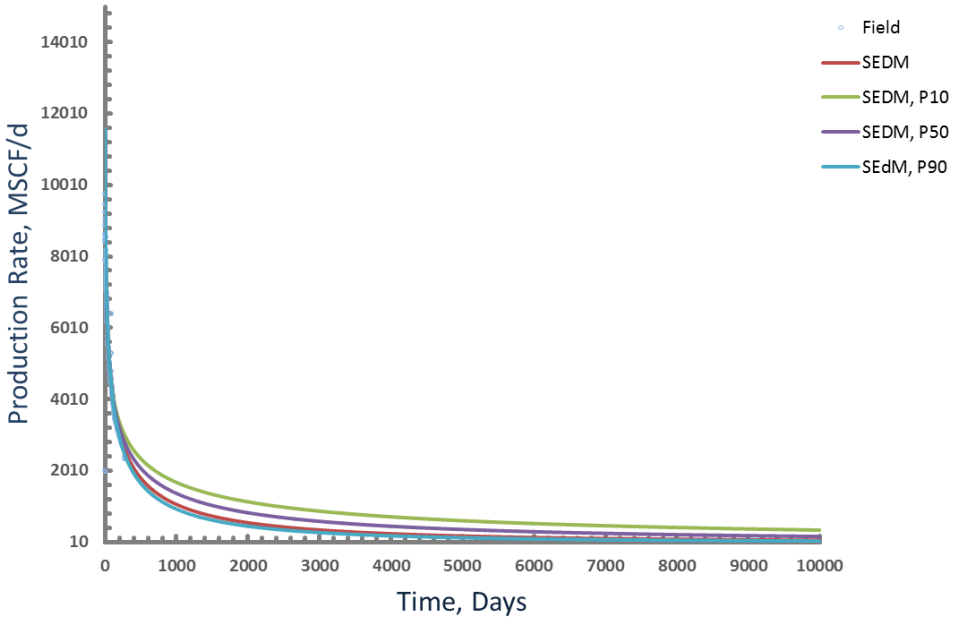
Field
SEDM
SEDM, P10
SEDM, P50
SEdM, P90
Production Rate, MSCF/d
14010
12010
10010
8010
6010
4010
2010
10
0
1000
2000
3000
4000
5000
6000
7000
8000
9000
10000
Time, Days

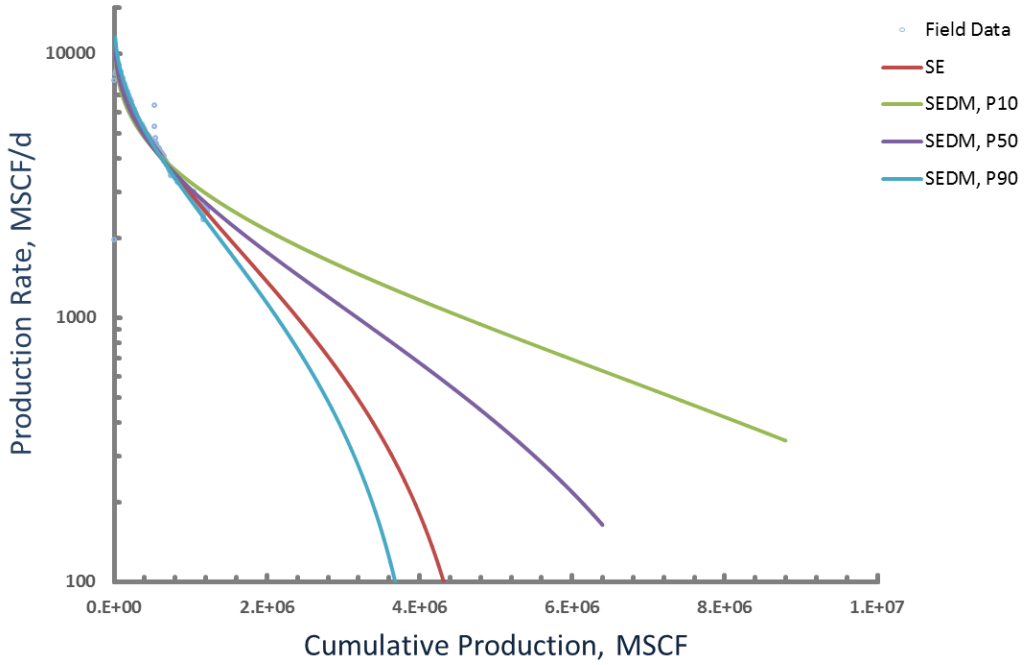
Field Data
SE
SEDM, P10
SEDM, P50
SEDM, P90
Production Rate, MSCF/d
10000
1000
100
0.E+00
2.E+06
4.E+06
6.E+06
8.E+06
1.E+07
Cumulative Production, MSCF

Well#10

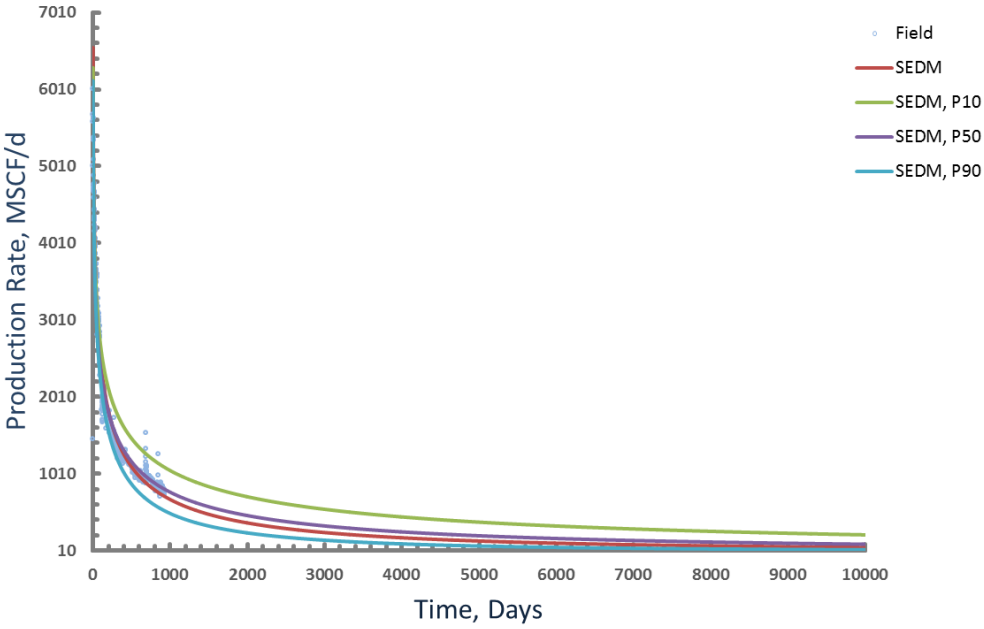
Production Rate, MSCF/d
7010
6010
5010
4010
3010
2010
1010
10
0
1000
2000
3000
4000
5000
6000
7000
8000
9000
10000
Time, Days
Field
SEDM
SEDM, P10
SEDM, P50
SEDM, P90

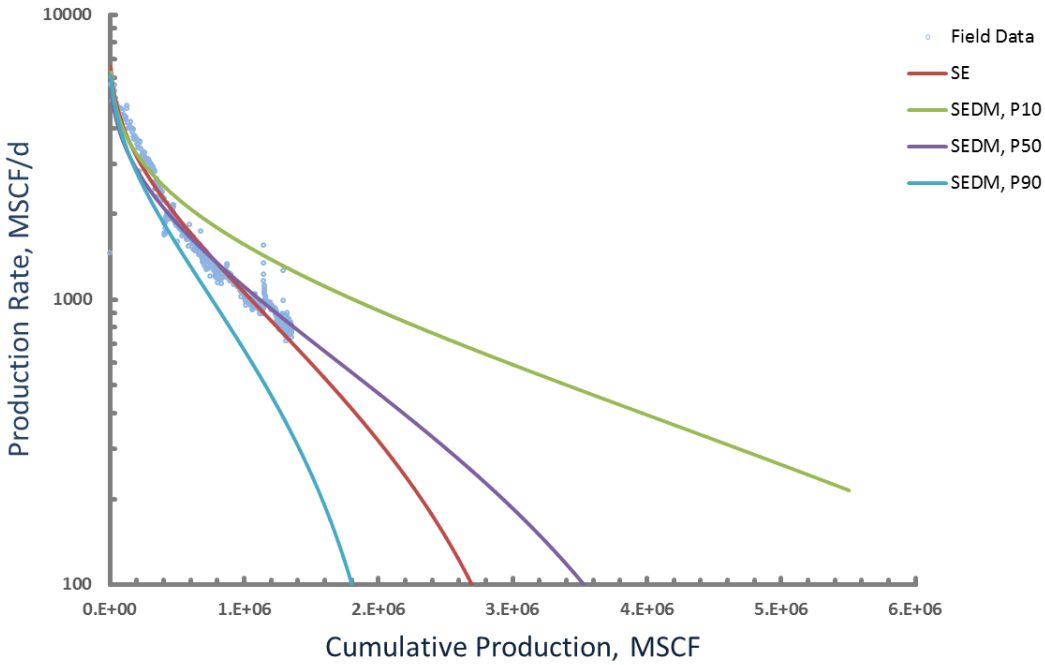
Production Rate, MSCF/d
10000
1000
100
0.E+00
1.E+06
2.E+06
3.E+06
4.E+06
5.E+06
6.E+06
Cumulative Production, MSCF
Field Data
SE
SEDM, P10
SEDM, P50
SEDM, P90

Well#11

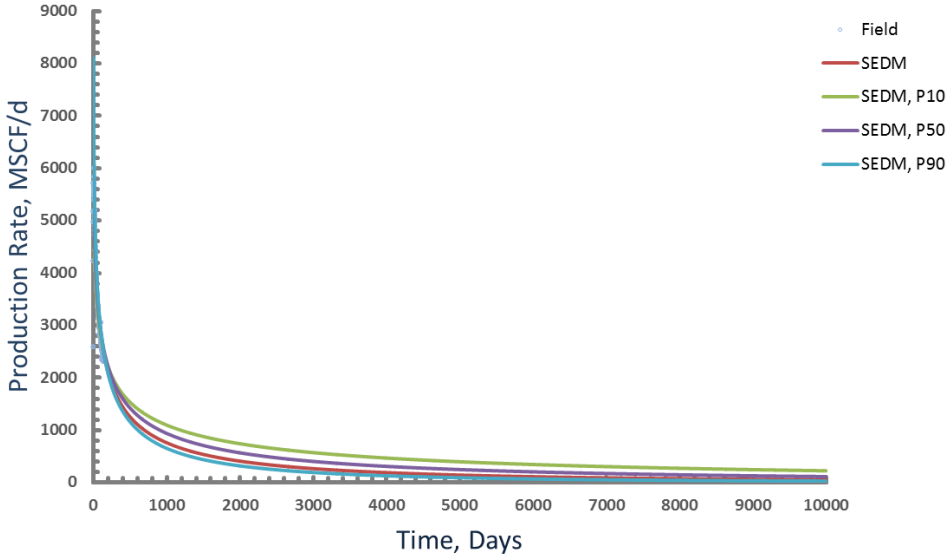
Production Rate, MSCF/d
9000
8000
7000
6000
5000
4000
3000
2000
1000
0
0
1000
2000
3000
4000
5000
6000
7000
8000
9000
10000
Time, Days
Field
SEDM
SEDM, P10
SEDM, P50
SEDM, P90

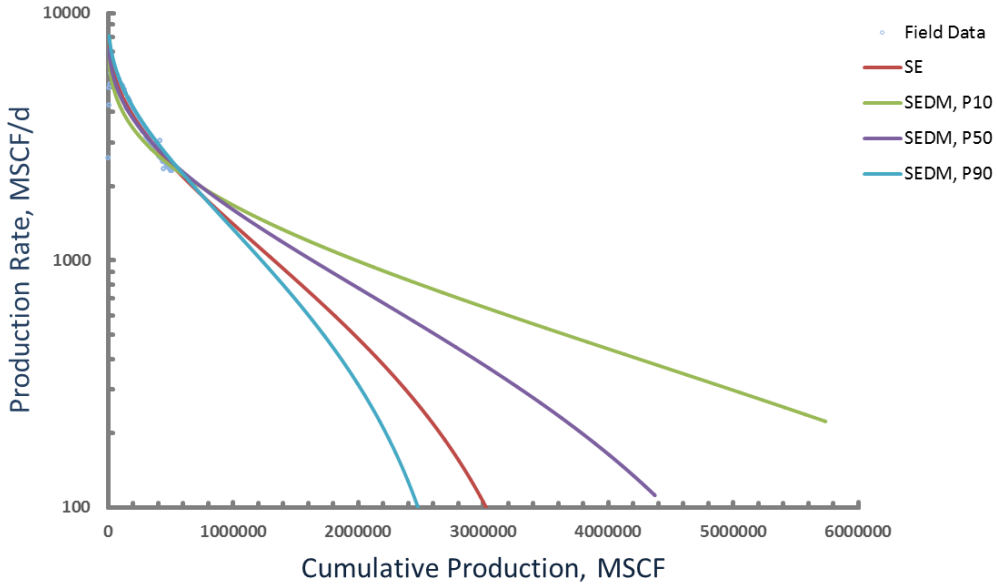
Production Rate, MSCF/d
10000
1000
100
0
1000000
2000000
3000000
4000000
5000000
6000000
Cumulative Production, MSCF
Field Data
SE
SEDM, P10
SEDM, P50
SEDM, P90

Well#12

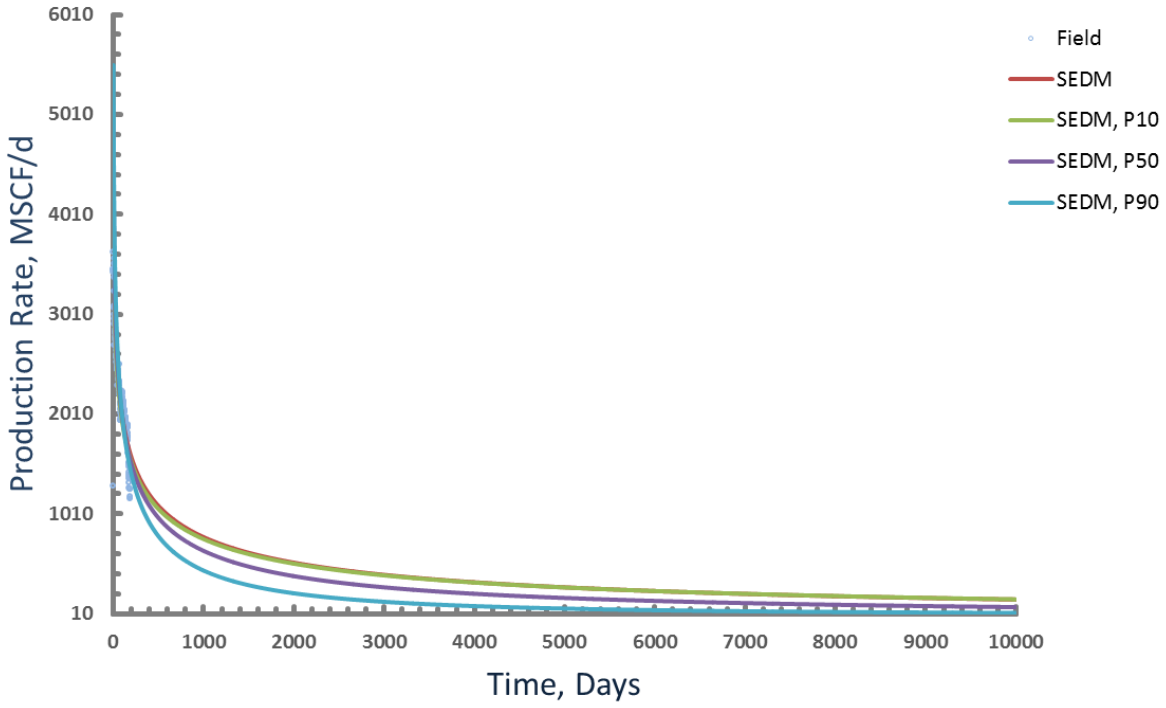
Production Rate, MSCF/d
6010
5010
4010
3010
2010
1010
10
0
1000
2000
3000
4000
5000
6000
7000
8000
9000
10000
Time, Days
Field
SEDM
SEDM, P10
SEDM, P50
SEDM, P90

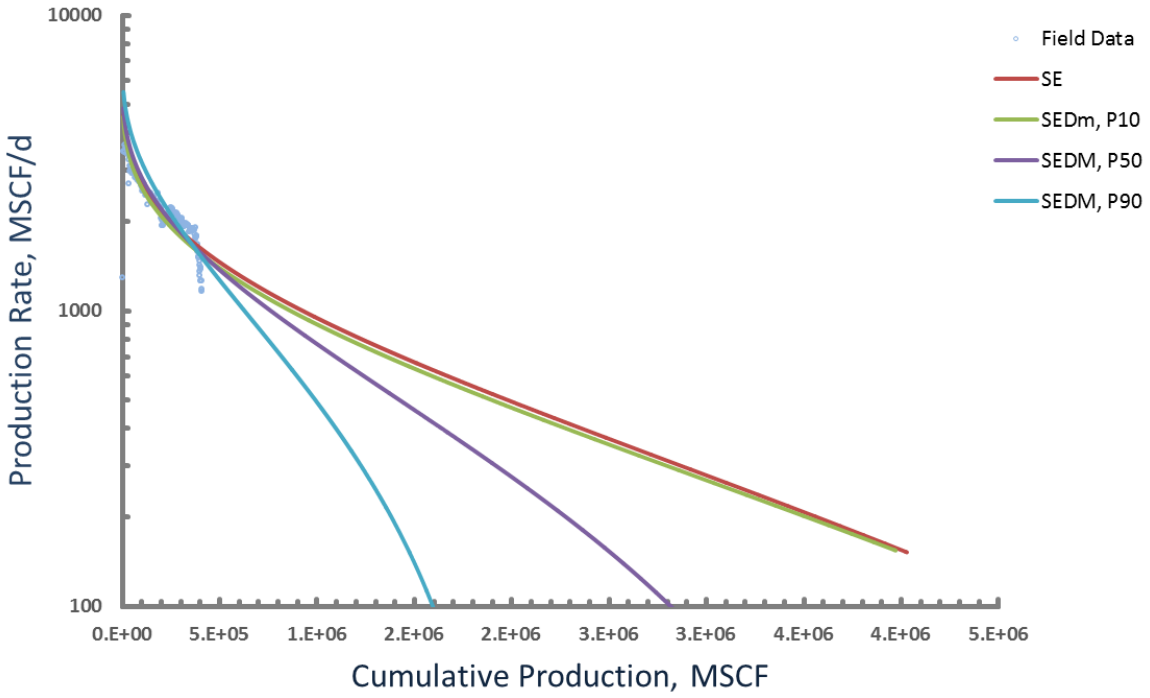
Production Rate, MSCF/d
10000
1000
100
0.E+00
5.E+05
1.E+06
2.E+06
2.E+06
3.E+06
3.E+06
4.E+06
4.E+06
5.E+06
Cumulative Production, MSCF
Field Data
SE
SEDm, P10
SEDM, P50
SEDM, P90

Well#13

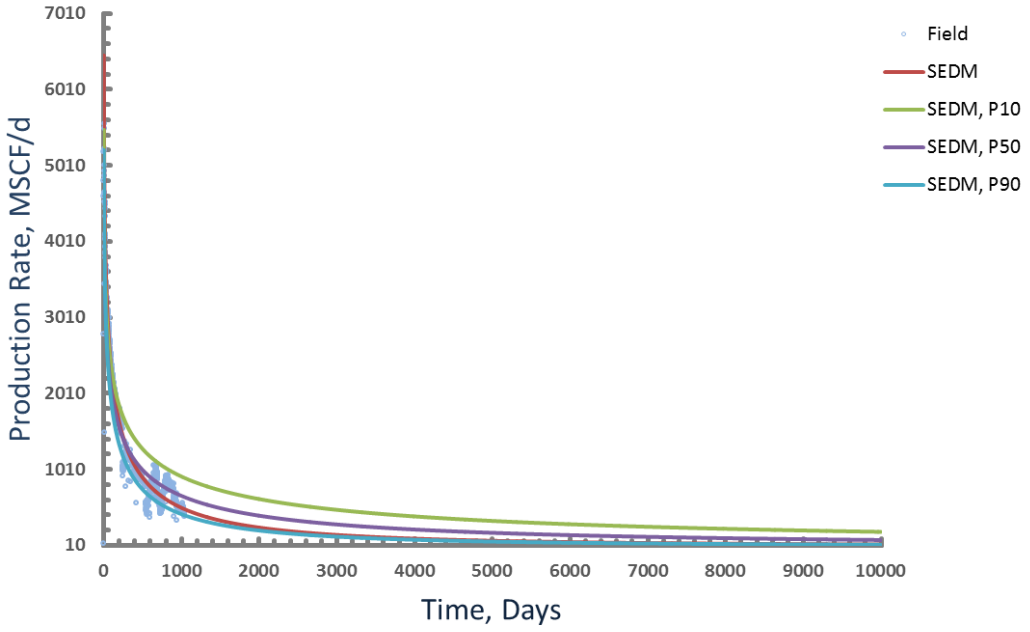
Production Rate, MSCF/d
7010
6010
5010
4010
3010
2010
1010
10
0
1000
2000
3000
4000
5000
6000
7000
8000
9000
10000
Time, Days
Field
SEDM
SEDM, P10
SEDM, P50
SEDM, P90

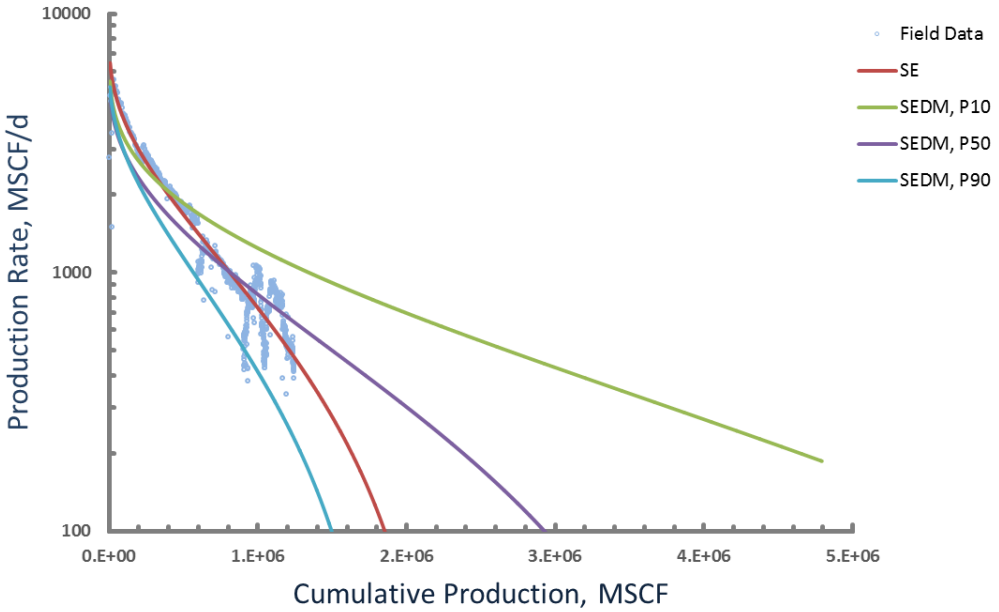
Production Rate, MSCF/d
10000
1000
100
0.E+00
1.E+06
2.E+06
3.E+06
4.E+06
5.E+06
Cumulative Production, MSCF
Field Data
SE
SEDM, P10
SEDM, P50
SEDM, P90

Well#14

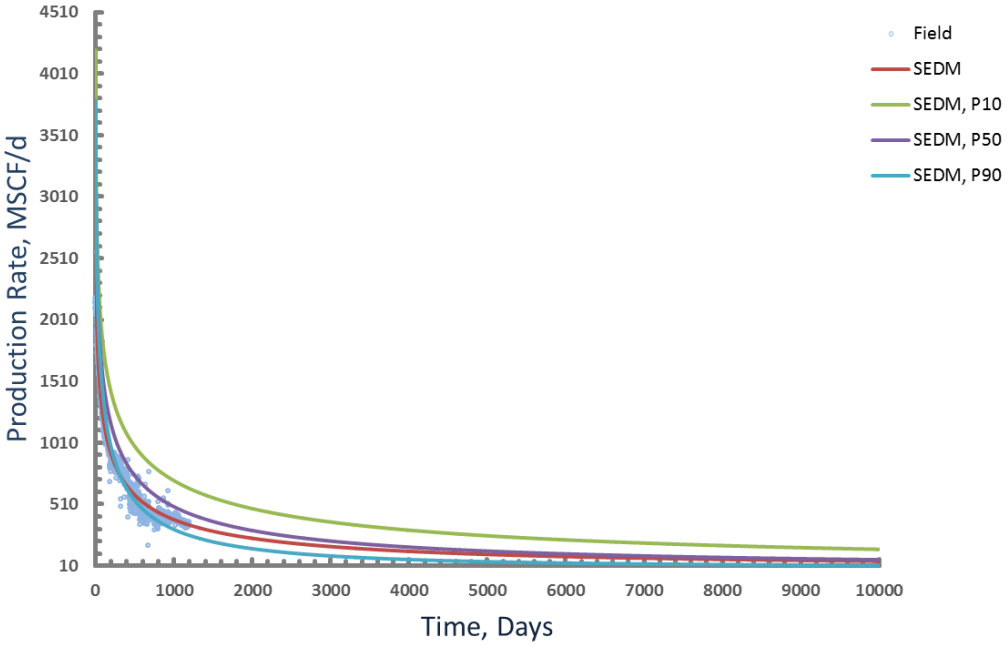
Production Rate, MSCF/d
4510
4010
3510
3010
2510
2010
1510
1010
510
10
0
1000
2000
3000
4000
5000
6000
7000
8000
9000
10000
Time, Days
Field
SEDM
SEDM, P10
SEDM, P50
SEDM, P90

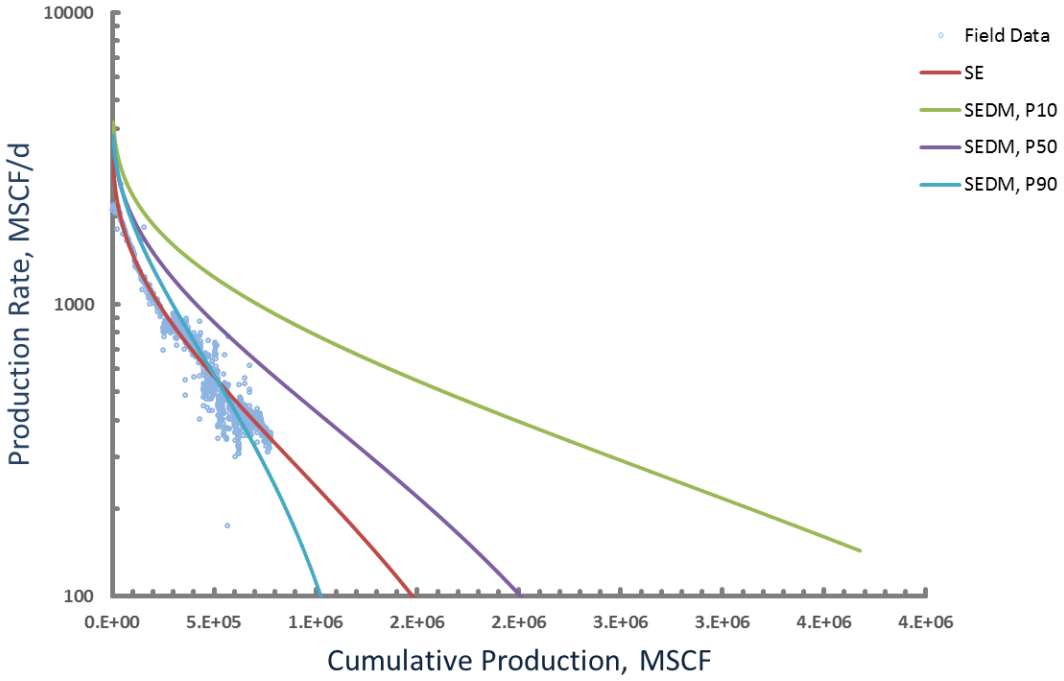
Production Rate, MSCF/d
10000
1000
100
0.E+00
5.E+05
1.E+06
2.E+06
2.E+06
3.E+06
3.E+06
4.E+06
4.E+06
Cumulative Production, MSCF
Field Data
SE
SEDM, P10
SEDM, P50
SEDM, P90

Well#15

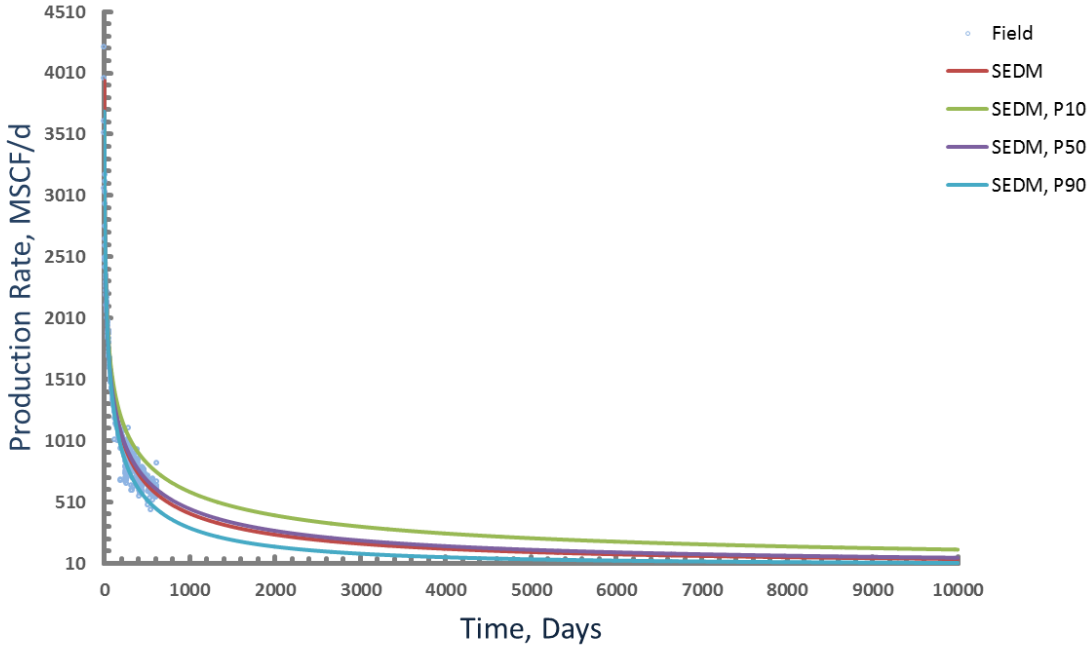
4510
4010
3510
3010
2510
2010
1510
1010
510
10
Production Rate, MSCF/d
0
1000
2000
3000
4000
5000
6000
7000
8000
9000
10000
Time, Days
Field
SEDM
SEDM, P10
SEDM, P50
SEDM, P90

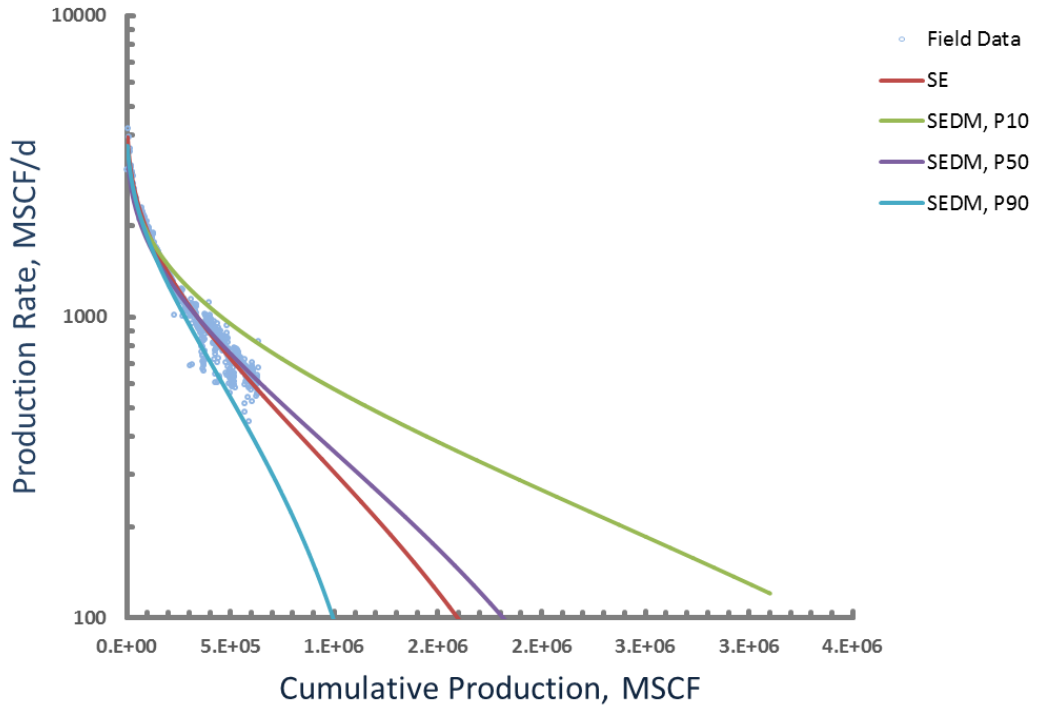
10000
1000
100
Production Rate, MSCF/d
0.E+00
5.E+05
1.E+06
2.E+06
2.E+06
3.E+06
3.E+06
4.E+06
Cumulative Production, MSCF
Field Data
SE
SEDM, P10
SEDM, P50
SEDM, P90

Well#16

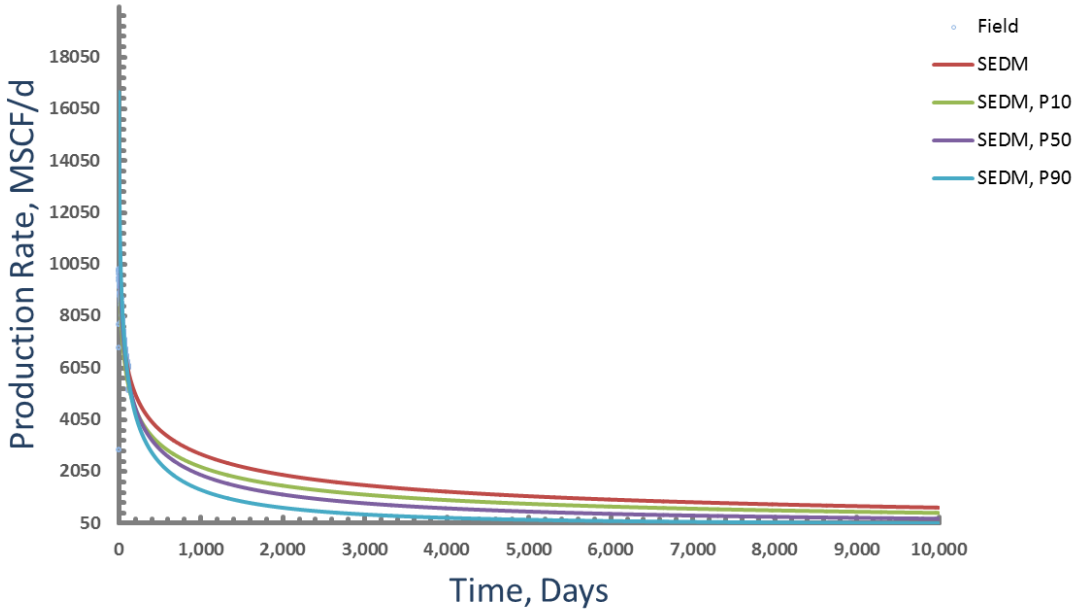
Production Rate, MSCF/d
18050
16050
14050
12050
10050
8050
6050
4050
2050
50
0
1,000
2,000
3,000
4,000
5,000
6,000
7,000
8,000
9,000
10,000
Time, Days
Field
SEDM
SEDM, P10
SEDM, P50
SEDM, P90

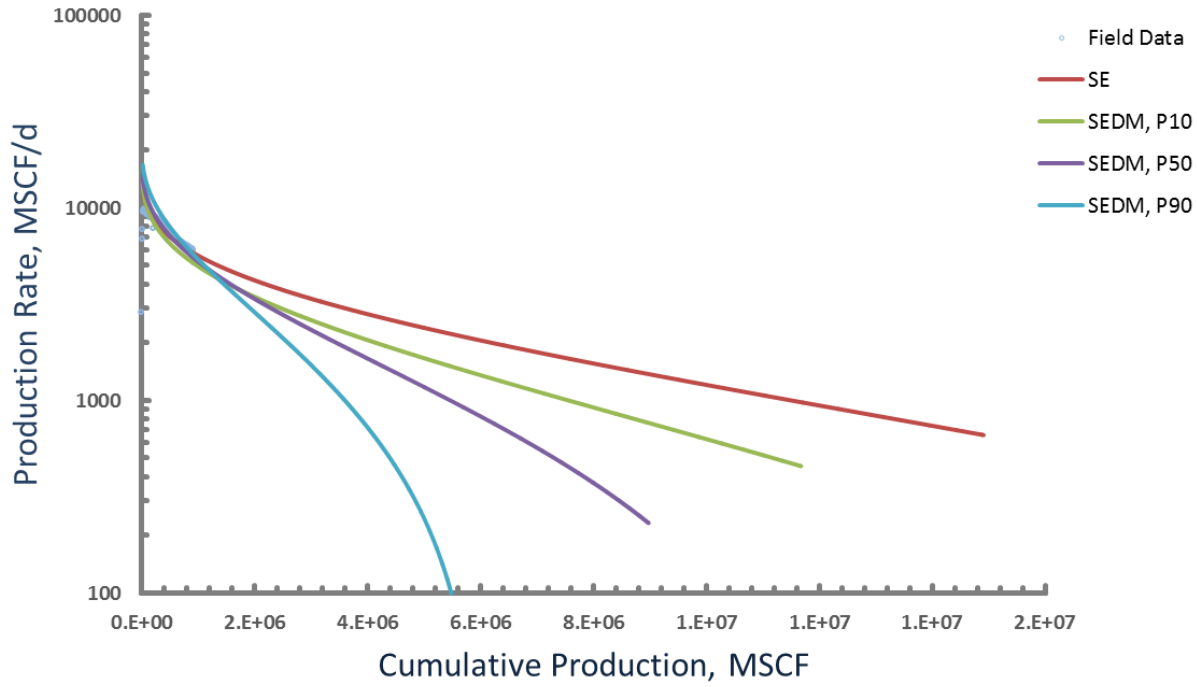
Production Rate, MSCF/d
100000
10000
1000
100
0.E+00
2.E+06
4.E+06
6.E+06
8.E+06
1.E+07
1.E+07
1.E+07
2.E+07
Cumulative Production, MSCF
Field Data
SE
SEDM, P10
SEDM, P50
SEDM, P90

Well#17

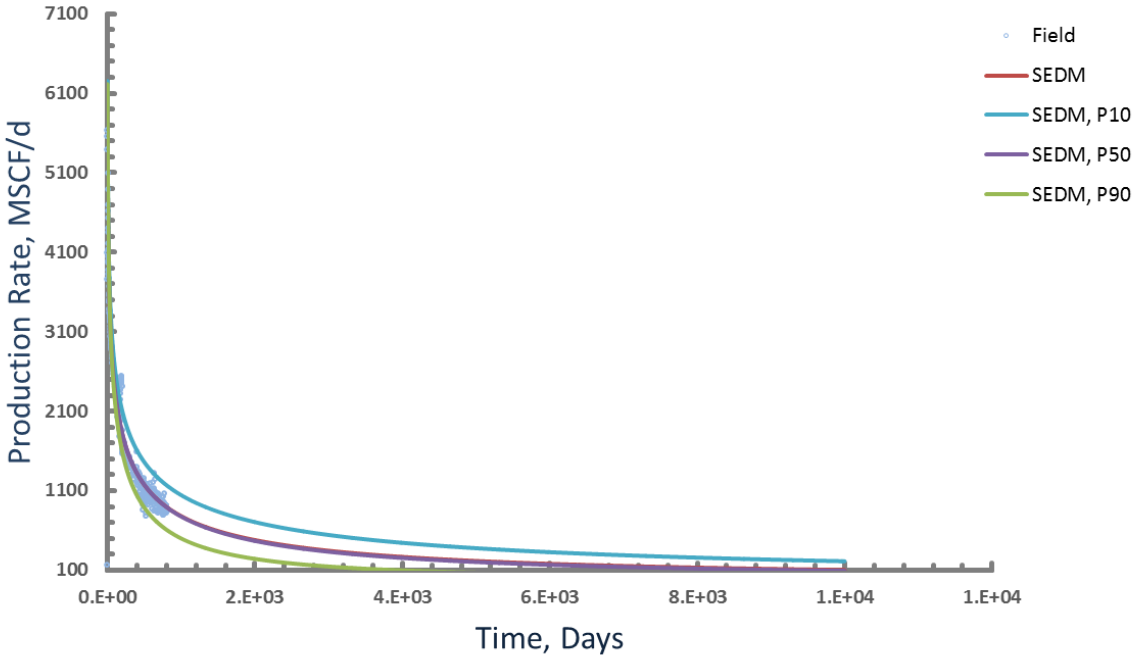
7100
6100
5100
4100
3100
2100
1100
100
Production Rate, MSCF/d
0.E+00
2.E+03
4.E+03
6.E+03
8.E+03
1.E+04
1.E+04
Time, Days
Field
SEDM
SEDM, P10
SEDM, P50
SEDM, P90

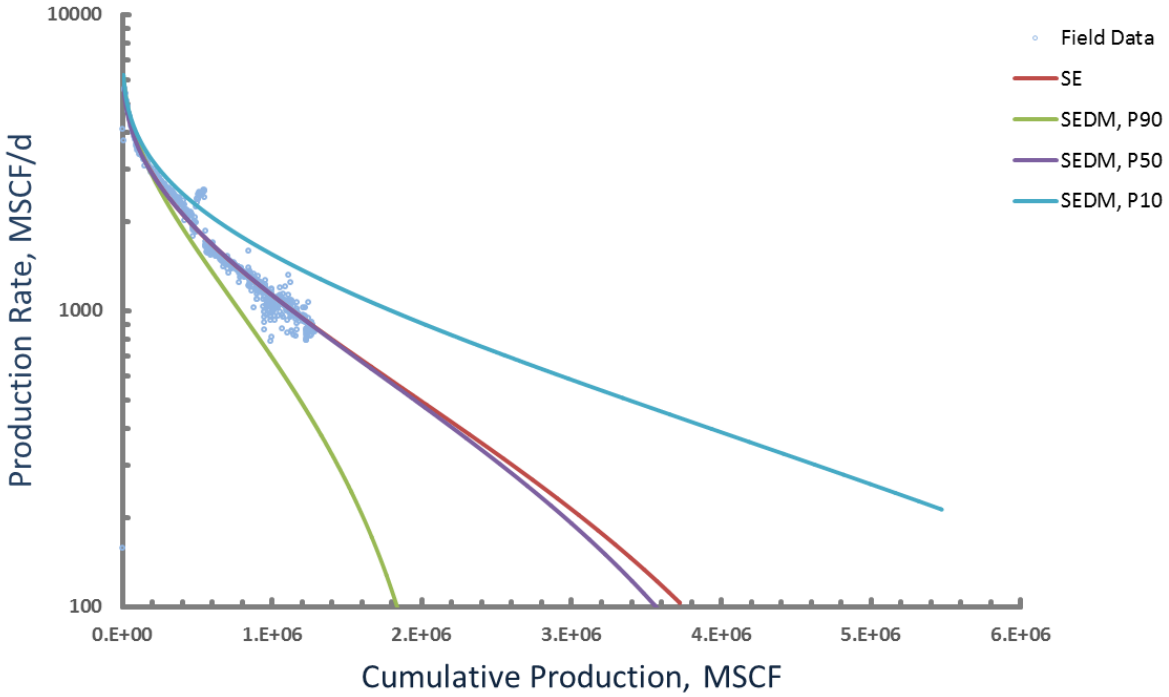
10000
1000
100
Production Rate, MSCF/d
0.E+00
1.E+06
2.E+06
3.E+06
4.E+06
5.E+06
6.E+06
Cumulative Production, MSCF
Field Data
SE
SEDM, P90
SEDM, P50
SEDM, P10

Well#18

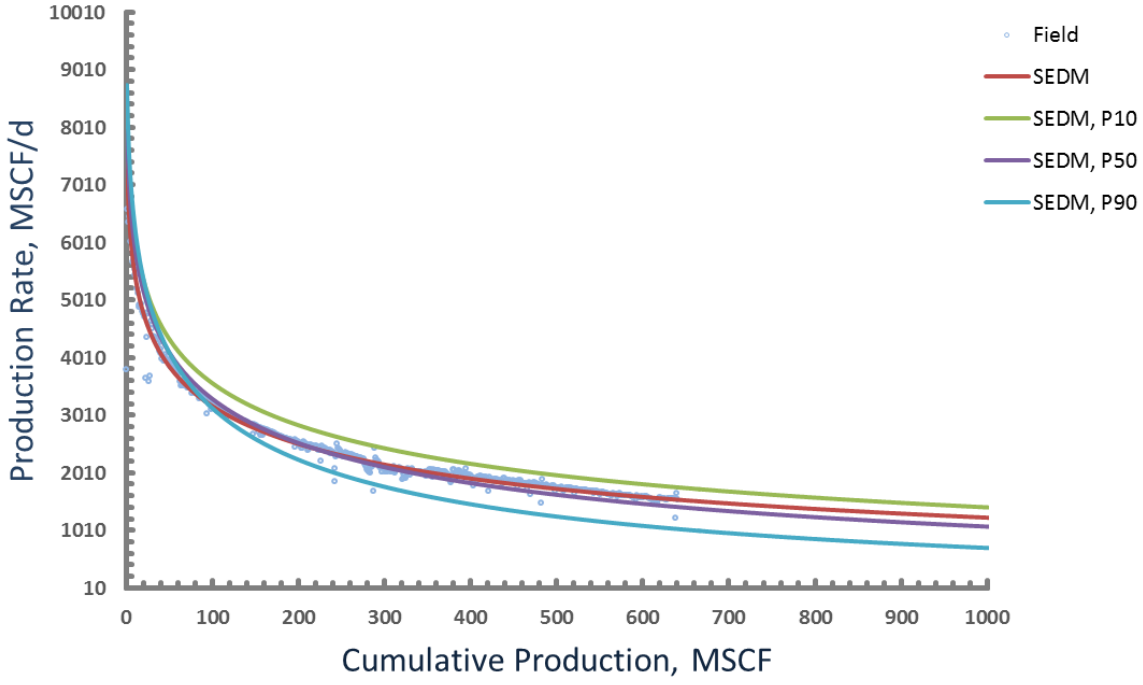
10010
9010
8010
7010
6010
5010
4010
3010
2010
1010
10
Production Rate, MSCF/d
0
100
200
300
400
500
600
700
800
900
1000
Cumulative Production, MSCF
Field
SEDM
SEDM, P10
SEDM, P50
SEDM, P90

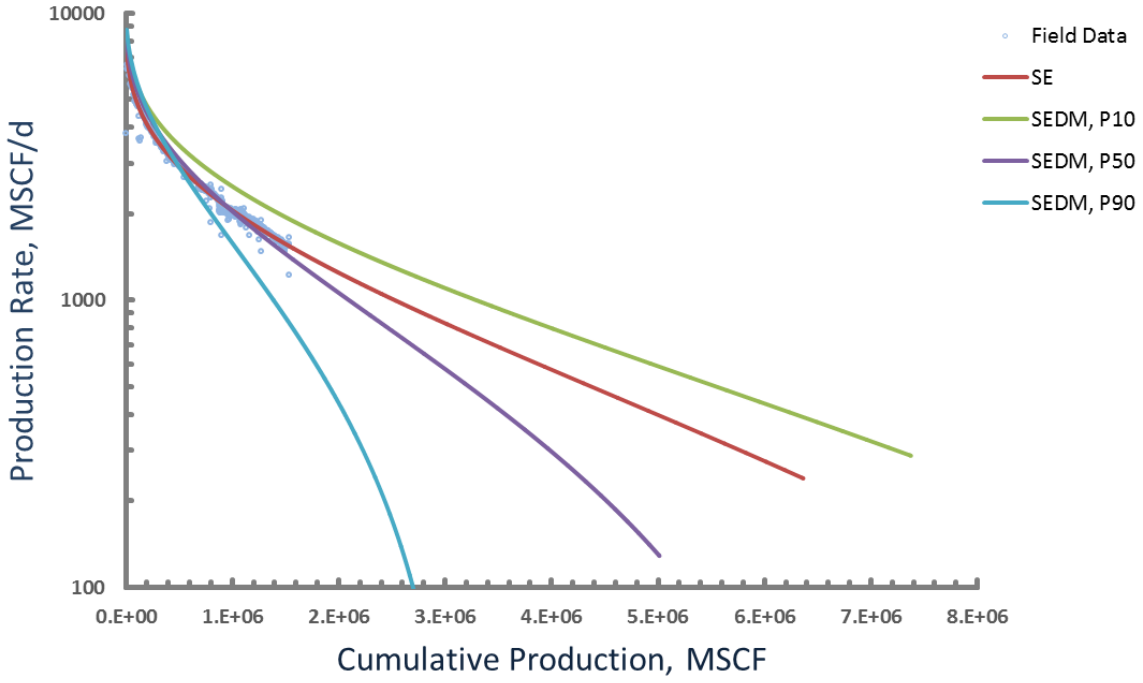
10000
1000
100
Production Rate, MSCF/d
0.E+00
1.E+06
2.E+06
3.E+06
4.E+06
5.E+06
6.E+06
7.E+06
8.E+06
Cumulative Production, MSCF
Field Data
SE
SEDM, P10
SEDM, P50
SEDM, P90

Well#19

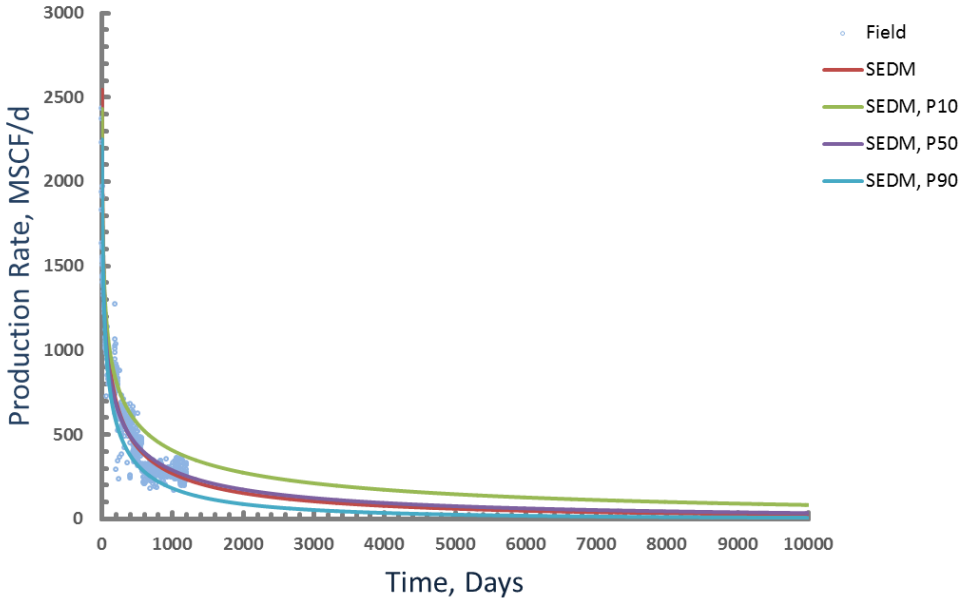
Production Rate, MSCF/d
3000
2500
2000
1500
1000
500
0
0
1000
2000
3000
4000
5000
6000
7000
8000
9000
10000
Time, Days
Field
SEDM
SEDM, P10
SEDM, P50
SEDM, P90

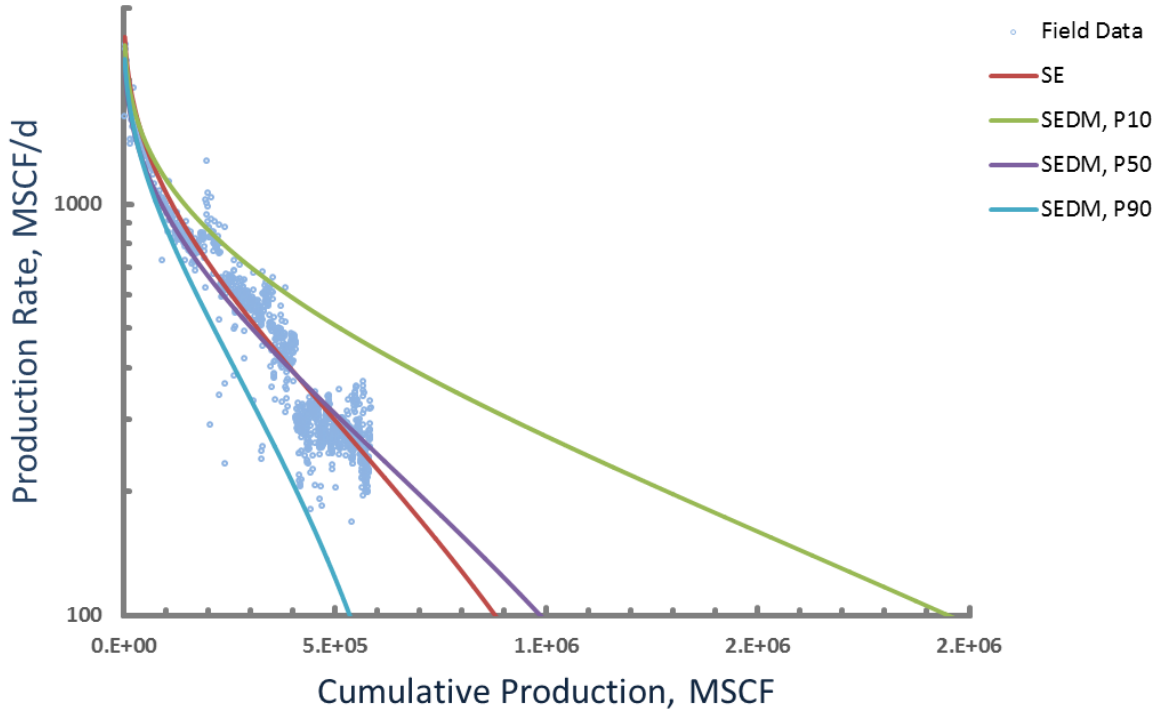
Production Rate, MSCF/d
1000
100
0.E+00
5.E+05
1.E+06
2.E+06
2.E+06
Cumulative Production, MSCF
Field Data
SE
SEDM, P10
SEDM, P50
SEDM, P90

Well#20

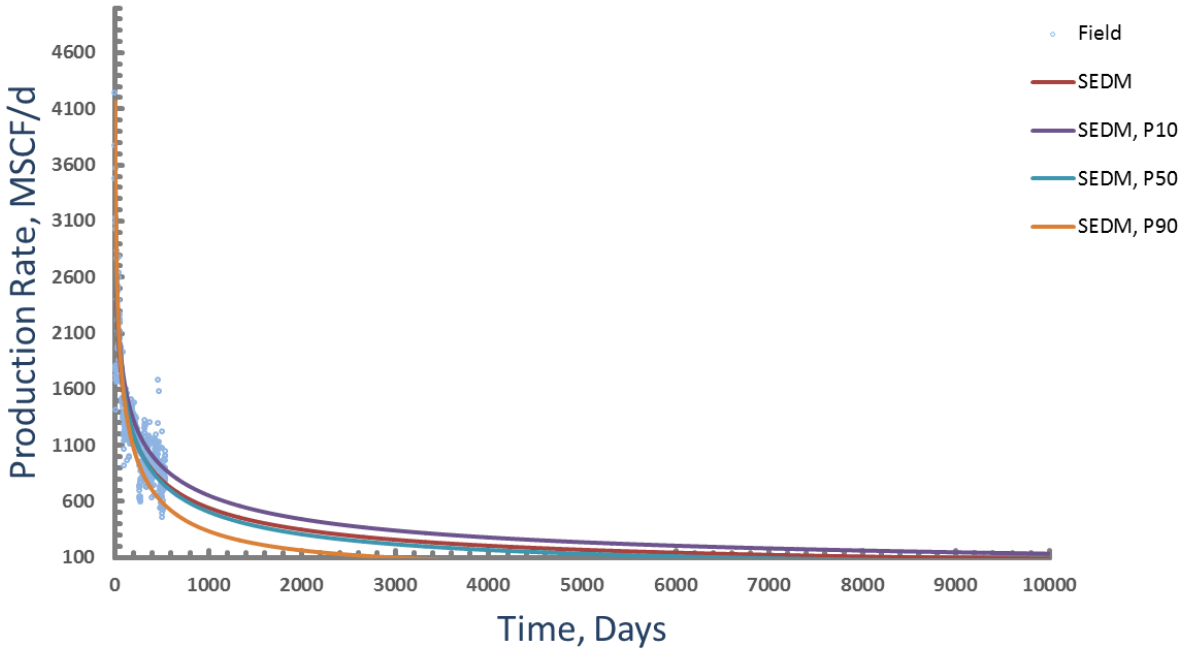
Production Rate, MSCF/d
4600
4100
3600
3100
2600
2100
1600
1100
600
100
0
1000
2000
3000
4000
5000
6000
7000
8000
9000
10000
Time, Days
Field
SEDM
SEDM, P10
SEDM, P50
SEDM, P90

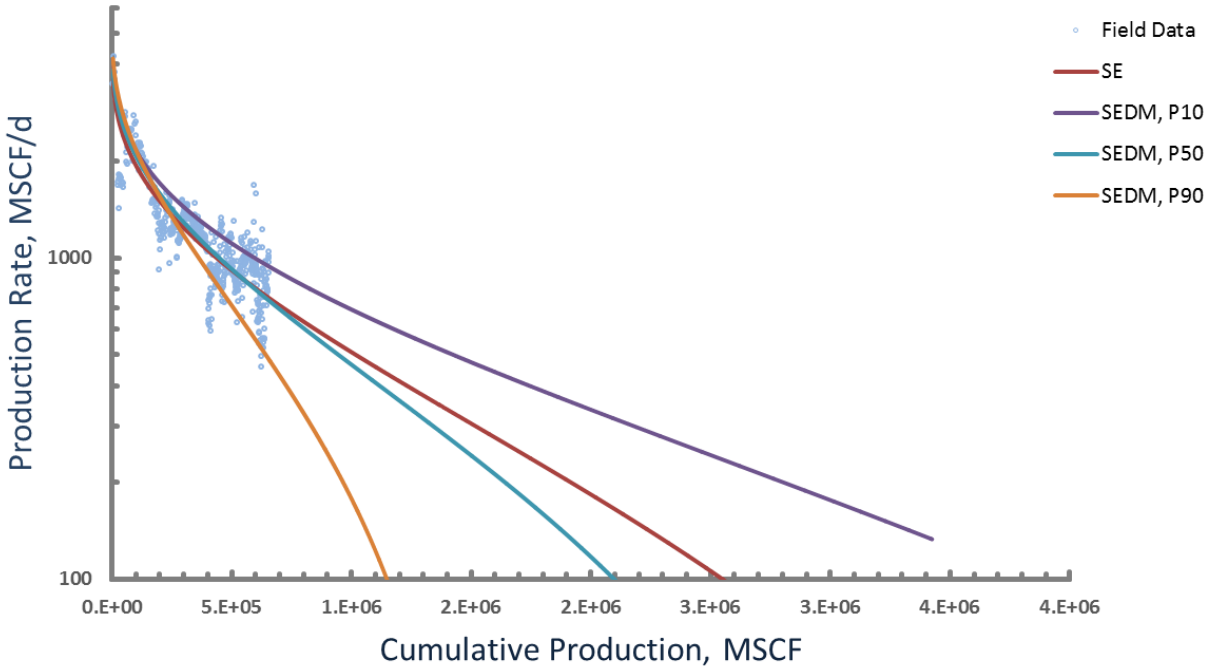
Production Rate, MSCF/d
1000
100
0.E+00
5.E+05
1.E+06
2.E+06
2.E+06
3.E+06
3.E+06
4.E+06
4.E+06
Cumulative Production, MSCF
Field Data
SE
SEDM, P10
SEDM, P50
SEDM, P90

Well#21

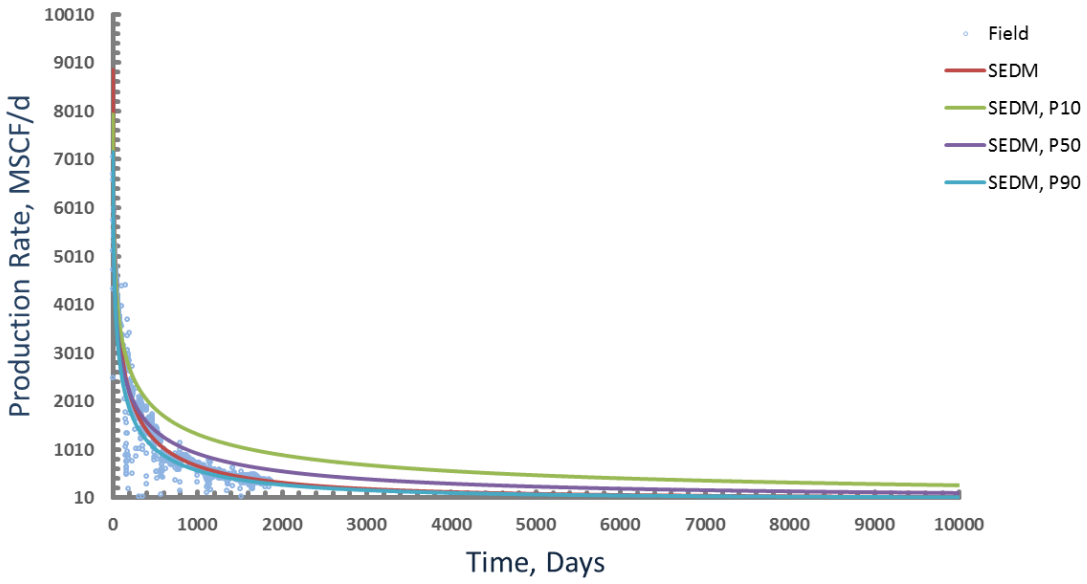
Production Rate, MSCF/d
10010
9010
8010
7010
6010
5010
4010
3010
2010
1010
10
0
1000
2000
3000
4000
5000
6000
7000
8000
9000
10000
Time, Days
Field
SEDM
SEDM, P10
SEDM, P50
SEDM, P90

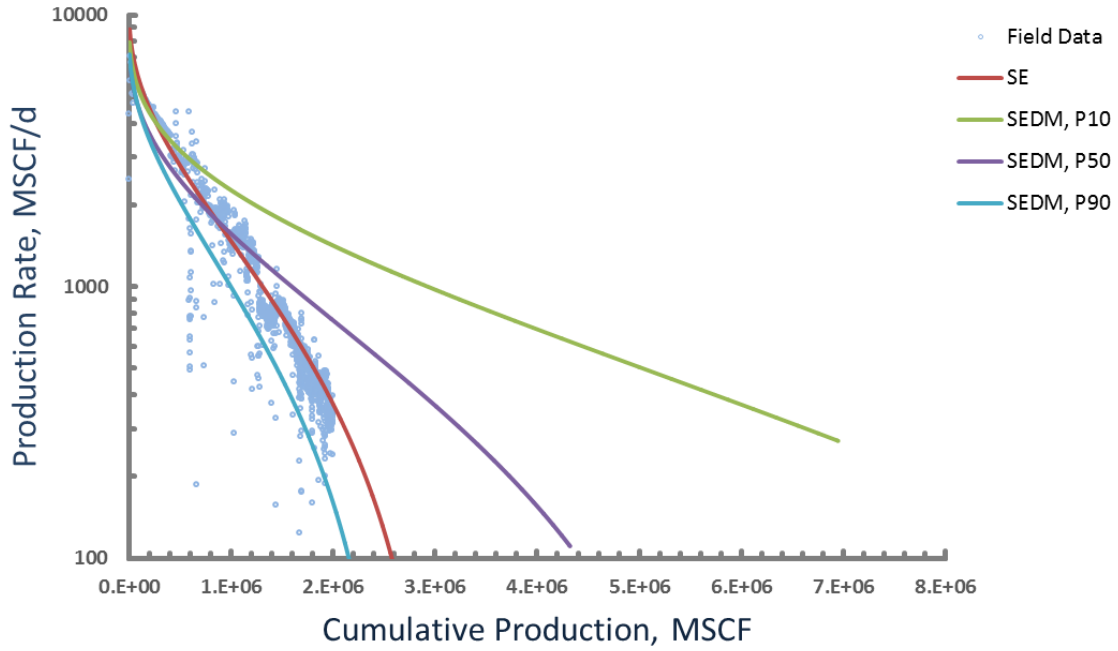
Production Rate, MSCF/d
10000
1000
100
0.E+00
1.E+06
2.E+06
3.E+06
4.E+06
5.E+06
6.E+06
7.E+06
8.E+06
Cumulative Production, MSCF
Field Data
SE
SEDM, P10
SEDM, P50
SEDM, P90

Well#22

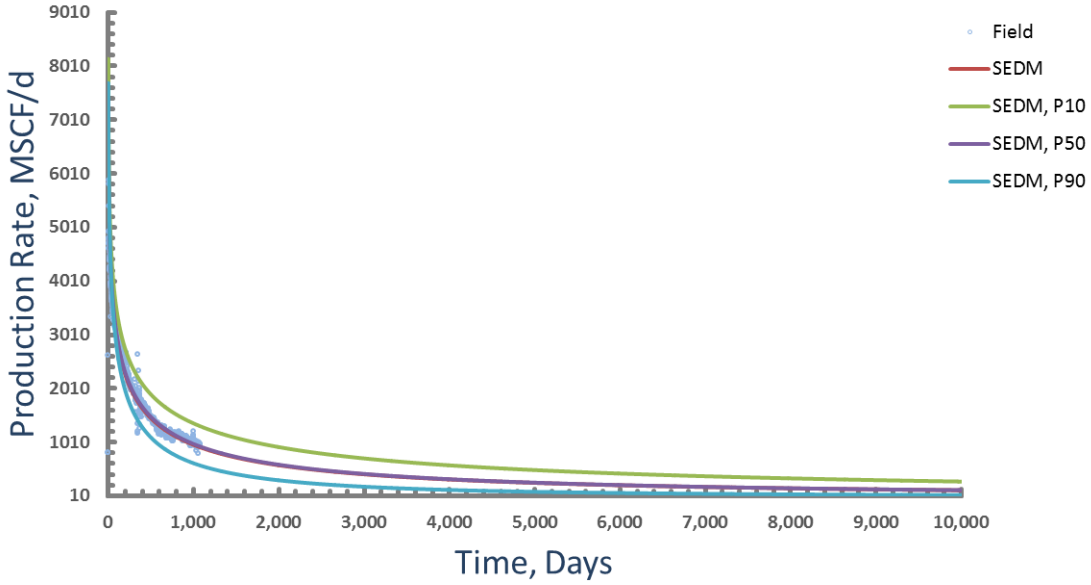
Production Rate, MSCF/d
9010
8010
7010
6010
5010
4010
3010
2010
1010
10
0
1,000
2,000
3,000
4,000
5,000
6,000
7,000
8,000
9,000
10,000
Time, Days
Field
SEDM
SEDM, P10
SEDM, P50
SEDM, P90

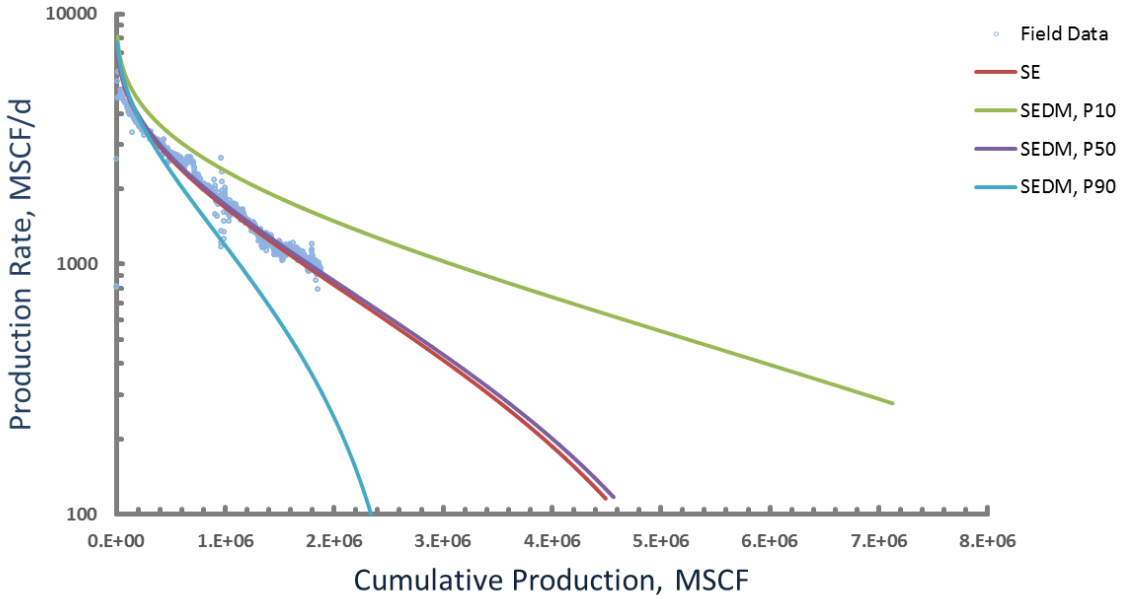
Production Rate, MSCF/d
10000
1000
100
0.E+00
1.E+06
2.E+06
3.E+06
4.E+06
5.E+06
6.E+06
7.E+06
8.E+06
Cumulative Production, MSCF
Field Data
SE
SEDM, P10
SEDM, P50
SEDM, P90

Well#23

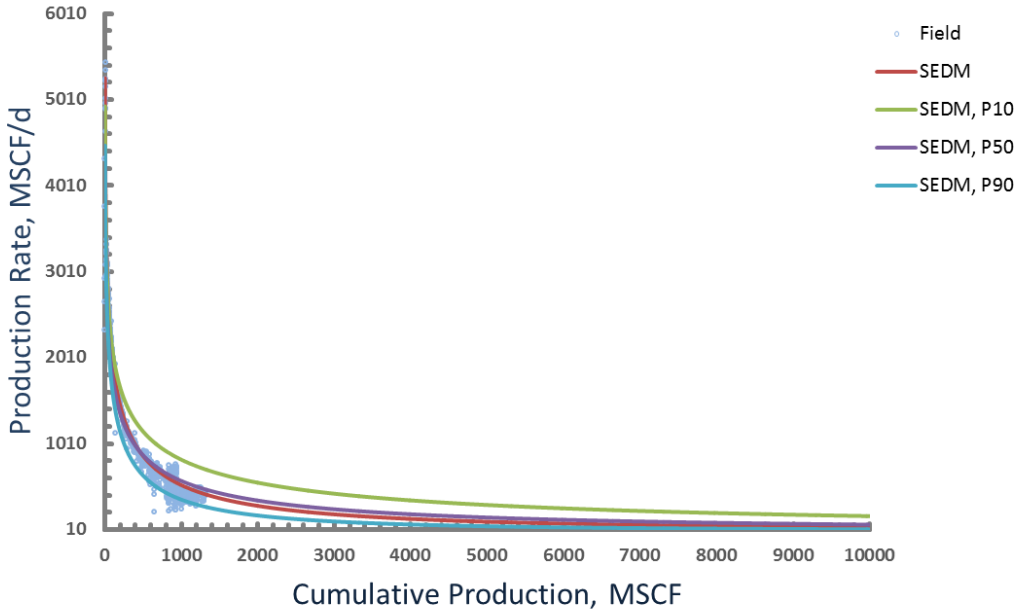
6010
5010
4010
3010
2010
1010
10
Production Rate, MSCF/d
0
1000
2000
3000
4000
5000
6000
7000
8000
9000
10000
Cumulative Production, MSCF
Field
SEDM
SEDM, P10
SEDM, P50
SEDM, P90

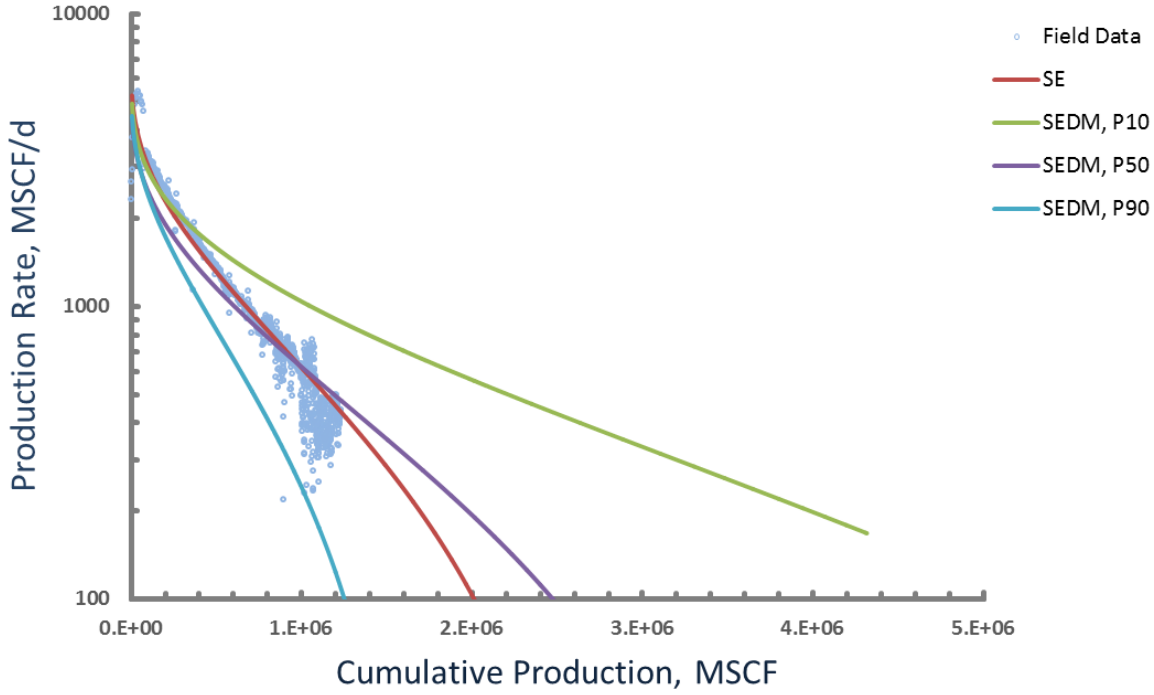
10000
1000
100
Production Rate, MSCF/d
0.E+00
1.E+06
2.E+06
3.E+06
4.E+06
5.E+06
Cumulative Production, MSCF
Field Data
SE
SEDM, P10
SEDM, P50
SEDM, P90

Well#24

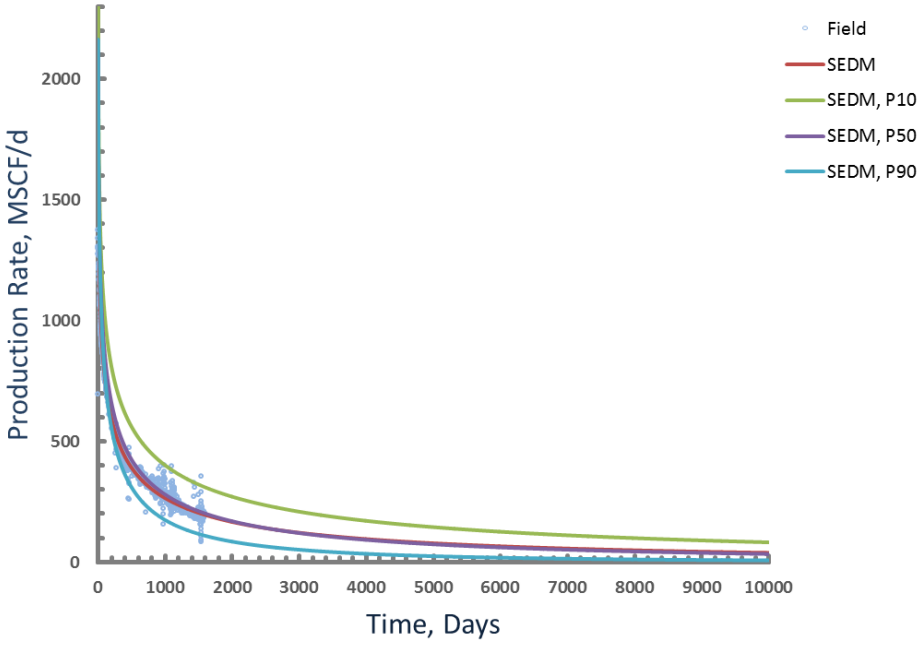
Field
SEDM
SEDM, P10
SEDM, P50
SEDM, P90
Production Rate, MSCF/d
2000
1500
1000
500
0
0
1000
2000
3000
4000
5000
6000
7000
8000
9000
10000
Time, Days

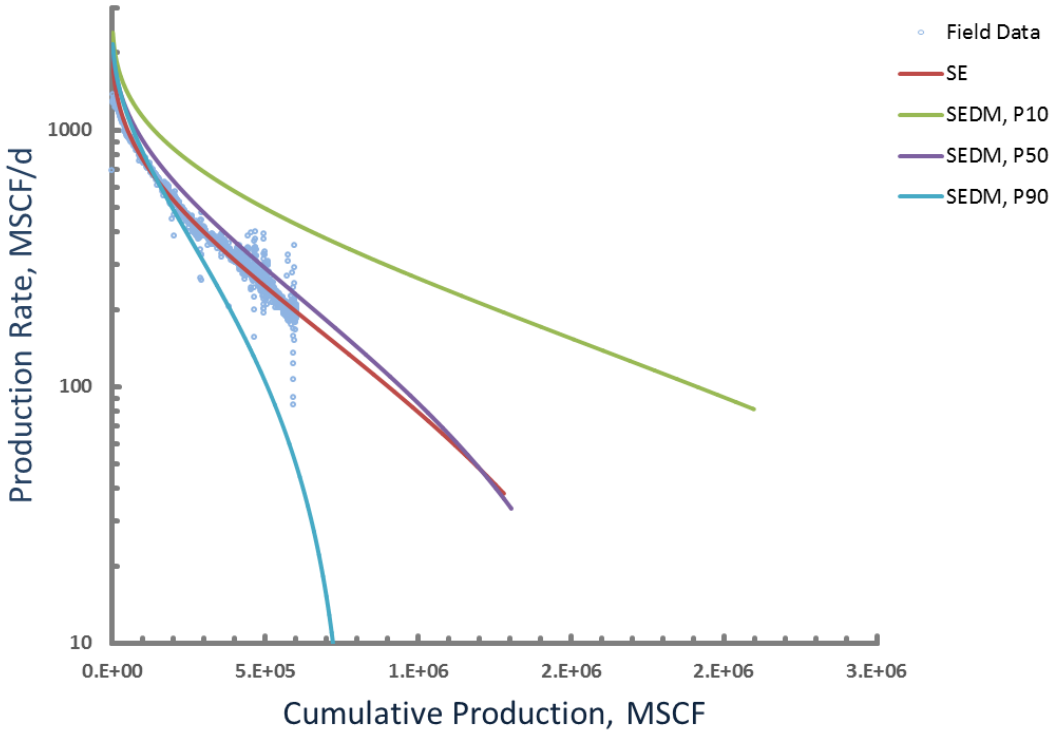
Field Data
SE
SEDM, P10
SEDM, P50
SEDM, P90
Production Rate, MSCF/d
1000
100
10
0.E+00
5.E+05
1.E+06
2.E+06
2.E+06
3.E+06
Cumulative Production, MSCF

Well#25

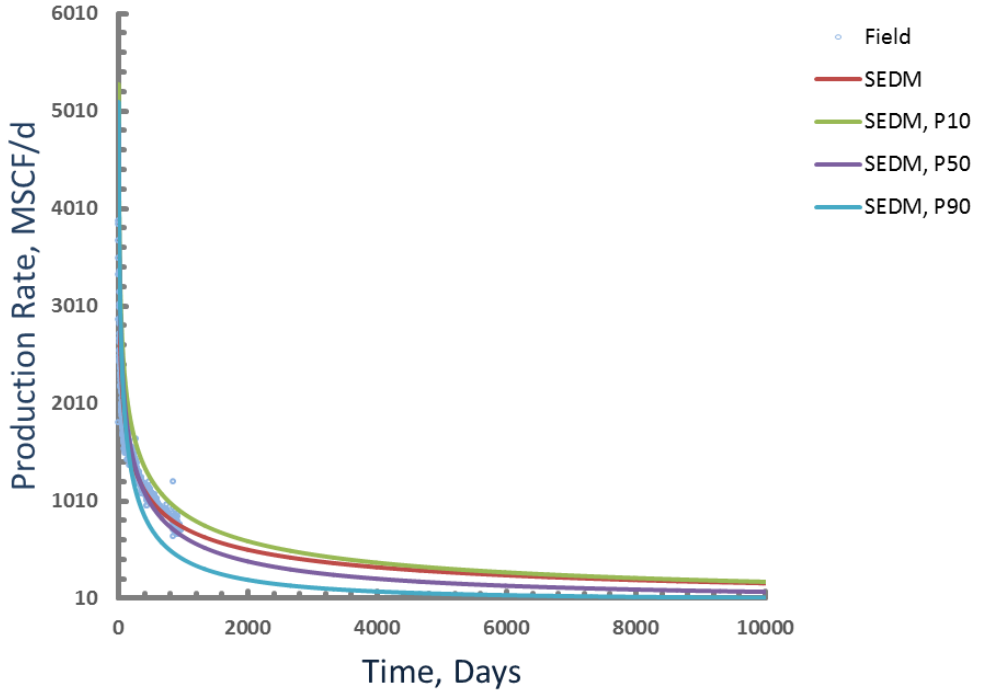
6010
5010
4010
3010
2010
1010
10
Production Rate, MSCF/d
0
2000
4000
6000
8000
10000
Time, Days
Field
SEDM
SEDM, P10
SEDM, P50
SEDM, P90

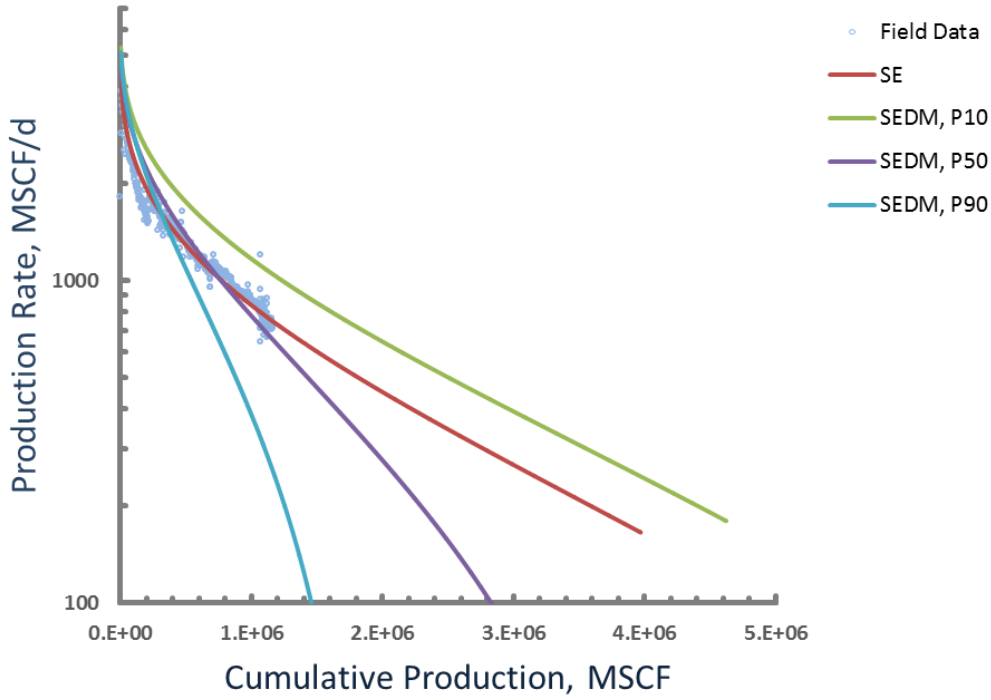
1000
100
Production Rate, MSCF/d
0.E+00
1.E+06
2.E+06
3.E+06
4.E+06
5.E+06
Cumulative Production, MSCF
Field Data
SE
SEDM, P10
SEDM, P50
SEDM, P90

VITA

Name:	Babak Akbarnejad Nesheli
Address:	C/O Dr. Valko, 3116 TAMU, College Station TX 77843-3116 (USA)
Email Address:	Babak.akbarnejad@pe.tamu.edu
Education:	B.A., Mining Engineering, Tehran University, 2002 M.S., Petroleum Engineering, Texas A&M University, 2006